MATERIALS FOR ADAPTIVE STRUCTURAL ACOUSTIC CONTROL

Period February 1, 1996 to January 31, 1997

Final Report

VOLUME V

OFFICE OF NAVAL RESEARCH
Contract No.: N00014-92-J-1510

APPROVED FOR PUBLIC RELEASE — DISTRIBUTION UNLIMITED

L. Eric Cross

PENNSTATE

THE MATERIALS RESEARCH LABORATORY
UNIVERSITY PARK, PA

REPORT DOCUMENTATION PAGE

OMB No. 0704-0188

1. AGENCY USE ONLY (Leave blank)	2. REPORT DATE	3. REPORT TYPE AND DATES COVERED
	4/14/97	FINAL REPORT 2/1/96-1/31/97

4. TITLE AND SUBTITLE

MATERIALS FOR ADAPTIVE STRUCTURAL ACOUSTIC CONTROL

5. FUNDING NUMBERS

ONR CONTRACT NO:
N00014-92-J-1510

6. AUTHOR(S)

L. ERIC CROSS

7. PERFORMING ORGANIZATION NAME(S) AND ADDRESS(ES)

MATERIALS RESEARCH LABORATORY
THE PENNSYLVANIA STATE UNIVERSITY
UNIVERSITY PARK, PA 16802-4800

8. PERFORMING ORGANIZATION REPORT NUMBER

9. SPONSORING/MONITORING AGENCY NAME(S) AND ADDRESS(ES)

OFFICE OF NAVAL RESEARCH
CODE 1513:NRJ
800 NORTH QUINCY STREET
ARLINGTON, VA 22217-5660

GERALD T. SMITH
OFFICE OF NAVAL RESEARCH RES. REP.
536 SOUTH CLARK STREET, RM 286
CHICAGO, ILLINOIS 60606-1588

10. SPONSORING/MONITORING AGENCY REPORT NUMBER

11. SUPPLEMENTARY NOTES

12a. DISTRIBUTION/AVAILABILITY STATEMENT

12b. DISTRIBUTION CODE

13. ABSTRACT *(Maximum 200 words)*

SEE FOLLOWING TWO PAGES

14. SUBJECT TERMS

15. NUMBER OF PAGES

16. PRICE CODE

17. SECURITY CLASSIFICATION OF REPORT	18. SECURITY CLASSIFICATION OF THIS PAGE	19. SECURITY CLASSIFICATION OF ABSTRACT	20. LIMITATION OF ABSTRACT

NSN 7540-01-280-5500

Standard Form 298 (Rev 2-89)
Prescribed by ANSI Std 239-18
298-102

GENERAL INSTRUCTIONS FOR COMPLETING SF 298

The Report Documentation Page (RDP) is used in announcing and cataloging reports. It is important that this information be consistent with the rest of the report, particularly the cover and title page. Instructions for filling in each block of the form follow. It is important to ***stay within the lines*** to meet ***optical scanning requirements***.

Block 1. Agency Use Only *(Leave blank)*.

Block 2. Report Date. Full publication date including day, month, and year, if available (e.g. 1 Jan 88). Must cite at least the year.

Block 3. Type of Report and Dates Covered. State whether report is interim, final, etc. If applicable, enter inclusive report dates (e.g. 10 Jun 87 - 30 Jun 88).

Block 4. Title and Subtitle. A title is taken from the part of the report that provides the most meaningful and complete information. When a report is prepared in more than one volume, repeat the primary title, add volume number, and include subtitle for the specific volume. On classified documents enter the title classification in parentheses.

Block 5. Funding Numbers. To include contract and grant numbers; may include program element number(s), project number(s), task number(s), and work unit number(s). Use the following labels:

C	- Contract	PR	- Project
G	- Grant	TA	- Task
PE	- Program Element	WU	- Work Unit Accession No.

Block 6. Author(s). Name(s) of person(s) responsible for writing the report, performing the research, or credited with the content of the report. If editor or compiler, this should follow the name(s).

Block 7. Performing Organization Name(s) and Address(es). Self-explanatory.

Block 8. Performing Organization Report Number. Enter the unique alphanumeric report number(s) assigned by the organization performing the report.

Block 9. Sponsoring/Monitoring Agency Name(s) and Address(es). Self-explanatory.

Block 10. Sponsoring/Monitoring Agency Report Number. *(If known)*

Block 11. Supplementary Notes. Enter information not included elsewhere such as: Prepared in cooperation with...; Trans. of...; To be published in.... When a report is revised, include a statement whether the new report supersedes or supplements the older report.

Block 12a. Distribution/Availability Statement. Denotes public availability or limitations. Cite any availability to the public. Enter additional limitations or special markings in all capitals (e.g. NOFORN, REL, ITAR).

DOD - See DoDD 5230.24, "Distribution Statements on Technical Documents."
DOE - See authorities.
NASA - See Handbook NHB 2200.2.
NTIS - Leave blank.

Block 12b. Distribution Code.

DOD - Leave blank.
DOE - Enter DOE distribution categories from the Standard Distribution for Unclassified Scientific and Technical Reports.
NASA - Leave blank.
NTIS - Leave blank.

Block 13. Abstract. Include a brief *(Maximum 200 words)* factual summary of the most significant information contained in the report.

Block 14. Subject Terms. Keywords or phrases identifying major subjects in the report.

Block 15. Number of Pages. Enter the total number of pages.

Block 16. Price Code. Enter appropriate price code *(NTIS only)*.

Blocks 17. - 19. Security Classifications. Self-explanatory. Enter U.S. Security Classification in accordance with U.S. Security Regulations (i.e., UNCLASSIFIED). If form contains classified information, stamp classification on the top and bottom of the page.

Block 20. Limitation of Abstract. This block must be completed to assign a limitation to the abstract. Enter either UL (unlimited) or SAR (same as report). An entry in this block is necessary if the abstract is to be limited. If blank, the abstract is assumed to be unlimited.

ABSTRACT

This report documents work carried out largely over the fifth and final year of the ONR sponsored University Research Initiative (URI) entitled "Materials for Adaptive Structural Acoustic Control." This program has continued to foster the successful development of new electroceramic single crystal and composite material combinations for both sensing and actuation functions in adaptive structural systems.

For the classical perovskite relaxor, dielectrics typified by lead magnesium niobate, continuing studies of properties in the temperature region above the dielectric maximum T_m have added strong additional support to the superparaelectric/spin glass model for the behavior developed earlier in the IMRL. The most exciting and important discovery of the year has been the ultra high strain capability of relaxor ferroelectric single crystal actuators. For crystal in the lead zinc niobate:lead titanate (PZN;PT) solid solution system, at compositions in the rhombohedral phase close to the morphotropic phase boundary to the tetragonal ferroelectric phase at 9 mole % PT in PZN, crystals cut and poled along the 001 cube axis exhibit massive field induced quasi linear anhysterestic strains up to 0.6%. For this poling d_{33} values up to 2,300 pC/N and coupling coefficients k_{33} of 94% have been achieved and it was the original hypothesis that these extreme numbers must be largely due to extrinsic domain wall motion. Now however it is very clear that the exact equivalence of the effect of an 001 oriented E field on the $111, \bar{1}11, 1\bar{1}1,$ and $\bar{1}\bar{1}1$ rhombohedral domains precludes this field from driving domain wall motion so that quite contrary to our earlier expectation the polarization and associated strain phenomena are purely intrinsic. At higher field levels there is an obvious step in both polarization and strain into an induced tetragonal phase which gives total reproducible induced strains up to 1.7%. Clearly the PZN:PT crystals represent a major breakthrough into a completely new regimen for piezoelectric actuation and sensing.

For antiferroelectric:ferroelectric switching compositions in the lead lanthanum zirconated titanate stannate family, new experimental studies have proven that the induced polarization P_3 and the strain x_{33} onset at different field levels. A new domain re-orientation model has been invoked to explain this startlingly unusual behavior. Both barium and strontium additives have also been explored to control hysteresis between forward and backward switching with good success. As well as being interesting for transduction we believe these compositions are sure to be important for energy storage dielectrics.

In composite sensing it is pleasing to report that the moonie flextensional patent has now been licensed to the Input:Output Corporation who have successfully fabricated and sold more than 80,000 moonie sensors. Work is continuing on the cymbal type modification of the moonie with focus now on array structures for large area panels. This topic is transitioning to a joint study between the IMRL and Penn State's ARL, on a new MURI initiative. For the very small hollow PZT spheres produced by blowing, the emphasis has been upon both poling and driving from outer surface electrodes, and exploring both by experiment and by finite element theoretical methods, the resonant mode structures which can be induced. Studies of the 2:2 composite structures confirm the very high effective hydrostatic sensitivity and are permitting closer consonance between measurement and theoretical analysis.

Actuation studies have been dominated by the initial exploration of the fantastic strain capability of the relaxor ferroelectric MPB single crystals. Obviously the induced strains are on order of magnitude larger than for conventional PZT ceramics, but the blocking force has

not yet been determined. It is expected that d_{31} will also be large and anhysteritic in these crystals, as spontaneous strain depends on Q_{44} which is a pure shear constant. The d_{15} however may be significantly more complex as an E_1 field will certainly drive domain walls in these E_3 poled crystals.

Reliability studies of conventional actuators are continuing with emphasis on using acoustic emission to explore and separate domain wall motion and crack propagation. Most earlier studies were indeterminate and difficult to interpret, recently for these strongly piezoelectric samples we have shown that electrical noise in the power supply induces very strong mechanical noise in the sample giving high spurious emission counts. New studies using a long time constant filter in the supply have permitted clear and effective separation. Over the last few years there has been a strong re-awakening of interest in bimorph type transducer amplifiers with new concepts like rainbow, cerambow and thunder appearing. Under our ONR program with Virginia Polytechnic it has been necessary to sort out the conflicting claims for these 'morph' types and these data are included for completeness. We have also begun serious study of the large electrostriction in the soft polyurethane elastomers where it has been necessary to derive new techniques to measure strain with ultra low constraint on the films.

Processing studies now involved both single crystal flux growth and a wide range of powder and ceramic processing. Current needs for integrity and better mechanical properties are driving new needs for fine grained PZT piezoceramics and new processing is permitting retention of excellent properties down to submicron grain sizes.

From the wide range of thin ferroelectric film activities in the laboratory, only those which refer to the thicker films being produced on silicon for MEMS devices are included.

MATERIALS FOR ADAPTIVE STRUCTURAL ACOUSTIC CONTROL

Period February 1, 1996 to January 31, 1997

Final Report

VOLUME V

OFFICE OF NAVAL RESEARCH
Contract No.: N00014-92-J-1510

L. Eric Cross

TABLE OF CONTENTS

APPENDICES

VOLUME I

General Summary Papers

1. Cross, L.E., "Ferroelectric Materials for Electromechanical Transducer Applications." *Mat. Chem. Phys* **43**, 108-115 (1996).

2. Cross, L.E., "Ferroelectric Ceramics: Materials and Application Issues." *Ceramic Transactions* **68**, 15-55 (1996).

3. Li. S., J.A. Eastman, Z. Li, C.M. Foster, R.E. Newnham, and L.E. Cross, " Size Effects in Ferroelectrics." *Phys. Lett. A* **212**, 341 (1996).

4. Li, Shaoping, J.A. Eastman, R.E. Newnham, and L.E. Cross, "Susceptibility of Nanostructured Ferroelectrics." *Japanese J. Appl. Physics* **35** (Part 2) [No. 4B], L502-L504 (1996).

5. Newnham, R.E., Chapter: Crystal Chemistry and Crystal Physics, in Innovative Ideas in Ceramics and Materials Curricula, edited by T. Stoebe and W. Huebner. Published by the *American Ceramic Society*, pp. 65-72 (1996).

6. Uchino, K., "New Applications of Photostriction." *Innovations in Mater. Res.* **1** (1), 11-22 (1996).

7. Aburatani, H. and K. Uchino, "Acoustic Emission (AE) Measurement Technique in Piezoelectric Ceramics." *Jpn. J. Appl. Phys.* **35** (2) [4B], L516-L518 (1996).

Materials Studies

8. Choi, S., J.M. Jung, and A.S. Bhalla, "Dielectric, Pyroelectric and Piezoelectric Properties of Calcium-Modified Lead Magnesium Tantalate-Lead Titanate Ceramics." *Ferroelectric Letters* **21**, 27-33 (1996).

9. Alberta, E. and A.S. Bhalla, "Preparation of Phase Pure Perovskite Lead Indium Niobate Ceramic." *Mater. Lett.* **29**, 127-129 (1996).

10. Zhang, Q.M., J. Zhao, T.R. Shrout, and L.E. Cross, "The Effect of Ferroelastic Coupling in Controlling the Abnormal Aging Behavior in Lead Magnesium Niobate-Lead Titanate Relaxor Ferroelectrics." *J. Mater. Res.* **12** (7), (1997).

11. Alberta, E., A.S. Bhalla, and T. Takenaka, "Piezoelectric, elastic and Dielectric Constants for Ceramics in the Solids Solution: $xPbZrO_3$ - $(1\text{-}x\text{-}z)Pb(Zn_{1/3}Nb_{2/3})\ O_3$ - $zPbTiO_3$." *Ferroelectrics* **188**, 109-124 (1996).

Materials Studies–continued

12. Zhang, Q.M. and J. Zhao, "Polarization Responses in Lead Magnesium Niobate Based Relaxor Ferroelectrics." *Applied Physics Letters* (submitted).

13. Müeller, V. and Q.M. Zhang, "Nonlinearity and Scaling Behavior in Donor Doped Lead Zirconate Titanate Piezoceramic." *Physics Review Letters* (submitted).

14. Zhang, Q.M., J. Zhao, K. Uchino, and J. Zheng, "Change of the Weak-Field Properties of $Pb(ZrTi)O_3$ Piezoceramics with Compressive Uniaxial Stresses and Its Links to the Effect of Dopants on the Stability of the Polarizations in the Materials." *J. Mat. Res.* **12**, 226 (1997).

15. Markowski, K., S.-E. Park, S. Yoshikawa, and L.E. Cross, "The Effect of Compositional Variations in the Lead Lanthanum Zirconate Stannate Titanate System on Electrical Properties." *J. Amer. Ceram.* **79** (12), 3297-3304 (1996).

16. Park, S.-E., K. Markowski, S. Yoshikawa, and L.E. Cross, "The Effect of Barium and Strontium Additions in the Lead Lanthanum Zirconate Stannate Titanate System on Electrical Properties." *J. Amer. Ceram.* **80** (2), 407-412 (1997).

VOLUME II

17. Yoshikawa, S., K. Markowski, S.-E. Park, M.-J. Pan, and L.E. Cross, "Antiferroelectric-to-Ferroelectric Phase Switching Lead Lanthanum Zirconate Stannate Titanate (PLZST) Ceramics." *SPIE Proceedings* **IV** (1997).

18. Blue, C.T., J.C. Hicks, S.-E. Park, S. Yoshikawa, and L.E. Cross, "In-situ X-ray Diffraction Study of the Antiferroelectric-Ferroelectric Phase Transition in PLSnZT." *Applied Physics Letter* **68** (21), 2942-2944 (1996).

19. Pan, M.-J., S.-E. Park, K. Markowski, and S. Yoshikawa, "Antiferroelectric-to-Ferroelectric PLZST Ceramics-II: The Effect of Pre-Stress Conditions on the Strain Behavior." Submitted *Proceedings of IEEE International Symposium on the Applications of Ferroelectrics*, Rutgers University, East Brunswick, New Jersey (August 1996).

20. M.-J. Pan, Markowski, K., S.-E. Park, S. Yoshikawa, and L.E. Cross. "Antiferroelectric-to Ferroelectric PLZSnT Ceramics-I: Structure, Compositional Modification and Electric Properties." Submitted *Proceedings of IEEE International Symposium on the Applications of Ferroelectrics*, Rutgers University, East Brunswick, New Jersey (August 1996).

Materials Studies–continued

21. Lopath, P.D., K.K. Shung, S.-E. Park, and T.R. Shrout, "Ultrasonic Transducers Using Piezoelectric Single Crystals Perovskites." Submitted *Proceedings of IEEE International Symposium on the Applications of Ferroelectrics*, Rutgers University, East Brunswick, New Jersey (August 1996).

22. Park, S.-E. and T.R. Shrout, "Characteristics of Relaxor-Based Piezoelectric Single Crystals for Ultrasonic Transducers." Proceedings of 1996 IEEE Ultrasonics Symposium, San Antonio, Texas (November 1996).

23. Park, S.-E., P.D. Lopath, K.K. Shung, and T.R. Shrout, "Relaxor-Based Single Crystal Materials for Ultrasonic Transducer Applications." Proceedings on SPIE's International Symposium on Medical Imaging, Newport Beach, California (February 1997).

24. Lopath, P.D., S.-E. Park, K.K. Shung, and T.R. Shrout, "$Pb(Zn_{1/3}Nb_{2/3})O_3/PbTiO_3$ Single Crystal Piezoelectrics for Ultrasonic Transducers." Proceedings on SPIE's International Symposium on Medical Imaging, Newport Beach, California (February 1997).

25. Park, S.-E. and T.R. Shrout, "Relaxor Based Ferroelectric Single Crystals for Electro-Mechanical Actuators." *Innovations in Materials Research* (accepted).

26. Park, S.-E. and T.R. Shrout, "Characteristics of Relaxor-Based Piezoelectric Single Crystals for Ultrasonic Transducers," *IEEE Trans. on Ultrasonics, Ferroelectric and Frequency Control Special Issue on Ultrasonic Transducers* (to be published).

27. Jin, B., R. Guo, and A.S. Bhalla, "Piezoelectric Properties and Equivalent Circuits of Ferroelectric Relaxor Single Crystals."

28. Mulvihill, M.L., K. Uchino, Z. Li, and W. Cao, "In-situ Observation of the Domain Configurations during the Phase Transitions in Barium Titanate." *Phil. Mag. B.* **74** (1), 25-36 (1996).

29. Mulvihill, M.L., L.E. Cross, and K. Uchino, "Dynamic Motion of the Domain Configuration in Relaxor Ferroelectric Single Crystals as a Function of Temperature and Electric Field." *Ferroelectrics* **186**, 325-328 (1996).

30. Sundar, V. and R.E. Newnham, "Conversion Method Measurements of Electrostriction Coefficients in Low-K Dielectrics." *Mat. Res. Bull.* **31** (5), 545-554 (1996).

31. Sundar, V., J.-F., Li, D. Viehland, and R.E. Newnham, "Interferometric Evaluation of Electrostriction Coefficients." *Mat. Res. Bull.* **31** (5), 555-563 91996).

Materials Studies–continued

32. Sundar, V., N. Kim, C. Randall, R. Yimnirun, and R.E. Newnham, "The Effect of Doping and Grain Size on Electrostriction in $PbZr_{0.52}Ti_{0.48}O_3$." Submitted *Proceedings of IEEE International Symposium on the Applications of Ferroelectrics*, Rutgers University, East Brunswick, New Jersey (August 1996).

33. Erdei, S., L. Galambos, I. Tanaka, L. Hesselik, F.W. Ainger, L.E. Cross, and R.S. Feigelson, "Segregation and Inhomogenities in Photorefractive SBN Fibers." *SPIE Proceedings V–Photorefractive Fiber and Crystal Devices: Materials, Optical Properties, and Applications II*, **2849**, 168-173 (1996).

34. Li, Shaoping, J.A. Eastman, J.M. Vertrone, R.E. Newnham, and L.E. Cross, "Coherent Coupling in Ferroelectric Superlattices." (1996).

35. Su, J., Q.M. Zhang, and R.Y. Ting, "Space Charge Enhanced Electromechanical Response in Thin Film Polyurethane Elastomers." *Applied Physics Letters* (submitted).

36. Zhang, Q.M., J. Su, and C.-H. Kim, "An Experimental Investigation of Electromechanical Responses in a Polyurethane Elastomer." *J. Appl. Phys.* **81** (6), 2770 (1997).

VOLUME III

37. Su, J., Q.M. Zhang, C.H. Kim, R.Y. Ting, and R. Capps, "Effects of Transitional Phenomena on the Electric Field Induced Strain-Electrostrictive Response of a Segmented Polyurethane Elastomer." *J. Appl. Polymer Sci.* (accepted).

Composite Sensors

38. Fernandez, J.F., A. Dogan, Q.M. Zhang, J.F. Tressler, and R.E. Newnham, "Hollow Piezoelectric Composites, Sensors and Actuators." *A: Physical* **51** (2,3), 183-192 (1996).

39. Fernandez, J.F., A. Dogan, Q.M. Zhang, and R.E. Newnham, "Piezoelectric Composites with Enclosed Hollow Spaces." Proceedings 4th Euroceramics Conference, *Electroceramics* **5**, 39-46 (1996).

40. Fernandez, J.F., A. Dogan, J.T. Fielding, K. Uchino, and R.E. Newnham, "Temperature Dependence of New Design Ceramic-Metal Piezocomposites Actuators." Proceeding 4th Euroceramics Conference, *Electroceramics* **5**, 133-138 (1996).

Composite Sensors–continued

41. Newnham, R.E., "Composite Sensors and Actuators," Disordered Materials, edited by G. Milton, K. Godlen, G. Grimmett, and P. Sen, Springer-Verlag, NY (accepted January 1997).

42. Tressler, J.F. and R.E. Newnham, "Doubly Resonant Cymbal Transducers, *IEEE Transactions of UFFC*, Special Issue on Transducers (accepted 1996).

43. Tressler, J.F., W. Cao, K. Uchino, and R.E. Newnham, "Ceramic Metal Composite Transducers for Underwater Acoustic Applications." Submitted *Proceedings of IEEE International Symposium on the Applications of Ferroelectrics*, Rutgers University, East Brunswick, New Jersey (August 1996).

44. Alkoy, S., A. Dogan, A.C. Hladky, J.K. Cochran, and R.E. Newnham, "Vibration Modes of PZT Hollow Sphere Transducers." Submitted *Proceedings of IEEE International Symposium on the Applications of Ferroelectrics*, Rutgers University, East Brunswick, New Jersey (August 1996).

45. Alkoy, S., A. Dogan, A.C. Hladky, and R.E. Newnham, "Miniature Piezoelectric Hollow Sphere Transducers (BBs)." 1996 Proceeding of IEEE International Frequency Control Symposium, pp. 586-594, Honolulu, Hawaii (1996).

46. Alkoy, S., A. Dogan, A.C. Hladky, and R.E. Newnham, "Piezoelectric Hollow Spheres." 1996 Proceeding 3rd Turkish Ceramic Society Meeting., Eds. V. Günay, H. Mandel, S. Ozgen. Istanbul, Turkey (October 1996).

47. Koc, B., A. Dogan, J.F. Fernandez, R.E. Newnham, and K. Uchino, "Accelerometer Application of the Modified Moonie (Cymbal) Transducer." *J. App. Phys.* **35**, 65-67 (1996).

VOLUME IV

48. Kumar, S., A. Bhalla, and L.E. Cross, "Underwater Acoustic Absorption by Collocated Smart Materials." *Ferroelectric Letters* **21**, 11-16 (1996).

49. Geng, X. and Q.M. Zhang, "Evaluation of Piezocomposites for Ultrasonic Transducer Applications–Influence of the Unit Cell Dimensions and the Properties of Constituents the Performance of 2-2 Piezocomposites." *IEEE Transactions of UFFC* (accepted).

50. Zhang, Q.M. and X. Geng, "Acoustic Properties of the Interface of a Uniform Medium-2-2 Piezocomposite and the Field Distributions in the Composite." *J. Appl. Phys.* (accepted).

Actuator Studies

51. Park, S.-E., and T.R. Shrout, "Ultrahigh Strain and Piezoelectric Behavior in Relaxor Based Ferroelectric Single Crystals."

52. Uchino, K. and S. Takahashi, "Multilayer Ceramic Actuators." *Current Opinion, Ceramic, Composites and Intergrowths*, p. 98-705 (1996).

53. Zheng, J., S. Takahashi, S. Yoshikawa, and K. Uchino, "Heat Generation in Multilayer Piezoelectric Actuators." *J. Amer. Ceram.* **79** (12), 3193-3198 (1996).

54. Dogan, A., J.F. Fernandez, K. Uchino, and R.E. Newnham, "New Piezoelectric Composite Actuator Designs for Displacement Amplification." *Proceeding Euroceramic Conference, Electroceramics* (5), 127-132 (1995) (in press).

VOLUME V

55. Poosanaas, P., A. Dogan., A.V. Prasadarao, S. Komarneni, and K. Uchino, "Photostriction of Sol-Gel Processed PLZT Ceramics." *J. Electroceramics* (1996) (in press).

56. Uchino, K., "Reliability of Ceramic Actuators." Submitted *Proceedings of IEEE International Symposium on the Applications of Ferroelectrics*, Rutgers University, East Brunswick, New Jersey (August 1996).

57. Uchino, K., "High Electromechanical Coupling Piezoelectrics-How High Energy Conversion Rate is Possible?-." *Proceeding MRS 1996* (1996) (in press).

58. Uchino, K., "Recent Developments in Ceramic Actuators-Comparison Among USA, Japan and Europe."

59. Xu, B., Q.M. Zhang, V.D. Kugel, Q. M. Wang, and L.E. Cross, "Optimization of Bimorph Based Double Amplifier Actuator under Quasistatic Situation." Submitted *Proceedings of IEEE International Symposium on the Applications of Ferroelectrics*, Rutgers University, East Brunswick, New Jersey (August 1996).

60. Kugel, V.D., S. Chandran, and L.E. Cross, "Caterpillar-Type Piezoelectric d_{33} Bimorph Transducer." *Appl. Phys. Lett.* **69** (14), 2021-2023 (1996).

61. Kugel, V.D., Q.M. Zhang, B. Xu, Q.-M. Wang, S. Chandran, and L.E. Cross, "Behavior of Piezoelectric Actuators under High Electric Field." Submitted *Proceedings of IEEE International Symposium on the Applications of Ferroelectrics*, Rutgers University, East Brunswick, New Jersey (August 1996).

62. Kugel, V.D., B. Xu, Q.M. Zhang, and L.E. Cross, "Bimorph-Based Piezoelectric Air Acoustic Transducer Model." *Sensors and Actuators A* (submitted 1996).

Actuator Studies–continued

63. Chandran, S., V.D. Kugel, and L.E. Cross, "CRESCENT: A Novel Piezoelectric Bending Actuator." *Proceeding SPIE's 4th Annual Symposium on Smart Structures* accepted 1997).

64. Kugel, V.D., S. Chandran, and L.E. Cross, "A Comparative Analysis of Piezoelectric Bending-Mode Actuators." Submitted *SPIE Proceedings*, Smart Structures and Materials: Smart Materials Technologies, 3040, 70-80 (1997).

65. Wang, Q.M., B. Xu, V.D. Kugel, and L.E. Cross, "Characteristics of Shear Mode Piezoelectric Actuators," Submitted *Proceedings of IEEE International Symposium on the Applications of Ferroelectrics*, Rutgers University, East Brunswick, New Jersey (August 1996).

Integration Studies

66. Elissalde, C., L.E. Cross, and C.A. Randall, "Structural-Property Relations in a Reduced and Internally Biased Oxide Wafer (RAINBOW) Actuator Material." *J. Amer. Ceram.* **79** (8), 2041-2048 (1996).

67. Xu. B., Q.M. Zhang, V.D. Kugel, Q. Wang, and L.E. Cross, "Optimization of Bimorph Based Double Amplifier Transducer under Quasistatic Conditions." Submitted *Proceedings of IEEE International Symposium on the Applications of Ferroelectrics*, Rutgers University, East Brunswick, New Jersey (August 1996).

68. Xu, B., Q. M. Zhang, V.D. Kugel, and L.E. Cross, "Piezoelectric Air Transducer for Active Noise Control." *Proceeding SPIE, Smart Structures and Integrated Systems* **271** (7), 388 (1996).

VOLUME VI

69. Chandran, S., V.D. Kugel, and L.E. Cross, "Characterization of the Linear and Non-Linear Dynamic Performance of RAINBOW Actuator." Submitted *Proceedings of IEEE International Symposium on the Applications of Ferroelectrics*, Rutgers University, East Brunswick, New Jersey (August 1996).

70. Wang, H., Q.M. Zhang, L.E. Cross, and C.M. Trottier, "Tailoring Material Properties by Structure Design–Radially Poled Piezoelectric Cylindrical Tube." *Ferroelectrics* **173**, 181-189 (1995).

Processing Studies

71. Park, S.-E., M. Mulvihill, P.D. Lopath, M. Zipparo, and T.R. Shrout, "Crystal Growth and Ferroelectric Related Properties of (1-x) Pb $(A_{1/3}Nb_{1/3})O_3$ - $xPbTiO_3$(A=Zn^{2+}, Mg^{2+})." Submitted *Proceedings of IEEE International Symposium on the Applications of Ferroelectrics*, Rutgers University, East Brunswick, New Jersey (August 1996).

72. Mulvihill, M., S.-E. Park, G. Risch, Z. Li, K. Uchino, and T.R. Shrout, "The Role of Processing Variables in the Flux Growth of PZN-PT Relaxor Ferroelectric Single Crystals." *Jpn. J. Appl. Phys.* **35** (Pt. 1; No. 7), 3984-3990 (1996).

73. Pan, M.-J., S.-E. Park, C.W. Park, K.A. Markowski, S. Yoshikawa, and C. Randall, "Superoxidation and Electrochemical Reactions during Switching in $Pb(Zr,Ti)O_3$ Ceramics." *J. Amer. Ceram.* **79** (11), 2971-2974 (1996).

74. Park, S.-E., M.L. Mulvihill, G. Risch, and T.R. Shrout, "The Effect of Growth Condition on Dielectric Properties of $Pb(Zn_{1/3}Nb_{2/3})O_3$ Crystal." *Jpn. J. Appl. Phys.* **36** (1) (1997).

75. Yoshikawa, Y. and K. Uchino, "Chemical Preparation of Lead-Containing Niobate Powders." *J. Amer. Ceram.* **79** (9), 2417-2421 (1996).

76. Ravindrathan, P., V. Srikanth, S. Komarneni, and A.S. Bhalla, "Processing of $Pb(Zn_{1/3}Nb_{2/3})O_3$: Ceramics at High Pressure." *Ferroelectrics* **188**, 135-141 (1996).

77. Ravindrathan, P., S. Komarneni, A.S. Bhalla, and R. Roy, "Low Temperature Chemical Routes to Smart Materials." *Ferroelectrics* **188**, 125-133 (1996).

78. Alberta, E.F. and A.S. Bhalla, "A Processing and Electrical Property Investigation of the Solid Solution: (x) $Pb(In_{1/2}Nb_{1/2})O_3$ - (1-x)$Pb(Sc_{1/2}Ta_{1/2})O_3$." *Ferroelectrics* **188**, 95-107 (1996).

Thin Film Ferroelectrics

79. Chen, H.D., K.R. Udayakumar, C.J. Gaskey, and L.E. Cross, "Fabrication and Electrical Properties of Lead Zirconate Titanate Thick Films." *J. Amer. Ceram.* **79** (8), 2189-2192 (1996).

80. Chen, H.D., K.K. Li, C.J. Gaskey, and L.E. Cross, "Thickness-Dependent Electrical Properties in Lanthanum-Doped PZT Thick Films." *Mat. Res. Soc. Symp. Proc.* **433**, 325-332 (1996).

81. Ravichandran, D., R. Meyer, Jr., R. Roy, R. Guo, A.S. Bhalla, and L.E. Cross, "Sol-Gel Synthesis of $Ba(Mg_{1/3}Ta_{2/3})O_3$: Phase Pure Powder and Thin Films." *Mat. Res. Bull.* **31** (7), 817-825 (1996).

82. Ravichandran, D., K. Yamakawa, R. Roy, A.S. Bhalla, S. Trolier-McKinstry, R. Guo, and L.E. Cross, "The Effect of Annealing Temperature on the Formation of $SrBi_2Ta_2O_9$ (SBT) Thin Films." Submitted *Proceedings of IEEE International Symposium on the Applications of Ferroelectrics*, Rutgers University, East Brunswick, New Jersey (August 1996).

Instrumentation

83. Su, J., P. Moses, and Q.M. Zhang, "A Bimorph Based Dilatometer for Field Induced Strain Measurement in Soft and Tin Free Standing Polymer Films." *Reviews of Scientific Instruments* (submitted).

ACTUATOR STUDIES

(continued)

APPENDIX 55

Accepted to be published in Journal of Electroceramics (1997)

PHOTOSTRICTION OF SOL-GEL PROCESSED PLZT CERAMICS

Patcharin Poosanaas, A. Dogan, A. V. Prasadarao, S. Komarneni, and K. Uchino.
International Center for Actuators and Transducers, Materials Research Laboratory,
The Pennsylvania State University, University Park, PA 16802

ABSTRACT

Lanthanum-modified lead zirconate titanate (PLZT) ceramic materials have gained considerable attention due to their photostriction, which is the superposition of photovoltaic and piezoelectric effects. However, the photovoltaic effect and the induced strain response are also influenced by the fabrication and processing conditions. The PLZT ceramics produced by conventional oxide mixing process exhibit moderate photostrictive properties due to the inhomogeneous distribution of impurities. In this study, ceramics of PLZT (3/52/48) doped with WO_3 and Nb_2O_5 were prepared by sol-gel technique using lead (II) acetate trihydrate, lanthanum (III) acetylacetonate hydrate, Zr, Ti, Nb, and W alkoxides. It was found that WO_3 and Nb_2O_5 were effective in suppressing the grain growth of PLZT, which lead to the enhancement of photovoltaic and photostrictive properties. Photovoltaic and photostrictive responses showed a maximum for samples with 0.5 at% WO_3 doped sol-gel PLZT. It has been shown that the sol-gel derived PLZT ceramics with proper density possess the possibility of enhancing the photostriction over ceramics produced by conventional oxide mixing process.

INTRODUCTION

Lanthanum-modified lead zirconate titanate (PLZT) ceramics are known to exhibit a range of interesting electro-optical properties. The advantages of PLZT ceramics are their high optical

transparency, desirable electrooptic properties, and fast response (Xu, 1991). There have been many successful demonstrations of the applications of PLZT. Recently, the application of PLZT in photostrictive actuators has drawn considerable attention (Uchino and Aizawa, 1985; Uchino *et al.*, 1985; Sada *et al.*, 1987; Chu *et al.*, 1994; Chu and Uchino, 1995)

Photostrictive effect is the superposition of the photovoltaic and piezoelectric effects. This effect is of interest in the development of wireless remote control photodriven actuators. Another promising application will be in the new generation photoacoustic devices. Photovoltaic effect and the strain response has been shown to vary greatly for the different preparation processes, even in the material with the same composition (Sada *et al.*, 1987). In a ceramic material for electro-optic application, a combination of good ferroelectricity and high transparency is required. This requirement can be met by a ceramic material with high density, low porosity, and a homogeneous composition. However, the conventional oxide mixing process provides inhomogeneous distribution of impurities, resulting in moderate photostriction properties. The sol-gel process, involving chemical precipitation (solution reaction) for preparation of powder materials, has gained attention in comparison to the conventional techniques due to its inherent advantages in producing high density homogeneous powder with a greater control on stoichiometry (Chiou and Kno, 1990; Rahaman, 1995). In addition, the obtained powders are finely divided and greatly enhanced in reactivity, sinterability and transparency over powders prepared by the conventional processing.

In this study, ceramics of PLZT (3/52/48) doped with WO_3 and Nb_2O_5 were prepared by both the conventional oxide mixing process and the sol-gel technique using lead (II) acetate trihydrate, lanthanum (III) acetylacetonate hydrate, Zr, Ti, Nb, and W alkoxides. Photostrictive effect and its dependence on dopant and fabrication method were investigated.

EXPERIMENTAL PROCEDURE

PLZT (3/52/48) ceramics with 3 at% La and a Zr/Ti ratio of 52/48 was selected due to its highest photovoltaic effect (Uchino and Aizawa, 1985). PLZT (3/52/48) doped with 0.5 at% WO_3 and various concentrations of Nb_2O_5 were prepared by the conventional oxide mixing process and the sol-gel technique. Figure 1 illustrates a flow chart for the sample preparation by the conventional oxide mixing process. In this method, $PbCO_3$, La_2O_3, ZrO_2, TiO_2 and dopants (WO_3 or Nb_2O_5) were mixed in the proper ratio corresponding to the composition and ball milled for 48 h. The slurry was dried and calcined at 950 °C for 10 h. The calcined powder was further ball milled for 48 h and subsequently sintered in air at 1270 °C for 2 h. The flow chart for the sample preparation by the sol-gel technique has been shown in Fig. 2. In the sol-gel processing, lead (II) acetate trihydrate, $Pb(CH_3COO)_2{\cdot}3H_2O$, lanthanum (III) acetylacetonate hydrate, $La(acac)_3{\cdot}H_2O$, zirconium (IV) butoxide, $Zr(OC_4H_9)_4$, and titanium (IV) isopropoxide, $Ti(OC_3H_7)_4$, were used as precursors while tungsten (VI) ethoxide, $W(OC_2H_5)_6$ and niobium (V) ethoxide, $Nb(OC_2H_5)_5$, were used as dopants and 2-methoxyethanol (2-MOE) was used as a solvent. Pb and La precursors were mixed in the proper ratio and dissolved in 2-MOE and used as precursor site A. The solution was distilled and refluxed at 125 °C and cooled to the room temperature. Precursor site B comprising of Zr, Ti and dopant were mixed in the proper ratio using 2-MOE as a solvent. The solution was refluxed in Ar at 125 °C and cooled to room temperature. Subsequently, the solution was added into the reflux solution of site A and was refluxed in Ar at 125 °C. The pH of this solution was adjusted to 10 by using nitric acid, before its hydrolysis. The solution was then aged to yield a gel which was dried to obtain the powder.

After the organic removal at 400 °C for 6 h, the powder was calcined at 600 °C for 1 h and sintered at 1250 °C for 2 h in air.

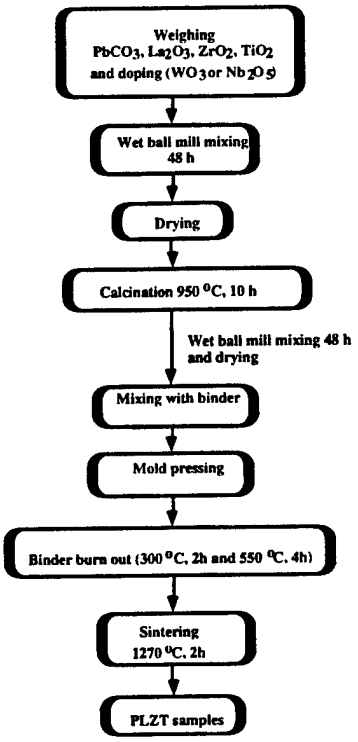

Fig. 1. Flow diagram of sample preparation by oxide mixing process.

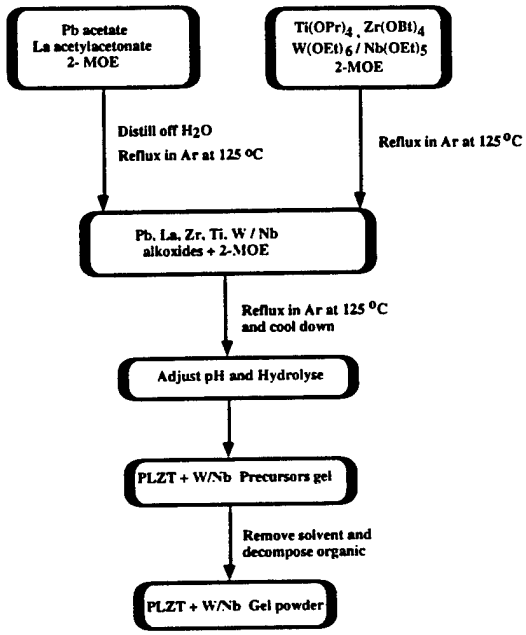

Fig. 2. Flow diagram of sample preparation by sol-gel process.
2-MOE: 2-methoxyethanol. $Ti(OPr)_4$: Titanium (IV) isopropoxide.
$Zr(OBt)_4$: Zirconium (IV) butoxide, $W(OEt)_6$: Tungsten (VI) ethoxide.
$Nb(OEt)_5$: Niobium (V) ethoxide.

The density of the sintered samples was determined by the Archimedes method. Microstructure and grain size of the samples were observed by scanning electron microscopy (ISI-SX-40X Scanning Electron Microscope, International Scientific Instruments, Inc., NY). Dielectric properties of PLZT samples were measured with an impedance analyzer (HP-4274A). Samples for dielectric measurements were polished to about 10 mm in diameter and 1 mm in thickness, then electroded with platinum (Pt) by sputtering. Piezoelectric properties of all the samples were measured by using a Berlincourt d33 meter (Channel Products, Inc.) at 100 Hz.

Samples for piezoelctric measurement were of the same configuration as for dielectric measurements, except they were poled in silicone oil at 120 °C under a 2 kV/mm electric field for 10 min.

Photovoltaic measurements were done by using a high-input-impedance electrometer (Keithley 617), while the photostriction measurement was done by using the displacement sensor (LVDT, Millitron model 1301). These measurements were done by radiating the light perpendicular to the polarization direction. The samples of 5x5x1 mm^3 were cut and polished for these measurements. The 5x1 mm^2 surfaces were silver electroded. Poling was performed by applying 2 kV/mm electric field for 10 min. in silicon oil at 120 °C. A high pressure mercury lamp (Ushio Electric USH-500D) was used as a light source for the measurement. The white radiation was passed through an IR blocking filter and an UV bandpass filter to obtain a beam with a maximum strength around 370 nm and an intensity of 3.25 mW/cm^2, before illuminating the samples (5x5 mm^2 polished surface). The light beam with this wavelength has been reported to yield the maximum photovoltaic properties (Uchino *et al.*, 1985). The experimental set-up for photovoltaic and photostriction measurements are shown in Figs. 3 and 4, respectively.

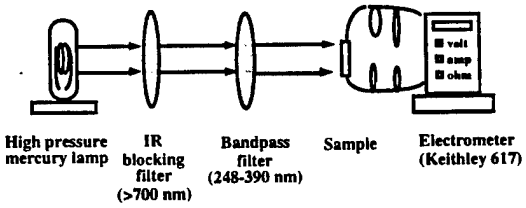

Fig. 3. Experimental set up for photovoltaic measurement.
Illumination
- High pressure Mercury lamp
- Without polarizer
- Filter - IR blocking filter
- Bandpass filter
- Wavelength - 370 nm
- Intensity - 3.25 mW/cm^2

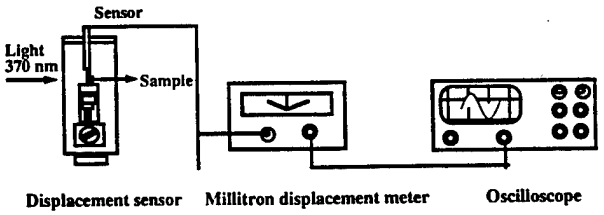

Fig. 4. Experimental set up for photostrictive measurement.

RESULTS AND DISCUSSION

Relative density

Figure 5 shows the relative sintered density of Nb_2O_5 doped PLZT as a function of sintering temperature. A relative density of 98% was achieved for PLZT oxide samples sintered at 1200 °C. The sintered density saturated and remained constant as the sintering temperature increases to 1300 °C. On the other hand, in the sol-gel PLZT a maximum density of 91% was observed at a sintering temperature of 1250 °C. The sintered density decreased as the sintering temperature was further increased. This was probably due to the evaporation of PbO during sintering. As evident from Fig. 5, the sol-gel PLZT exhibits lower density as compared to the oxide PLZT at all the sintering temperatures. This lower density was probably due to finer and agglomerated particles, resulting in aggregation which was observed in some areas of Nb_2O_5 doped sol-gel PLZT. However, the aggregation was not observed in 0.5 at% WO_3 doped sol-gel PLZT, which is one reason for the higher relative density of this ceramic (93%) than Nb_2O_5 doped sol-gel PLZT. The high density in PLZT oxide samples is probably due to higher packing density without agglomeration as compared to sol-gel ceramics. Figure 6 shows the SEM micrographs of the sintered ceramic surfaces. The 1.0 at % Nb_2O_5 doped sol-gel PLZT in (b) clearly showed large pores which caused by the particle agglomeration.

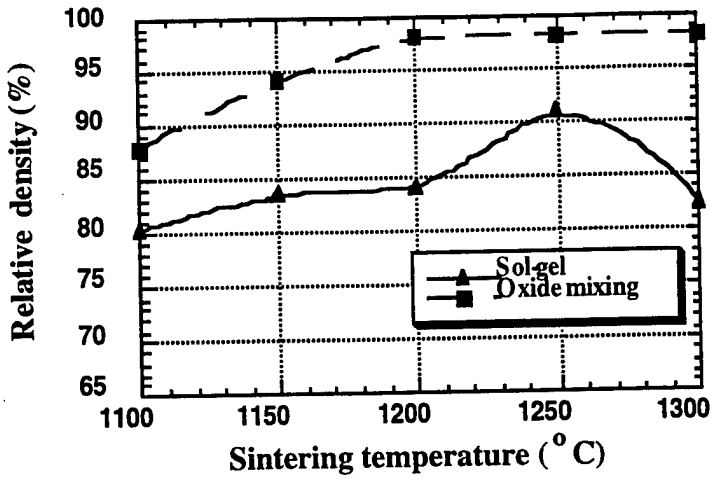

Fig. 5. Relative density as a function of sintering temperature after 2h sintering.

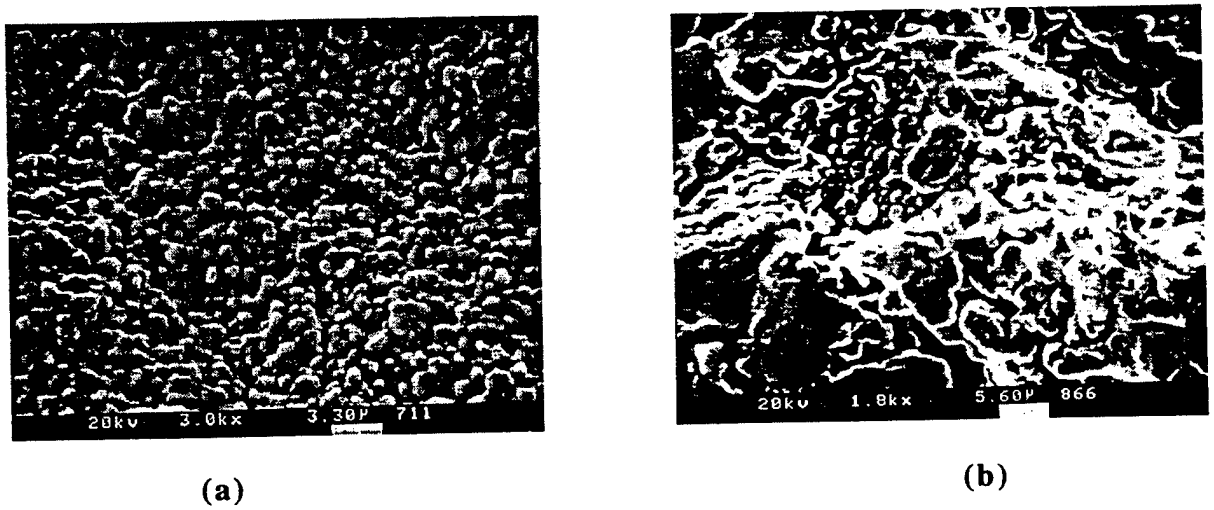

(a) **(b)**

Fig. 6. SEM micrographs of 1.0 at% Nb_2O_5 doped PLZT ceramics prepared by (a) oxide mixing (b) sol-gel methods.

Grain size

The average grain size is shown in Fig. 7 as a function of doping concentration. The average grain size decreases with increasing doping concentration. Nb_2O_5 was found to be more effective in suppressing the grain size as compared to WO_3 as a dopant. The grain size of the sol-gel ceramics was smaller than that of the oxide mixing ceramics when sintered at 1250 °C for 2h.

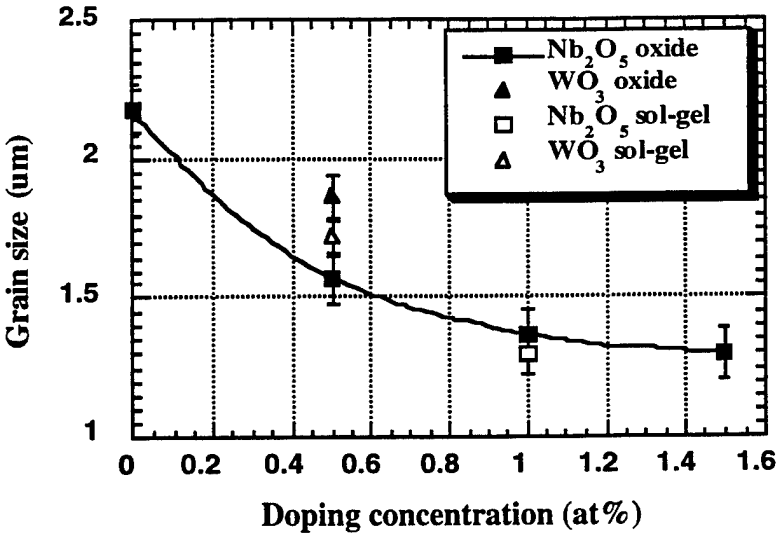

Fig. 7. Variation of average grain size with doping concentration.

Dielectric and piezoelectric properties

Figure 8 (a) shows the change in the maximum dielectric constant with doping concentration. The number shown in the figure represents the relative density of the samples at each composition. The dielectric loss (tan δ) as a function of doping concentration is shown in Fig. 8 (b). The maximum dielectric constant was found to decrease with increasing doping concentration for the case of oxide mixing samples. This was partially due to the lower grain size observed in PLZT doped oxide mixing ceramics. The dielectric constant showed a minimum at 1.0 at% Nb_2O_5 doped oxide PLZT. Also, the sol-gel PLZT doped with WO_3 has a lower dielectric constant compared to the oxide PLZT due to the smaller grain size. However, the Nb_2O_5 doped sol-gel PLZT exhibits higher dielectric constant as compared to the oxide PLZT at the same composition. This may be due to the high dielectric loss observed in this ceramic (Fig.8 (b)). Higher dielectric loss in sol-gel samples may be due to loss through grain boundaries and pores.

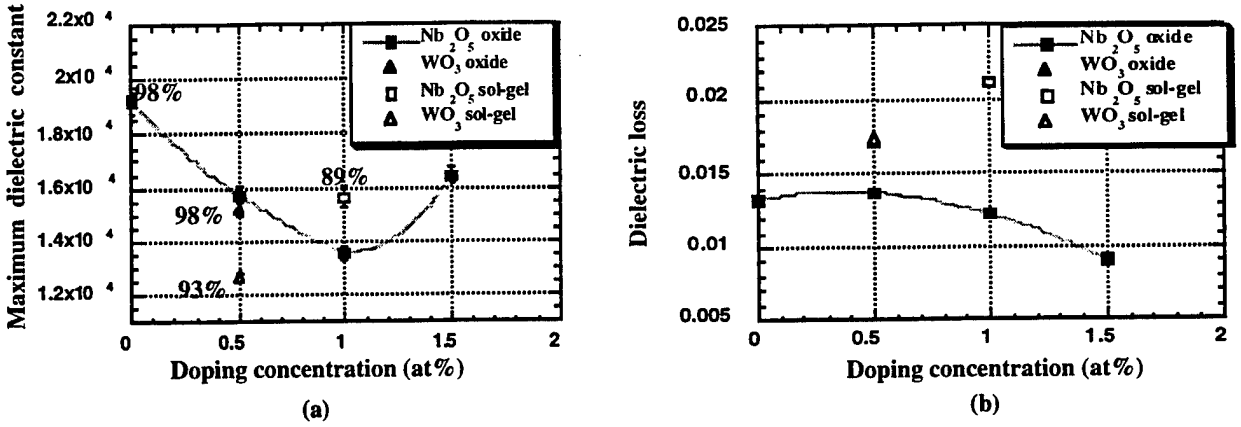

Fig. 8 Variation of (a) maximum dielectric constant (b) maximum dielectric loss with doping concentration.

The piezoelectric constant as a function of doping concentration is shown in Fig. 9. The measured value of d33 decreases with increasing doping concentration. Also, the sol-gel ceramics exhibit lower d33 as compared to the oxide ceramics. With decrease in grain size, the domain wall contribution to the piezoelectric properties drops off, leading to this decrease in piezoelectric constant.

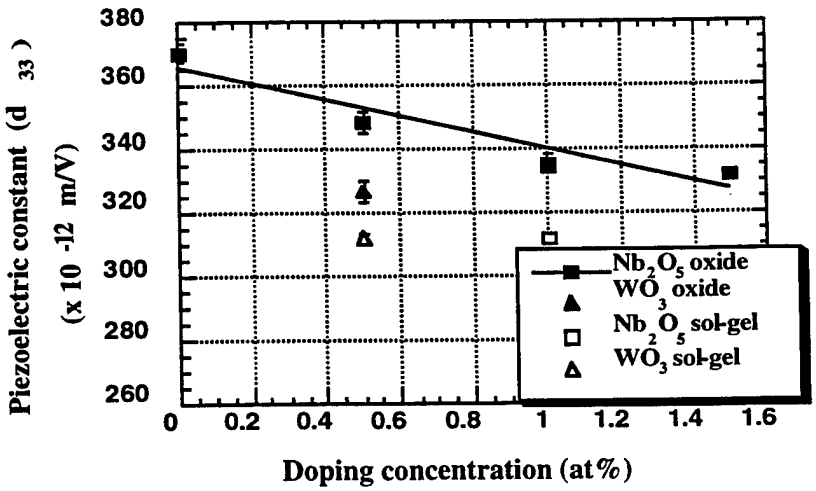

Fig. 9. Variation of piezoelectric constant with doping concentration.

Photovoltaic and photostrictive properties

Figure 10 shows the variation of photovoltaic responses with doping concentration for the samples doped with WO_3 and Nb_2O_5. All dopants were found to enhance the photovoltaic responses. The photovoltage reached more than 1 kV/cm and the photocurrent was of the order of nA/cm. As in the previous papers, the current density was normalized only with respect to the width of the illuminated surface, but not to the depth. Both the photovoltage and photocurrent revealed a maximum at 1 at% of doped Nb_2O_5 in the oxide PLZT. WO_3 doped sol-gel PLZT showed the maximum photovoltaic response among all the samples. This may be attributed to higher degree of homogeneity and uniform distribution of dopant and a stoichiometry in compositions for this sample. Lower photovoltatic properties were observed in Nb_2O_5 doped sol-gel PLZT. In general, increase in photovoltage will enhance photostriction and increasing photocurrent will increase the response speed. The photostriction is estimated as the product of the photovoltage and the piezoelectric coefficient (Uchino and Aizawa, 1985, Sada *et al.*, 1987; Chu and Uchino, 1995). It can be expressed by

$$x_{ph} = d_{33} E_{ph} (1- \exp (-t/RC))$$

where x_{ph} is photoinduced strain, d_{33} is piezoelectric coefficient, E_{ph} is the saturated photovoltage, t is time, R is the resistance, and C is the capacitance of samples. The RC is referred to as time constant or response speed which suggests that sample with high photocurrent will give fast response speed as compared to slow response samples. These effects are confirmed in Figs. 11 (a) and 11 (b), where the change in photostriction and response speed are shown as a function of doping concentration. Similar changes in photovoltaic behavior with doping concentration was observed in photostrictive effect. The maximum photostriction was

found in WO_3 doped sol-gel PLZT. In the Nb_2O_5 doped oxide PLZT, the largest photostriction was observed in the sample with 1.0 at% Nb_2O_5. Also, the WO_3 doped sol-gel PLZT exhibited the fastest response time among all the samples. The fastest response time among Nb_2O_5 doped oxide PLZT, was obtained at 1.0 at% Nb_2O_5. The lower photostriction and the slow response speed in Nb_2O_5 doped sol-gel PLZT can be due to the agglomeration of fine powder which resulted in a lower density.

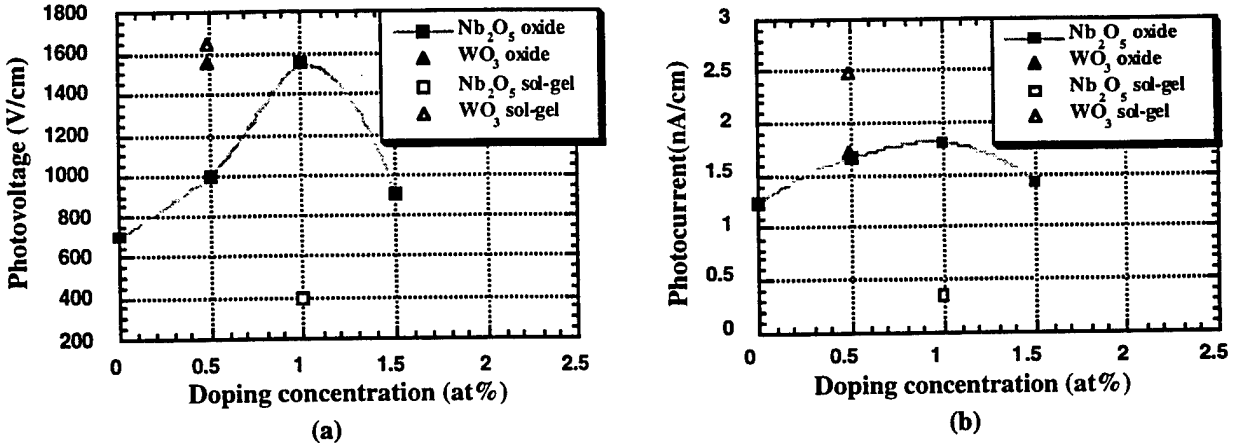

Fig. 10. Variation of (a) photovoltage (b) photocurrent with doping concentration.

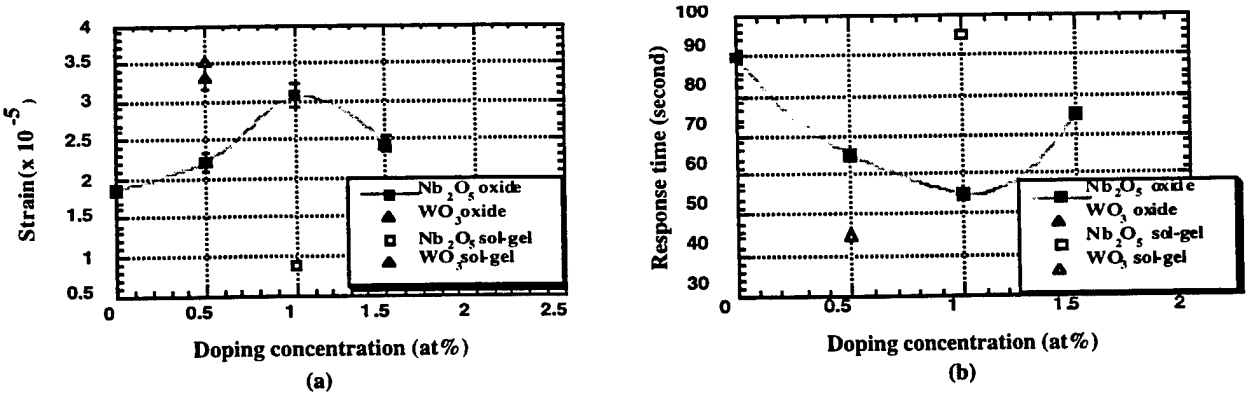

Fig. 11. Variation of (a) photoinduced strain (b) response time with doping concentration.

CONCLUSIONS

WO_3 and Nb_2O_5 were effective in suppressing the grain growth which leads to the enhancement of photovoltaic and photostrictive properties in PLZT. Although, WO_3 was less effective in suppressing the grain size, due to its inherent dopant property, it was more effective in enhancing the photovoltaic and photostrictive responses. Dielectric and piezoelectric properties were found to decrease with increasing doping concentration due to the smaller grain size. In general, the dielectric and piezoelectric properties can be enhanced by doping with donors such as WO_3 and Nb_2O_5. However, they also decrease with decreasing grain size due to drop in domain wall contribution. The lower dielectric and piezoelectric properties found in doped ceramics indicate the dominance of the grain size effect. Although the relative density of sol-gel PLZT is lower than oxide PLZT at the same composition, the preliminary results showed that the maximum photovoltaic and photostrictive effect were obtained for 0.5 at% WO_3 doped sol-gel PLZT. This may suggest that a better homogeneity and a closer control of stoichiometry in sol-gel technique as compared to oxide mixing process give rise to higher photovoltaic and photostrictive properties. The aggregation and low density observed in Nb_2O_5 doped sol-gel PLZT was the reason for lower photovoltatic and photostrictive responses as compared to the WO_3 doped sol-gel PLZT. In conclusion, the preliminary results in this study suggests that the sol-gel technique possess the possibility in enhancing the photostriction in PLZT. It must also be noted that if the density of sol-gel processed PLZT can be increased through particle size distribution and by controlling the agglomeration, even further improvement in photostrictive response will be achieved.

ACKNOWLEDGMENTS

This work is partially supported by Army Research Office through Grant No. DAAL 03-92-G-0244. One of the authors (P. Poosanaas) would like to acknowledge the Royal Thai Government and Dr. Harit Sutabutr from the National Metal and Materials Technology Center (Thailand) for granting MOSTE fellowship.

BIBLIOGRAPHY

Chiou, B.-S., and Kno, J. N., 1990, The Preparation of PLZT Ceramics from a Sol-Gel Process, J. Elec. Mater., 19 (4), 393-397.

Chu, S.-Y., and Uchino, K., 1995, Photostrictive Effect in PLZT-Based Ceramics and its Application, Ferroelectrics, 174, 185-196.

Chu, S.-Y., Ye, Z., and Uchino, K., 1994, Photovoltaic Effect for the Linearly Polarized Light in (Pb, La) (Zr, Ti) O_3, Ceramics, Smart Mater. Struct., 3, 114-117.

Rahaman. M. N., 1995, Ceramic Processing and Sintering, Marcel Dekker. Inc., New York, 207.

Sada, T., Inoue, M., and Uchino, K., 1987, Photostriction in PLZT Ceramics, J. Ceram. Soc. Jpn., Inter. Ed., 95, 499-504.

Uchino, K., and Aizawa, M., 1985, Photostrictive Actuator Using PLZT Ceramics, Jpn. J. Appl. Phys. Suppl., 24, 139-141.

Uchino, K., Aizawa, M., and, Nomura, S., 1985, Photostrictive Effect in (Pb, La) (Zr, Ti) O_3, Ferroelectrics, 64, 199-208.

Xu, Y., 1991, Ferroelectric Materials and Their Application, Elsevier Science Pub. Co., New York, 1991, 164.

APPENDIX 56

ISAF '96 Proc. (in press)

Reliability of Ceramic Actuators

Kenji Uchino
International Center for Actuators and Transducers
Materials Research Laboratory, The Pennsylvania State University
University Park, PA 16802 USA

Abstract-Reliability of ceramic actuators is dependent on complex factors, which are divided into three major categories: reliability of the ceramic material, reliability of the device design and drive technique. The reliability issues are reviewed from whole points of view, with a particular focus on multilayer structures.

I. INTRODUCTION

The application field of ceramic actuators has become remarkably wide [1,2]. There still remain, however, problems in durability and reliability that need to be addressed before these devices can become general-purpose commercialized products. Investigations are primarily focused on the areas of ceramic preparation, device design and drive technique to improve the reliability.

II. MATERIALS IMPROVEMENTS

The reproducibility of the strain characteristics depends strongly on grain size, porosity and impurity content. Increasing the grain size enhances the magnitude of the field-induced strain, but degrades the fracture toughness and increases the hysteresis [3]. The grain size should be optimized for each application. Hence, fine powders made from wet chemical processes such as coprecipitation and sol-gel will be required.

Porosity does not affect the strain behavior significantly. Figure 1 shows the tip deflection of a unimorph made from $Pb(Mg_{1/3}Nb_{2/3})O_3$ based material plotted as a function of sample porosity [4]. The deflection did not show a difference below 8 % of porosity.

The impurity, donor- or acceptor-type, provides remarkable changes in strain. Figure 2 shows dopant effect on the field induced strain in $(Pb_{0.73}Ba_{0.27})(Zr_{0.75}Ti_{0.25})O_3$ [5]. Since donor doping provides "soft" characteristics, the sample exhibits larger strains and less hysteresis when driven under a high electric field (1 kV/mm). On the contrary, the acceptor doping provides "hard" characteristics, leading to a very small hysteretic loss and a large mechanical quality factor when driven under a small AC electric field (i. e. ultrasonic motor applications!).

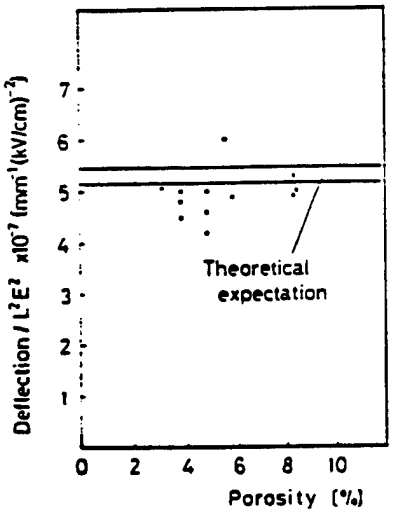

Fig.1. Tip deflection of a PMN unimorph plotted as a function of the sample porocity.

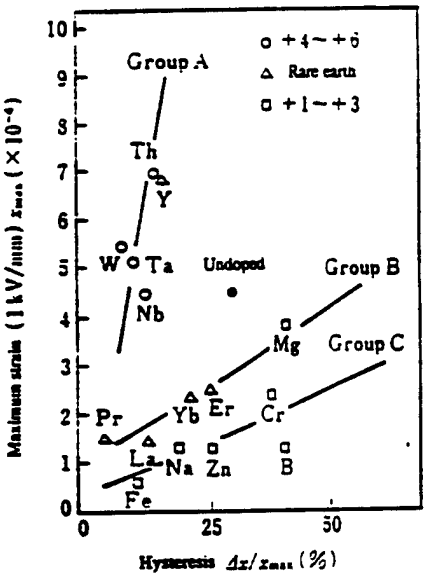

Fig.2. Dopant effect on the field induced strain in $(Pb_{0.73}Ba_{0.27})(Zr_{0.75}Ti_{0.25})O_3$.

Figure 3 shows the temperature rise versus vibration velocity for undoped, Nb-doped and Fe-doped $Pb(Zr,Ti)O_3$ samples. The suppression of heat generation is remarkable in the Fe-doped (acceptor-doped) ceramic [6].

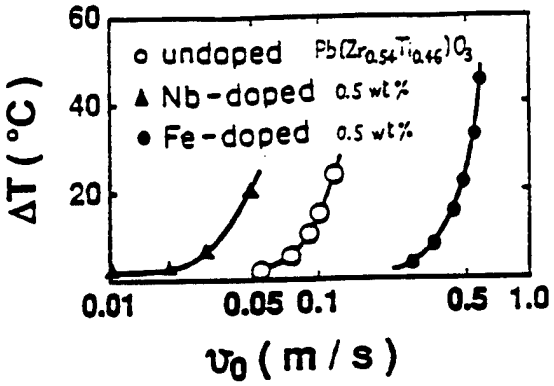

Fig.3. Temperature rise vs. effective vibration velocity for PZT samples doped with Nb or Fe.

The temperature dependence of the strain characteristics must be stabilized using either composite or solid solution techniques [7]. The recent new trends are found in developing high temperature actuators for engine surroundings and cryogenic actuators for laboratory equipment and space structures.

Ceramic actuators are recommended to be used under bias compressive stress. Figure 4 shows compressive uniaxial stress dependence of the weak-field piezoelectric constants d in various PZT. Note the significant enhancement in the d values for hard piezoelectric ceramics [8]. Systematic studies on stress dependence of induced strains are eagerly awaited, including the composition dependence of mechanical strength.

Although the aging effect is very important, not many investigations have been done so far. The aging effect arises from two factors: depoling and destruction. Creep and zero-point drift of the displacement are caused by the depoling of the ceramic. Another serious degradation of the strain is produced by a very high electric field under an elevated temperature, humidity and mechanical stress. Change in lifetime of a multilayer piezoelectric actuator with temperature and DC bias voltage has been reported by Nagata [9]. The lifetime under DC bias voltage obeys an empirical rule:

$$t_{DC} = A\, E^{-n} \exp(W_{DC}/kT) \qquad (1)$$

where W_{DC} is an activation energy ranging from 0.99 - 1.04 eV.

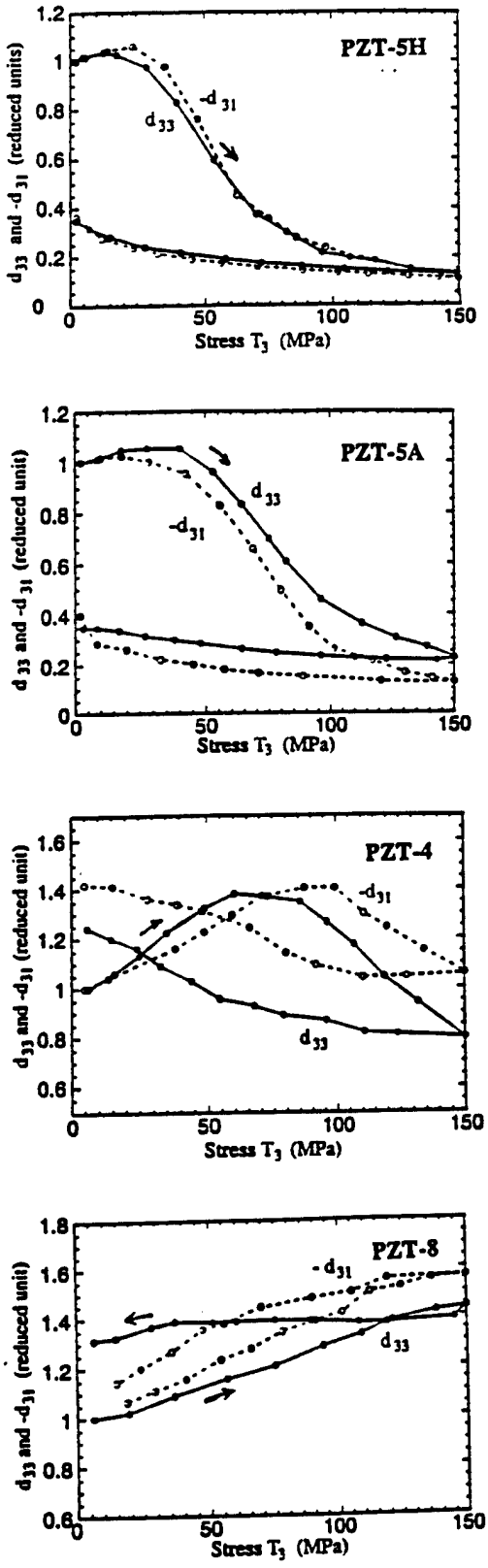

Fig.4. Compressive uniaxial stress dependence of the weak-field piezoelectric constant d in PZT (from top to bottom, "soft" to "hard").

III. RLIABILITY OF DEVICES

Popular silver electrodes have a serious problem of migration under a high electric field and high humidity. This problem can be overcome with usage of a silver-palladium alloy (or more expensive Pt). To achieve inexpensive ceramic actuators, we need to introduce Cu or Ni electrodes, which requires a sintering temperature as low as 900°C. Low temperature sinterable actuator ceramics will be the next target to research.

Delamination of the electrode layer is another problem in multilayer types as well as bimorphs. To enhance adhesion, composite electrode materials with metal and ceramic powder colloid, ceramic electrodes, and electrode configurations with via holes are recommended for use [10]. To suppress the internal stress concentration which initiates the crack in the actuator device, several electrode configuations have been proposed, as shown in Fig.5: plate-through type, slit-insert type, and float-electrode-insert type [11]. The reason why the lifetime is extended with decreasing layer thickness has not yet been clarified.

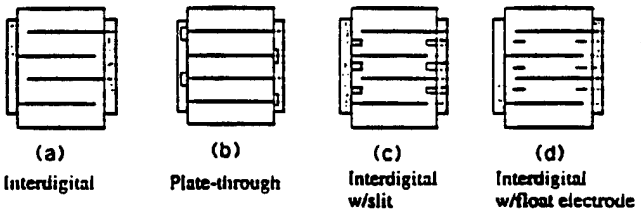

Fig.5. Various electrode configurations for multilayer ceramic actuators.

Lifetime prediction or health monitoring systems have been proposed using failure detection techniques [12]. Figure 6 shows such an "intelligent" actuator system with AE monitoring. The actuator is controlled by two feedback mechanisms: position feedback, which can compensate the position drift and the hysteresis, and breakdown detection feedback which can stop the actuator system safely without causing any serious damages to the work, e.g. in a lathe machine. Acoustic emission measurement of a piezo-actuator under a cyclic electric field is a good predictor for lifetime. AE was detected largely when a crack propagates in the ceramic actuator at the maximum speed. During a normal drive of a 100-layer piezoelectric actuator, the number of AE was counted and a drastic increase by three orders of magnitude was detected just before complete destruction. Note that part of the piezo-device can be utilized as an AE sensor.

A recent new electrode configuration with a strain gauge type (Fig.7) is another intriguing alternative for the health monitoring. By measuring the resistance of the strain gauge shaped electrode embedded in a ceramic actuator, we can monitor both electric-field induced strain and the symptom of cracks in the ceramic.

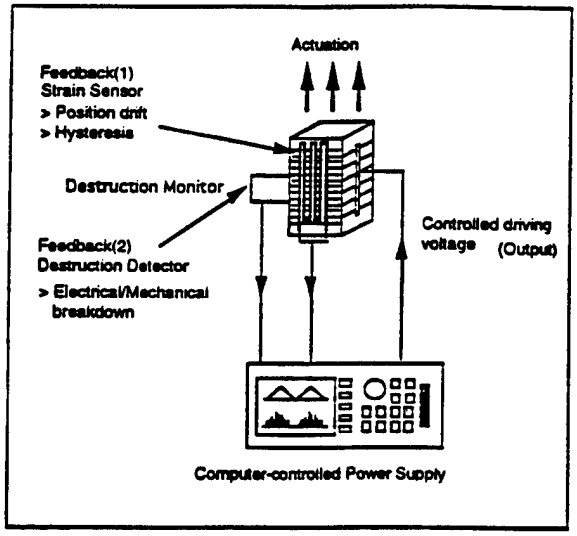

Fig.6. Intelligent actuator system with both position feedback and breakdown detection feedback mechanisms.

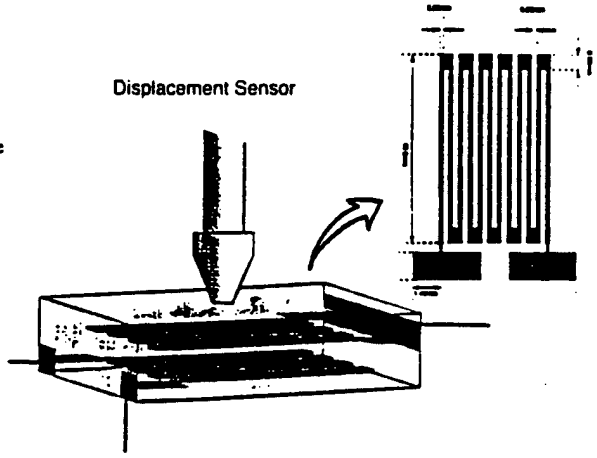

Fig.7. Multilayer ceramic actuator with a strain-gauge type electrode.

IV. DRIVE TECHNIQUES

Pulse drive of the piezoelectric / electrostrictive actuator generates very large tensile stress in the device, sometimes large enough to initiate cracks. In such cases, compressive bias stress should be employed on the device through clamping mechanisms such as a helical spring and a plate spring.

Temperature rise is occasionally observed particularly when the actuator is driven cyclically, i.e. in pulse drive or ultrasonic motor applications.

Temperature rise is due to the imbalance between heat generation basically caused by dielectric hysteresis loss and the heat dissipation determined by the device size (surface area!) [13]. Figure 8 shows a linear relation between temperature rise and the v_e/A value, where v_e is the effective volume and A the surface area of a multilayer actuator, when driven at a fixed magnitude and frequency of the electric field. We need to select a suitable drive power or a driving duty ratio so as not to produce a temperature rise of more than 20°C.

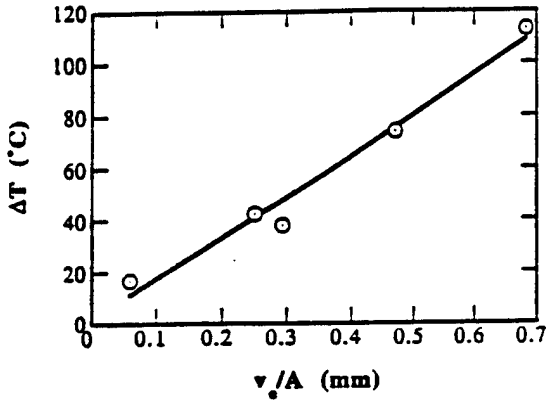

Fig.8. Temperature rise versus v_e/A for various size multilayer ceramic actuators (applied field: 3 kV/mm at 300Hz).

Regarding ultrasonic motors, the usage of the antiresonance mode has been proposed [14]. Quality factor Q and temperature rise have been investigated on a PZT ceramic rectangular bar, and the results for the fundamental resonance (A-type) and antiresonance (B-type) modes are illustrated in Fig.9 as a function of vibration velocity. It is recognized that Q_B is higher than Q_A over the whole vibration velocity range. In other words, the antiresonance mode can provide the same mechanical vibration level without generating heat.

All the previous ultrasonic motors have utilized the mechanical resonance mode at the so-called "resonance" frequency. However, the mechanical resonant mode at the "antiresonance" frequency reveals higher Q and efficiency than the "resonance" state. Moreover, the usage of "antiresonance," whose admittance is very low, requires low current and high voltage for driving, in contrast to high current and low voltage for the "resonance." This means that a conventional inexpensive power supply may be utilized for driving the ultrasonic motor.

V. CONCLUSION

There are many possibilities to improve the durability and reliability of ceramic actuators. Future wide commercialization will be rather promising.

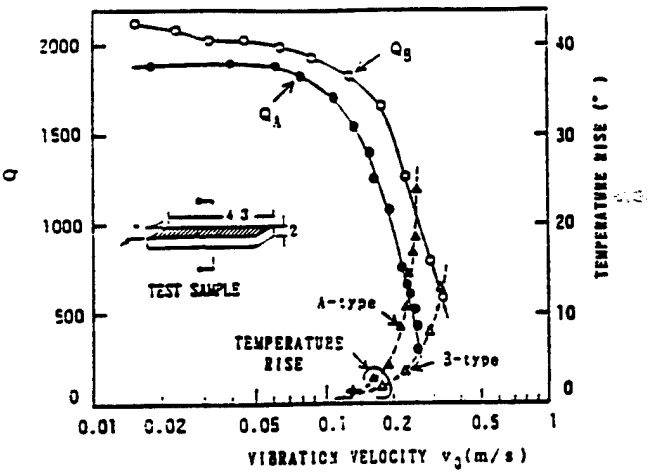

Fig.9. Vibration velocity dependence of the quality factor and temperature rise for both A- and B-type resonances of a PZT resonator.

REFERENCES

[1] K.Uchino, *Ceramic Actuators and Ultrasonic Motors*, Kluwer Academic Pub., 1996.

[2] K.Uchino, "Ceramic Actuators: Principles and Applications," MRS Bull., vol.18, p.42, 1993.

[3] K.Uchino and T.Takasu, "Evaluation Method of Piezoelectric Ceramics from a Viewpoint of Grain Size," Inspec., vol.10, p.29, 1986.

[4] K.Abe, K.Uchino and S.Nomura, "The Electrostric-tive Unimorph for Displacement Control," Jpn. J. Appl. Phys., vol.21, p.L408, 1982.

[5] A.Hagimura and K.Uchino, "Impurity Doping Effect on Electrostrictive Properties of $(Pb,Ba)(Zr,Ti)O_3$," Ferroelectrics, vol.93, p.373, 1989.

[6] S.Takahashi and S.Hirose, Jpn. J. Appl. Phys., vol.32, Pt.1, p.2422, 1993.

[7] K.Uchino, J.Kuwata, S.Nomura, L.E.Cross and R.E. Newnham, "Interrelation of Electrostriction with Phase Transition Diffuseness," Jpn. J. Appl. Phys., vol.20, Suppl.20-4, p.171, 1981.

[8] Q.M.Zhang, J.Zhao, K.Uchino and J.Zheng, "Change of the Weak Field Properties of $Pb(Zr,Ti)O_3$ Piezoceramics with Compressive Uniaxial Stresses," J. Mater. Res. (submitted).

[9] K.Nagata, "Lifetime of Multilayer Actuators," Proc. 49th Solid State Actuator Study Committee, JTTAS, Tokyo, 1995.

[10] K.Abe, K.Uchino and S.Nomura, "Barium Titanate-Based Actuator with Ceramic Internal Electrodes," Ferroelectrics, vol.68, p.215, 1986.

[11] H.Aburatani, K.Uchino, A.Furuta and Y.Fuda, "Destruction Mechanism and Destruction Detection Technique for Multilayer Ceramic Actuators," Proc. 9th Int'l Symp. Appl. Ferroelectrics, p.750, 1995.

[12] K.Uchino and H.Aburatani, "Destruction Detection Techniques for Safety Piezoelectric Actuator Systems," Proc. 2nd Int'l Conf. Intelligent Mater., p.1248, 1994.

[13] J.Zheng, S.Takahashi, S.Yoshikawa, K.Uchino and J.W.C. de Vries, "Heat Generation in Multilayer Piezoelectric Actuators," J. Amer. Ceram. Soc. (in press).

[14] S.Hirose, M.Aoyagi, Y.Tomikawa, S.Takahashi and K. Uchino, "High-Power Characteristics at Anti-resonance Frequency of Piezoelectric Transducers," Proc. Ultrasonic Int'l, p.1, 1995.

APPENDIX 57

MRS Fall Mtg. '96, Proc. (in press)

HIGH ELECTROMECHANICAL COUPLING PIEZOELECTRICS - HOW HIGH ENERGY CONVERSION RATE IS POSSIBLE ? -

KENJI UCHINO
International Center for Actuators and Transducers, Materials Research Laboratory
The Pennsylvania State University, University Park, PA 16802

ABSTRACT

A new category of piezoelectric ceramics with very high electromechanical coupling was discovered in a lead zinc niobate:lead titanate solid solution in a single crystal form. The maximum coupling factor k_{33} reaches 95%, which corresponds to the energy conversion rate twice as high as the conventional lead zirconate titanate ceramics. This paper reviews the previous studies on superior piezoelectricity in relaxor ferroelectric: lead titanate solid solutions and on the possible mechanisms of this high electromechanical coupling.

KEY WORDS: electromechanical coupling, piezoelectric, relaxor ferroelectric, domain motion

INTRODUCTION

Lead zirconate-titanate (PZT) ceramics are well known piezoelectrics widely used in many transducers. Their applications include gas igniters, force/acceleration sensors, microphones, buzzers, speakers, surface acoustic wave filters, piezoelectric transformers, actuators, ultrasonic motors, ultrasonic underwater transducers, and acoustic scanners [1,2]. Particularly in recent medical acoustic imaging, higher electromechanical coupling materials are eagerly required to improve the image resolution. Under these circumstances, relaxor ferroelectric: lead titanate solid solution systems with superior electromechanical coupling factors to the conventional PZT have been refocused, which were initially discovered in a lead zinc niobate:lead titanate system by the author's group in 1981 [3].

This paper reviews the previous studies on superior piezoelectricity in relaxor ferroelectric: lead titanate solid solutions, then on peculiar domain motions in these materials, finally possible mechanisms are considered for this extremely high electromechanical coupling.

ELECTROMECHANICAL COUPLING FACTORS

The terminologies, electromechanical coupling factor and efficiency are sometimes confused. Let us consider them at first. The electromechanical coupling factor k is defined as

$$k^2 = (\text{Stored mechanical energy / Input electrical energy}) \quad (1)$$

or

$$= (\text{Stored electrical energy / Input mechanical energy}). \quad (2)$$

When an electric field E is applied to a piezoelectric actuator, since the input electrical energy is $(1/2)\,\varepsilon_0\varepsilon\,E^2$ per unit volume and the stored mechanical energy per unit volume under zero external stress is given by $(1/2)\,x^2 / s = (1/2)\,(d\,E)^2 / s$, k^2 can be calculated as

$$k^2 = [(1/2)\,(d\,E)^2 / s] / [(1/2)\,\varepsilon_0\varepsilon\,E^2] = d^2 / \varepsilon_0\varepsilon \cdot s. \quad (3)$$

On the other hand, the efficiency η is defined as

$$\eta = \text{(Output mechanical energy)} / \text{(Consumed electrical energy)} \quad (4)$$

or

$$= \text{(Output electrical energy)} / \text{(Consumed mechanical energy)}. \quad (5)$$

In a work cycle (e. g. an electric field cycle), the input electrical energy is transformed partially into mechanical energy and the remaining is stored as electrical energy (electrostatic energy like a capacitor) in an actuator. Then, this ineffective energy can be returned to the power source, leading to near 100 % efficiency, if the loss is small. Typical values of dielectric loss in PZT are about 1 - 3 %.

The electromechanical coupling factor is different according to the sample geometry. Figure 1 shows two sample geometries corresponding to k_{33} and k_{31}, which we will discuss later. In some particular applications such as Non-Destructive Testing, large piezoelectric anisotropy, i. e. a large value of the ratio k_{33}/k_{31}, is required to improve the image quality in addition to a large value of k_{33} itself. However, the empirical rule suggests that these two requirements are contradictory to each other. In Figure 2 we plotted the k_{33} versus k_{31} relation for various perovskite oxide piezoelectric polycrystal and single crystal samples such as $Pb(Zr,Ti)O_3$, $PbTiO_3$, $Pb(Zn_{1/3}Nb_{2/3})O_3$ and $Pb(Mg_{1/3}Nb_{2/3})O_3$ based compositions [4]. It is obvious from this convex tendency that the piezoelectricity becomes isotropic (i. e. the k_{33}/k_{31} ratio approaches to 1) with increasing the electromechanical coupling factor (i. e. the k_{33} value).

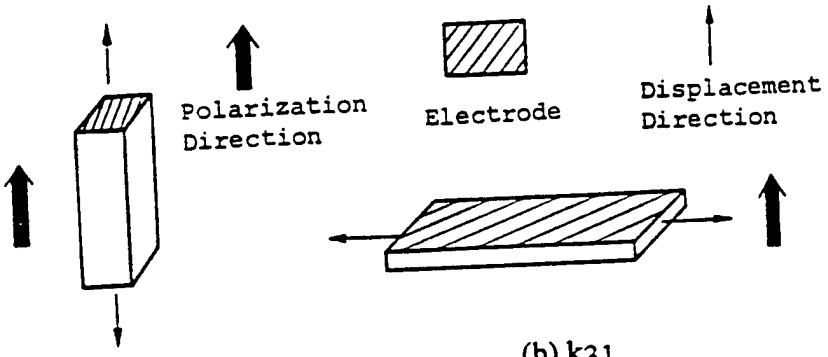

(a) k_{33} (b) k_{31}

Fig.1 Typical vibration modes of piezoelectric devices.

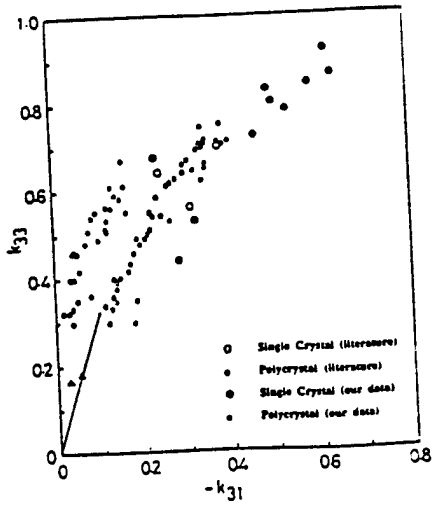

Fig.2 Relation between k_{33} and k_{31} for various perovskite oxide piezoelectrics.

HIGH ELECTROMECHANICAL COUPLING MATERIALS

Morphotropic Phase Boundary Composition

Conventionally, $Pb(Zr,Ti)O_3$ (PZT), $PbTiO_3$ (PT) and PZT based ternary ceramics with a small amount of a relaxor ferroelectric have been utilized for piezoelectric applications. Figure 3 shows the composition dependence of permittivity and electromechanical coupling factor k_p in the PZT system. It is notable that the morphotropic phase boundary (MPB) composition between the rhombohedral and tetragonal phases exhibits the maximum enhancement in dielectric and piezoelectric properties; this is explained in terms of a phenomenological theory [5]. The physical properties of a perovskite solid solution between A and B, (1-x) A - x B, can be estimated through the Gibbs elastic energy of a solid solution, if we suppose a linear combination of the Gibbs elastic energy of each component:

$$G_1(P,X,T) = (1/2)[(1 - x)\alpha_A + x\alpha_B] P^2 + (1/4)[(1 - x)\beta_A + x\beta_B] P^4 + (1/6)[(1 - x)\gamma_A + x\gamma_B] P^6 - (1/2)[(1 - x)s_A + xs_B] X^2 - [(1 - x)Q_A + xQ_B] P^2 X, \quad (6)$$

where $\alpha_A = (T - T_{0,A}) / \varepsilon_0 C_A$ and $\alpha_B = (T - T_{0,B}) / \varepsilon_0 C_B$.

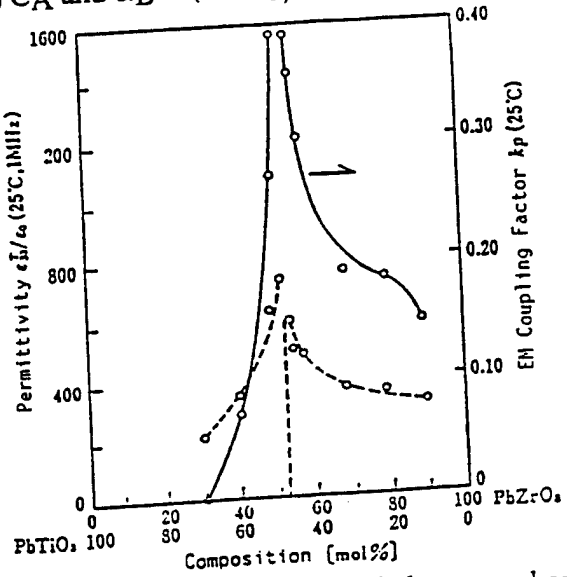

Fig.3 Composition dependence of permittivity and electromechanical coupling factor k_p in the PZT system.

The solution provides reasonable first-order estimates of the Curie temperature, spontaneous polarization and strain, as well as the enhancement of the permittivity, piezoelectric constant and electromechanical coupling at the MPB composition.

Note that in virgin samples of piezoelectric ceramics, the polarizations of grains (micro single crystals making up a polycrystalline sample) are randomly oriented (or domains are oriented randomly even in each grain, if the grain size is large enough for a multi-domain state) so as to cancel the net polarization in total. In a similar fashion, the net strain is negligibly small under an external electric field. Hence, before use, it is necessary to apply a relatively large electric field (> 3 kV/mm) to align the polarization direction of each grain as much as possible. Such a treatment is called electric poling.

Relaxor Ferroelectric Based Composition

On the other hand, relaxor ferroelectrics such as $Pb(Mg_{1/3}Nb_{2/3})O_3$:$PbTiO_3$ compositions have been focused due to their giant electrostriction [6]. Few work has been conducted on piezoelectric properties at the MPB region before the trial by the author's group.

We focused on single crystals of $(1-x)Pb(Zn_{1/3}Nb_{2/3})O_3$- $xPbTiO_3$ (PZN-PT) which are relatively easily grown by a flux method over the whole composition range, compared with the case in the $Pb(Zr,Ti)O_3$ (PZT) system. This system exhibits a drastic change from a diffuse phase transition to a sharp transition with an increase of the PT content, x, correlating to the existence of a morphotropic phase boundary from a rhombohedral to a tetragonal phase around x = 0.1 [7]. Figure 4 shows the phase diagram of this system near the MPB region.

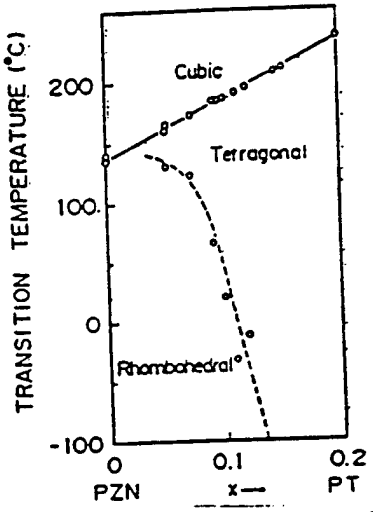

Fig.4 Phase diagram of $(1-x)Pb(Zn_{1/3}Nb_{2/3})O_3$- $xPbTiO_3$ (PZN-PT).

The most intriguing piezoelectric characteristics have been found in the MPB compositions with $0.05< x <0.143$, which exhibit two multiple phase transitions, changing the crystal symmetry from rhombohedral to tetragonal, then to cubic during heating [3]. Figure 5 shows the composition dependence of the pyroelectric coefficient λ_3^T, piezoelectric constants d_{ij}, electromechanial coupling factors k_{ij}, elastic compliances s_{ij}^E and dielectric constant ε_3^T measured at room temperature [3]. The superscript * is for the crystal with the rhombohedral symmetry at room temperature poled along the pseudocubic [001] direction. Figure 6 shows the temperature dependence of electromechanical coupling factors k_{33} and k_{31} measured with bar-shaped specimens of 0.91PZN-0.09PT [8]. Special notations have been introduced to describe the elastic and electromechanical constants for a sample poled in a certain direction. The $s^E[001]//$ or $s^E[111]//$ are defined from the resonance frequency of a bar sample elongated and poled in the pseudocubic [001] or [111] axes, respectively. The [001] and [111] axes are the principle axes of the tetragonal and rhombohedral phases and also the poling directions for each sample. The coupling coefficients $k[001]//$ and $k[111]//$ are consequently calculated from the resonance and antiresonance frequencies of the same sample. All the electromechanical components show a very large kink anomaly at the rhombohedral-tetragonal transition temperature, and a rapid decrease in k or an increase in d and s^E on approaching the Cuie point. These components vanish just above the Curie point.

Table I summarizes the elastic, piezoelectric, electromechanical and dielectric constants and the spontaneous polarization of 0.91PZN-0.09PT for the rhombohedral and tetragonal phases. It is important that the sample electrically poled along the pseudocubic [001] axis (not the principal axis in the rhombohedral phase!) reveals a very large piezoelectric constant $d[001]// = 1.5x10^{-9}$

C/N and a high electromechanical coupling factor k[001]// = 0.92 at room temperature, both of which are much larger than d[111]// and k[111]//, respectively. Also these are the highest values among all perovskite piezoelectric materials reported so far. It was found that such a high electromechanical coupling factor could not be explained consistently in terms of a mono-domain single crystal model without considering the complicated domain dynamical motion.

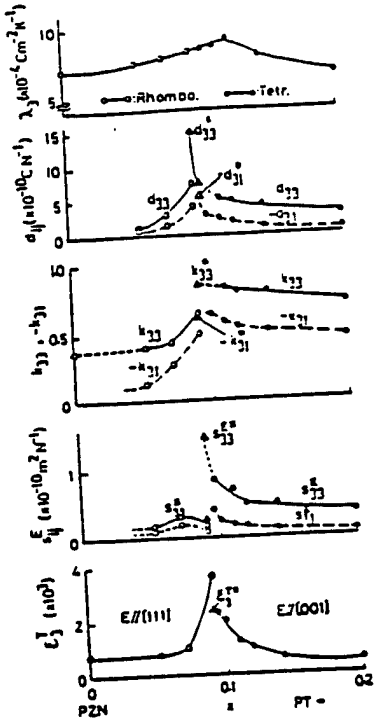

Fig.5 Composition dependence of the pyroelectric coefficient λ_3^T, piezoelectric constants d_{ij}, electromechanial coupling factors k_{ij}, elastic compliances s_{ij}^E and dielectric constant ε_3^T measured at room temperature.

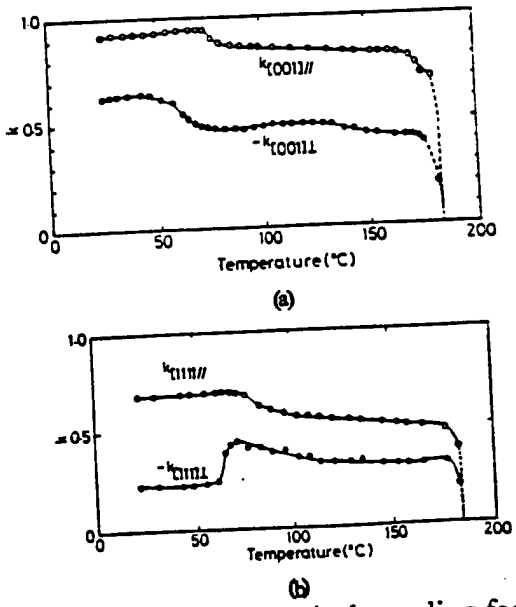

Fig.6 Temperature dependence of electromechanical coupling factors k33 and k31 measured with bar-shaped specimens of 0.91PZN-0.09PT.

Table I Elastic, piezoelectric, electromechanical and dielectric constants and the spontaneous polarization of 0.91PZN-0.09PT for the rhombohedral and tetragonal phases.

	Rhomb. phase	Tet. phase	Unit
Temp.	25	130	°C
$s^E_{[111]\perp}$	18	15.5	
$s^E_{[111]//}$	13.6	10.3	
$s^E_{[001]\perp}$	36.9	17.7	
$s^E_{[001]//}$	143	56	$(TPa)^{-1}$
$s^D_{[111]\perp}$	17.1	13.9	
$s^D_{[111]//}$	7.6	7.3	
$s^D_{[001]\perp}$	22.6	13.6	
$s^D_{[001]//}$	21.8	17.6	
$-d_{[111]\perp}$	194	352	
$d_{[111]//}$	625	450	pC/N
$-d_{[001]\perp}$	493	266	
$d_{[001]//}$	1570	795	
$-k_{[111]\perp}$	0.23	0.32	
$k_{[111]//}$	0.68	0.53	—
$-k_{[001]\perp}$	0.62	0.48	
$k_{[001]//}$	0.92	0.83	
$\varepsilon^T_{[111]//}$	4100	8200	
$\varepsilon^T_{[001]//}$	2200	1880	—
$\varepsilon^S_{[111]//}$	2200	—	
$\varepsilon^S_{[001]//}$	295	570	
P_s	0.52	0.30	C/m^2

Recently, two groups of Yamashita (Toshiba) and Shrout (Penn State) reconfirmed the author's original work, and extended the investigation to a wide range of relaxor ferroelectrics such as $Pb(Mg_{1/3}Nb_{2/3})O_3$-PT, $Pb(Sc_{1/2}Ta_{1/2})O_3$-PT and $Pb(Sc_{1/2}Nb_{1/2})O_3$-PT. Large electromechanical coupling factors k_p, k_{33} and piezoelectric constant d_{33} of these binary systems are listed in Table II.

Table II Large electromechanical coupling factors k_p, k_{33} and piezoelectric constant d_{33} of relaxor ferroelectric binary systems.

MATERIAL	FEATURE	k_p (%)	k_{33} (%)	d_{33} (pC/N)	REFERENCE
PZT 53/47	Polycrystal	52	67	220	[9]
		67	76	400	[10]
PZN:PT 91/9	Single crystal		92	1500	[8]
PMN:PT 67/33	Polycrystal	63	73	690	[11]
	Single crystal			1500	[12]
PST:PT 55/45	Polycrystal	61	73	655	[13]
PSN:PT 58/42	Polycrystal	71	77	450	[14]

Measurements on electric field-induced polarization and strain were carried out on a pure PZN single crystal by Shrout et al [15]. The polarization and strain curves are plotted for the <111> (the spontaneous polarization direction!) and <100> orientations in Fig. 7. Even though the [100] plate sample showed the "ideal" P vs. E or strain vs. E behaviors of a mono-domain crystal, notice that the absolute value of P is much larger in the [111] plate sample; this indicates again the spontaneous polarization along the <111> axis. He also reported the poling direction-dependent electromechanical coupling factors in PZN: k[001]// = 0.85 was much larger than k[111]// = 0.38, in a similar fashion to 0.91PZN-0.09PT. These results also suggest the importance of the domain contribution to dielectric and piezoelectic properties.

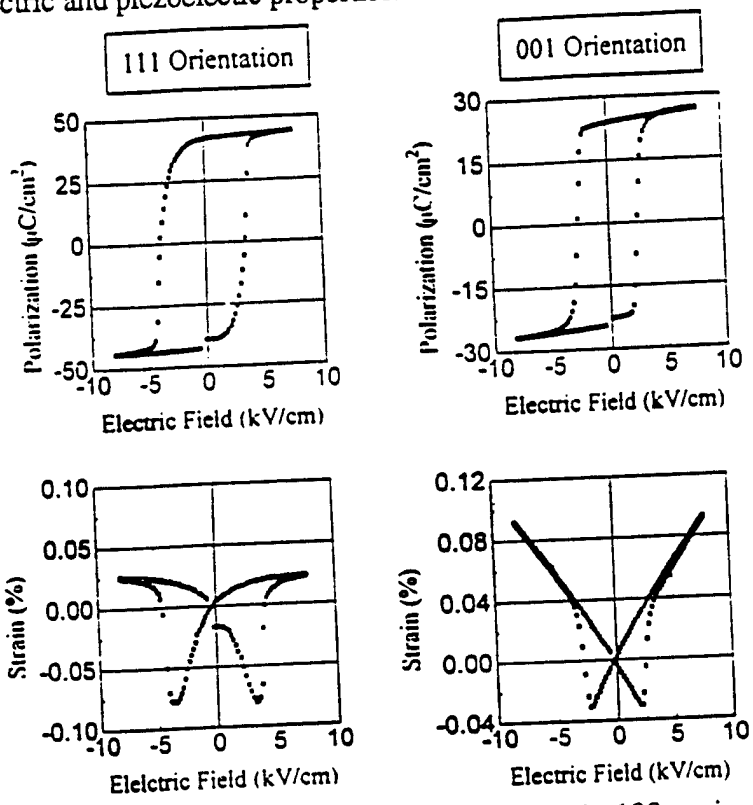

Fig.7 Polarization and strain curves plotted for the <111> and <100> orientations in pure PZN.

DOMAIN MOTION IN RELAXOR FERROELECTRICS

Historical Background of Domain-Controlled Piezoelectric Transducers

Historically, most of the studies on ferroelectric single crystals and polycrystalline materials have aimed to simulate the mono-domain state, desiring to derive the better characteristics from the specimens; ceramics as well as single crystals were poled electrically and/or mechanically to reorient the domains along one direction. Researches on controlling domains intentionally can be found in electrooptic devices and ferroelectric memory devices in particular. However, the intentional domain control has not been utilized or applied occasionally in the actuator and transducer areas. Recent requirements for the higher performance transducers encourages the investigation on the possibility of domain-related effect usage.

Developments in high resolution CCD optical microscope systems and in single crystal growth techniques are also accelerating these domain-controlled piezoelectric devices. A high resolution CCD (Charge Coupled Device) camera was attached to a Nikon Transmission Petrographic Microscope which was connected to a monitor and VCR (illustrated in Fig.8)[16]. The birefringence between the domains permits the observation of the domains with the polarizing light

microscope. The microscope system also allows magnifications up to x1300 on the monitor. The temperature-controlled sample stage (Linkam Inc.) in conjunction with the deep focal point of the objective lenses allows an electric field to be safely applied across the sample between -185 and 600°C. The stationary and switching domains can be instantaneously recorded by the VCR and observed on the monitor.

Single crystal growth methods of PZN-PT are described here for example [8]. The powders used were Pb_3O_4, TiO_2, ZnO and Nb_2O_5. Excess ZnO was added in some cases to counteract the evaporation during crystal growth. PbO was used as the flux. The mole ratio of the flux to composition was varied from 1:1 to 3:2. The batch sizes were changed from 75 grams to 500 grams. The raw powders were loaded into a platinum crucible and charged several times at 900°C until the crucible was full. The crucible was then partially sealed with a Pt lid. The sealed Pt crucible was placed in an alumina crucible and sealed once again. The crucibles were placed in a box furnace with a temperature controller. The cooling rate was veried from 0.5 to 3°C/hr down to 900°C. After the temperature reaches 900°C, the furnace was fast cooled at 50°C/hr to room temperature. The single crystals were leached from from the flux with warm 25 vol% nitric acid. Single crystals with a dimension of 1 cm^3 could be obtained.

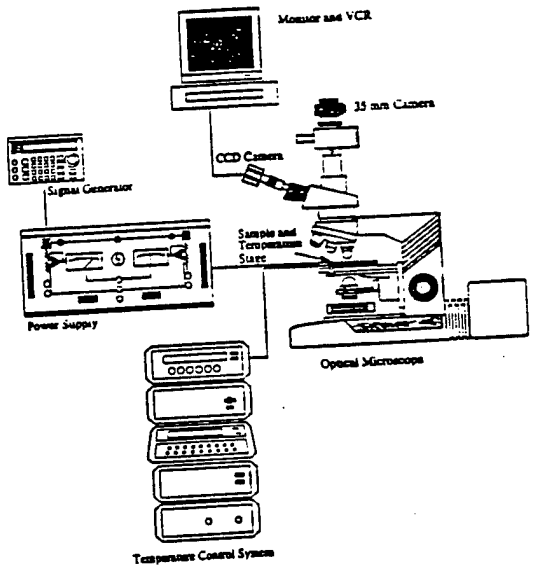

Fig.8 CCD optical microscope system.

Domain Configurations in PZN-PT

Let us review the relation between domain configurations and physical properties in relaxor ferroelectrics. Figure 9 shows the static domain configurations for the samples of x = 0, 0.07 and 0.095 of $(1-x)Pb(Zn_{1/3}Nb_{2/3})O_3$- $xPbTiO_3$ (PZN-PT) [17]. The pure PZN did not exhibit large clear domains in the whole temperature range when it was unpoled (i. e. micro-domains). Rhombohedral domains could be described as having an ambiguous spindle-like morphology. Ambiguity refers to the variation of domain widths and lengths which appear as an interpenetrating structure. With increasing the PT content, this small spindle-like domain was enlarged and the domain wall became sharp. Tetragonal domains appear to have a well defined lamellar morphology, and are either at right angles or antiparallel. Therefore, even though the widths and lengths of the tetragonal domains vary, the divisions between the domains are well defined and no interpenetrating structure is observable. Notice that the morphotropic phase boundary (MPB) composition (x = 0.095) shows the coexistence of both rhombohedral (spindle-like) and tetragonal domains (sharp straight line); the two-phase coexistence can not be found statically in normal ferroelectric materials such as $BaTiO_3$.

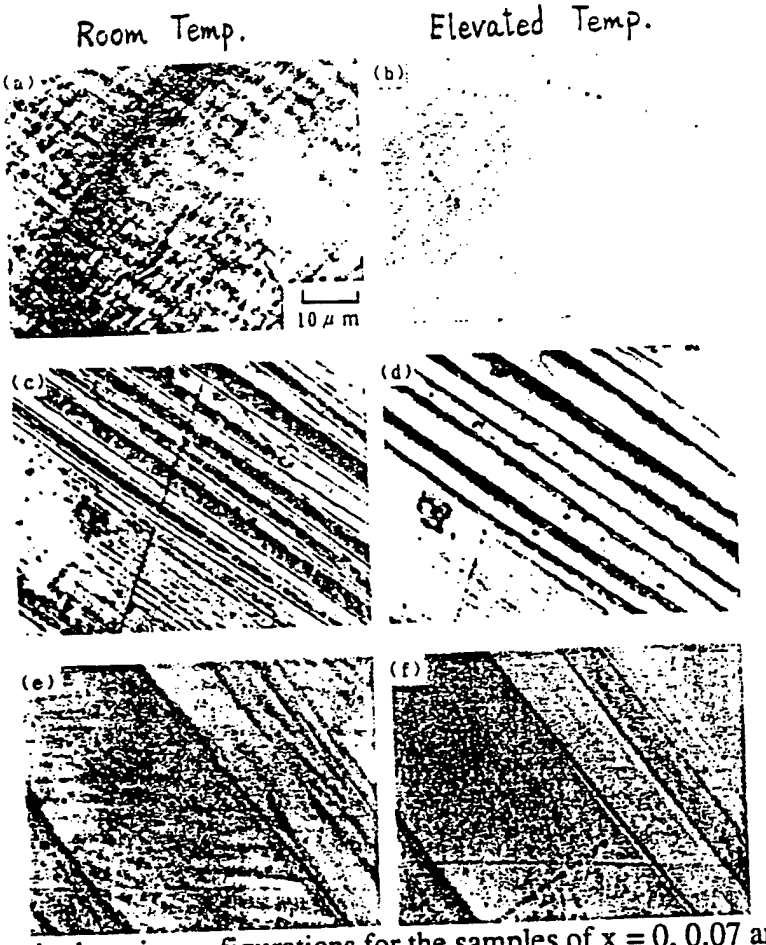

Fig.9 Static domain configurations for the samples of x = 0, 0.07 and 0.095 of (1-x)Pb($Zn_{1/3}Nb_{2/3}$)O_3- x$PbTiO_3$ (PZN-PT).

Figures 10 and 11 show the actual domain reversal processes and their schematical illustration under an applied electric field [18]. Sharp 90° domain walls corresponding to the tetragonal symmetry in the sample with x = 0.2 moved abruptly and rather independently each other above a coercive field of 1 kV/mm. The situation resembles to the case in normal ferroelectrics. On the contrary, pure PZN (x = 0.0) revealed very different domain motion. During electric field cycles, micro- to macro-domain growth occurred, and long narrow spindle-like domains (aspect ratio = 10) were arranged rather perpendicularly to the electric field (18 degree canted). When a field above 0.5 kV/mm was applied, the ambiguous domain walls rippled simultaneously in a certain size region, so that each domain should change synchronously like cooperative phenomena. The domain reversal front (180° domain wall) moved rather slower than in the sample of x = 0.2. It is noteworthy that the stripe period of the dark and bright domains (probably corresponding to up and down polarizations) was not changed by the domain reversal, and that each domain area changed under an AC external field with zero net polarization at zero field. Thus, the relaxor crystal is electrically-poled easily when an electric field is applied around the transition temperature, and depoled completely without any remanent polarization. This can explain large apparent secondary non-linear effects in physical properties such as electrostrictive and electrooptic phanomena, without exhibiting any hysteresis.

The relation between the dielectric property and the domain structure was clearly demonstrated in the permittivity measurement of the pure PZN. Figures 12(a) and 12(b) show the permittivity vs. temperature curves taken for the annealed (unpoled) and poled states of the PZN sample[19]. Large dielectric relaxation (frequency dependence of the permittivity) was observed in a wide temperature range below the Curie point for the unpoled state, while the dielectric dispersion was measured only in a narrow temperature range between 100°C and the Curie point for the poled

state. Considering that below 100°C the PZN exhibits the micro- to macro-domain growth under a high electric field, we can conclude that the dielectric relaxation is attributed to the micro-domains. Thus, we learned how to control the micro- and macro-domains through temperature change and an external electric field, and how to change the dielectric dispersion, elastic and piezoelectric constants according to these phase transitions.

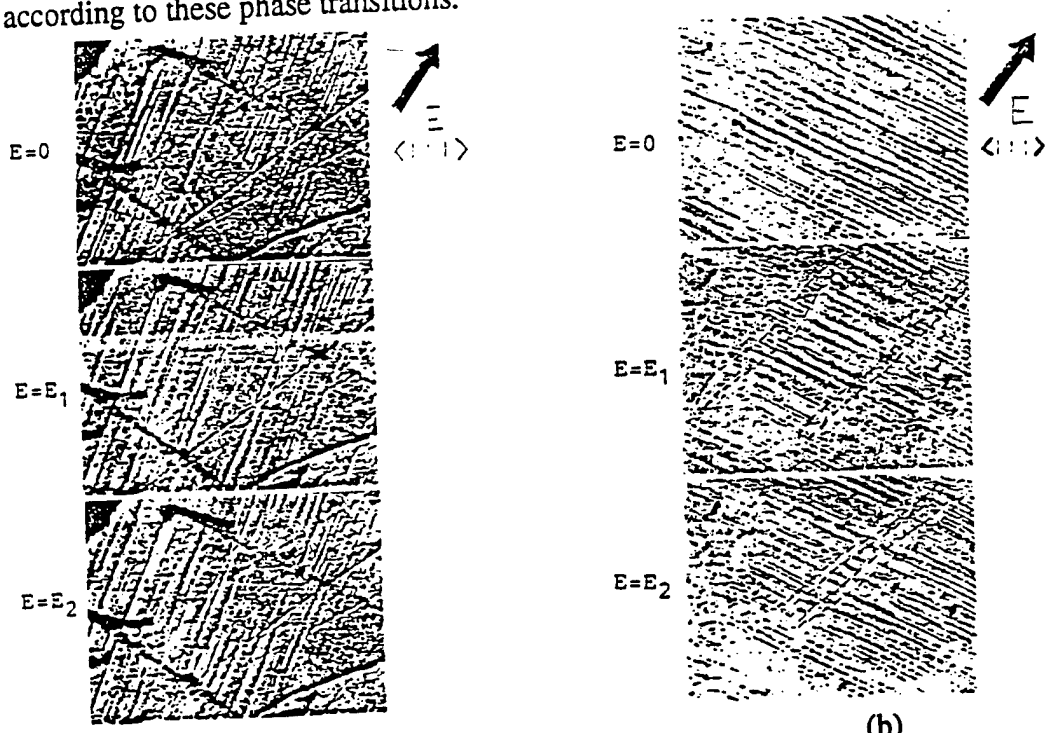

(a) (b)

Fig.10 Actual domain reversal processes under an applied electric field for the samples of x = 0.2 (a) and 0 (b) of (1-x)Pb(Zn1/3Nb2/3)O3- xPbTiO3.

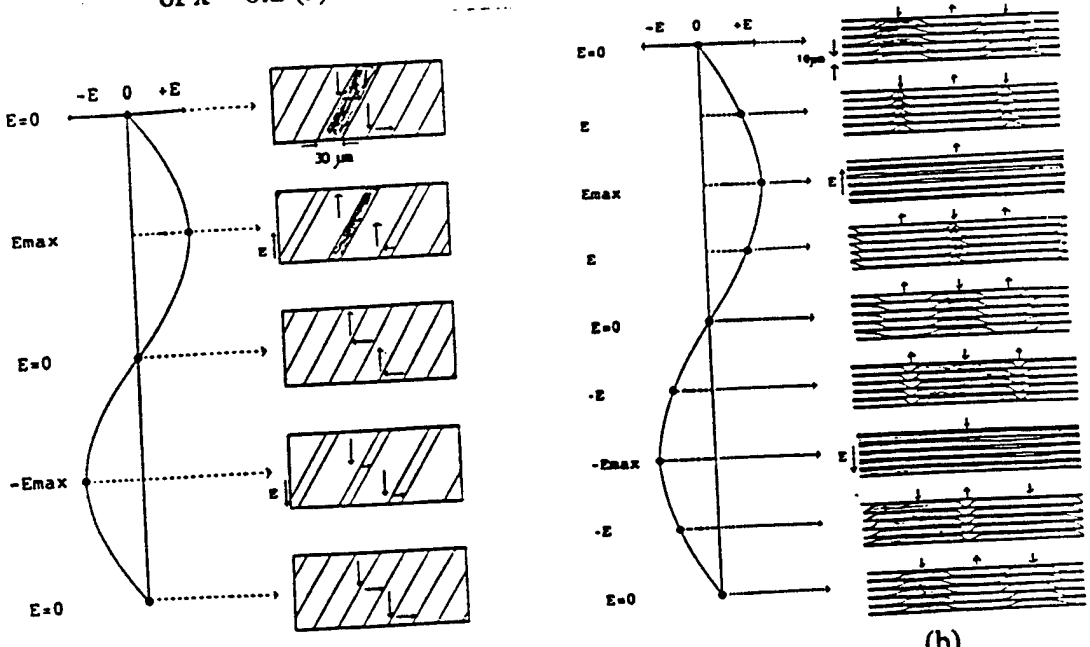

(a) (b)

Fig.11 Schematical illustration of the domain reversal processes under an applied electric field for the samples of x = 0.2 (a) and 0 (b) of (1-x)Pb(Zn1/3Nb2/3)O3- xPbTiO3.

a.) A depoled 100% PZN single crystal measured on the <111>.

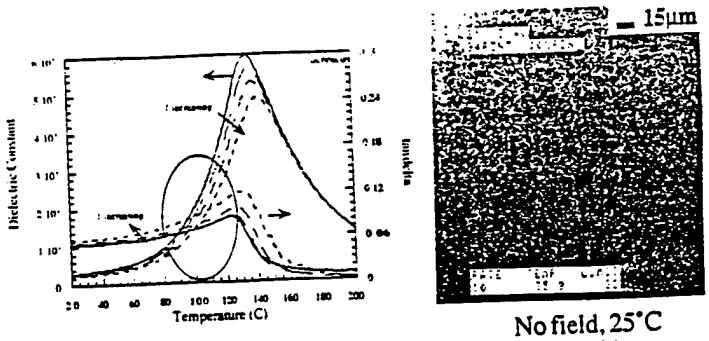

b.) A poled 100% PZN single crystal measured on the <111>.

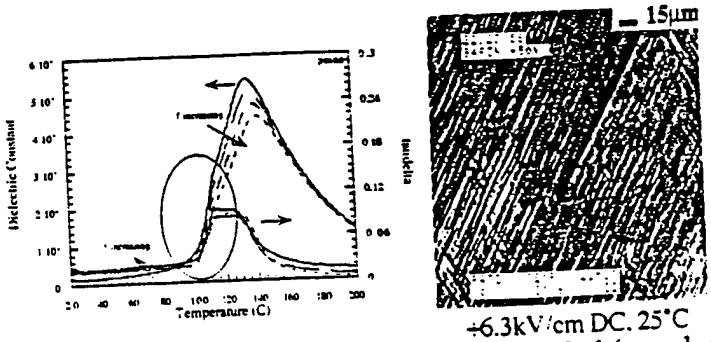

Fig.12 Permittivity vs. temperature curves taken for the annealed (unpoled) state (a) and poled state (b) of the PZN sample.

Hierarchical Domain Structures

Figure 13 shows the domain structures observed in a 0.89PZN-0.11PT crystal, which exists on the morphotropic phase boundary. The typical tetragonal stripe domain pattern was observed without an external electric field at room temperature, while the spindle-like rhombohedral domain pattern appeared as overlapped on the stripe pattern, when the electric field was applied along the perovskite pseudo-cubic [111] directions. This domain hierarchy suggests that the morphotropic phase boundary composition may easily change the domain configuration and the crystal symmetry according to the applied electric field direction, much easily than in the normal ferroelectric PZT.

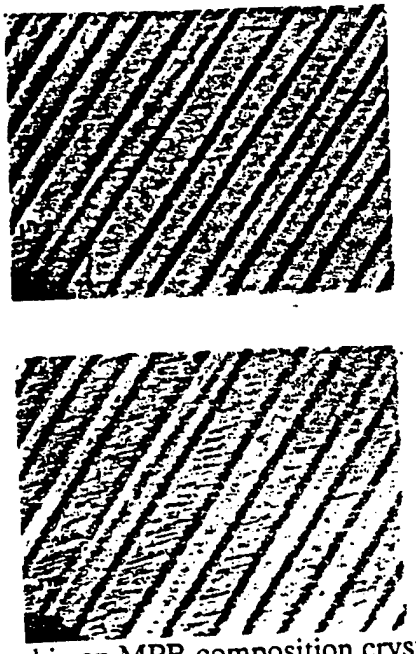

Fig.13 Domain structures observed in an MPB composition crystal 0.89PZN-0.11PT.

Future work will include the dynamic domain observation in the 0.91PZN-0.09PT sample (rhombohedral phase is stable at room temperature) poled along the perovskite [100] axis; this enhances remarkably the electromechanical coupling factor k up to 92 - 95 %. Also the possibility of the different poling direction which enhances the coupling factor more will be explored.

CONCLUSIONS

1. The electromechanical coupling factor k33 of more than 90 % can be obtained in the solid solutions between the relaxor and normal ferroelectrics.

2. Promising compositions include: $Pb(Zn_{1/3}Nb_{2/3})O_3$-$PbTiO_3$, $Pb(Mg_{1/3}Nb_{2/3})O_3$-$PbTiO_3$ and $Pb(Sc_{1/2}Nb_{1/2})O_3$-$PbTiO_3$.

3. The highest k in a single crystal form can be obtained when it is electrically-poled along a different axis from the spontaneous polarization direction.

Domain cotrolled single crystals (not in the monodomain state!) may be the key for obtaining the highest electromechanical coupling. The important factors to the domain reconstruction will be realized by changing external electric field, stress and temperature, as well as the sample preparation history.

REFERENCES

1. K. Uchino, Proc. 4th Int'l Conf. on Electronic Ceramics & Appl. Vol.1, p.179, Aachen, Germany, Sept. 5-7 (1994).
2. K. Uchino, Piezoelectric Actuators and Ultrasonic Motors, Kluwer Academic Publ., Boston (1996).
3. J. Kuwata, K. Uchino and S. Nomura, Ferroelectrics 37, 579 (1981).
4. K. H. Hellwege et al.: Landolt - Bornstein, Group III, Vol.11, Springer-Verlag, N.Y. (1979).
5. K. Uchino and S. Nomura, Jpn. J. Appl. Phys. 18, 1493 (1979).
6. K. Uchino, Bull. Amer. Ceram. Soc. 65(4), 647 (1986).
7. S. Nomura, T. Takahashi and Y. Yokomizo, J. Phys. Soc., Jpn. 27, 262 (1969).
8. J. Kuwata, K. Uchino and S. Nomura, Jpn. J. Appl. Phys. 21(9), 1298 (1982).
9. B. Jaffe, R. S. Roth and S. Marzullo, J. Res. Nat'l. Bur. Stand. 55,, 239 (1955).
10. H. Igarashi, Mem. Nat'l. Def. Adad. 22, 27 (1982).
11. S. W. Choi, T. R. Shrout, S. J. Jang and A. S. Bhalla, Ferroelectrics 100, 29 (1989).
12. T. R. Shrout, Z. P. Chang, N. Kim and S. Markgraf, Ferroelectrics Lett. 12, 63 (1990).
13. J. F. Wang, J. R. Giniewicz and A. S. Bhalla, Ferroelectics Lett. 16, 113 (1993).
14. Y. Yamashita, Jpn. J. Appl. Phys. 33, 4652 (1994).
15. T. R. Shrout, ONR Transducer Workshop, State College (March, 1996)
16. M. L. Mulvihill, L. E. Cross and K. Uchino, J. Amer. Ceram. Soc. 78, 3345 (1996).
17. K. Kato, K. Suzuki and K. Uchino, J. Jpn. Ceram. Soc. 98(8), 840 (1990).
18. R. Ujiie and K. Uchino, Proc. IEEE Ultrasonic Symp. '90, Hawaii, 2, 725 (1991).
19. M. L. Mulvihill, L. E. Cross and K. Uchino, Proc. 8th Europian Mtg. on Ferroelectrics, Ferroelectrics 186, 325 (1996).

APPENDIX 58

Recent Developments in Ceramic Actuators - Comparison among USA, Japan and Europe

In these several years, piezoelectric and electrostrictive materials have become key components in smart actuator/sensor systems such as precision positioners, miniature ultrasonic motors and adaptive mechanical dampers. This paper reviews recent developments of piezoelectric and related ceramic actuators with particular focus on the improvement of actuator materials, device designs and drive/control techniques of actuators. Developments will be compared among USA, Japan and Europe.

1 Introduction

Piezoelectric actuators are forming a new field between electronic and structural ceramics [1-4]. Application fields are classified into three categories: positioners, motors and vibration suppressors. The manufacturing precision of optical instruments such as lasers and cameras, and the positioning accuracy for fabricating semiconductor chips, which must be adjusted using solid-state actuators, is of the order of 0.1 µm. Regarding conventional electromagnetic motors, tiny motors smaller than 1 cm³ are often required in office or factory automation equipment and are rather difficult to produce with sufficient energy efficiency. Ultrasonic motors whose efficiency is insensitive to size are superior in the mini-motor area. Vibration suppression in space structures and military vehicles using piezoelectric actuators is also a promising technology.

This article reviews recent applications of piezoelectric and related ceramics to smart actuator/sensor systems, including the improvement of actuator materials, design of the devices, drive/control techniques and integration of actuators and sensors. The developments are compared among USA, Japan and Europe.

2 Ceramic Actuator Materials

2.1 PRACTICAL ACTUATOR MATERIALS

Actuator materials are classified into three categories; piezoelectric, electrostrictive and phase-change materials. Modified lead zirconate titanate [PZT, $Pb(Zr,Ti)O_3$] ceramics are currently the leading ma-

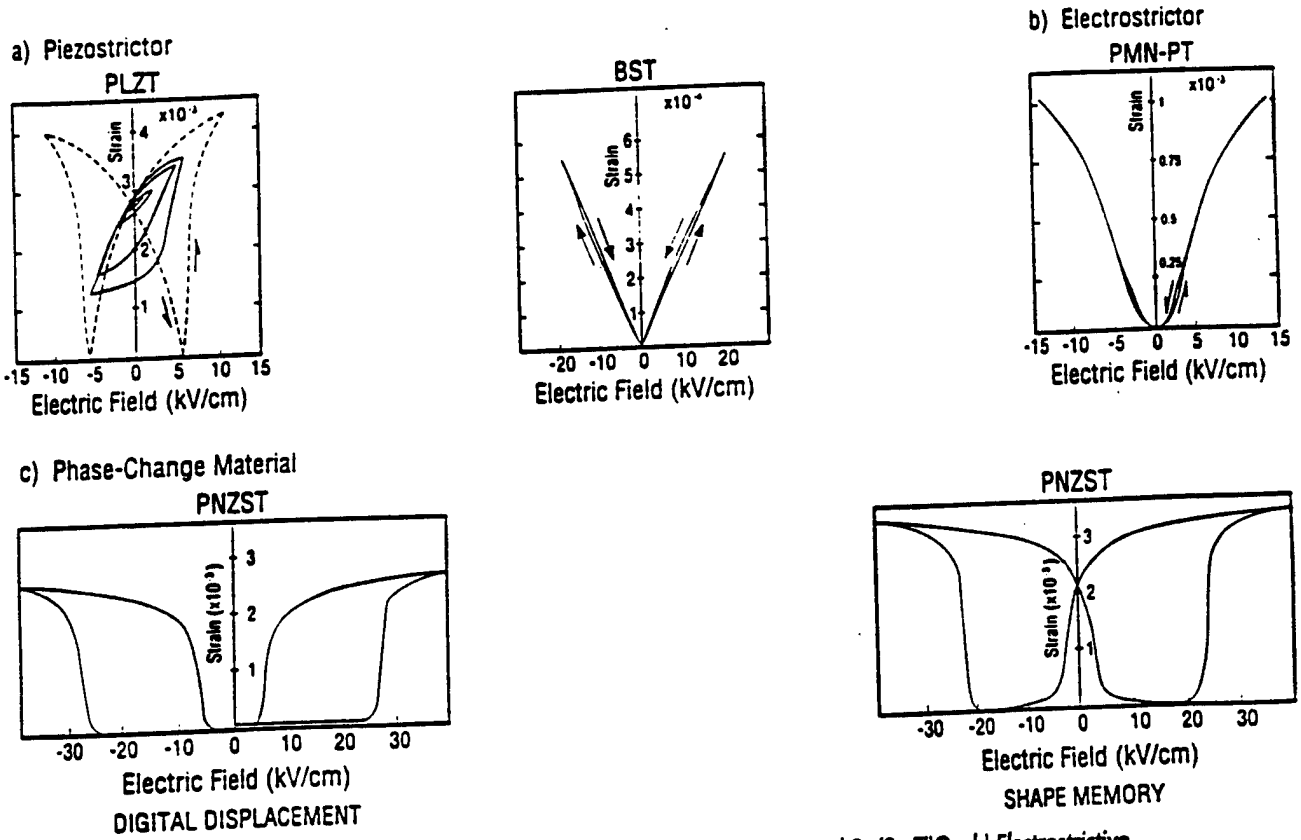

Fig. 1: Electric field-induced strains in ceramics; a) Piezoelectric $(Pb,La)(Zr,Ti)O_3$ and $Ba(Sn,Ti)O_3$. b) Electrostrictive $Pb(Mg1/3Nb2/3,Ti)O_3$. c) Phase-change material $Pb(Zr,Sn,Ti)O_3$.

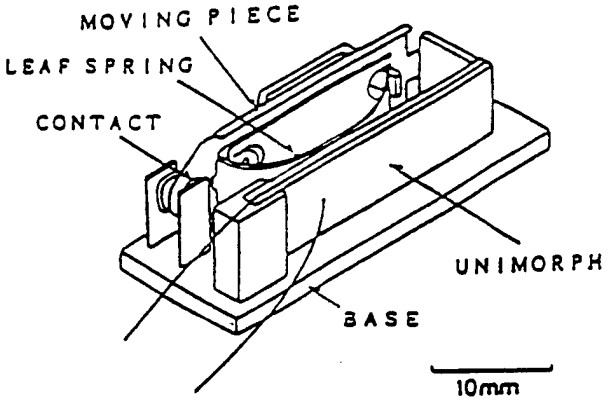

Figure 2: Latching relay using a shape memory ceramic unimorph

terials for piezoelectric applications. The PLZT [(Pb,La)(Zr,Ti)O_3] 7/62/38 compound is one such composition [5]. The strain curve is shown in Fig.1(a) left. When the applied field is small, the induced strain is nearly proportional to the field (x = dE). As the field becomes larger (i.e., greater than about 100 V/mm), however, the strain curve deviates from this linear trend and significant hysteresis is exhibited due to polarization reorientation. This sometimes limits the usage of this material in actuator applications that require nonhysteretic response.

An interesting new family of actuators has been fabricated in Germany from a barium stannate titanate system [Ba(Sn,Ti)O_3] [6]. The useful property of $Ba(Sn_{0.15}Ti_{0.85})O_3$ is its unusual strain curve, in which the domain reorientation occurs only at low fields, and there is then a long linear range at higher fields (Fig.1(a) right); i.e., the coercive field is unusually small. Moreover, this system is particularly intriguing because no Pb ion is contained, which will be essential as ecological materials in the future.
On the other hand, electrostriction in PMN [$Pb(Mg_{1/3}Nb_{2/3})O_3$] based ceramics developed in USA, though a second-order phenomenon of electromechanical coupling (x = ME^2), is extraordinarily large (more than 0.1 %) [7]. An attractive feature of these materials is the near absence of hysteresis (Fig.1(b)). The superiority of PMN to PZT was demonstrated in a Scanning Tunneling Microscope (STM) [8]. The PMN actuator could provide extremely small distortion of the image even when the probe was scanned in the opposite direction.

Concerning the phase-change-related strains, polarization induction by switching from an antiferro-electric to a ferroelectric state, has been proposed by our group[9]. Figure 1(c) shows the field-induced strain curves taken for the lead zirconate stannate based system $[Pb_{0.99}Nb_{0.02}((Zr_xSn_{1-x})_{1-y}Ti_y)_{0.98}O_3]$. The longitudinally induced strain reaches up to 0.4%, which is much larger than that expected in normal piezostrictors or electrostrictors. A rectangular-shape hysteresis in Fig.1(c) left, referred to as a „digital displacement transducer" because of the two on/off strain states, is interesting. Moreover, this field-induced transition exhibits a shape memory effect in appropriate compositions (Fig.1(c) right). Once the ferroelectric phase has been induced, the material will „memorize" its ferroelectric state even under zero-field conditions, although it can be erased with the application of a small reverse bias field [10]. This shape memory ceramic is used in energy saving actuators. A latching relay in Fig. 2 is composed of a shape memory ceramic unimorph and a mechanical snap action switch, which is driven by a pulse voltage of 4ms. Compared with the conventional electromagnetic relays, the new relay is much simple and compact in structure with almost the same response time.

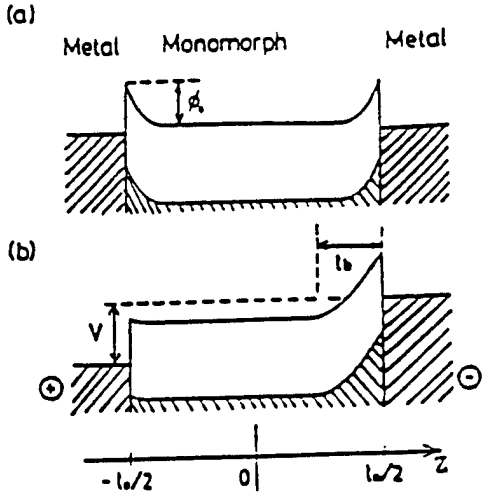

Figure 3: Electron energy band (Schottky barrier) model in monomorph devices (n-type semiconductor).

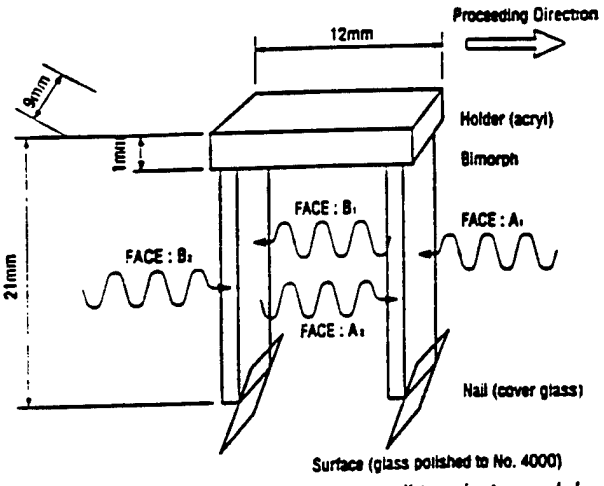

Figure 4: Structure of a photo-driven walking device and the illumination directions

2.2 NOVEL ACTUATOR MATERIALS

A monomorph device has been developed to replace the conventional bimorphs, with simpler structure and manufacturing process. The principle is a superposed effect of piezoelectricity and semiconductivity (Fig. 3) [11]. The contact between a semiconductor and a metal (Schottky barrier) causes non-uniform distribution of the electric field, even in a compositionally uniform ceramic. Suppose that the ceramic possesses also piezoelectricity, only one side of a ceramic plate tends to contract, leading to a bending deformation in total. A monomorph plate with 30 mm in length and 0.5 mm in thickness can generate 200 µm tip displacement, in equal magnitude of that of the conventional bimorphs [12]. The „rainbow" actuator by Aura Ceramics [13] is a modification of the above-mentioned semiconductive piezoelectric monomorphs, where half of the piezoelectric plate is reduced so as to make a thick semiconductive electrode to cause a bend. A photostrictive actuator is a fine example of an intelligent material, incorporating „illumination sensing" and self production of „drive/control voltage" together with final „actuation." In certain ferroelectrics, a constant electromotive force is generated with exposure of light, and a photostrictive strain results from the coupling of this bulk photovoltaic effect to inverse piezoelectricity. A bimorph unit has been made from PLZT 3/52/48 ceramic doped with slight addition of tungsten [14]. The remnant polarization of one PLZT layer is parallel to the plate and in the direction opposite to that of the other plate. When a violet light is irradiated to one side of the PLZT bimorph, a photovoltage of 1 kV/mm is generated, causing a bending motion. The tip displacement of a 20 mm bimorph 0.4 mm in thickness was 150 µm, with a response time of 1 sec.

A photo-driven micro walking device, designed to begin moving by light illumination, has been developed [15]. As shown in Fig. 4, it is simple in structure, having neither lead wires nor electric circuitry,

Actuator materials developments

USA	Japan	Europe
POSITIONER $Pb(Mg_{1/3}Nb_{2/3})O_3$-$PbTiO_3$ Electrostrictor - Low hysteresis, non-linear	$Pb(Zr,Ti)O_3$-based Piezostrictor - Large strain (0,15%)	$Ba(Sn,Ti)O_3$ Piezostrictor - Low hysteresis
ULTRASONIC MOTOR $Pb(Zr,Ti)O_3$-based Piezostrictor - High Q_m, low loss	$Pb(Zr,Ti)O_3$-based Piezostrictor - High Q_m, low loss	
SPECIAL PURPOSE $Pb(Zr,Sn,Ti)O_3$-based Phase chnge material - Large strain (0,4%) - Shape memory effect $(Pb,La)(Zr,Ti)O_3$-based Photostrictor - Remote Control (photo-driven)		

Table I

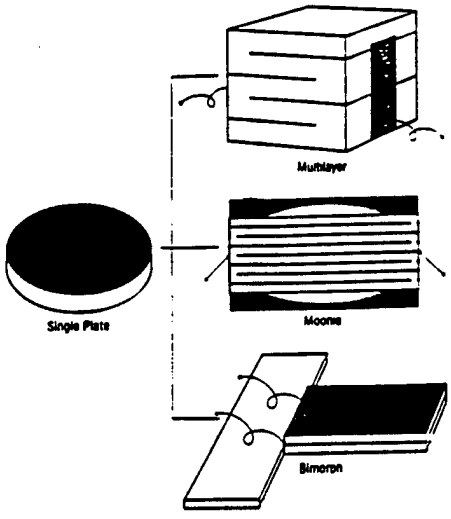

Figure 5: Typical designs for ceramic actuators: multilayer, moonie and bimorph

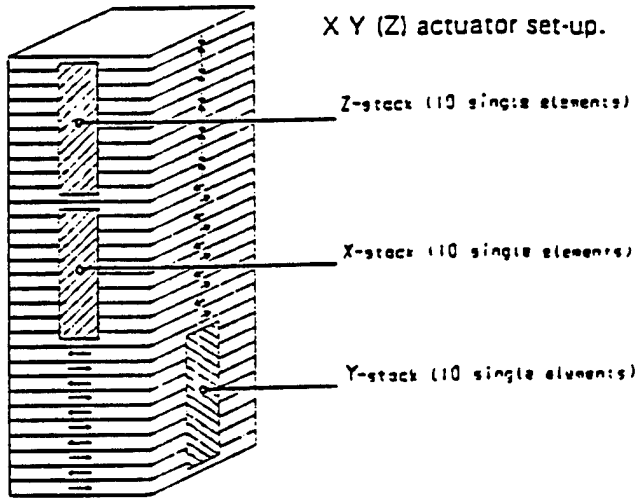

Figure 6: 3-D positioning multilayer actuator

Actuator designs developments

USA	Japan	Europe
RELIABILITY		
Multilayer with float electrodes	Multilayer with plate-through electrodes	Multilayer with very thin layers
Monomorph Rainbow		
AMPLIFICATION MECHANISM		
Moonie, cymbal	Multilayer & Impact mechanisms	
SPECIAL FUNCTION		
		Multilayer with 3-D function

Table II

with two bimorph legs fixed to a plastic board. When the legs are irradiated alternately with light, the device moves like an inchworm with a speed of 100 µm/min. Table I summarizes the material developments in USA, Japan and Europe.

3 Actuator Designs

Two of the most popular actuator designs are multilayers and bimorphs (see Fig.5). The multilayer, in which roughly 100 thin piezoelectric/electrostrictive ceramic sheets are stacked together, has advantages in low driving voltage (100 V), quick response (10 µsec), high generative force (100 kgf) and high electromechanical coupling. But the displacement in the range of 10 µm is not sufficient for some applications. This contrasts with the bimorph, consisting of multiple piezoelectric and elastic plates bonded together to generate a large bending displacement of several hundred µm, but the response (1 msec) and the generative force (100gf) are low.

A composite actuator structure called the „moonie" has been developed at Penn State to provide characteristics intermediate between the multilayer and bimorph actuators; this transducer exhibits an order of magnitude larger displacement than the multilayer, and much larger generative force with quicker response than the bimorph [16]. The device consists of a thin multilayer piezoelectric element and two metal plates with narrow moon-shaped cavities bonded together as shown in Fig.5. The moonie with a size of 5 x 5 x 2.5 mm^3 can generate a 20 mm displacement under 60 V, eight times as large as the generative displacement of the multilayer with the same size [17]. This new compact actuator has been applied to make a miniaturized laser beam scanner.
A 3-D positioning actuator with a stacked structure was also proposed by a German company as in Fig.6, where shear strain was utilized to generate the x and y displacements. Table II summarizes the developments in actuator designs compared among USA, Japan and Europe.

4 Drive/Control Techniques

Piezoelectric/electrostrictive actuators may be classified into two categories, based on the type of driving voltage applied to the device and the nature of the strain induced by the voltage (Fig.7): (1) rigid displacement devices for which the strain is induced unidi-

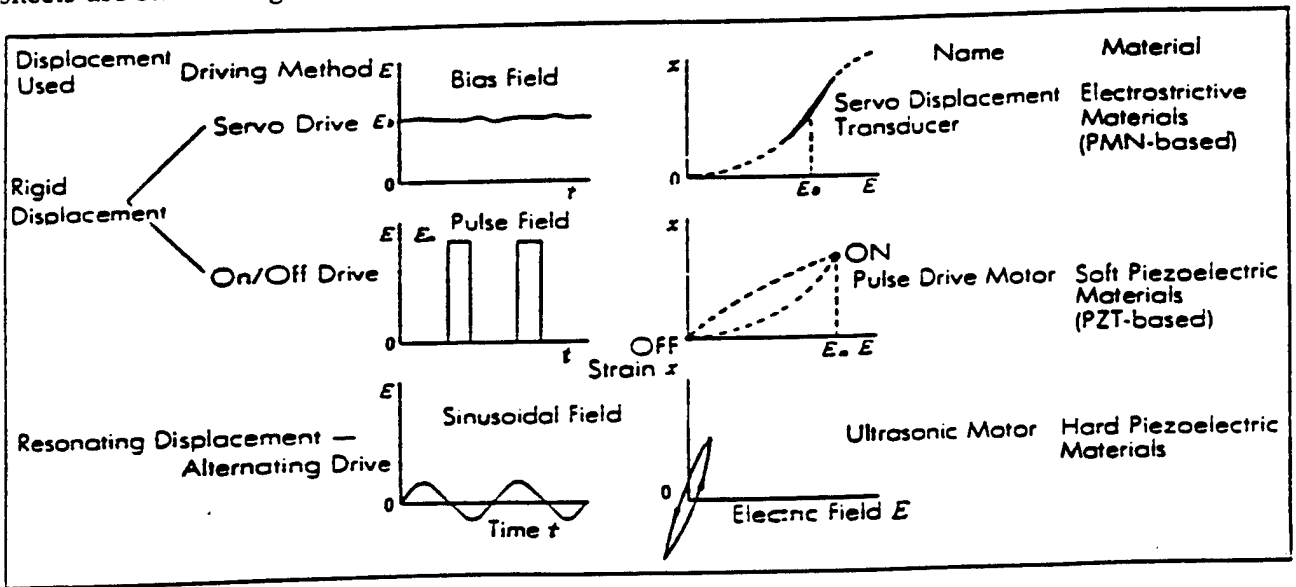

Figure 7: Classification of piezoelectric/electrostrictive actuators

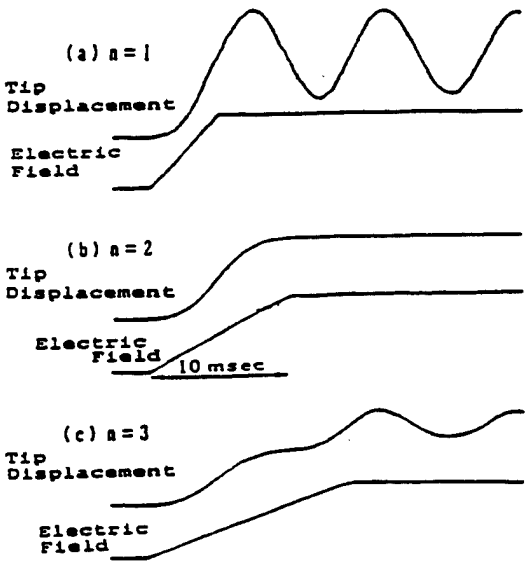

Fig.8: Transient vibration of a bimorph excited after a pseudo-step voltage applied. (2n=resonance period)

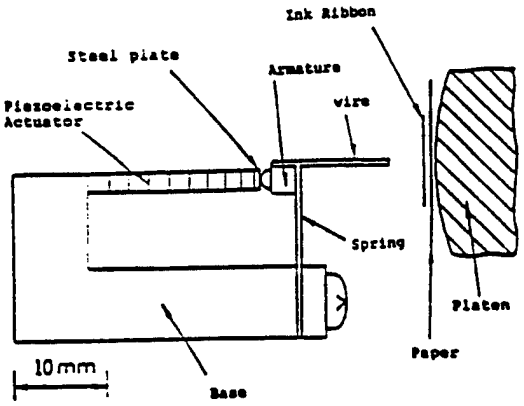

Fig.9: Dot-matrix printer head using a flight actuator mechanism.

rectionally along an applied dc field, and (2) resonating displacement devices for which the alternating strain is excited by an ac field at the mechanical resonance frequency (ultrasonic motors). The first can be further divided into two types: servo displacement transducers (positioners) controlled by a feedback system through a position-detection signal, and pulse-drive motors operated in a simple on/off switching mode, exemplified by dot-matrix printers.

The materials requirements for these classes of devices are somewhat different, and certain compounds will be better suited to particular applications. The ultrasonic motor, for instance, requires a very hard type piezoelectric with a high mechanical quality factor Q, leading to the suppression of heat generation. Driving the motor at the antiresonant frequency, rather than at the resonant state, is also an intriguing technique to reduce the load on the piezo-ceramic and the power supply [18]. The servo-displacement transducer suffers most from strain hysteresis and, therefore, a PMN electrostrictor is used for this purpose. The pulse-drive motor requires a low permittivity material aiming at quick response with a certain power supply rather than a small hysteresis so that soft PZT piezoelectrics are preferred to the high-permittivity PMN for this application.

Pulse drive techniques of the ceramic actuator is very important for improving the response of the device [19]. Figure 8 shows transient vibrations of a bimorph excited after a pseudo-step voltage is applied. The rise time is varied around the resonance period. It is concluded that the overshoot and ringing of the tip displacement is completely suppressed when the rise time is precisely adjusted to the resonance period of the piezo-device. A flight actuator was developed using a pulse-drive piezoelectric element and a steel ball. A 2

Difference in the ceramic actuator developments among USA, Japan and Europe

USA	Japan	Europe
TARGET		
Military-oriented product	Mass-consumer product	Lab-equipment product
CATEGORY		
Vibration suppressor	Mini-motor Positioner	Mini-motor Positioner Vibration suppressor
APPLICATION FIELD		
Space structure Military vehicle	Office equipment Camera Precision machine Automobile	Lab stage/stepper Airplane Hydraulic system
ACTUATOR SIZE		
Up-sizing (30 cm)	Down-sizing (1 cm)	Intermed. size (10 cm)
MAJOR MANUFACTURER		
AVX/Kyocera Morgan Matroc Itek Opt. Systems Burleigh AlliedSignal	Tokin Corp. NEC Hitachi Metal Mitsui-Sekka Canon Seiko Instruments	Philips Siemens Hoechst CeramTec Ferroperm Physik Instrumente

Table III

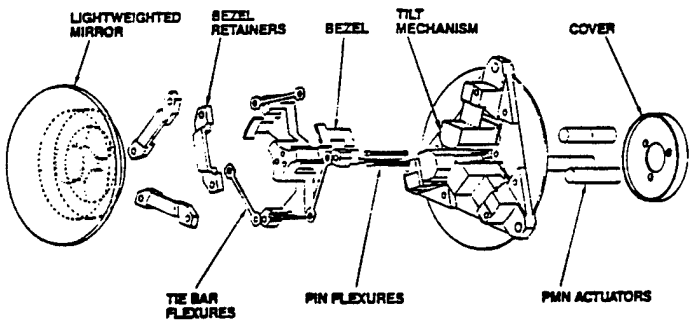

Fig.10: „Hubble" telescope using PMN electrostrictive actuators.

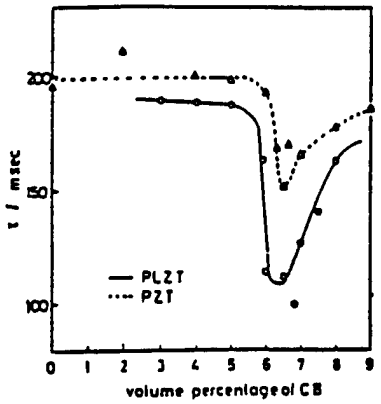

Fig.11: Damping time constant change with volume percentage of carbon black in piezoelectric composite dampers.

mm steel ball can be hit up to 20 μm by a 5 mm displacement induced in a multilayer actuator with quick response [19]. A dot-matrix printer head has been trially manufactured using a flight actuator as shown in Fig.9 [20]. By changing the drive voltage pulse width, the movement of the armature was easily controlled to realize no vibrational ringing or double hitting.

5 Device Applications

Table III compares the difference in the ceramic actuator developments among USA, Japan and Europe. The details will be described in this section.

5.1 USA

The target of the development is mainly for military-oriented applications such as vibration suppression in space structures and military vehicles. Notice the up-sizing trend of the actuators for these purposes.

A typical example is found in a space truss structure proposed by Jet Propulsion Laboratory [21]. A stacked PMN actuator was installed at each truss nodal point and functioned actively so that unne-

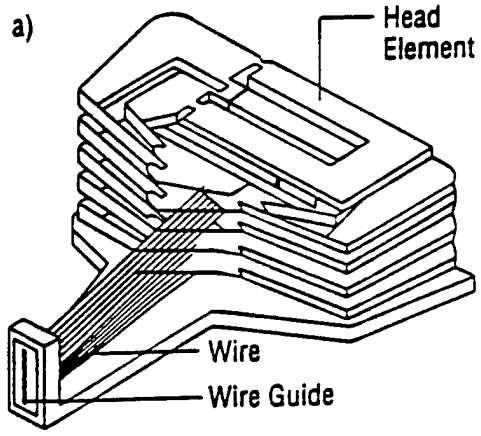

Fig.12: Structure of a printer head (a), and a differential-type piezoelectric printer-head element (b).

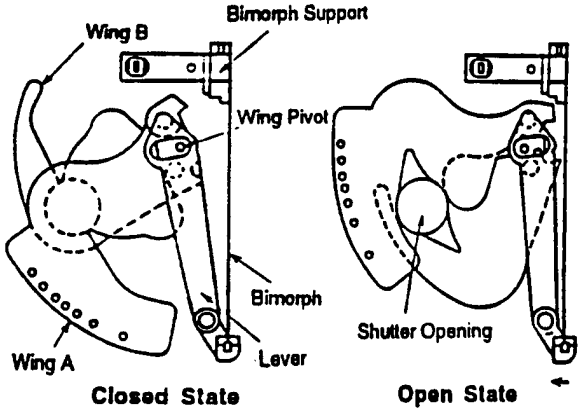

Fig.13: Piezoelectric camera shutter.

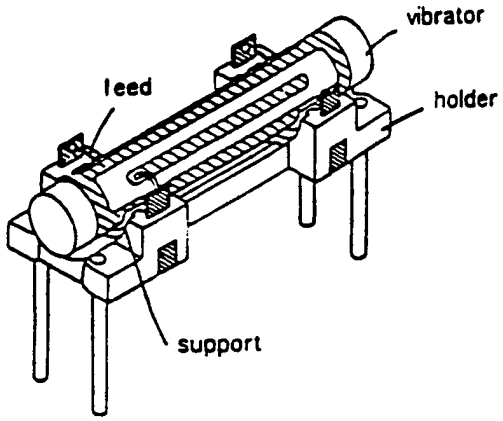

Fig.14: Piezo-ceramic cylinder vibratory gyroscope.

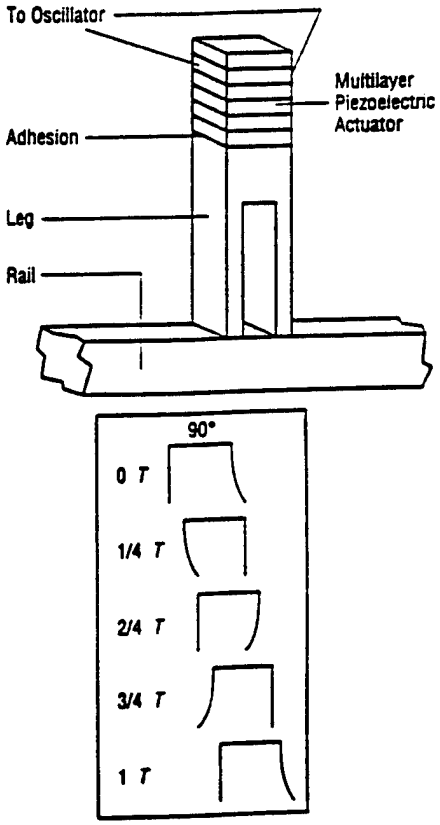

Fig.15: Ultrasonic linear motor of a vibratory coupler type.

cessary mechanical vibration was suppressed immediately. A „hubble" telescope has also been proposed using multilayer PMN electrostrictive actuators to control the phase of the incident light wave in the field of optical information processing (Fig.10) [22]. The PMN electrostrictor provided superior adjustment of the telescope image because of negligible strain hysteresis.

Passive damper application is another smart usage of piezoelectrics, where mechanical noise vibration is radically suppressed by the converted electric energy dissipation through Joule heat when a suitable resistance, equal to an impedance of the piezoelectric element $1/\omega C$, is connected to the piezo-element [23]. Piezoceramic:carbon black: polymer composites are promising useful designs for practical application. Figure 11 shows the damping time constant change with volume percentage of the carbon black. The minimum time constant (i.e. quickest damping) is obtained at 6 % of carbon black, where a drastic electric conductivity change is observed (percolation threshold) [24]

A dot matrix printer is the first widely-commercialized product using ceramic actuators. Each character formed by such a printer is composed of a 24 x 24 dot matrix. A printing ribbon is subsequently impacted by a multiwire array. A sketch of the printer head appears in Fig. 12(a) [25]. The printing element is composed of a multilayer piezoelectric device, in which 100 thin ceramic sheets 100 µm in thickness are stacked, together with a sophisticated magnification mechanism (Fig.12(b)). The magnification unit is based on a monolithic hinged lever with a magnification of 30, resulting in an amplified displacement of 0.5 mm and an energy transfer efficiency greater than 50%. A piezoelectric camera shutter is currently the largest production quantity item (Fig.13). A piece of piezoelectric bimorph can open and close the shutter in a milli-second through a mechanical wing mechanism [26]. Piezoelectric gyro-sensors are now widely used to detect the noise motion of a handy video camera. Figure 14 shows a Tokin's cylinder type gyroscope [27]. Among the 6 electrode strips, two of them are used to excite total vibration and the other two pairs of electrode are used to detect the Corioli's force or the rotational acceleration cause by the hand motion. By using the gyro signal, the image vibration can be compensated electrically on a monitor display.

5.2 JAPAN

Japanese industries seek to develop mass-consumer products, and the categories are only limited to minimotor and positioner areas, aiming at the applications to office equipment and cameras/video cameras. In that sense, tiny actuators smaller than 1 cm are the main focus.

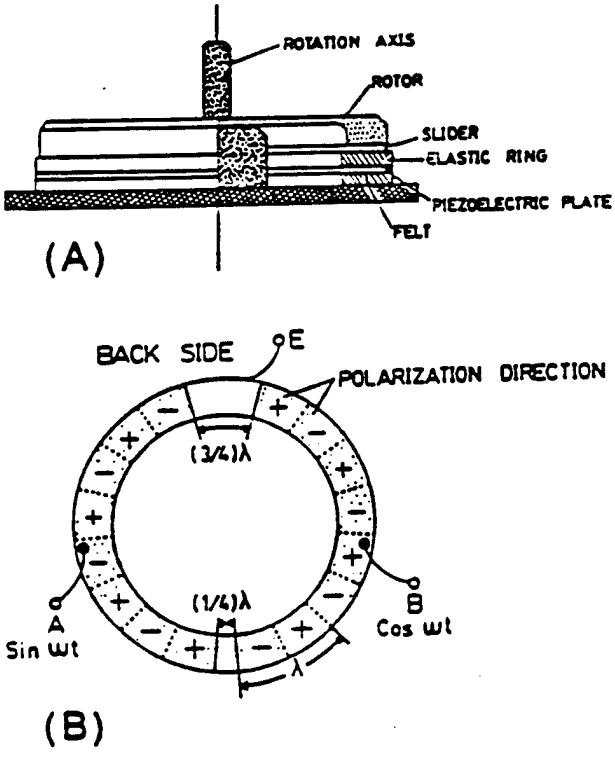

Fig.16: Design of the surface wave type motor (a), and its electrode configuration.

Efforts have been made to develop high-power ultrasonic vibrators as replacements for conventional electromagnetic motors. The ultrasonic motor is characterized by „low speed and high torque," which is contrasted with „high speed and low torque" of the electromagnetic motors. Two categories are being investigated in Japan for ultrasonic motors: a standing-wave type and a propagating-wave type.

The standing-wave type is sometimes referred to as a vibratory-coupler type or a „woodpecker" type, where a vibratory piece is connected to a piezoelectric driver and the tip portion generates flat-elliptical movement. Attached to a rotor or a slider, the vibratory piece provides intermittent rotational torque or thrust. The standing-wave type has , in general, high efficiency, but lack of control in both clockwise and counterclockwise directions is a problem. An ultrasonic linear motor equipped with a multilayer piezoelectric actuator and fork-shaped metallic legs has been developed as shown in Fig.15 [28]. Since there is a slight difference in the mechanical resonance frequency between the two legs, the phase difference between the bending vibrations of both legs can be controlled by changing the drive frequency. The walking slider moves in a way similar to a horse using its fore and hind legs when trotting. A trial motor 20 x 20 x 5 mm³ in dimension exhibited a maximum speed of 20 cm/s and a maximum thrust of 0.2 kgf with a maximum efficiency of 20%, when driven at 98 kHz of 6 V (actual power = 0.7 W). This motor has been employed in a precision X-Y stage.

By comparison, the propagating-wave type (a surface-wave or „surfing" type) combines two standing waves with a 90 degree phase difference both in time and in space, and is controllable in both rotational directions (Fig.16) [29]. By means of the traveling elastic wave induced by the thin piezoelectric ring, a ring-type slider in contact with the „rippled" surface of the elastic body bonded onto the piezoelectric is driven in both directions by exchanging the sine and cosine voltage inputs. Another advantage is its thin design, which makes it suitable for installation in cameras as an automatic focusing device. 80 % of the exchange lenses in Canon's „EOS" camera series have already been replaced by the ultrasonic motor mechanism.

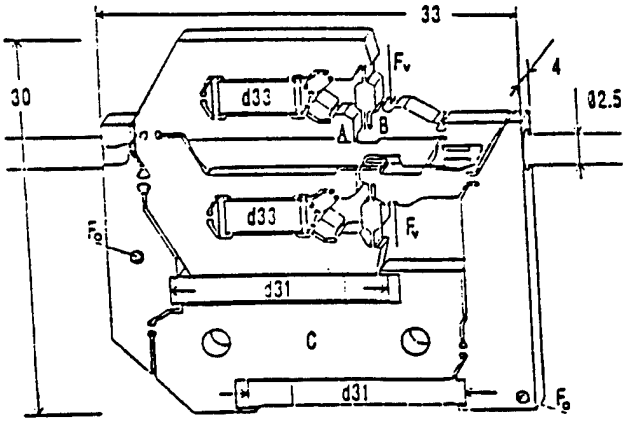

Fig.17: Walking piezo motor.

Figure 17 shows a walking piezo motor with 4 multilayer actuators [30]. Shorter two are used to function as clamplers and longer two provide the proceeding distance in an inchworm mechanism.

5.3 EUROPE

Ceramic actuator development has started relatively recently in Europe, and the research topics diverges very widely. However, the current focus by major manufacturers is probably put on lab-equipment products such as lab-stages and steppers with sophisticatedly complicated structures.

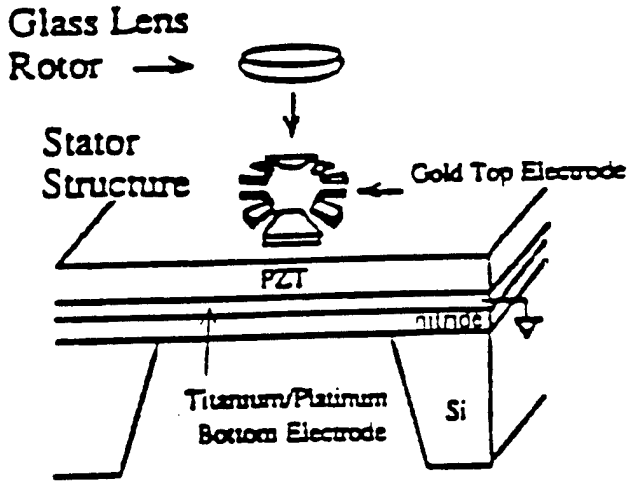

Fig.18: Ultrasonic micro-motor.

6 Future of Ceramic Actuators

18 years have passed since the intensive development of piezoelectric actuators began in Japan, then spreaded worldwidely. Presently, the focus has been shifted to practical device applications.

The markets in USA is limited to military and defense applications, and it is difficult to estimate the sales amount. The current needs from Navy are smart submarine skins, hydrophone actuators, prop noise cancellation etc., and smart aircraft skins from Air Force, while Army requires hilicopter rotor twisting, aeroservoelastic control and cabin noise/seat vibration cancellation.

On the contrary in Japan, piezoelectric shutters (Minolta Camera) and automatic focusing mechanisms in cemeras (Canon), dot-matrix printers (NEC) and part-feeders (Sanki) are now commercialized and mass-produced by tens of thousands of pieces per month. During the commercialization, new designs and drive-control techniques of the ceramic actuators have been mainly developed in the past few years. A number of patent disclosures have been found particularly in NEC, TO-

TO Corporation, Matsushita Electric, Brother Industry, Toyota Motors, Tokin, Hitachi Metal, Toshiba etc.

Several years ago Mr. T. Sekimoto, Former President of NEC, expressed his desire to the piezoelectric actuators in his New Year's speech that the market-share of piezoelectric actuators and their employed devices would reach up to $10 billion (S1010) in the future. If we estimate the annual sales in 2000 (without considering the current serious economical recession in Japan), ceramic actuator units, camera-related devices and ultrasonic motors will be expected to reach $500 million, $300 million and $150 million, respectively. Regarding the final actuator-related products, $10 billion will not be very different from the realistic amount.

Future research trends will be divided into two ways: up-sizing in space structures and down-sizing in office equipment. Further down-sizing will also be required in medical diagnostic applications such as blood test kits and surgical catheters. Piezoelectric thin films campatible with silicon technology will be much focused in microelectromechanical systems. An ultrasonic rotary motor as tiny as 2 mm in diameter fabricated on a silicon membrane is a good example (see Fig.18) [31].

With expanding the application field of ceramic actuators, the durability/reliability issue becomes more important. The final goal is, of course, to develop much tougher actuator ceramics mechanically and electrically. However, the reliability can be improved significantly if the destruction symptom of the actuator is monitored.

Safety systems or health monitoring systems have been proposed with two feedback mechanisms: position feedback which can compensate the position drift and the hysteresis, and breakdown detection feedback which can stop the actuator system safely without causing any serious damages onto the work, e.g. in a lathe machine [32]. Acoustic emission and internal potential measurements, and resistance monitoring of a strain-gauge type internal electrode embedded in a piezo-actuator under a cyclic electric field drive are good predictors for the life time [33].

Future research and development should focus on superior systems ecologically (i.e. fit for human!) as well as technologically. Safety systems, which can monitor the fatigue or the destruction symptom of materials/devices, and stop the equipment safely without causing serious problems, will be desired.

7 References

[1] K.Uchino, Piezoelectric/Electrostrictive Actuators, Morikita Publishing, Tokyo 1986

[2] K.Uchino, Bull.Am.Ceram.Soc., 65(4), 647 (1986)

[3] K.Uchino, MRS Bull., 18(4), 42 (1993)

[4] K.Uchino, Proc. 4th Int'l Conf. Electronic Ceramics & Appl., p.179(1994)

[5] K.Furuta and K.Uchino, Adv.Ceram.Mater., 1, 61 (1986)

[6] J.von Cieminski and H.Beige, J.Phys.D, 24, 1182 (1991)

[7] L.E.Cross, S.J.Jang, R.E.Newnham, S.Nomura and K.Uchino, Ferroelectrics, 23(3), 187(1980)

[8] K.Uchino, Ceramic Data Book'88 (Chap.:Ceramic Actuators), Inst. Industrial Manufacturing Tech., Tokyo 1988

[9] K.Uchino and S.Nomura, Ferroelectrics, 50(1), 191 (1983)

[10] A.Furuta, K.Y.Oh and K.Uchino, Sensors and Mater., 3(4), 205 (1992)

[11] K.Uchino, M.Yoshizaki, K.Kasai, H.Yamamura, N.Sakai and H.Asakura, Jpn.J.Appl.Phys., 26(7), 1046 (1987)

[12] K.Uchino, M.Yoshizaki and A.Nagao, Ferroelectrics, 95, 161 (1989)

[13] Aura Ceramics, Inc., Catalogue „Rainbow"

[14] M.Tanimura and K.Uchino, Sensors and Mater., 1, 47 (1988)

[15] K.Uchino, J.Rob.Mech., 1(2), 124 (1989)

[16] Y.Sugawara, K.Onitsuka, S.Yoshikawa, Q.C.Xu, R.E.Newnham and K.Uchino, J.Am.Ceram.Soc., 75(4), 996 (1992)

[17] H.Goto, K.Imanaka and K.Uchino, Ultrasonic Techno, 5, 48 (1992)

[18] N.Kanbe, M.Aoyagi, S.Hirose and Y.Tomikawa, J.Acoust.Soc.Jpn.(E), 14(4), 235 (1993)

[19] S.Sugiyama and K.Uchino, Proc. Int'l.Symp.Appl.Ferroelectrics'86, IEEE, p.637 (1986)

[20] T.Ota, T.Uchikawa and T.Mizutani, Jpn.J.Appl.Phys., 24, Suppl.24-3, 193 (1985)

[21] J.T.Dorsey, T.R.Sutter and K.C.Wu, Proc. 3rd Int'l Conf. Adaptive Structures, p.352 (1992)

[22] B.Wada, JPL Document D-10659, p.23 (1993)

[23] K.Uchino and T.Ishii, J.Jpn.Ceram. Soc., 96(8), 863 (1988)

[24] Y.Suzuki, K.Uchino, H.Gouda, M.Sumita, R.E.Newnham and A.R.Ramachandran, J. Jpn. Ceram. Soc., 99(11), 1135 (1991)

[25] T.Yano, I.Fukui, E.Sato, O.Inui and Y.Miyazaki, Proc. Electr. & Commun.Soc., p.1-156 (Spring,1984)

[26] Y.Tanaka, Handbook on New Actuators for Precision Control, Fuji Technosystem, p.764 (1994

[27] Tokin Corporation, Catalogue „Ceramic Gyro"

[28] M.Tohda, S.Ichikawa, K.Uchino and K.Kato, Ferroelectrics, 93, 287 (1989)

[29] Y.Akiyama (Editor), Ultrasonic Motors/Actuators, Triceps, Tokyo 1986

[30] M.P.Koster, Proc. 4th Int'l Conf. New Actuators, Germany, p.144 (1994)

[31] A.M.Flyn, L.S.Tavrow, S.F.Bart, R.A.Brooks, D.J.Ehrlich, K.R.Udayakumar and L.E.Cross, J. Microelectromechanical Systems, 1, 44 (1992)

[32] K.Uchino, J.Industrial Education Soc. Jpn., 40, 28 (1992)

[33] K.Uchino and H.Aburatani, Proc. 2nd Int'l Conf. Intellgent Materials, p.1248 (1994)

Kenji Uchino
International Center for Actuators and Transducers (ICAT)
134 Materials Research Laboratory
The Pennsylvania State University
University Park, PA 16802-4800, USA
phone (814) 863-8035
fax (814) 865-2326

APPENDIX 59

ISAF,96

Optimization of Bimorph Based Double Amplifier Actuator under Quisistatic Situation

Baomin Xu, Q. M. Zhang, V. D. Kugel, Qingming Wang , L. E. Cross

Materials Research Laboratory, Pennsylvania State University, University Park, PA 16802

Abstract -- Bimorph based double amplifier actuator is a new type of piezoelectric actuation structure which combines both bending and flextensional amplification concepts. As a result the displacement of the actuator can be more than ten times larger than the tip displacement of bimorphs and can be used in air acoustic transducers as an actuation element. This paper studied the dependence of displacement on actuator parameters and optimum design issues for the cover plate (the flextensional part of the actuator) theoretically and experimentally.

I. INTRODUCTION

How to get larger displacements is always a main objective in the development of piezoelectric transducer and actuator devices. Since the direct extensional strain in most piezoelectric ceramic materials is at best a few tenths of one percent, the means of enhancing or amplifying the displacement is essential in many device designs[1].

Except for multilayer type actuators, which enhance the displacement by a direct dimension effect, presently there are two ways to amplify the extensional strain of piezoelectric materials[2]. One is to make use of bending amplification mechanism, which leads to the development of bimorph type actuators. Another way is the utilization of flextentional amplification scheme, which leads to the development of flextensional transducers widely used in underwater acoustics, moonie and cymbal actuators[3].

Recently, we presented a new kind of piezoelectric actuation structure named bimorph based double amplifier[4], because it can be considered as the combination of bending-type actuators and flextensional elements, as shown in Fig. 1. As a result the displacement of the new actuator can be more than ten times larger than the tip displacement of bimorphs, and can be used in air acoustic transducers as an actuation element. Some theoretical analyses have been given earlier[5]. In this work, the displacement of the actuator is studied in detail, with emphasis on the optimum dimension design of the cover plate of the actuator.

II. PRINCIPLE AND THEORETICAL ANALYSIS

This work was supported by the Office of Naval Research under the contract No. N00014-94-1-1140.

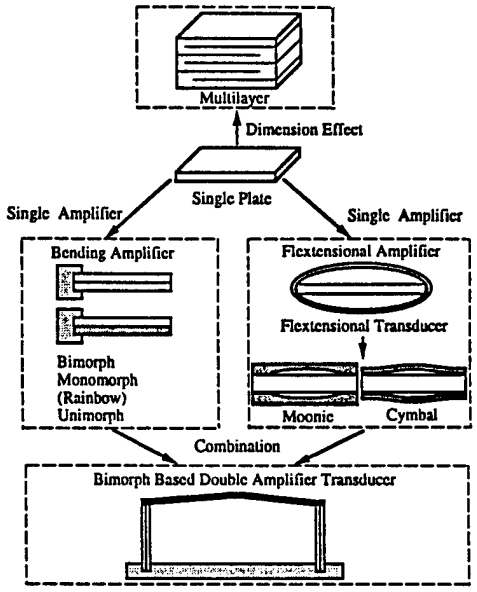

Fig. 1. Evolution of piezoelectric actuators with larger displacement

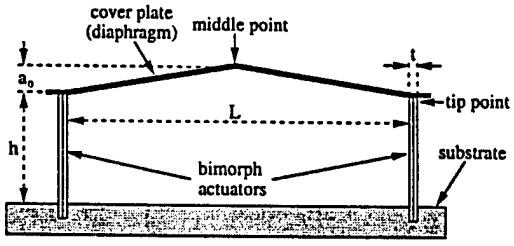

L: length of the cover plate h: height of bimorphs
t: thickness of bimorphs a_0: initial height of the cover plate

Fig. 2. Basic configuration of bimorph based double amplifier

The basic configuration of bimorph based double amplifier is shown in Fig. 2. The structure mainly consists of two parallel-mounted bimorphs with a triangle shaped cover plate as an active diaphragm fixed on the top of the bimorphs. Higher displacement is achieved by converting the tip displacement of bimorphs to the motion of the cover plate. Since one of the objective of the actuator is to work in air acoustic transducers as an actuation element, loudspeaker

paper is chosen as cover plate material in this work because of its excellent mechanical-acoustic property and light weight.

The relationship between displacement of the cover plate (middle point) and actuator parameters is explained below: as shown in Fig. 3, letters A, B, and C represent the joint parts of the cover plate, which are called as hinge regions. Generally, the deformation of the cover plate can be considered to concentrate in these hinge regions. When a displacement of the cover plate is generated, moments will be induced in these hinge regions due to the deformation, which will balance the moments produced by the bimorphs. Therefore, the motion of the cover plate is rotation-dominated and can be treated as two rigid beams connected by a torsional spring at the middle point. When a voltage V is applied to the bimorphs, a tip displacement Δ and force F are generated, which in turn produces a displacement ξ at the middle point of the cover plate and induces a moment M in the torsional spring due to the displacement. From the geometric consideration, it can be found that:

$$\xi = a_1 - a_0 = \sqrt{a_0^2 + L\cdot\Delta} - a_0 \qquad (1)$$

The moment balance equation is:

$$2F\cdot(a_0+\xi) = M = k\cdot 2\cdot(\theta_1 - \theta_0)$$

or
$$F(a_0+\xi) = k(\theta_1-\theta_0) \approx k\cdot 2\xi / L \qquad (2)$$

Since ξ is much smaller than L. k in equation (2) is the spring constant. It has been known that[6]:

$$F = \frac{t^3 w}{4h^3 s_{11}^E}(\Delta_0 - \Delta) = c_0(\Delta_0 - \Delta) \qquad (3)$$

where w is the width and s_{11}^E is the elastic compliance of the piezoelectric material, Δ_0 is the tip displacement under free condition, and

$$\Delta_0 = 3d_{31}V(h/t)^2 \qquad (4)$$

if parallel type bimorph is used.

The equivalent torsional spring constant k can be determined in this way: Suppose the original length of the hinge region is b, and it is also the neutral line length of the deformation area. R_A, R_B and R_C are the elastic curvature radii at hinge regions A, B, and C respectively. From Fig. 3 we can get:

$$R_{B,i} = R_{C,i} \approx b/\tan\theta_i \text{ , and } R_{A,i} \approx b/(2\tan\theta_i),\ i = 0,\ 1$$

Let M_A, M_B and M_C represent the induced moments at areas A, B and C due to the displacement, then the total induced moment is[7]:

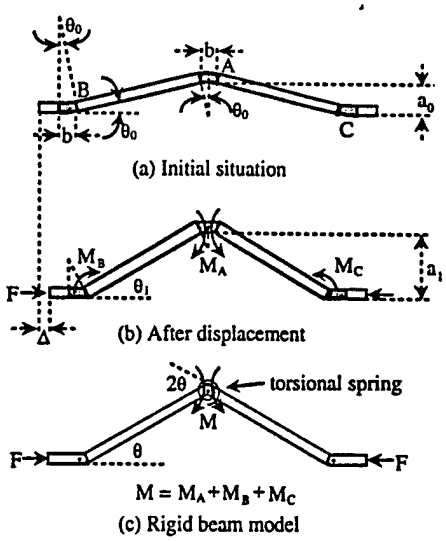

Fig. 3. Rigid-beam model for rotation-dominated cover plate motion

$$\begin{aligned} M &= M_A + M_B + M_C \\ &= EI(1/R_{A,1} - 1/R_{A,0}) + 2\cdot EI(1/R_{B,1} - 1/R_{B,0}) \\ &= 4EI(\tan\theta_1 - \tan\theta_0)/b \\ &\approx 4EI(\theta_1 - \theta_0)/b \end{aligned}$$

where E is the Young's modulus of the cover plate material and I is area moment of inertia of cross section of the hinge region. Compare to equation (2) we get the spring constant:

$$k = 2EI/b \qquad (5)$$

This means that k just depends on the properties of the cover plate material. Substituting equations (3) and (5) in equation (2) yields:

$$c_0(\Delta_0 - \Delta)(a_0 + \xi) = (2EI/b)\cdot(2\xi/L) \qquad (6)$$

From equations (1), (6) and (4), the dependence of Δ and ξ on the actuator parameters and driving voltage can be obtained, so that optimization on actuator design can be conducted. However, the analysis is rather complicated because the relationship between Δ and ξ is nonlinear according to equation (1).

Considering a simple situation, that is, if $L\cdot\Delta \ll a_0^2$, we get the linear approximations for equations (1) and (6):

$$\xi = L\cdot\Delta/(2a_0) \qquad (7)$$

$$c_0(\Delta_0 - \Delta)\cdot a_0 = (2EI/b)\cdot(2\xi/L) \qquad (8)$$

Hence Δ and ξ can be obtained as:

$$\Delta = \frac{\Delta_0}{1+2EI/(a_0^2 c_0 b)} \tag{9}$$

$$\xi = \frac{L \cdot \Delta_0}{2a_0 + 4EI/(a_0 c_0 b)} \tag{10}$$

Equation (10) indicates that ξ will increase linearly with L, but there is an optimum value for a_0 where ξ is maximum. This optimum value is:

$$2a_0 = 4EI/(a_0 c_0 b), \text{ or } a_0 = \sqrt{2EI/(c_0 b)} \tag{11}$$

However, as the initial height a_0 is very small, another possibility is that the deformation of the cover plate becomes larger and can not be neglected, that is, flextensional motion of the cover plate will occur. Hence the rigid-beam model shown in Fig. 3 is not valid. From elastic theory[8,9], when a triangle shaped continuous beam is under the action of compressed axial force P, the displacement of middle point is:

$$\xi = a_0\left(\frac{\tan(\pi/2)\sqrt{P/P_{cr}}}{(\pi/2)\sqrt{P/P_{cr}}} - 1\right) \tag{12}$$

where $P_{cr}=\pi^2 EI/L^2$ is Euler load.

Equation (12) shows that ξ will increase linearly with a_0. Actually, this is the situation similar for cymbal actuators where the displacement is linearly related to the cavity depth of endcaps and exponentially related to the cavity diameter because of the flextensional motion of endcaps[10].

Therefore, if flextensional motion of the cover plate occurs above the optimum a_0 value determined from the rotation-dominated situation, the real optimum cover plate height will be in the vicinity from rotation-dominated situation to the flextension-dominated situation.

III. EXPERIMENTS

The bimorphs used in this work are operated in parallel configuration and made from Motorala 3203HD (PZT type 5H) material. Their dimensions are $20.0 \times 7.7 \times 1.5$mm. The loudspeaker paper with the same width and 0.56mm thickness is fixed on the top of bimorphs by super glue. The displacement of middle point and tip point are measured by using MTI 2000 Fotonic Sensor under different dimensions of cover plate. The applied voltage on bimorphs is fixed at 150V (p-p value) and frequency is 1Hz.

IV. RESULTS AND DISCUSSIONS

Fig. 4 is the dependence of middle point displacement and tip point displacement on the height of cover plate. The

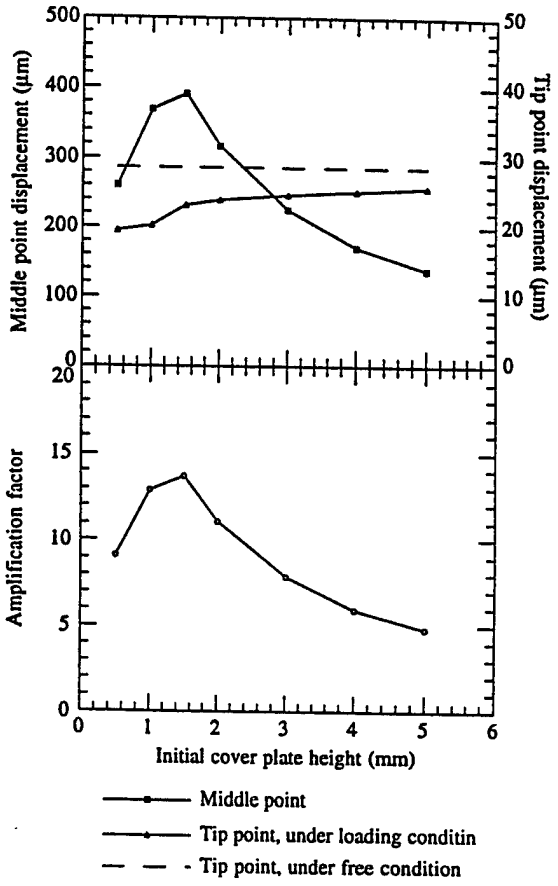

Fig. 4. Dependence of displacement and amplification factor on the initial cover plate height

length of cover plate is fixed at 56.0mm in this experiment. It really shows that there is an optimum value for initial cover plate height (about 1.5mm) at which middle point displacement reaches the maximum. Defining the amplification factor as the ratio of middle point displacement to the free tip displacement of bimorphs, Fig. 4 shows that the amplification factor is more than 10 in the vicinity of optimum initial cover plate height.

In order to determine the motion situation of the cover plate, the middle point displacement is also calculated by using equations (1) and (7) with measured tip point displacement and compared to experimental values in Fig. 5. It can be seen that when the cover plate height is larger than 3.0mm, the linear approximation can be used. When the cover plate height is between 1.5mm and 3.0mm, the calculated value using equation (1) is consistent with experimental results. This means it is still rotation-dominated situation but nonlinear effect must be considered. When the cover plate height is smaller than 1.5mm, the calculated value still increases but the measured value decreases, which means

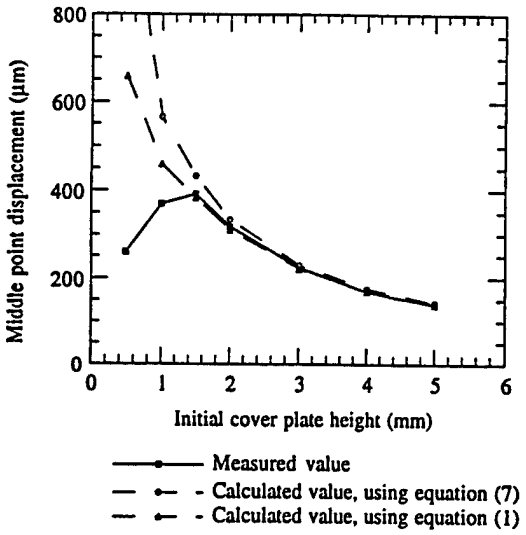

Fig. 5. Measured and calculated middle point displacement

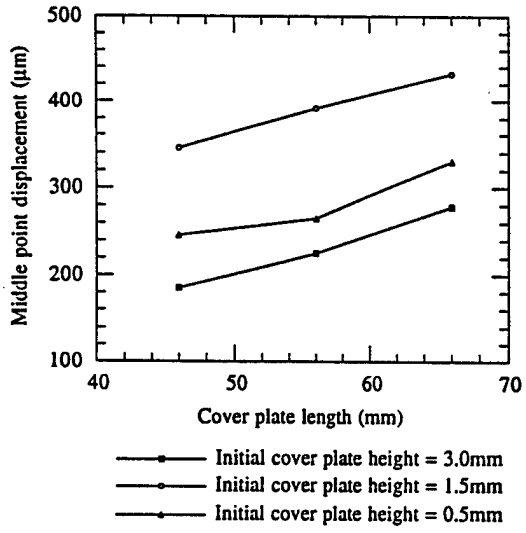

Fig. 6. Dependence of middle point displacement on cover plate length

flextensional motion of cover plate becomes obvious. Therefore, the optimum initial cover plate height for the present design is in the vicinity from rotation-dominated to flextention-dominated situation.

Fig. 6 shows the dependence of middle point displacement on the length of cover plate. When the cover plate height is 3.0mm, the linear approximation can be used so that the middle point displacement will linearly increase with the length of cover plate. When the cover plate height is 0.5mm, flextensional motion becomes dominated, and the middle point displacement increased with cover plate length more rapidly than linearly. This is consistent with our theoretical analysis.

V. CONCLUSIONS

The displacement of bimorph based double amplifier actuators can be more than ten times larger than the tip displacement of bimorphs. The displacement strongly depends on the initial height of cover plate. When the cover plate height decreases, the motion of cover plate is from rotation-dominated to flextension-dominated. And the optimum cover plate height is in the transfer region of these two kinds of situations. The displacement increases with cover plate length, but the relationship in detail is quite different according to rotation-dominated or flextension-dominated situation.

REFERENCES

[1] G. H. Haertling, "Rainbow ceramics – a new type of ultra-high-displacement actuator", *Amer. Ceram. Soc. Bull.*, Vol. 73, pp. 93 - 96, Jan. 1994.

[2] K. Uchino, "Ceramic Actuators: Principles and Applications", *MRS Bulletin*, Vol. 18, pp. 42 - 47, April 1993.

[3] A. Dogan, "Flextensional 'moonie' and 'cymbal' actuators", Ph.D. thesis, Pennsylvania State University, 1994.

[4] Baomin Xu, Q. M. Zhang, V. D. Kugel, L. E. Cross, "Piezoelectric air transducer for active noise control", *SPIE Proc.*, Vol. 2717, pp. 388 - 398, Feb. 1996.

[5] V. D. Kugel, Q. M. Zhang, Baomin Xu, Qingming Wang, L. E. Cross, "Bimorph-based air transducer: a model", presented at 1996 ONR Transducer Materials and Transducer Workshop, State College, Pennsylvania, March 25 - 27, 1996.

[6] J. G. Smits, S. I. Dalke, T. K. Cooney, "The constituent equations of piezoelectric bimorphs", *Sensors and Actuators A*, Vol. 28, pp. 41 -61, Jan. 1991.

[7] L. D. Landau and E. M. Lifshitz, *Theory of Elasticity*, 3rd. ed., Oxford: Pergamon Press, 1986, Chapter 2.

[8] S. P. Timoshenko, J. P. Gene, *Theory of Elastic Stability*, 2nd. ed., New York: McGraw-Hill, 1961, Chapter 1.

[9] H. G. Allen, P. S. Bulson, *Background to Buckling*, London: McGraw-Hill, 1980, Chapter 1.

[10] A. Dogan, J. F. Fernandez, K. Uchino, R. E. Newnham, "New piezoelectric composite actuator designs for displacement applications," in press *Proc. Euroceram 95* (1995).

APPENDIX 60

Caterpillar-type piezoelectric d_{33} bimorph transducer

V. D. Kugel,[a] Sanjay Chandran, and L. E. Cross
187 Materials Research Laboratory, The Pennsylvania State University, University Park, Pennsylvania 16802

(Received 12 June 1996; accepted for publication 24 July 1994)

A piezoelectric bimorph transducer utilizing piezoelectric d_{33} coefficient was developed. This bimorph consists of piezoelectric segments bonded by a polymeric agent and was fabricated by a dicing and layering technique. The transducer has superior piezoelectric characteristics compared to standard piezoelectric d_{31} bimorphs. Piezoelectric coefficients, electrical admittance, mechanical compliance, and losses of the actuator were found to increase with increasing driving electric field.
 [S0003-6951(96)04040-5]

Piezoelectric bimorph actuators have been known for many years[1] and are widely used for efficient interconversion of electrical and mechanical energy. A typical piezoelectric bimorph transducer consists of two similar piezoelectric plates poled along their thickness (Z axis) and adhesively bonded together (Fig. 1); in the case of a piezoelectric/metal bimorph a metal plate is replaced for one of the piezoelectric plates. Instead of a "piezoelectric/metal bimorph" notation, we will use "unimorph" in the sense that this type of bimorph has only one piezoelectric plate. Clearly, the flexural displacement in this actuator is caused by the piezoelectric effect (d_{31})in the direction perpendicular to the polar **P** axis. The static tip displacement η and corresponding blocking force $F_{bl}(\eta=0)$ of the piezoelectric bimorph cantilever can be written as[2]

$$\eta=\frac{3}{2}d_{31}\frac{l^2}{t}E,$$
$$F_{bl}=\frac{3}{8}\frac{d_{31}wt^2}{s_{11}^E}\frac{1}{l}E, \tag{1}$$

where d_{31} is the piezoelectric coefficient, s_{11}^E is the mechanical compliance in the direction X under the constant electric field, and E, l, w, and t are the dimensions of the cantilever (Fig. 1). Mechanical stress T_1 arising in the unloaded piezoelectric cantilever under the applied electric field is directed along the X axis.

Commercial piezoelectric bimorph actuators are usually made from soft PZT ceramics with the composition near the morphotropic phase boundary. For these compositions, piezoelectric coefficient d_{33} along the polar axis and corresponding coupling factor k_{33} are 2–2.2 times larger than d_{31} and k_{31}. Studies of the effect of the mechanical stress on piezoelectric properties of the ceramics also show that piezoelectric coefficient d_{33} is much less sensitive to the compressive stress T_3 along the polar axis than coefficient d_{31} is to the compressive stress T_1 perpendicular to the polar axis.[3] Thus, the piezoelectric bimorph actuator utilizing d_{33} coefficient can be expected to have superior characteristics compared to a standard d_{31}-type bimorph transducer.

In this letter, we report on a novel type of piezoelectric bimorph and unimorph in which the piezoelectric effect along the polar axis is used to generate flexural displacement. A schematic view of the developed caterpillar-type d_{33} unimorph is shown in Fig. 2. From Fig. 2 it is clear that, when the piezoelectric plate changes its length under the applied voltage V, it causes bending of the cantilever. Unlike in the standard d_{31}-type bimorph actuator (Fig. 1), the bending moment in these transducers is caused by piezoelectric d_{33} coefficient. To fabricate the d_{33} bimorph the metal plate is replaced by an identical piezoelectric plate. In this case the driving voltage is applied in such a way that mechanical strains generated in the top and bottom piezoelectric plates have opposite signs.

The experimental process adopted for fabricating the d_{33}-type transducer is described below. Initially, a stack of similar piezoelectric electroded plates poled along their thickness is fabricated. Adjacent plates have opposite directions of spontaneous polarization **P**. The plates are bonded to each other by a very thin layer of conductive polymer. Then the stack is sliced by means of a diamond saw in the plane parallel to the direction of spontaneous polarization. To fabricate a unimorph transducer, the sliced plate is glued to a metal substrate (see Fig. 2). Conducting electrodes are deposited on the surface of the piezoelectric plate in such a way that voltage V applied to these electrodes produces the same piezoelectric strain (positive or negative) in each of the piezoelectric segments comprising this plate. To make a d_{33} bimorph, a metal plate is replaced by an identical piezoelectric plate. It is important to note that the conductive polymer serves not only for electric connecting, but also for improving fracture toughness. Therefore, the transducer developed

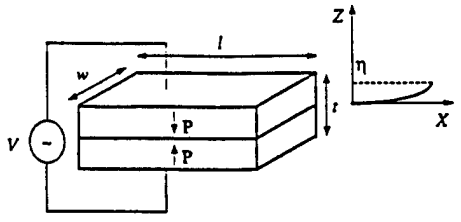

FIG. 1. Bimorph piezoelectric d_{31} element with series connection. The vector of the spontaneous polarization **P** is directed along the Z axis.

[a]Electronic mail: vxk7@psuvm.psu.edu

 0003-6951/96/69(14)/2021/3/$10.00

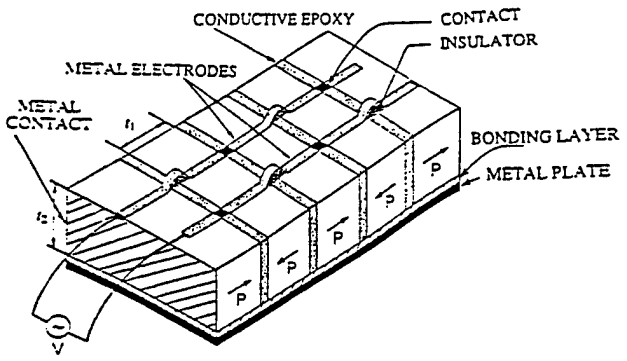

FIG. 2. A schematic view of the caterpillar-type d_{33} unimorph actuator. In the case of a bimorph consisting of two similar piezoelectric plates, the metal plate is replaced for the same piezoelectric plate.

can sustain a much larger bending force without mechanical failure.

In our experiments we used soft piezoelectric ceramics PKI550 (Piezo Kinetic, Inc.) and stainless steel SS302. The ceramic plates in the stack were bonded using commercial conductive adhesives EP21TDCS (Master Bond, Inc.) and E-Solder 3025 (Insulating Materials, Inc.). J-B Weld epoxy (J-B Weld Company) was used for bonding metal and sliced ceramic plates. Each piezoelectric segment in the piezoelectric plates (Fig. 2) had the following dimensions: $t_1=t_2=1.09$ mm, $w=11$ mm. Stainless steel plates had thicknesses, $t_m=0.25$, 0.29, and 0.37 mm. For comparison, standard d_{31}-type bimorphs and unimorphs of identical dimensions were also fabricated.

To characterize the transducer developed, the following parameters of these transducers in the cantilever configuration ($l=26.0$ mm), were measured: (i) displacement η of the free end; (ii) blocking force F_{bl}, and (iii) electrical admittance as a function of the applied electric field. All measurements were done at a frequency of 100 Hz which is greatly

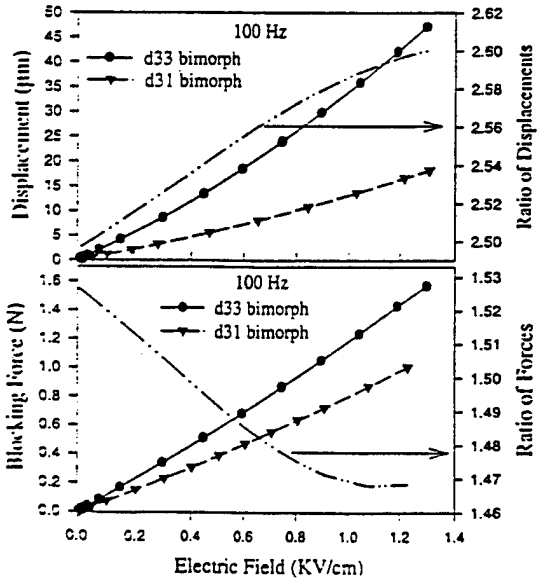

FIG. 3. The dependence of displacement and blocking force for bimorphs on the electric field. The thickness of bimorphs is $t=2t_2=2.18$ mm.

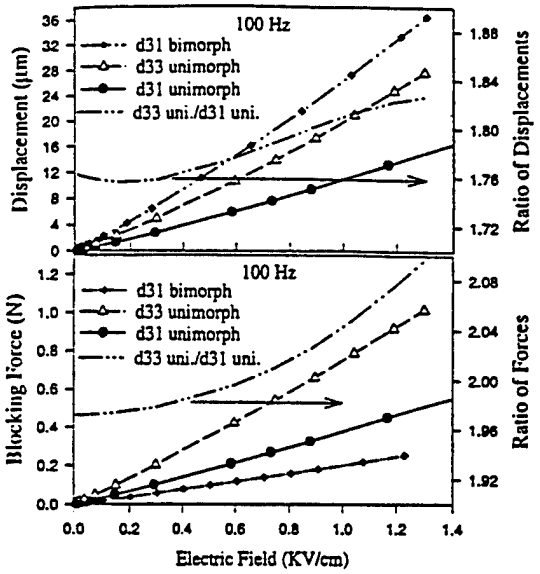

FIG. 4. The dependence of displacement and blocking force for unimorphs on the electric field. The thickness of the metal plate is 0.37 mm. The thickness of the d_{31} bimorph is $t=1.09$ mm.

below (~ 1 kHz) the first resonant frequency of the bending vibrations.

The displacement and blocking force (rms) for bimorphs and unimorphs are shown in Fig. 3 and 4, respectively. It is clear that the displacement of the d_{33} bimorph is about 2.5 times larger than that of the d_{31} bimorph and the blocking force is about 1.5 times larger. Although the displacement of the d_{33} unimorph is smaller than the displacement of the d_{33} bimorph, it is approximately 1.8 times that of the d_{31} unimorph. The blocking force of d_{33} unimorphs is about 2.0 times that of the d_{31} unimorph. Thus, the developed d_{33} bimorph and unimorph actuators have superior piezoelectric characteristics compared to those of d_{31} actuators. Relative characteristics of the above mentioned transducers for a low electric field (~10 V/cm) are given in Table I.

There is clearly an optimal ratio t_m/t_2 for unimorphs that gives maximum displacement.[4] Equation (1) for d_{33} unimorphs can be written (thorough analysis will be given elsewhere) as

TABLE I. Relative characteristics of various types of transducers.

Type of piezoelement	Displacement	Blocking force
d_{31} bimorph	1	1
d_{31} unimorph (PKI550/SS302, 1.09/0.37)	0.41	1.80
d_{33} bimorph	2.50	1.52
d_{33} unimorph (PKI550/SS302, 1.09/0.37)	0.72	3.50

$$\eta=\frac{3}{2}d_{33}\frac{l^2}{t_2}E\cdot k_d,\quad k_d=\frac{2xy(1+x)}{1+4xy+6x^2y+4x^3y+x^4y^2},$$

$$x=\frac{t_m}{t_2},\quad y=Y_m s_{33}^E, \tag{2}$$

$$F_{bl}=\frac{3}{8}\frac{d_{33}wt_2^2}{s_{33}^E l}E\cdot k_{df},\quad k_{df}=2xy\frac{1+x}{1+xy},$$

where $E=V/t_1$, Y_m is the Young's modulus of the metal plate, and s_{33}^E is the mechanical compliance of ceramics in the direction of the polar axis. For bimorph cantilevers the coefficients k_d and k_{df} in Eq. (2) are equal to 1. Theoretical values of k_d and k_{df} and corresponding experimental data obtained from the comparison of displacements and blocking forces of the d_{33} bimorph and unimorphs are given in Fig. 5. A relatively large difference between the theoretically derived and experimentally observed values for the blocking force can be attributed to the effect of the bonding layer (Fig. 2) whose thickness has been neglected in the theoretical calculations.

A close analysis of the displacement, blocking force (Figs. 2 and 3) by means of Eqs. (1) and (2), and electrical impedance of the actuators studied shows that piezoelectric, mechanical, and dielectric properties of the transducers fabricated from soft piezoelectric ceramics depend upon the magnitude of the electric field (Fig. 6). We also found that the imaginary parts of d_{31}, d_{33}, s_{11}^E, s_{33}^E and the electrical admittance increase with increasing electric field (thorough analysis will be given elsewhere). Clearly, the relative displacement is proportional to the piezoelectric coefficient d and the blocking force is proportional to the ratio d/s where s is the mechanical compliance of the whole transducer. From Fig. 6 it can be seen that the increase in d_{33} and s with increasing electric field is more than that in d_{31} and s_{11}^E. According to known results[5] the nonlinear behavior of PZT ceramics has an extrinsic nature, i.e., it is caused by domain wall and interphase interface motion. In a bimorph transducer, two factors can affect the behavior of piezoelectric coefficients under an external electric field. The first one is an increase in the piezoelectric coefficients with increasing

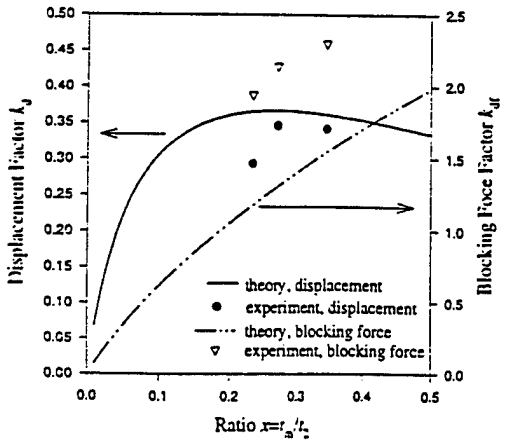

FIG. 5. Theoretical dependence and experimental data for the displacement factor k_d and blocking force factor k_{df} of d_{33} unimorphs. The coefficient $Y_m s_{33}^E$ is equal to 3.90.

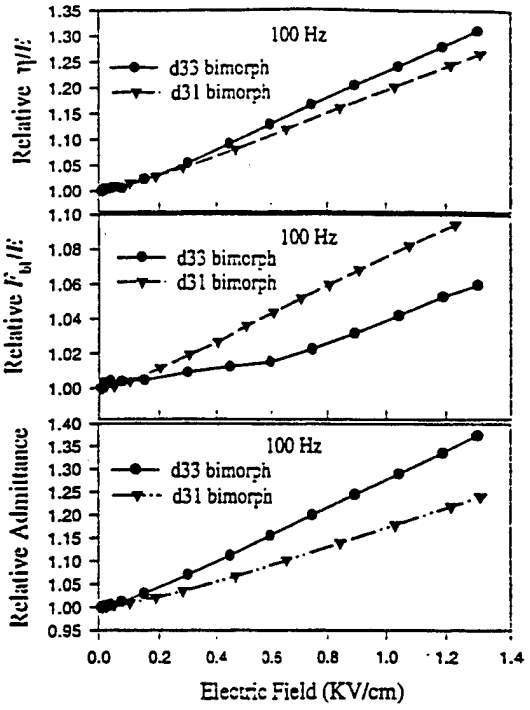

FIG. 6. Relative changes in piezoelectric characteristics of bimorph transducers. The electrical impedance was measured under free vibrations. The coercive field of PKI550 ceramics is 3.2 kV/cm.

electric field.[5] The second one is the effect of the internal stress that exists in the bimorph even without the external load. It is known that the decrease in d_{31} due to the stress T_1 is much greater than the decrease in d_{33} due to T_3.[3] Therefore, it is reasonable to expect that the enhancement of the displacement of the d_{33} bimorph under the electric field will be larger than that of the d_{31} bimorph; this is consistent with the experimental data (Fig. 6). The same two factors also affect the mechanical compliances and dielectric permittivities; in addition, the conductive polymer causes mechanical "softening" of d_{33} actuators as well.

In summary, we have developed and studied in significant detail a novel type of piezoelectric bimorph transducer based on the piezoelectric d_{33} coefficient. Superior piezoelectric characteristics compared to piezoelectric d_{31} bimorphs were obtained. Piezoelectric coefficients, electrical admittance, mechanical compliance, and losses of the actuator increase with increasing driving electric field.

This work was supported by the Office of Naval Research and under Contract No. N00014-94-1-1140.

[1] W. P. Mason, *Electrical Transducers and Wave Filters* (Van Nostrand, New York, 1942), pp. 199–200; 209–215.
[2] J. K. Lee and M. A. Marcus, Ferroelectrics 32, 93 (1981); J. G. Smith, S. I. Daike, and T. K. Cooney, Sens. Actuators 28, 41 (1992).
[3] H. H. A. Krueger, J. Acoust. Soc. Am. 42, 636 (1967); 43, 583 (1968); Q. M. Zhang, J. Zhao, K. Uchino, and J. Zheng, J. Mater. Research (to be published).
[4] M. R. Steel, F. Harrison, and P. G. Harper, J. Phys. D 11, 979 (1978).
[5] S. Li, W. Cao, and L. E. Cross, J. Appl. Phys. 69, 7219 (1991).

APPENDIX 61

Proceedings of ISAF 10, East Brunswick, NJ
(Submitted)

Behavior of Piezoelectric Actuators under High Electric Field

V. D. Kugel, Q. M. Zhang, Baomin Xu, Qing-ming Wang, Sanjay Chandran, and L. E. Cross
187 Materials Research Laboratory, The Pennsylvania State University, University Park, PA 16802

Abstract-Behavior of piezoelectric actuators (bimorph, unimorph, RAINBOW, and shear-mode) fabricated from soft ceramics has been investigated in a wide electric field and frequency range. The electrical admittance, mechanical displacement, and blocking force of these transducers have been found to be highly dependent on the magnitude of driving field. The resonant frequency and mechanical quality factor of bending vibrations for all but shear-mode actuators decreases significantly with increasing driving field. Analysis shows that despite a large variation in the quasi-static electrical admittance and reduced tip displacement of bimorph, unimorph, and RAINBOW cantilevers with driving field, their ratio is almost a constant, which characterizes the ratio of dielectric permittivity ε_{33}^{T} to piezoelectric coefficient d_{31}.

I. Introduction

Studies of last few years have demonstrated that piezoelectric transducers have significant potential as actuators for acoustic noise control [1]. These transducers are operated at such high power levels that the ferroelectric ceramic used in them begins to exhibit nonlinear behavior. It is known that piezoelectricity-related properties of ceramic materials are highly dependent on the level of driving electric field and mechanical vibrations [2-6]. A common feature in this behavior of piezoelectric ceramics is an increase in dielectric and piezoelectric coefficients, and losses even at electric fields much lesser than the coercive one. It is believed that the nonlinear behavior has extrinsic nature, i.e., is related to the domain wall and interphase boundaries' motion [4]. Till now, most of the studies were focused on the investigation of materials properties. The purpose of this work was to study the behavior of the potential piezoelectric transducers such as bimorph, unimorph, RAINBOW, and shear-mode vibrators under high electric field.

II. Experimental Procedure

All transducers investigated had a rectangular cross-section and the following dimensions: 0.45-2 mm in thickness, 5-15 mm in width, and 15-35 mm in length. Piezoelectric bimorph and metal/piezoelectric unimorph actuators were fabricated from PKI550 (Piezo Kinetic, Inc.) ceramic plates poled along their thickness. This category of piezoelectric ceramics is analogous to "soft" PZT5H ceramics. Stainless steel SS302 was used to make the unimorphs. The plates were bonded using commercial J-B Weld epoxy (J-B Weld Company). Rainbow transducers were cut from piezoelectric RAINBOW disks which were purchased from Aura Ceramics, Inc. Shear-mode actuators were fabricated from 3203HD ceramic plates (Motorola). The plates were poled along their length and the driving electric field was applied across the thickness of the plates. Clearly, the flexural displacement generated in the bimorph, unimorph and RAINBOW actuators is caused by piezoelectric d_{31} coefficient while linear displacement in the shear-mode actuators is caused by piezoelectric d_{15} coefficient.

To characterize these transducers, their electromechanical properties as a function of the driving electric field well below and close to the fundamental frequency of bending vibrations were investigated. The following parameters of these transducers in the cantilever configuration were measured: i) displacement η of the free end; ii) blocking force F_{bl} ($\eta = 0$), and iii) electrical admittance as a function of the applied electric field and frequency.

A block diagram of the experimental set-up is show in Fig. 1. The tip displacement of piezoelectric cantilevers was measured by a photonic sensor MTI 2000 (MTI Instruments). The measuring head of the sensor was mounted on a manual micropositioner which provided the linear displacement and rotation for adjusting height and angle of the head against the measured transducer. The transducer (in the Figure, bimorph is shown as an example) was mounted on XYZ micropositioner (Ealing Electro-Optics, Inc). To measure the blocking force, a special metal head of a load cell ELF-TC500 (Entran Devices, Inc) was glued by Super Glue to the vibration end of the transducer. The load cell was mounted on a micropositioner which provided a horizontal displacement for adjusting the position of the load cell against the measured transducer. The load cell was driven by power supply PS-15 (Entran Devices, Inc). The electrical admittance was measured by means of a small (several ohm) resistor R connected in series with the transducer. All lock-in amplifiers (SR830 DSP, Stanford

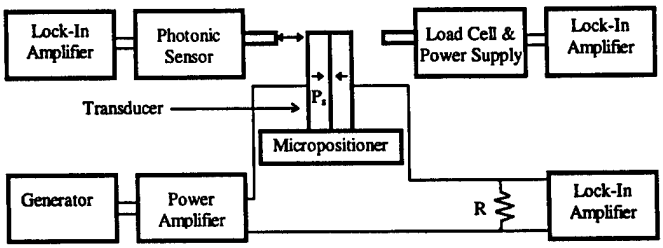

Fig. 1. Block diagram of the experimental set-up adopted to measure electromechanical properties of piezoelectric transducers. $\mathbf{P}_s$ denotes the vector of spontaneous polarization.

Research Systems, Inc) were synchronized with the output voltage of the power amplifier (790 Series, PCB Piezotronics, Inc or PA-250H, Julie Research Laboratories, Inc). The input AC signal to the power amplifier was supplied by a generator DS345 (Stanford Research Systems, Inc). The developed experimental set-up made it possible to measure the mechanical displacement and electrical admittance in the frequency range of 0-20 kHz and the blocking force in the frequency range from DC to several kilohertz. The maximum driving voltage was 300 Volt RMS.

III. Representation of Experimental Data

The quasi-static tip displacement η and corresponding blocking force F_{bl} of unimorph actuators can be written as [7]

$$\eta = \frac{3}{2} d_{31} \frac{l^2}{t_c} E \cdot k_d, \quad k_d = \frac{2xy(1+x)}{1+4xy+6x^2y+4x^3y+x^4y^2},$$
$$x = \frac{t_m}{t_c}, \quad y = Y_m s_{11}^E,$$
$$F_{bl} = \frac{3}{8} \frac{d_{31}}{s_{11}^E} \frac{wt_c^2}{l} E \cdot k_{df}, \quad k_{df} = 2xy \frac{1+x}{1+xy}, \tag{1}$$

where l, and w are the length and width of the cantilever, correspondingly; t_c and t_m are the thickness of the ceramic and metal plates, correspondingly; E is the driving electric field, Y_m is the Young's modulus of the metal plate, and s_{11}^E is the mechanical compliance of ceramics in the direction perpendicular to the polar axis. For bimorph cantilevers the coefficients k_d and k_{df} in (1) are equal to 1. Corresponding equations for pure shear-mode actuator can be written as:

$$\eta = d_{15} l E,$$
$$F_{bl} = \frac{1}{4} \frac{d_{15}}{s_{33}^E} \frac{wt_c^3}{l^2} E, \tag{2}$$

where s_{33}^E is the component of the mechanical compliance of ceramics in the direction of polar axis. It should be noted that blocking force in shear-mode thin plates causes bending. As follows from (1, 2) reduced amplitudes η/E and F_{bl}/E are proportional to dk_d and dk_{df}/s correspondingly (in the case of bimorph and shear-mode cantilevers k_d and k_{df} are equal to 1). Consequently, a relative change in the ratios η/E and F_{bl}/E as a function of the driving electric field gives information about the change in the piezoelectric and mechanical properties of the actuators.

The electrical admittance of the transducers at frequencies well below the fundamental bending resonance can be written as

$$Y = j\omega \frac{S}{t_c} \varepsilon \cdot k_Y, \tag{3}$$

where S is the area of the one of the electrodes, ε is the component of the tensor of the dielectric permittivity (ε_{33}^T for bimorphs and unimorphs and ε_{11}^T for shear-mode transducers) and k_Y is the coefficient depending the corresponding electromechanical coupling coefficient. For bimorphs this coefficient equals $1 - 0.5 d_{31}^2 / \varepsilon_{33}^T s_{11}^E$, for shear-mode actuators it equals 1. As follows from (3) the relative change in the electrical admittance as a function of the driving electric field gives information about the change in the dielectric permittivity and electromechanical coupling coefficient of the transducer.

To characterize the change in the properties of transducers near fundamental resonance, the following parameters as a function of the driving electric field were measured: i) a change in the resonant frequency $\Delta\nu_r$, ii) ratio of vibration amplitudes at resonant and low frequencies, η_r/η. The relative change in $\Delta\nu_r$ gives an idea of the change in the mechanical compliance and losses at the resonance. The relative change in η_r/η encompasses the change in the mechanical quality factor Q_m since the amplitude of the damped harmonic vibrations is proportional to this factor [8]

$$\eta_r \cong \eta Q_m. \tag{4}$$

Thus, the relative values of Y, η/E, F_{bl}/E, $\Delta\nu_r$, and η_r/η as a function of electric field calculated from experimental data were chosen to characterize nonlinear properties of transducers. It should be noted that the lock-in amplifiers used (Fig. 1) made it possible to measure complex values of η, F_{bl}, and Y, i.e., the amplitude and phase characteristics.

IV. Experimental Results

All chosen functions (RMS) were normalized relatively their values at a low electric field (~5-10 V/cm). The dependence of relative values of Y, η/E, F_{bl}/E on the electric field is shown in Figs. 2-5. Instead of the phase of the electrical admittance the phase of Y/j was plotted since it is directly related to tangent of the dielectric losses (see (3)). All measurements were done at a frequency at least 10 times lesser than the fundamental frequency of bending vibrations. Maximum electric fields used in these experiments were much less than the coercive field of the ceramics (8-9 kV/cm). As is seen from these graphs, an increase in the driving electric field causes an increase in the amplitude and phase delay of mechanical displacement, electrical admittance, and blocking force. For bimorphs, the dependencies of Y and η/E on the electric field are almost identical and are more pronounced than the dependence of corresponding reduced blocking force F_{bl}/E (Fig. 2). For unimorph cantilevers the effect of the driving electric field is stronger and function η/E increases more rapidly at a high electric field than Y (Fig. 3). A close analysis of experimental data presented in Figs. 2 and 3 shows that

there is a certain threshold electric field (10-50 V/cm) above which measured parameters begin to increase monotonically. As follows from Fig. 4, the dependence of piezoelectric properties of RAINBOW actuators on the electric field is extremely high. Functions Y and η/E behave almost in the same manner and, unlike for unimorphs, have convex shape. This type of actuators is characterized by very high losses. It should be noted that the blocking force for RAINBOW cantilevers has been found to be increased markedly with increasing shear force, which can be generated externally by the horizontal displacement of the load cell (Fig. 1). Behavior of F_{bl}/E was similar to that of Y. Experimental data for shear-mode cantilevers are given in Fig. 5. Clearly, in this case the electrical admittance increases much more rapidly with electric field than the reduced displacement.

Resonant characteristics of transducers are presented in Figs. 6 and 7. All actuators demonstrate a decrease in the resonant frequency of bending vibrations with increasing electric field (Fig. 6). The most pronounced decrease is shown by bimorph cantilevers and the smallest one is shown by shear-mode cantilevers. Measurements of the electrical impedance of the shear-mode vibrator show that there is no resonance in the impedance despite the fact that mechanical resonance of bending vibrations does occur. As is seen from Fig. 7, the relative decrease in the ratio of amplitudes at resonance and low frequency, η_r/η (and, consequently, in Q_m), is highly dependent on the type of transducers. A drastic change is obtained with bimorph actuators while a moderate change is observed with shear-mode actuators. It is important to note that the magnitude of the change in η_r/η has been found to depend on its value at low electric field.

V. Discussion and Summary

The results presented here distinctly show that electromechanical properties of the actuators fabricated from soft ceramics depend on the level of the driving electric field. Data for bimorph transducer (Fig. 2) demonstrate that the electrical admittance Y and reduced tip displacement η/E behave in a very similar manner. This functions are proportional to $\varepsilon_{33}^{T}\left(1-0.5d_{31}^{2}/\varepsilon_{33}^{T}s_{11}^{E}\right)$ and d_{31} correspondingly. Since the factor in parentheses does not change much it means that there is a close relation between electric field dependencies of ε_{33}^{T} and d_{31}. Our studies of the material properties of various soft PZT ceramics also demonstrate the same results [9]. As follows from the graph of the reduced blocking force $F_{bl}/E \propto d_{31}/s_{11}^{E}$ (Fig. 2), an increase in s_{11}^{E} is more moderate than in ε_{33}^{T} and d_{31}. This graph also shows the behavior of electromechanical coupling coefficient $d_{31}^{2}/\varepsilon_{33}^{T}s_{11}^{E}$ because the ratio $d_{31}/\varepsilon_{33}^{T}$ is a constant. As follows from the comparison of Figs. 2 and 3 a change in coefficients k_d, k_{df}, and k_y with electric field takes place for unimorphs. Data for RAINBOW actuators (Fig. 4) also confirm that there is a close relation between ε_{33}^{T} and d_{31}. As follows from Fig. 5 and (2, 3), d_{15} increases much more rapidly with the electric field than ε_{11}^{T}.

Data of resonant measurements show that bimorph vibrator is more sensitive to the electric field than other transducers. In unimorph actuator there is a non-piezoelectric metal plate which stabilize the behavior of the transducer since its properties do not depend on the electric field. In RAINBOW actuator, in addition to this effect, the internally biased compressive stress may affect resonant behavior. A relatively

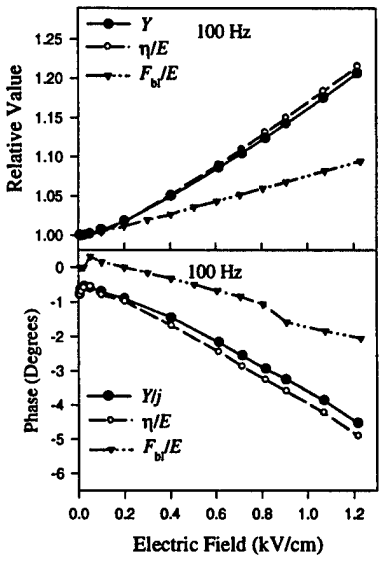

Fig. 2. Amplitude and phase characteristics of bimorph cantilever.

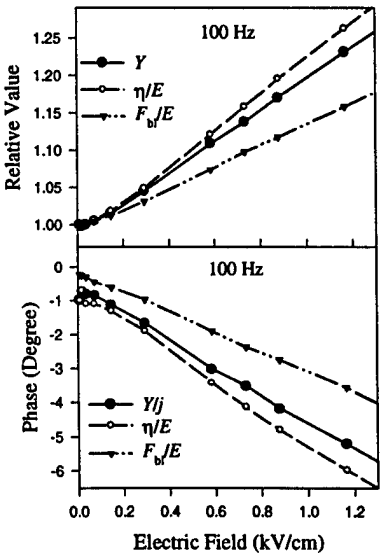

Fig. 3. Amplitude and phase characteristics of unimorph cantilever with t_m/t_c=0.34.

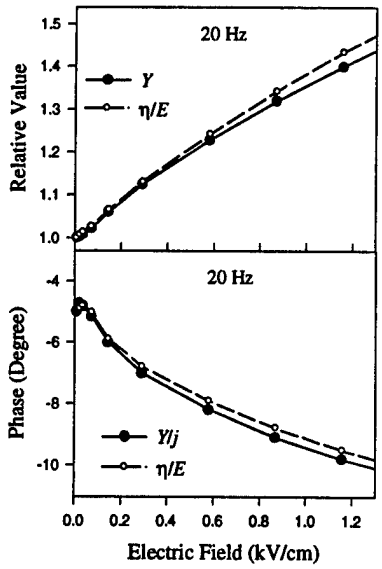

Fig. 4. Amplitude and phase characteristics of RAINBOW cantilever.

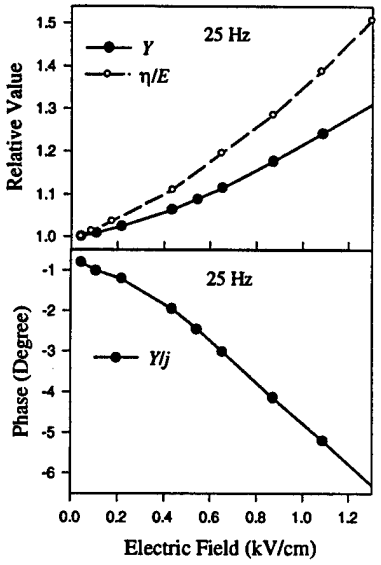

Fig. 5. Amplitude and phase characteristics of shear-mode cantilever.

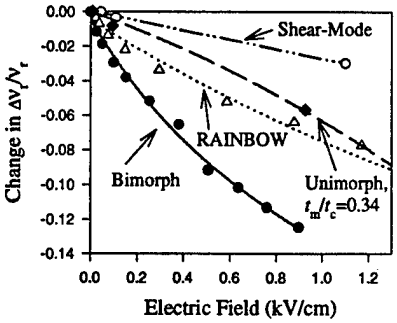

Fig. 6. Dependence of the resonant frequency v_r of bending vibrations on electric field. Low-field resonant frequency is: 1394 Hz (bimorph), 1015 Hz (unimorph), 595 (RAINBOW), and 286 Hz (shear-mode).

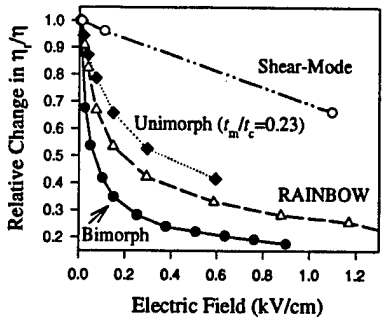

Fig. 7. Dependence of the ratio of amplitudes at resonant and low frequencies on electric field. Low-field quality factor Q_m is: 55 (bimorph), 48 (unimorph), 62 (RAINBOW), and 31 (shear-mode).

weak dependence of v_r and Q_m in shear-mode actuator can be related to the lack of the electromechanical coupling for the bending mode and to relatively low level of resonant vibrations. We assume that bending vibrations in the transducer appear as a results of elastic instability [10] of pure shear vibrations because of the action of inertia forces.

In summary, we have studied piezoelectric properties of bimorph, unimorph, RAINBOW, and shear-mode actuators in a wide electric field and frequency range. An appropriate experimental measurement system has been developed. The quasi-static and resonant piezoelectric properties of these structures have been found to be highly dependent on the magnitude of driving field.

ACKNOWLEDGMENT

This work was supported by the Office of Naval Research under the contract N00014-94-1-1140.

REFERENCES

[1] Baomin Xu, Qiming Zhang, V. D. Kugel, and L. E. Cross, "Piezoelectric air transducer for active noise control", *Proceedings of SPIE*, vol. 2717, pp. 388-398 (1996).

[2] J. H. Belding, M. G. McLaren, " Behavior of Modified Lead Zirconate-Lead Titanate Piezoelectric Ceramics Under High Electric Fields", *Ceramic Bulletin* vol. 49, pp. 1025-1029, 1970.

[3] R. S. Woollett and C. L. LeBlanc, "Ferroelectric Nonlinearities in Transducer Ceramics", *IEEE Trans. Sonics and Ultrasonics*, vol. 20, pp. 24-31, January 1973.

[4] Shaoping Li, Wenwu Cao, and L. E. Cross, "The Extrinsic Nature of Nonlinear Behavior Observed in Lead Zirconate Titanate Ferroelectric Ceramic", *J. Appl. Phys.* vol. 69, pp. 7219-7224, 15 May 1991.

[5] Sadayuki Takahashi, Seiji Hirose, and Kenji Uchino, "Stability of PZT Piezoelectric Ceramics under Vibration Level Change", *J. Am. Cer. Soc.* vol. 77, pp. 2429-2432, 1994.

[6] Q. M. Zhang, H. Wang, and J. Zhao, "Effect of Driving Field and Temperature on the Response Behavior of Ferroelectric Actuator and Sensor Materials", *Journal of Intelligent Material Systems and Structures*, vol. 6, pp. 84-93, January 1995.

[7] V. D. Kugel, Sanjay Chandran, and L. E. Cross, "Caterpillar-Type Piezoelectric d_{33} Bimorph Transducer", Accepted to *Appl. Phys. Lett.* (1996).

[8] R. F. Steidel, Jr., *An Introduction to Mechanical Vibrations*, John Willey & Sons: New York, 1979, pp. 212-216.

[9] V. D. Kugel and L. E. Cross, to be published.

[10] L. D. Landau and E. M. Lifshitz, *Theory of Elasticity*, Pergamon Press, Oxford, 1986, pp. 83-86.

APPENDIX 62

Submitted to Sensors and Actuators A (1996)

Bimorph-Based Piezoelectric Air Acoustic Transducer: Model

V. D. Kugel*, Baomin Xu, Q. M. Zhang, and L. E. Cross

187 Materials Research Laboratory,

The Pennsylvania State University,

University Park, PA 16802

Keywords: piezoelectricity, piezoelectric transducers, bimorph, air acoustics

ABSTRACT

A new type of bimorph-based piezoelectric air transducer with the working frequency range of 200-1000 Hz has been recently developed [1]. In the present work, basic acoustic characteristics of this device and its piezoelectric elements are analyzed. To model the vibration spectrum of the transducer, one-dimensional approach is developed where inertia, elastic and damping forces are included. Analytical equations describing mechanical vibrations and electrical impedance of piezoelectric bimorph cantilevers under external forces are derived. In order to describe various losses in the transducer, complex piezoelectric, dielectric, and elastic constants are used. Results of the modeling are in good accord with experimental data. Suggested model can be used for the device optimization.

* Author to whom correspondence should be addressed. e-mail: vxk7@psuvm.psu.edu

1. Introduction

Piezoelectric ceramics offer many advantages as sensors and actuators. Relatively high coefficient of electromechanical coupling makes it possible to use the material in ultrasonic devices and tweeters. However, in the low frequency applications such as air acoustics, a larger displacement is often required, which is far beyond the range reachable by ceramics materials. In order to overcome this problem, a new type of bimorph-based piezoelectric transducer has been recently suggested [1]. The main peculiarity of this devices is that through double amplification scheme a large displacement can be generated which makes it suitable for acoustic applications at low frequency range such as from 200 to 1000 Hz. It has been demonstrated that the device can a produce a sound pressure level of 90-100 dB that makes this device very attractive for active noise control and flat panel acoustic source [1].

The purpose of this study was to develop a model capable of characterizing the vibration behavior and structure performance relationship of this transducer. The paper is structured as follows. In section 2, an approach that will be used to describe this bimorph-based piezoelectric air transducer is discussed. In section 3, analytical equations describing mechanical vibrations and electrical impedance of piezoelectric bimorph cantilevers are derived. In section 4, calculation of various forces acting in the transducer is carried out. Results of the device modeling and comparison with experimental data are presented in section 5. Finally, in section 6 a summary and conclusions are presented.

2. Model

The piezoelectric transducer to be analyzed consists of two arrays of piezoelectric bimorph cantilevers bridged by a curved diaphragm (Fig. 1); inactive lateral faces are covered with non-radiating plates. The diaphragm serves for acoustic matching: it amplifies the tip displacement of the cantilevers and it also increases the sound-emitting area. Amplification factor K_{amp} is defined as the ratio of the displacement of the diaphragm apex η_d to the tip displacement of the bimorph cantilever $\eta(l)$, where l is the cantilever length (Fig. 1). A typical amplification factor lies in the range of 5 to 20. In a current design the bimorphs are made from soft piezoelectric ceramics PZT5H (Morgan Metroc, Inc) and a loudspeaker paper is used as a triangle-shape diaphragm. Experimental results [2] have demonstrated that if the amplification factor is less than 10 and the length of the diaphragm is less than 50 mm the diaphragm can be considered as a rigid plate without buckling at frequencies below 800-1000 Hz. Therefore for calculating vibrations of the diaphragm the quantities to be evaluated are: the displacement of the moving end of the cantilevers and the amplification factor. It is clear that the interaction between the diaphragm and the piezoelectric elements is through the forces acting in hinges for diaphragm fastening (Fig. 1). We will assume that the transducer is constructed in such a way that in the working range of frequencies the load produced by the diaphragm acts evenly along piezoelectric driving elements of both arrays, i.e., force variation through piezoelectric arrays is neglected. We also will assume that both arrays are equivalent. Under theses conditions, vibrations of the transducer can be analyzed from a one-

dimensional model. Moreover, because of the symmetry it is enough to consider a single piezoelectric element with the corresponding part of the diaphragm (Fig. 2).

In general, vibrating diaphragm generates several types of mechanical forces acting on the bimorph: inertia force $\mathbf{F}_{in}$ that is created by the motion of the mass of the diaphragm, elastic forces $\mathbf{F}_{el}$ that are caused by stiffness of the air enclosed in the cabinet and the stiffness of hinges. The last force is the air damping force $\mathbf{F}_{dm}$ that is caused by the acoustic radiation. The force diagram is shown in Fig. 2 where $\mathbf{R}_1$ and $\mathbf{R}_2$ are the reaction forces and $\mathbf{F}_{push}$ is the force generated by bimorph cantilever, which drives the diaphragm. Introducing $\mathbf{F}_{push}$ makes it possible to analyze separately vibrations of the bimorph cantilever and the motion of the diaphragm. In the model it is assumed, that the hinges for diaphragm fastening generating the elastic force only.

3. Analysis of piezoelectric bimorph cantilever

To define bending vibration of the piezoelectric bimorph cantilever, equations describing vibrations of the neutral surface η of the vibrating beam are used [3]. In the case of the piezoelectric beam, the neutral surface is defined in a such way that any extension strain, even if allowed to exist there, does not contribute a bending moment [3]. The equation of bending of uniform symmetric piezoelectric bimorph beams (in which the thicknesses of two piezoelectric plates are equal) with rectangular cross-section can be written as (Fig. 2)

$$\begin{cases} S_2 = -z\dfrac{\partial^2 \eta}{\partial y^2}, & \text{Mechanical strain of the neutral plane describing bending [3],} \\ S_2 = s_{22}^{\mathrm{E}} T_2 + d_{32} E_3, & -h < z \le h \quad \text{Piezoelectric equation constitutive equation,} \\ E_3 \cong -\dfrac{U}{h}, & 0 < z \le h \quad \text{Electric field across bimorph with parallel connection,} \\ E_3 \cong \dfrac{U}{h}, & -h \le z \le 0 \quad \text{Electric field across the bimorph with parallel connection,} \end{cases} \tag{1}$$

where S_2 is the mechanical strain along the Y axis, s_{22}^{E} is the mechanical compliance, T_2 is the mechanical stress, d_{32} is the piezoelectric coefficient, E is the electric field across the sample, U is the applied voltage, and $2h$ is the bimorph thickness. The neutral surface of the symmetrical bimorph, which is not subjected to external forces and electric fields, lies in the plane of symmetry of the bimorph. A coordinate system XYZ is chosen such that this plane passes through $z = 0$ and the bimorph cantilever is clamped at $y = 0$ (Fig. 2). The translation force F_t that causes the displacement of the neutral plane in the Z direction (Fig. 2) is [3]

$$F_t = \frac{\partial F_s}{\partial y} dy, \tag{2}$$

where F_s is the internal shear force along the Z axis [3]:

$$F_s = -\frac{\partial M}{\partial y}, \tag{3}$$

where M is the internal bending moment along the X axis:

$$M = -\iint_{\text{cross-section}} z T_2 \, dx dz. \tag{4}$$

By using Eqs. (2, 3) the law of linear momentum conservation, i.e.,

$$\dot{F}_t = \rho(2hw)dy\frac{\partial^2\eta}{\partial t^2}, \tag{5}$$

where ρ is the density of the bimorph, w is the width of the bimorph beam, and $2hw$ is the area of the cross-section of the bimorph, can be written as

$$-\frac{\partial^2 M}{\partial y^2} = \rho(2hw)\frac{\partial^2\eta}{\partial t^2}. \tag{6}$$

Substitution of T_2 from Set (1) into Eq. (4) yields

$$M = \frac{2wh^3}{3s_{22}^E}\frac{\partial^2\eta}{\partial y^2} - \frac{Uwhd_{32}}{s_{22}^E}. \tag{7}$$

Thus, one can see that in the case of the symmetrical bimorph beam the external electric tension generates a pure bending moment only. Substituting this expression into Eq. (6), gives

$$\frac{\partial^4\eta}{\partial y^4} + \frac{3\rho s_{22}^E}{h^2}\frac{\partial^2\eta}{\partial t^2} = 0. \tag{8}$$

To find a solution of Eq. (8) the following boundary conditions should be used [4]:

$$\begin{cases} y = 0: \\ \qquad \eta = 0;\ \dfrac{\partial\eta}{\partial y} = 0; \\ y = l: \\ \qquad \dfrac{2wh^3}{3s_{22}^E}\dfrac{\partial^2\eta}{\partial y^2} - \dfrac{Uwhd_{32}}{s_{22}^E} = M_{ex} = 0; \\ \qquad -\dfrac{2wh^3}{3s_{22}^E}\dfrac{\partial^3\eta}{\partial y^3} = F_{ex} \end{cases} \tag{9}$$

where M_{ex} is the x component of the external angular momentum applied at $y=l$; F_{ex} is the z component of the external force acting at the vibrating end of the cantilever. In our

derivations the effect of forces acting along Y and X axes was neglected. Before proceedings further with calculations of force F_{ex} for the transducer under consideration, a general expression for vibrations of the piezoelectric bimorph cantilever under the applied voltage and external forces will be derived. Assuming that harmonic electric voltage $U_m e^{j\omega t}$ is applied to the cantilever and external forces $F_{ex}^m e^{j\omega t}$ are linear functions of the displacement, the displacement of the cantilever can be written as $\eta_m e^{j\omega t}$ where ω is the angular frequency. Therefore Eq. (8) can be written as

$$\frac{\partial^4 \eta_m}{\partial y^4} - \lambda^4 \eta_m = 0, \tag{10}$$

where

$$\lambda^4 = \frac{3\omega^2 s_{22}^E \rho}{h^2}. \tag{11}$$

The solution of Eq. (10) with boundary conditions (9) is

$$\eta_m = \frac{1}{2}\frac{\frac{3}{2}\frac{d_{32}U_m}{\lambda^2 h^2}(cosh[\lambda l]+cos[\lambda l])+\frac{3}{2}\frac{s_{22}^E F_{ex}^m}{\lambda^3 wh^3}(sinh[\lambda l]+sin[\lambda l])}{1+cosh[\lambda l]cos[\lambda l]}(cosh[\lambda y]-cos[\lambda y])+$$
$$\frac{1}{2}\frac{\frac{3}{2}\frac{d_{32}U_m}{\lambda^2 h^2}(-sinh[\lambda l]+sin[\lambda l])-\frac{3}{2}\frac{s_{22}^E F_{ex}^m}{\lambda^3 wh^3}(cosh[\lambda l]+cos[\lambda l])}{1+cosh[\lambda l]cos[\lambda l]}(sinh[\lambda y]-sin[\lambda y]). \tag{12}$$

The resonant frequencies ν_r, which is determined from zero value of the denominator in Eq. (12), coincides with the resonant frequencies of a free piezoelectric cantilever:

$$\cosh[\lambda l]\cos[\lambda l] = -1. \tag{13}$$

In the low-frequency limit $(\lambda l \to 0)$ Eq. (12) may be rewritten as

$$\eta_m = 3d_{32}U_m\left(\frac{y}{2h}\right)^2 - \frac{s_{22}^E F_{ex}^m}{w}\frac{(2y^3 - 6ly^2)}{(2h)^3}. \quad (14)$$

In most practical cases the external force F_{ex} acting at the vibrating end of the piezoelectric cantilever $(y = l)$ is a combination of linear damping, inertia, and elastic forces. For harmonic driving voltage $U_m e^{j\omega t}$ applied to the cantilever these forces are expressed by

$$F_{ex} = K\eta_m e^{j\omega t}, \quad (15)$$

where K is a complex coefficient. Substitution of the force amplitude from Eq. (15) into Eq. (12) produces

$$\eta_m = \frac{3}{4}\frac{d_{32}U_m}{\lambda^2 h^2}\frac{\lambda^3\left(cosh[\lambda l] + cos[\lambda l]\right) + \frac{3}{2}\frac{s_{22}^E K}{wh^3}\left(sinh[\lambda l] - sin[\lambda l]\right)}{\lambda^3\left(1 + cosh[\lambda l]cos[\lambda l]\right) - \frac{3}{2}\frac{s_{22}^E K}{wh^3}\left(cosh[\lambda l]sin[\lambda l] - sinh[\lambda l]cos[\lambda l]\right)} \times$$
$$\left(cosh[\lambda y] - cos[\lambda y]\right) +$$
$$\frac{3}{4}\frac{d_{32}U_m}{\lambda^2 h^2}\frac{\lambda^3\left(-sinh[\lambda l] + sin[\lambda l]\right) - \frac{3}{2}\frac{s_{22}^E K}{wh^3}\left(cosh\, h[\lambda l] - cos[\lambda l]\right)}{\lambda^3\left(1 + cosh[\lambda l]cos[\lambda l]\right) - \frac{3}{2}\frac{s_{22}^E K}{wh^3}\left(cosh[\lambda l]sin[\lambda l] - sinh[\lambda l]cos[\lambda l]\right)} \times$$
$$\left(sinh[\lambda y] - sin[\lambda y]\right). \quad (16)$$

Eq. (16) reveals that the external force of the type (15) changes the resonant characteristics of the vibrating cantilever. If the piezoelectric material has no losses and the external force does not tend to damp vibrations of the bimorph cantilever, i.e., K is real, the resonant frequencies may be calculated from the following equation

$$\lambda^3\left(1 + cosh[\lambda l]cos[\lambda l]\right) - \frac{3}{2}\frac{s_{22}^E K}{wh^3}\left(cosh[\lambda l]sin[\lambda l] - sinh[\lambda l]cos[\lambda l]\right) = 0. \quad (17)$$

As follows from Eq. (16) the displacement of the moving end ($y = l$) is

$$\eta_m(l) = \frac{3}{2}\frac{d_{32}U_m}{h^2}\frac{\lambda\, sinh[\lambda l]sin[\lambda l]}{\lambda^3\left(1+cosh[\lambda l]cos[\lambda l]\right)-\frac{3}{2}\frac{s_{22}^E K}{wh^3}\left(cosh[\lambda l]sin[\lambda l]-sinh[\lambda l]cos[\lambda l]\right)}. \tag{18}$$

Apparently, the amplitude of the tip displacement is equal to zero when $sin(\lambda l) = 0$ and the value of the corresponding frequency does not depend on external loading. It can also be shown that the lowest frequency of the zero vibrations is about 2.8 times higher than the fundamental frequency of bending vibrations of unloaded cantilever. In the low-frequency limit Eq. (18) may be written as

$$\eta_m(l) = \frac{3}{2}\frac{d_{32}U_m}{h^2}\frac{l^2}{2-\frac{s_{22}^E K(0) l^3}{wh^3}}, \tag{19}$$

where $K(0)$ is the low-frequency value of the force coefficient (15).

To calculate the electrical impedance of the piezoelectric bimorph cantilever we will start with the piezoelectric constitutive equations:

$$\begin{cases} S_2 = s_{22}^E T_2 + d_{32} E_3, \\ D_3 = d_{32} T_2 + \varepsilon_{33}^T E_3, \end{cases} \quad -h < z \le h, \tag{20}$$

where D_3 is the component of electric displacement along the Z axis. Using Eqs. (1) and (20) one can get

$$D_3 = -z\frac{\partial^2 \eta}{\partial y^2}\frac{d_{32}}{s_{22}^E} + \left(\varepsilon_{33}^T - \frac{d_{32}^2}{s_{22}^E}\right)E_3. \tag{21}$$

Total charge on the surfaces of the bimorph $(z = \pm h)$, Q_s, can be written as [5]:

$$Q_s = -\iint_{\text{electrode surface}} D_3(h)dS + \iint_{\text{electrode surface}} D_3(-h)dS. \tag{22}$$

Substituting (21) into (22) gives

$$Q_s = 2\frac{d_{32}}{s_{22}^E} hw\left(\frac{\partial \eta}{\partial y}_{|y=l} - \frac{\partial \eta}{\partial y}_{|y=0}\right) - \left(\varepsilon_{33}^T - \frac{d_{32}^2}{s_{22}^E}\right)\iint_{\text{electrode surface}} (E_3(h) - E_3(-h))dxdy. \tag{23}$$

Electrical current through the bimorph can be written as

$$I = \frac{dQ_s}{dt} = j\omega Q_s \tag{24}$$

and the electrical admittance of the bimorph using boundary conditions at $y=0$ (9) is

$$Y = j\omega\left(2\frac{d_{32}}{s_{22}^E} hw\frac{\partial \eta}{\partial y}_{|y=l} - \left(\varepsilon_{33}^T - \frac{d_{32}^2}{s_{22}^E}\right)\iint_{\text{electrode surface}} (E_3(h) - E_3(-h))dxdy\right)\frac{1}{U_m}. \tag{25}$$

Using Eqs. (1) and (16) one can get the numerical value of electrical admittance of the piezoelectric bimorph cantilever. Analysis shows that at frequencies far below the fundamental bending resonance this numerical value is slightly higher than experimental one. The reason for this is that in the calculation an approximate electric field (Eq. (1)) was used.

4. Calculation of vibrations of the piezoelectric cantilever loaded with the diaphragm

To evaluate vibrations of the piezoelectric cantilever loaded with diaphragm (Figs. 1 and 2) by means of Eq. (16), external mechanical force F_{ex} acting on the vibrating end of the cantilever along the Z axis should be determined (forces acting along the Y axis are

neglected). This force may be calculated using the laws of angular and linear momentum conservation [6] for the diaphragm:

$$\begin{aligned}
&\mathbf{r}\times\left(\mathbf{R}_1+\mathbf{R}_2+\mathbf{F}_{\text{push}}+\mathbf{F}_{\text{el}}\right)+\int_{\text{diaphragm}}\mathbf{r}\times\mathbf{F}_{\text{in}}dV+\int_{\text{diaphragm}}\mathbf{r}\times\mathbf{F}_{\text{dm}}dS=\frac{d}{dt}\left(\int_{\text{diaphragm}}(\mathbf{r}\times\rho_d\mathbf{v})dV\right),\\
&\mathbf{R}_1+\mathbf{R}_2+\mathbf{F}_{\text{push}}+\mathbf{F}_{\text{el}}+\int_{\text{diaphragm}}\mathbf{F}_{\text{in}}dV+\int_{\text{diaphragm}}\mathbf{F}_{\text{dm}}dS=\frac{d}{dt}\left(\int_{\text{diaphragm}}\rho_d\mathbf{v}dV\right),
\end{aligned} \tag{26}$$

where $\mathbf{v}(\mathbf{r})$ is the diaphragm velocity. Assuming that the thickness of the diaphragm is small, volume integrals in Eq. (26) can be transformed to surface integrals. The air damping force (surface density) $\mathbf{F}_{\text{dm}}$ can be written as [7]:

$$\mathbf{F}_{\text{dm}}=-k_{\text{v}}\mathbf{v}, \tag{27}$$

where k_{v} is the damping coefficient depending on the shape of the transducer (it is directly related to the acoustic impedance of the transducer [7]). By substituting various quantities, set of equations (2) in $X'Y'Z'$ coordinate system can be transformed to

$$\begin{aligned}
&-F_{\text{push}}+F_{el}+R_1+k_{\text{v}}\frac{wL_{\text{d}}^2}{2}\sin\varphi\frac{d\varphi}{dt}=-\rho_{\text{d}}\frac{t_{\text{d}}wL_{\text{d}}^2}{2}\left(\sin\varphi\frac{d^2\varphi}{dt^2}+\cos\varphi\left[\frac{d\varphi}{dt}\right]^2\right), && Z' \text{ axis}\\
&R_2-P_{\text{in}}-k_{\text{v}}\frac{wL_{\text{d}}^2}{2}\cos\varphi\frac{d\varphi}{dt}=\rho_{\text{d}}\frac{t_{\text{d}}wL_{\text{d}}^2}{2}\left(\cos\varphi\frac{d^2\varphi}{dt^2}-\sin\varphi\left[\frac{d\varphi}{dt}\right]^2\right), && Y' \text{ axis}\\
&R_1\sin\varphi-R_2\cos\varphi+\frac{P_{\text{in}}}{2}\cos\varphi+k_{\text{v}}\frac{wL_{\text{d}}^2}{6}\frac{d\varphi}{dt}=-\rho_{\text{d}}\frac{t_{\text{d}}wL_{\text{d}}^2}{6}\frac{d^2\varphi}{dt^2}, && X' \text{ axis}
\end{aligned} \tag{28}$$

where P_{in} is the weight of the one half of the diaphragm with the width w and φ is the angle between the diaphragm and Z' axis (Fig. 2). From set of equations (28) one can solve the magnitude of $\mathbf{F}_{\text{push}}$ acting along the Z' axis:

$$F_{\text{push}} = \frac{F_{\text{in}}}{2} ctn\varphi + \frac{1}{3} k_v w L_d^2 \frac{1}{\sin\varphi} \frac{d\varphi}{dt} + \frac{1}{3} \rho_d t_d w L_d^2 \frac{1}{\sin\varphi} \frac{d^2\varphi}{dt^2} + F_{\text{el}},$$
$$\mathbf{F}_{\text{push}} = -\mathbf{k} F_{\text{push}}, \tag{29}$$

where **k** is the unit vector along the Z axis. Right hand side of the first equation in (29) is the external force F_{ex} acting at the moving end of the bimorph cantilever parallel to the Z axis since according to Newton's third law $\mathbf{F}_{\text{ex}} = -\mathbf{F}_{\text{push}}$ and the Z and Z' axes coincide. Clearly, the external force F_{ex} is a non-linear one in a general case since $ctn\varphi$ and $\sin\varphi$ are non-linear functions of φ and, hence, displacement. For air acoustic transducer it is desirable to work in a linear regime when the amplitude of the diaphragm vibrations is much lesser than the diaphragm height h_d (Fig. 1). In this case:

$$ctn\varphi \cong \frac{1}{\sin\varphi} \cong \frac{L_d}{h_d},$$
$$\frac{d\varphi}{dt} \cong -\frac{1}{h_d} \frac{d\eta}{dt}_{|y=l}, \tag{30}$$
$$K_{\text{amp}} = \frac{L_d}{h_d}.$$

Therefore the displacement of the diaphragm apex η_d is

$$\eta_d = K_{\text{amp}} \eta(l). \tag{31}$$

We also assume that the elastic force is linear:

$$F_{\text{el}} = -k_{spr} \eta(l), \tag{32}$$

where k_{spr} is the equivalent spring constant of the air enclosed in the cabinet and hinges (Fig. 1). Thus, under linear approximation F_{ex} can be expressed as:

$$F_{\text{ex}} = K_{\text{amp}} \frac{F_{\text{in}}}{2} - \frac{1}{3} K_{\text{amp}}^2 \left(k_v w L_d \frac{d\eta}{dt}_{|y=l} + \rho_d t_d w L_d \frac{d^2\eta}{dt^2}_{|y=l} \right) - k_{spr} \eta(l). \tag{33}$$

Since for harmonic excitation the tip displacement of the bimorph cantilever can be written as $\eta_m e^{j\omega t}$, Eq. (33) can be rewritten as:

$$F_{ex} = K_{amp}\frac{F_{in}}{2} + \eta_m(l)e^{j\omega t}\left(-\frac{1}{3}K_{amp}^2\left(k_v w L_d j\omega - \rho_d t_d w L_d \omega^2\right) - k_{spr}\right). \quad (34)$$

First term in Eq. (34) produces constant deflection only, therefore it can be neglected in calculations of the spectrum of vibrations. Comparing Eqs. (15) and (34) one can find coefficient K in the expression of the tip displacement (Eq. (18)):

$$K = -\left(\frac{1}{3}K_{amp}^2\left(k_v w L_d j\omega - \rho_d t_d w L_d \omega^2\right) + k_{spr}\right). \quad (35)$$

Thus, vibrations of the bimorph cantilever and diaphragm can be calculated by means of Eqs. (11), (18), (31), (35).

5. Results of modeling

The strategy in calculating the spectrum of the diaphragm vibrations was as follows. Initially, electromechanical properties of the piezoelectric bimorphs were determined by experimental studying characteristics of the ceramics and vibration spectrum of unloaded piezoelectric bimorph cantilevers. Then, these data were used to calculate the vibrations of the cantilevers loaded with the diaphragm. Since the equivalent spring constant k_{spr} of the air enclosed in the cabinet and hinges was unknown, its value was determined experimentally by measuring the diaphragm vibrations at low frequencies under the assumption that k_{spr} is frequency independent. As follows from Eqs. (19), (30),

(31), (35), the magnitude of low-frequency vibrations of the diaphragm apex is directly related to the spring constant:

$$\eta_d = \frac{3}{2} d_{32} U_m \left(\frac{l}{h}\right)^2 \frac{1}{2 - \frac{s_{22}^E k_{spr}}{w}\left(\frac{l}{h}\right)^3} K_{amp}. \quad (36)$$

To determine of the damping coefficient k_v, it was assumed that the vibrating diaphragm behaves as a baffled piston [7]:

$$k_v = 2\rho_{air} c_{air} \left(\frac{\left[2\pi \nu r_{eq}\right]^2}{2 c_{air}^{\ 2}} + j \frac{16}{3} \frac{\nu r_{eq}}{c_{air}} \right), \quad (37)$$

where ρ_{air} is the air density, c_{air} is the sound velocity in the air, ν is the frequency, and r_{eq} is the equivalent radius of the transducer diaphragm with the area $A = 2L_d w_d$, $r_{eq} = \sqrt{A/\pi}$.

Thus, the procedure described above made it possible to determine all parameters essential for calculating vibration spectrum of the transducer. It is important to note that complex piezoelectric, dielectric, and elastic constants should be determined for including losses in the piezoelectric elements. Parameters of the diaphragm and piezoelectric bimorph cantilevers used in the transducer are given in the Table 1 [1].

Soft piezoelectric ceramics was used for the bimorph fabricating [1]. It is known that electromechanical properties of these piezoelectric bimorph cantilevers are highly dependent on the magnitude of the applied electric field [8]. Found in [8] and [9] electromechanical coefficients of PZT5H ceramics for the electric field E=0.71 kV/cm rms are shown in the Table 2. Frequency dispersion of these coefficients was neglected in the device modeling since it is not significant in the working frequency range. Calculated vibration spectrum of the unloaded bimorph cantilever is shown in Fig. 3. Resonant

frequency at 0.71 kV/cm was ν_r=1044 Hz and the mechanical quality factor was Q_m=10.1. At small electric fields (E<0.01 kV/cm) the corresponding parameters ν_r=1167 and Q_m=55 were the same as the experimental data [1]. It should be noted that the vibration amplitude at the resonance depends on the mechanical losses. As follows from Eq. (18), complex amplitude of the tip displacement of the unloaded bimorph (K=0) with low losses can be written as:

$$\eta_m(l)=\frac{3}{2}\frac{|d_{32}|U_m e^{-j\left(\theta_d-\frac{\theta_s}{2}\right)}}{h^2|\lambda|^2}\frac{sinh|\lambda l|\,sin|\lambda l|-j|\lambda l|\frac{\theta_s}{4}\left(cosh|\lambda l|\,sin|\lambda l|+sinh|\lambda l|\,cos|\lambda l|\right)}{1+cosh|\lambda l|\,cos|\lambda l|+j|\lambda l|\frac{\theta_s}{4}\left(cosh|\lambda l|\,sin|\lambda l|-sinh|\lambda l|\,cos|\lambda l|\right)}, \tag{38}$$

where θ_d is the phase of the piezoelectric coefficient d_{32} and θ_s is the phase of the mechanical compliance s_{22}^E. At the fundamental frequency of bending vibrations (λl=1.875) Eq. (38) gives:

$$\eta_m^{\nu_r}(l)=3U_m\left(\frac{l}{2h}\right)^2|d_{32}|\frac{0.89}{\theta_s}e^{-j\left(\frac{\pi}{2}+\theta_d-0.16\theta_s\right)} \tag{39}$$

Thus, the amplitude of the resonant displacement is inversely proportional to the phase of the mechanical compliance.

Calculated vibration spectrum of the diaphragm apex is shown in Fig. 4. Magnitude of the equivalent spring constant (N/m) shown in the Fig. 4 is for the width of the part of the diaphragm w driven by one bimorph (w=5 mm). Clearly, at the low loss limit the value of the resonance frequency derived from the model does not depend on the losses of the equivalent spring constant and it reproduces the experimental values $\nu_r \cong 550$ Hz. Nevertheless, only k_{spr} having imaginary part can fit the amplitude of the

diaphragm vibrations at the resonance. These results indicate that the elastic force caused by hinges and the air enclosed in the cabinet has losses. Thus, the model developed is capable of describing basic characteristics of the vibration spectrum of the transducer.

As seen from Fig. 4 the width of the experimental peak is narrower than that of the theoretical one. It may be caused by an increase in the amplification factor of the diaphragm (Eq. (31)) around the resonant frequency that was observed experimentally. Nonlinear dependence of electromechanical properties on the level of vibrations maybe another reason for this discrepancy. Data of Fig. 4 show that the model cannot describe minimum in the diaphragm vibrations observed near 800 Hz. Experimental study of the frequency dependence of the amplification factor K_{amp} of the diaphragm shows that the diaphragm has its own bending resonance near this frequency, i.e., it does not keep its shape. Additional factor that can affect the diaphragm vibrations at high frequencies is losses in the hinges.

The model developed makes it possible to analyze mechanical vibrations and sound pressure generated by the transducer for various dimensions of the diaphragm and piezoelectric elements. Vibration characteristics and on-axis sound pressure at the distance r=1 m for different thicknesses of cantilevers and constant rms magnitude of the electric field E=0.71 kV/cm are shown in Fig. 5. Complex value of the spring constant $k_{spr} = 9500(0.916 + 0.4j)$ N/m was used in the modeling. The sound pressure p of the transducer was calculated assuming that the transducer behaves as a baffled piston [7]:

$$p = 2\pi\nu^2 A\rho_{air}\overline{\eta}_d, \tag{40}$$

where $\overline{\eta}_d$ is the average amplitude (rms) of the diaphragm vibrations, $\overline{\eta}_d \cong 0.5\eta_d$. The calculated value of the sound pressure for $2h$=1 mm is close to the experimental one [1]. It should be noted that the results of the model (Fig. 5) are valid for the given equivalent spring constant only. As is seen from the Fig. 5 the optimal value of the bimorph thickness lies between 1 and 1.5 mm. Clearly, sound pressure developed by the transducer sharply decreases below 300 Hz. Data of Fig. 5 shows that the resonant frequency of the transducer is highly dependent on the thickness of piezoelectric elements.

The model developed makes also possible to analyze the change in the resonant frequency of a double-amplifying structure [1]. The structure consists of two piezoelectric bimorph cantilever bridged by a triangular diaphragm (as in the air transducer but much narrower in the x direction and without non-radiating plates covering inactive sides). Assuming that the spring constant and air damping coefficient in this structure are equal to zero, Eq. (17) can be rewritten as:

$$\lambda^3\left[1+cosh[\alpha]cos[\alpha]-\frac{1}{3}K_{amp}^2\frac{m_d}{m}\alpha(cosh[\alpha]sin[\alpha]-sinh[\alpha]cos[\alpha])\right]=0, \qquad (41)$$

where $\alpha=\lambda l$, m_d is the mass of the one half of the diaphragm and m is the mass of the piezoelectric cantilever. The value α obtained from Eq. (41) is directly related to the resonant frequency of the double-amplifying structure,

$$\nu_r=\frac{\alpha^2}{4\pi}\frac{2h}{l^2}\frac{1}{\sqrt{3s_{22}^E\rho}}. \qquad (42)$$

Results of modeling and experimental data for the structure with $2h$=1 mm, w=7 mm, l=20 mm, m=1.092 g, L_d=25 mm, and m_d=0.057 g are given in Fig. 6. As is seen from the Figure, Eq. (41) describes very well experimental data for the apex height above 1.5 mm.

Below this height the thickness of the diaphragm, t_d=0.59 mm, becomes comparable with the height of the diaphragm apex that can increase the contribution of elastic forces and bending moments in the hinges.

6. Conclusions

In this work, a model describing basic acoustic characteristics of the bimorph-based piezoelectric transducer [1] has been developed. One-dimensional approach was suggested in which inertia, elastic and damping forces are included. As integral part of this model, analytical equations describing the spectrum of mechanical vibrations and electrical impedance of piezoelectric bimorph cantilevers under external forces was derived. In the model, complex electromechanical parameters of the transducer were used to include losses in the transducer. Results of modeling and experimental data are in good agreement. The model developed can be used for optimizing acoustics characteristics of the transducer.

Nomenclature

h_d height of the diaphragm apex

$2L_d$ length of the diaphragm

w_d width of the diaphragm

t_d thickness of the diaphragm

η_d displacement of the diaphragm apex

$\overline{\eta}_d$ average displacement of the diaphragm

ρ_d density of the diaphragm

m_d mass of the part of diaphragm acting on piezoelectric bimorph cantilever

$2h$ thickness of piezoelectric bimorph cantilever

l length of the piezoelectric bimorph cantilever

w width of piezoelectric bimorph cantilever

η displacement of the of the neutral plane of the piezoelectric bimorph cantilever

η_m amplitude of the displacement of the of the neutral plane of the piezoelectric bimorph cantilever

$\eta_m^{v_r}$ amplitude of the displacement of the of the neutral plane of the piezoelectric bimorph cantilever at resonance

ρ density of the piezoelectric bimorph cantilever

m mass of the piezoelectric bimorph cantilever

s_{22}^E y component of the mechanical compliance of the piezoelectric bimorph cantilever

d_{32} piezoelectric coefficient along the Y axis

θ_d phase angle of the piezoelectric coefficient d_{32}

θ_s phase angle of the mechanical compliance s_{22}^E

λ wave coefficient describing bending vibrations of the piezoelectric bimorph cantilever

ω angular frequency

v frequency

ν_r is the fundamental frequency of bending vibrations

φ angle between the diaphragm and Z' axis

j imaginary unit

r_{eq} equivalent radius of the diaphragm

c_{air} sound velocity in the air

k_v air damping coefficient

ρ_{air} density of the air

p sound pressure

α coefficient determining the resonant frequency of the loaded piezoelectric bimorph cantilever

k_{spr} equivalent spring constant

t time

x, y, z rectangular Cartesian coordinates

k unit vector along the Z axis

r radius-vector in the $X'Y'Z'$ coordinate system

v diaphragm velocity

XYZ, $X'Y'Z'$ Cartesian coordinate systems

A area of the diaphragm

E_3 electrical field along the Z axis

D_3 electric displacement along the Z axis

I electrical current through the piezoelectric bimorph cantilever

K_{amp} amplification factor of the diaphragm

Q_s total electric charge on surfaces of the piezoelectric bimorph cantilever

S_2 mechanical strain along the Y axis

U voltage across the piezoelectric bimorph cantilever

U_m amplitude of the voltage across the piezoelectric bimorph cantilever

Y electrical admittance of the piezoelectric bimorph cantilever

F_{el} elastic force acting along the Z'axis

F_{ex} external force acting along the Z axis

F_{ex}^{m} amplitude of the external force acting along the Z axis

F_{in} inertia force directed along the Y' axis

F_s internal shear force along the Z axis

F_t internal translation force along the Z axis

K complex force coefficient

M internal bending moment along the X axis

M_{ex} external bending moment along the X axis

$\mathbf{F}_{el}$ vector elastic force

$\mathbf{F}_{in}$ vector inertia force (volume density)

$\mathbf{F}_{dm}$ vector air-damping force (surface density)

$\mathbf{F}_{push}$ vector force driving the diaphragm

$\mathbf{R}_1$, $\mathbf{R}_2$ vector reaction forces

$\mathbf{P}$ vector of spontaneous polarization

Acknowledgment

This work was supported by the Office of Naval Research under the contract N00014-94-1-1140.

References

[1]. Baomin Xu, Qiming Zhang, V. D. Kugel, and L. E. Cross, Piezoelectric air transducer for active noise control, Proceedings of SPIE, 2717, (1996) 388-398.

[2]. V. D. Kugel and L. E. Cross, unpublished.

[3]. T. Ikeda, *Fundamentals of Piezoelectricity,* Oxford University Press, Oxford, 1990. pp. 105-107, 246-249.

[4]. L. D. Landau and E. M. Lifshitz, *Theory of Elasticity,* Pergamon Press, Oxford, 1986. pp. 71-83.

[5]. C. R. Paulans S. A. Nasar, *Introduction to Electromagnetic Field,* McGraw-Hill, New York, 1987. pp. 127-131.

[6]. J. Zelenka, *Piezoelectric Resonators and their Applications,* ELSEVIER, Amsterdam, 1986. pp. 64-66.

[7]. D. E. Hall, *Basic Acoustics,* HARPER & ROW, New York, 1987. pp. 161-182, 232-235, 262-268.

[8]. V. D. Kugel, Q. M. Zhang, Baomin Xu, Qing-ming Wang, Sanjay Chandran, and L. E. Cross, Behavior of Piezoelectric Actuators under High Electric Field, Accepted to *IEEE Proceedings on Application of Ferroelectrics, ISAF'96* (1996).

[9]. V. D. Kugel and L. E. Cross, unpublished.

Biographies

Valery D. Kugel received his M.Sc. degree in EE from Riga Polytechnic Institute, Latvia in 1984 and the Ph.D. degree in EE (Ferroelectricity) from Tel Aviv University, Israel in 1995. He is currently a Postdoctoral fellow at the Materials Research Lab of the Pennsylvania State University. His research interests include ferroelectricity, piezoelectric, pyroelectric, and dielectric materials and devices for sensor, actuator and transducers applications.

Baomin Xu received the B. Sc. degree in materials science from Tsinghua University, China in 1986 and the Ph.D. degree in ceramics from Shanghai Institute of Ceramics, Chinese Academy of Sciences in 1991. He is currently a Postdoctoral fellow at the Materials Research Lab of the Pennsylvania State University. His research interests involve piezoelectric materials and devices for sensor, actuator and transducer applications, dielectric materials and ceramic processing. Dr. Xu is a member of the American Ceramic Society.

Q. M. Zhang is currently an Associate Professor of Electrical Engineering at the Materials Research Laboratory and Department of Electrical Engineering of the Pennsylvania State University. His research interests involve ferroelectric ceramic, polymer, and composite for actuator, sensor, and transducer applications; new design and modeling of piezocomposites; characterization of piezoelectric and electrostrictive effects in ferroelectrics; smart materials and structures; effect of defect structure on electromechanical properties of ferroelectrics; structural studies of interfaces in

ferroelectrics. Dr. Zhang is a member of IEEE, American Ceramic Society, and Materials Research Society.

L. Eric Cross is Evan Pugh Professor of Electrical Engineering at the Pennsylvania State University. His research interests are in dielectric and ferroelectric crystals; piezoelectric and electrostrictive ceramics; composites for sensor , actuator and transducer applications, and as components in "smart" materials and structures. He has co-authored mere than 500 technical papers, and sections of six books. Dr. Cross is a member of the National Academy of Engineering, a Fellow of the American Institute of Physics, of the American Ceramic Society, and the American Optical Society, and a member of the Japanese Physical Society. He is chairman of the IEEE Committee of Ferroelectrics, US representative for ferroelectrics on IUPAP, and a member of the Defense Sciences Council of ARPA.

CAPTIONS OF FIGURES

Fig. 1 Schematic view of bimorph-based piezoelectric air transducer with double amplification.

Fig. 2. Diagram of the forces included in one-dimensional model. **P** denotes the vector of spontaneous polarization in the piezoelectric bimorph cantilever.

Fig. 3. Spectrum of mechanical vibrations of unloaded piezoelectric bimorph cantilever.

Fig. 4. Comparison between experimental and theoretical magnitudes of the vibrations of the diaphragm apex.

Fig. 5. Theoretical diaphragm vibrations and on-axis sound pressure at the distance r=1 m under electric field E=0.71 kV/cm rms for different thicknesses of cantilevers.

Fig. 6. Theoretical and experimental dependencies of the fundamental resonance on the height of the diaphragm apex in the double-amplifying structure. Material of the piezoelectric bimorphs: soft piezoelectric ceramics 3203HD (Motorola).

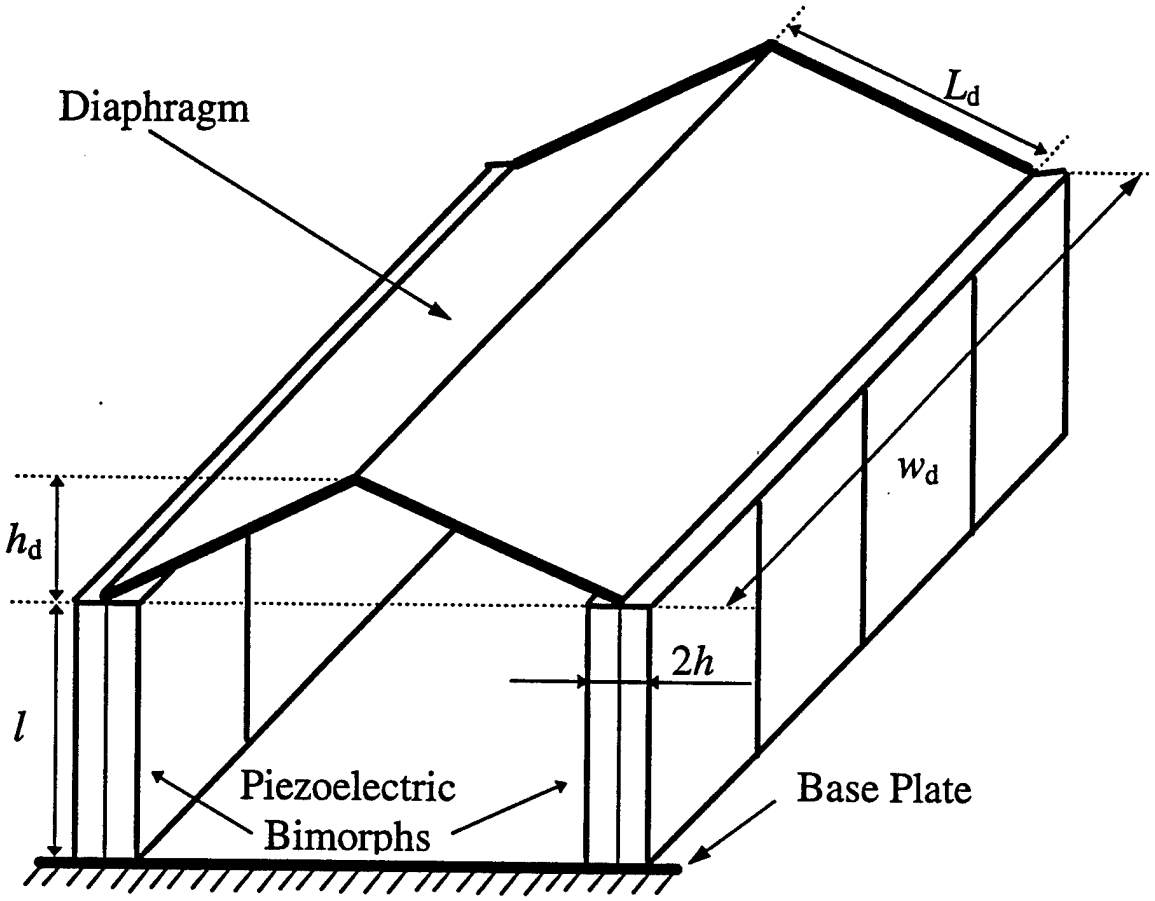

Fig. 1

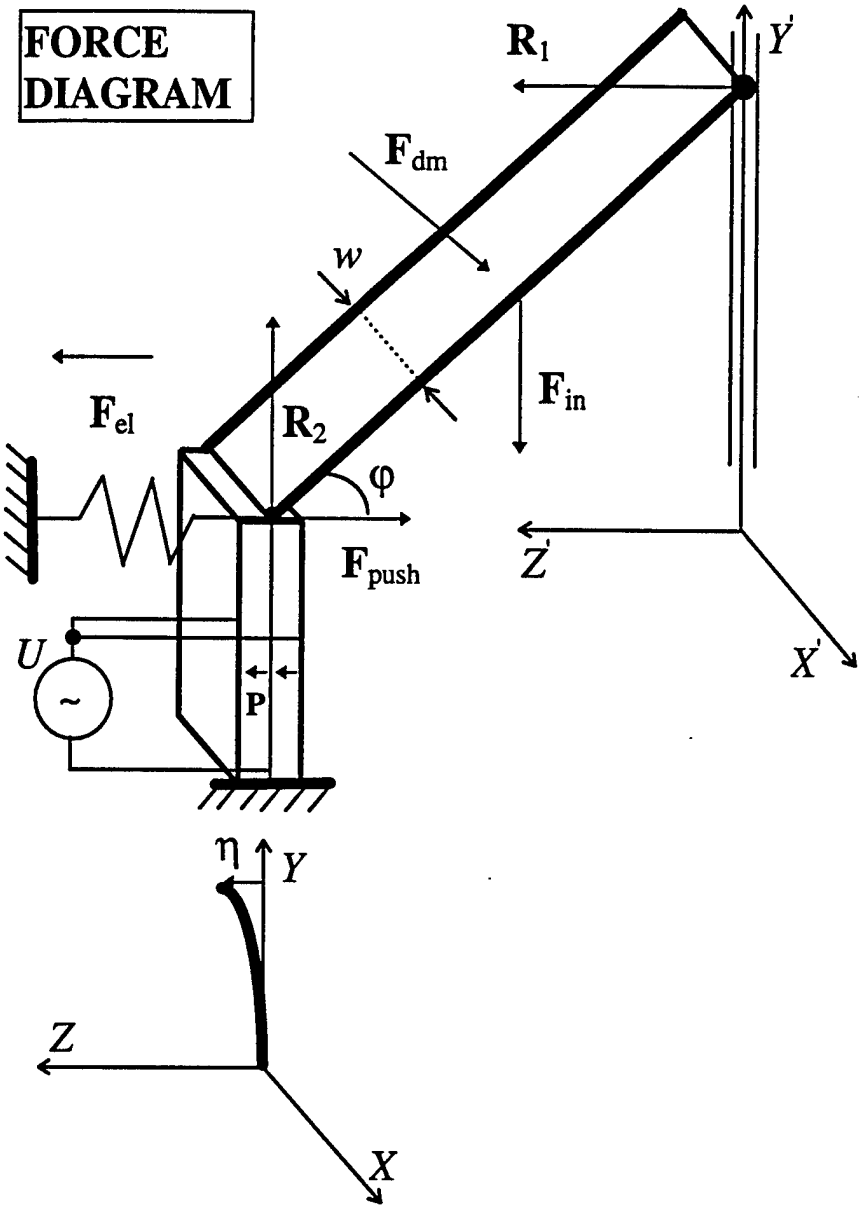

Fig. 2

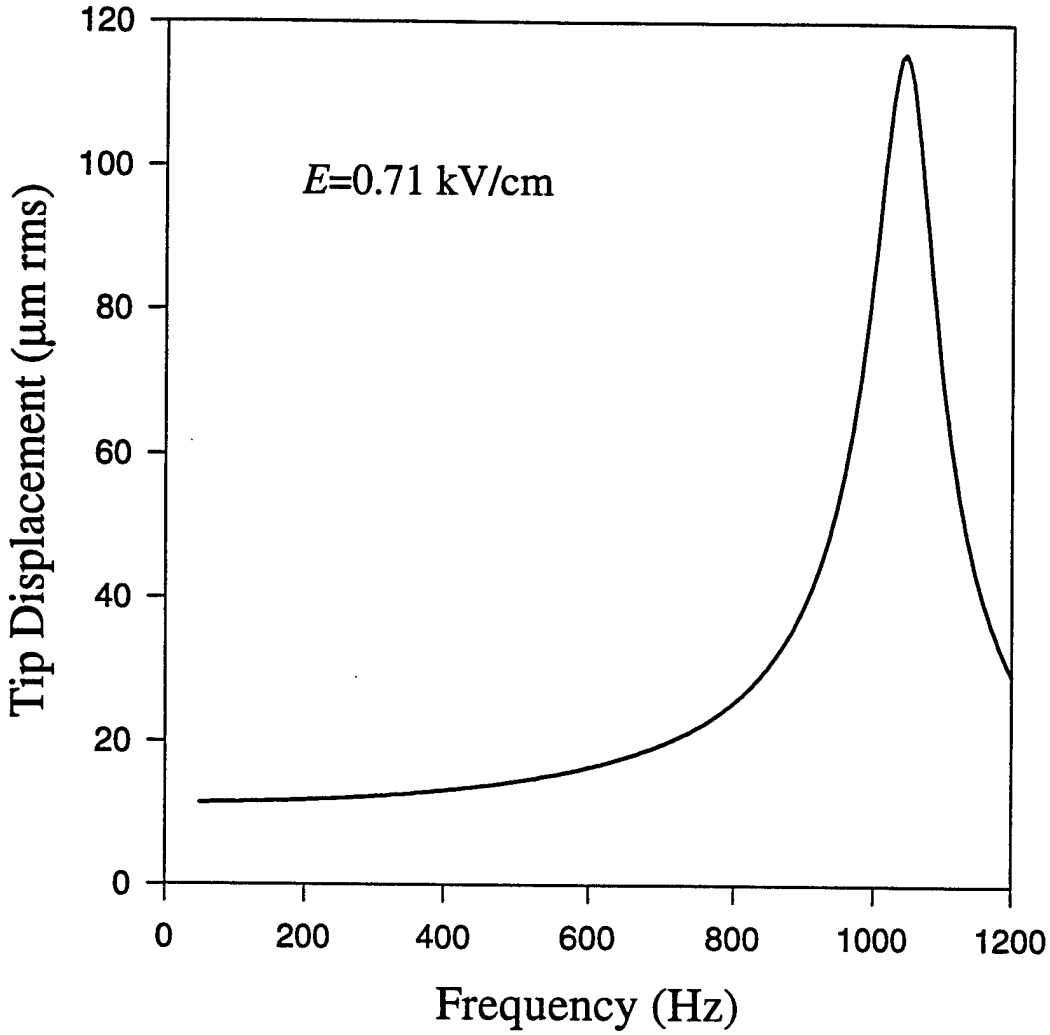
120
100
80
60
40
20
0
Tip Displacement (μm rms)
E=0.71 kV/cm
0
200
400
600
800
1000
1200
Frequency (Hz)

Fig. 3

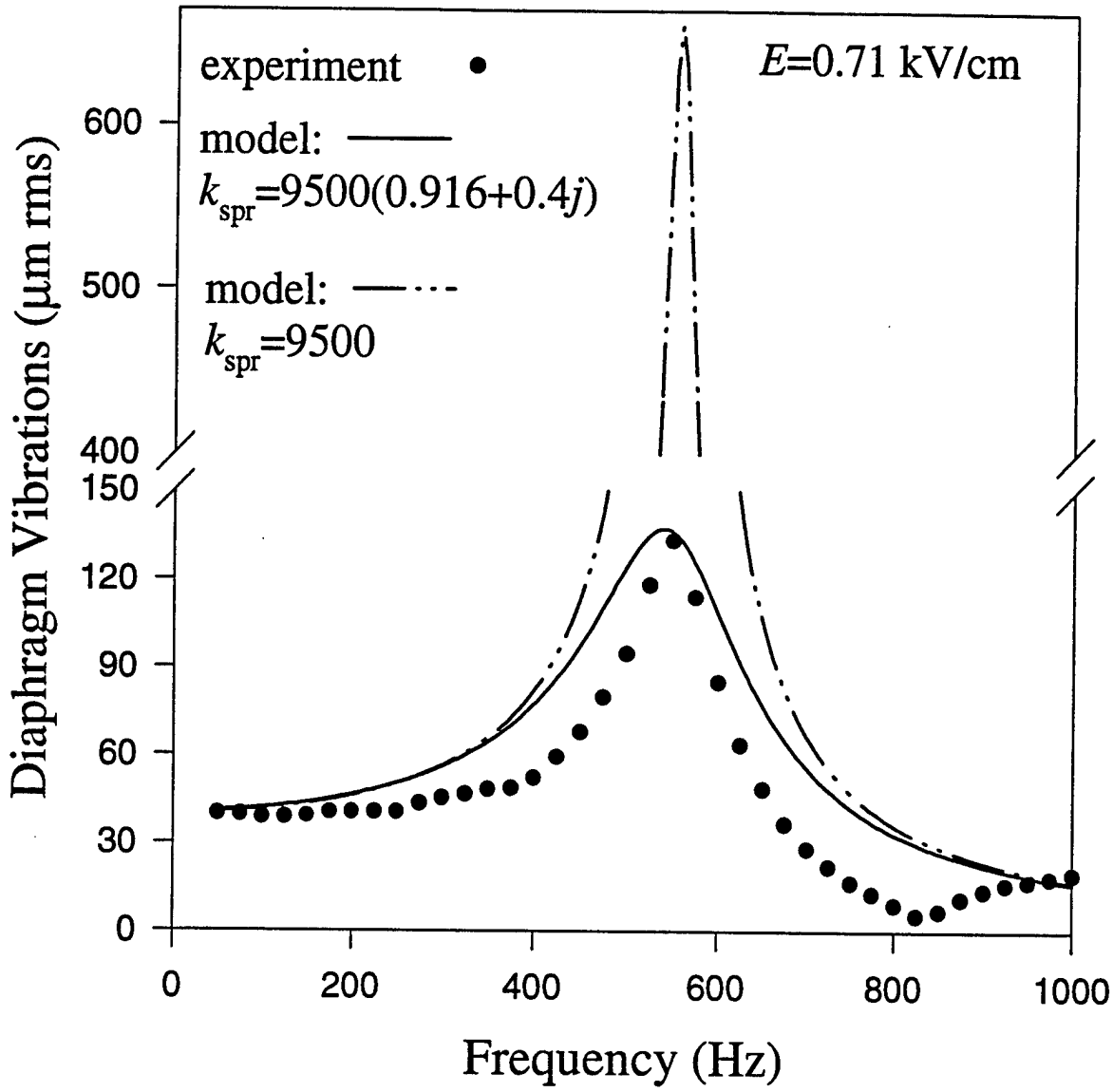
experiment
model:
k_{spr}=9500(0.916+0.4j)
model:
k_{spr}=9500
E=0.71 kV/cm
Diaphragm Vibrations (μm rms)
600
500
400
150
120
90
60
30
0
0
200
400
600
800
1000
Frequency (Hz)

Fig. 4

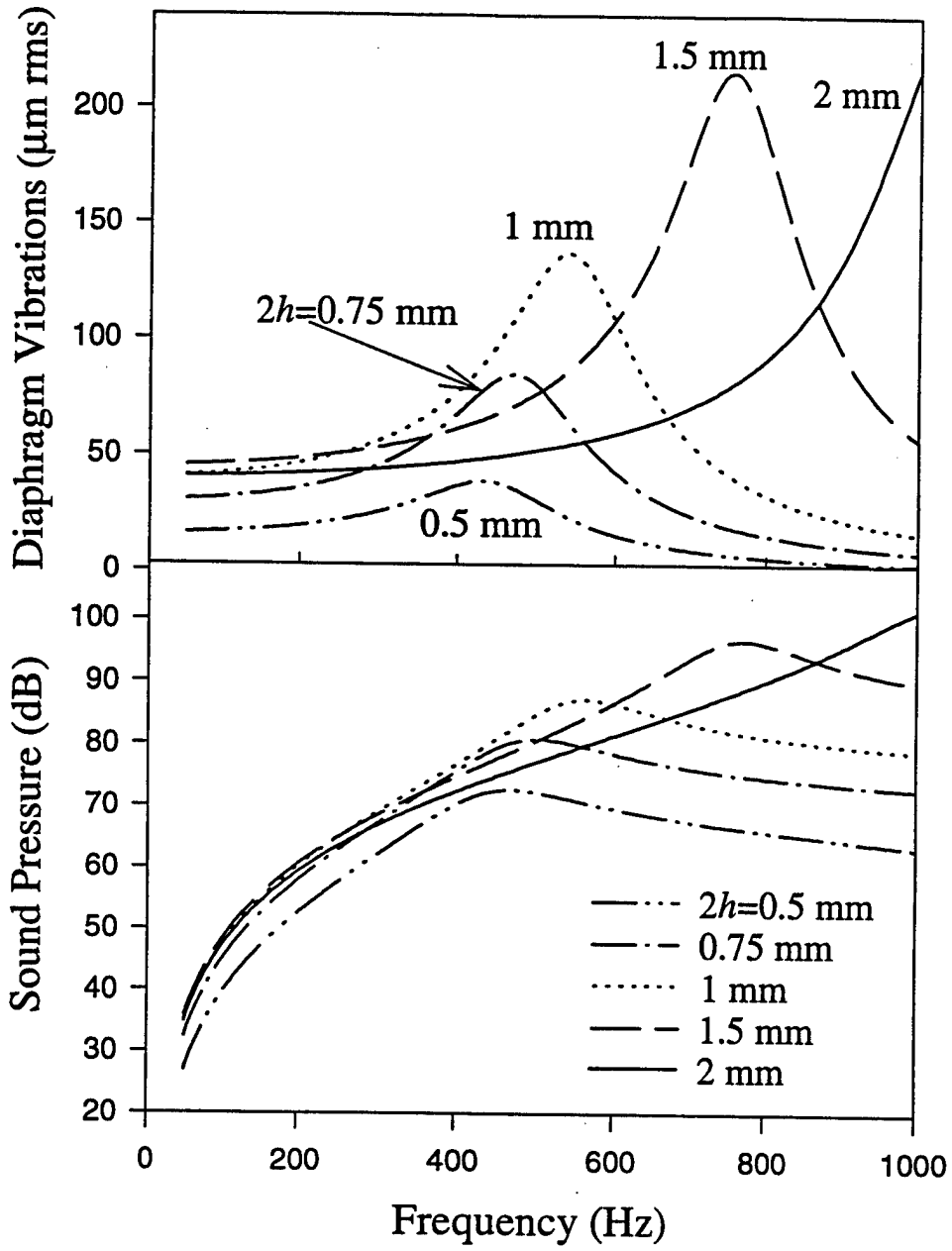
Diaphragm Vibrations (μm rms)
200
150
100
50
0
1.5 mm
2 mm
1 mm
2h=0.75 mm
0.5 mm
Sound Pressure (dB)
100
90
80
70
60
50
40
30
20
2h=0.5 mm
0.75 mm
1 mm
1.5 mm
2 mm
0
200
400
600
800
1000
Frequency (Hz)

Fig. 5

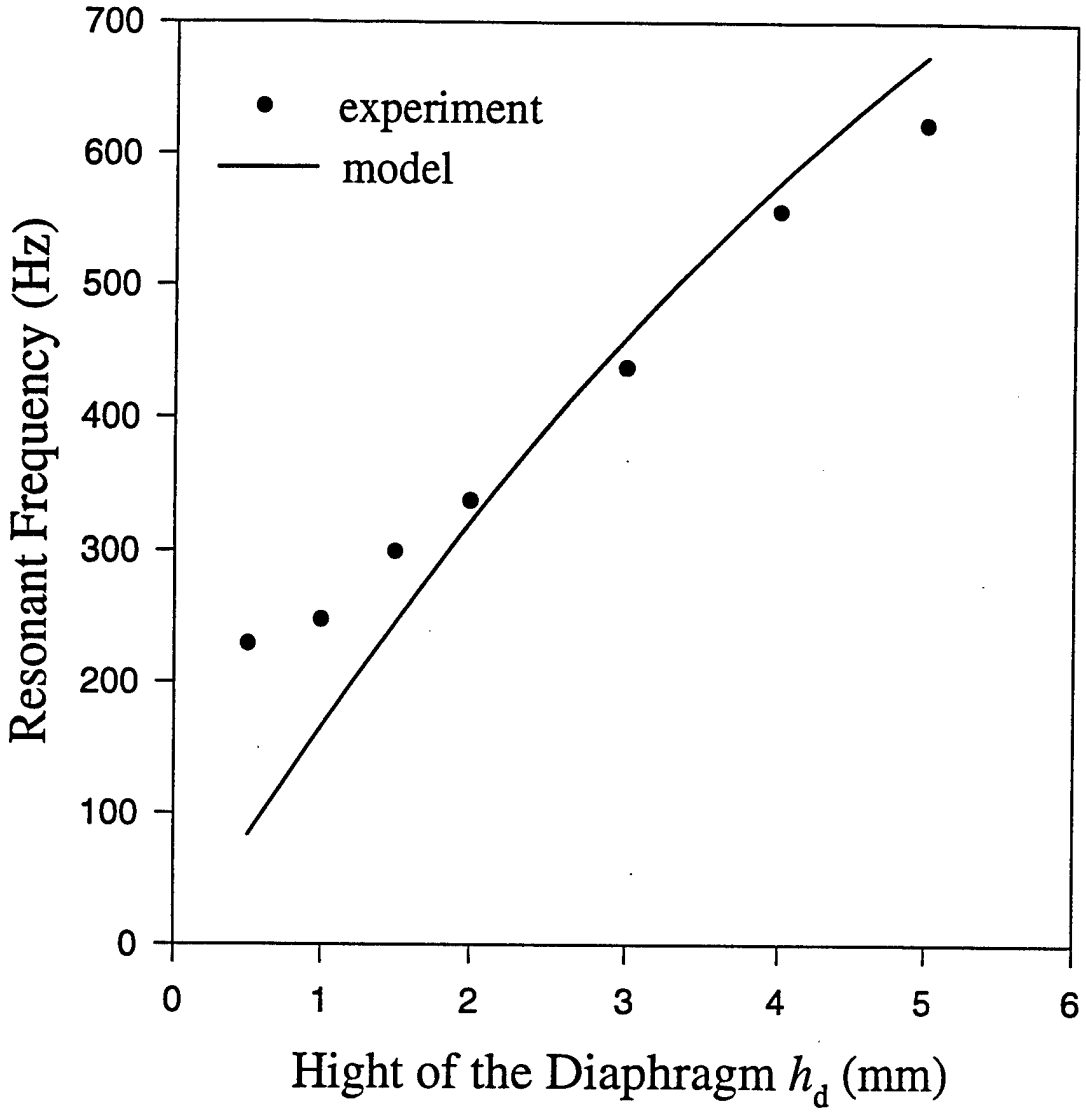
700
600
500
400
300
200
100
0
Resonant Frequency (Hz)
experiment
model
0
1
2
3
4
5
6
Hight of the Diaphragm h_d (mm)

Fig. 6

Table 1. Diaphragm and bimorph cantilever characteristics.

Parameters of the loudspeaker paper diaphragm					Dimensions of the piezoelectric bimorph cantilevers		
h_d (mm)	L_d (mm)	w_d (mm)	t_d (mm)	ρ_d (g/cm^3)	l (mm)	w (mm)	$2h$ (mm)
2.8	23	63	0.59	0.55	18	5	1.0

Table 2. Magnitude of electromechanical coefficients of PZT5H for E=0.71 kV/cm

coefficient	$\varepsilon_{33}^{T}/\varepsilon_0$	d_{32} (m/V)	s_{22}^{E} (m^2/N)
	$3770(0.997-0.078j)$	$333\cdot10^{-12}(0.996-0.091j)$	$30.3\cdot10^{-12}(0.996-0.088j)$

APPENDIX 63

CRESCENT : A novel piezoelectric bending actuator

Sanjay Chandran, V. D. Kugel, and L. E. Cross
Intercollege Materials Research Laboratory, The Pennsylvania State University, University Park, PA 16802

ABSTRACT

Piezoelectric actuators have significant potential for use in smart systems like vibration suppression and acoustic noise canceling devices. In this work, a novel piezoelectric bending actuator CRESCENT was developed. CRESCENT is a stress-biased ceramic-metal composite actuator. The technology involves the use of the difference in thermal contraction between the ceramic and the metal plates bonded together at a high temperature by a polymeric agent to produce a stress-biased curved structure. An extensive experimental investigation of this device in the cantilever configuration was carried out. The tip displacement, blocking force and electrical admittance and were chosen to characterize the performance of the actuator under quasistatic conditions. The device fabricated at optimum temperature exhibits large tip displacement and blocking force and possesses superior electromechanical characteristics to conventional unimorph actuators.

Keywords: piezoelectric actuators, unimorph, bimorph, CRESCENT

1. INTRODUCTION

Piezoelectric ceramic materials are being increasingly investigated for use as solid-state actuators in applications requiring large displacements (>10 μm) such as loudspeakers, pumps, vibration suppression and acoustic noise canceling devices. Since the direct extensional strain in piezoelectric ceramics is quite small, novel strain amplification mechanisms are being explored. The bending mechanism is an effective strain amplification technique and actuators utilizing this mechanism are widely used for the above mentioned applications. A classical example of such a device is the unimorph actuator[1] which consists of the non-piezoelectric and electroded piezoelectric plates bonded together. A schematic view of the unimorph actuator with rectangular cross-section in the cantilever configuration is shown in Fig. 1a. The flexural displacement η under applied voltage U (Fig. 1b) is caused by the piezoelectric effect in the direction perpendicular to the polar Z axis (piezoelectric d_{31} coefficient).

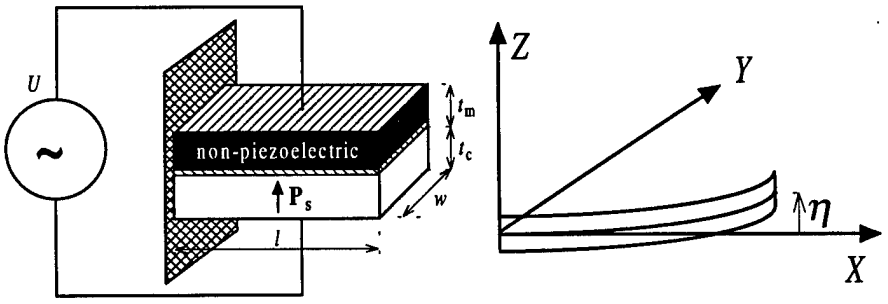

(a) (b)

Fig. 1. (a) A schematic view of the unimorph actuator in cantilever configuration. $\mathbf{P}_s$ denotes the vector of the spontaneous polarization. (b) Flexural displacement η of the unimorph in the ZX plane under the applied voltage.

Recently, a novel technique of using pre-stress produced during the device fabrication was introduced.[2] The piezoelectric actuator made using this technique was named RAINBOW (Reduced And Internally Biased Oxide Wafer). RAINBOW is made by subjecting the ceramic to a selective high temperature reduction with graphite in an oxidizing atmosphere resulting in a reduced electrically conductive layer and an unreduced piezoelectric layer. The resulting stress-biased monolithic unimorph has a dome or saddle-shaped structure because of difference in the thermal contraction between the reduced and unreduced layers of the ceramic plate. It was stated that this dome shape enables the actuator to generate significant axial displacement.[3]

In this work, the authors describe a novel piezoelectric stress-biased bender called CRESCENT. This device is very promising considering that it generates fairly large displacement and blocking force at reasonable driving fields. In addition, ease of fabrication, low cost and surface mountable configuration are some of its other attractive features. Details regarding the fabrication of CRESCENT and its electromechanical characterization are given below.

2. FABRICATION OF CRESCENT

The technology of fabricating CRESCENT involves the use of the difference in thermal contraction between the piezoelectric ceramic and metal plates bonded together by a polymeric agent to produce a stress-biased curved structure. The electroded piezoelectric plate is cemented to a metal plate by a thin layer of high temperature curing epoxy by subjecting it to high temperature (200-400°C) for a fixed period of time (typically 30 minutes - 6 hours) so that the epoxy cures and hardens. Then the structure is rapidly cooled (typically air cooled) to room temperature to achieve the differential thermal contraction. This process produces a dome-shaped structure with significant internal stresses. After the device is fabricated it is poled. A schematic view of the CRESCENT is given in Fig. 2.

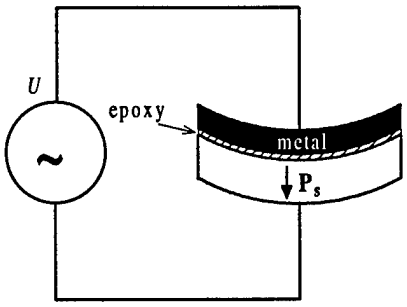

Fig. 2. Schematic view of CRESCENT.

3. EXPERIMENTAL PROCEDURE

In all experiments, soft piezoelectric ceramics PKI550 (Piezo Kinetics, Inc.) and stainless steel SS302 were used. This category of piezoelectric ceramics is analogous to soft piezoelectric ceramics PZT5H. Stainless steel SS302 was used because of its very high Young's modulus. Two epoxies with different curing temperatures were used: one of the epoxies was cured at 250 °C for 6 hours and the other was cured at 350 °C for 45 minutes.

Each piezoelectric plate was rectangular in cross-section and had the following dimensions: total length $L \cong 30$ mm, width $w \cong 11$ mm and thickness $t_c \cong 1.09$ mm (Fig. 1). The SS 302 plates had dimensions: total length $L \cong 30$ mm, width $w \cong 11$ mm and thickness $t_m \cong 0.37$ mm (Fig. 1). Since the Curie temperature (~200 °C) was lower than the device fabrication temperature, the actuators were poled after fabrication. The radius of the curvature of both the CRESCENT actuators before poling was about 0.4 m and after poling it increased to 0.8-0.9 m. For comparison, standard d_{31} unimorph actuator of identical dimensions was fabricated. In case of unimorph, the piezoelectric ceramic plate was first poled along its thickness and then bonded to the SS302 plate using commercially available J-B Weld epoxy (J-B Weld Company) at

room temperature for 24 hours. Hence the unimorph has a greatly reduced level of internal stress compared to the CRESCENT actuators.

The piezoelectric d_{33} coefficients of the CRESCENT and unimorph actuators after poling were measured using the piezoelectric d_{33} meter ZJ-2 (Institute of Acoustics, Academia Sinica). To characterize the CRESCENT and unimorph actuators, their electromechanical response as a function of the applied electric field well below the fundamental frequency of bending vibrations (quasistatic conditions) was investigated. Under quasistatic conditions, the following parameters of these devices in the cantilever configuration (Fig. 1) were measured as a function of amplitude of the electric field: (*i*) displacement η of the free end of the cantilever, (*ii*) blocking force F_{bl} (when η=0), and (*iii*) electrical admittance *Y*. The vibrating length of the cantilever was $l \cong 26$ mm.

A block diagram of the experimental set-up is shown in Fig. 3.[4] The tip displacement of piezoelectric cantilevers was measured by a photonic sensor MTI 2000 (MTI Instruments). The actuator (in Fig. 3, bimorph is shown as an example) was mounted on a XYZ micropositioner (Ealing Electro-Optics, Inc.). To measure the blocking force, a special metal head of a load cell ELF-TC500 (Entran Devices, Inc.) was glued by Super Glue to the vibration end of the actuator. Power supply PS-15 (Entran Devices, Inc.) was used to drive the load cell. The electrical admittance was measured by means of a small (a few ohms) resistor R connected in series with the actuator. The lock-in amplifiers (SR830 DSP, Stanford Research Systems, Inc.) used to measure the signals corresponding to the tip displacement and admittance were synchronized with the output voltage of the power amplifier (790 Series, PCB Piezotronics, Inc. or PA-250H, Julie Research Laboratories, Inc.). The input AC signal to the power amplifier was provided by a generator DS345 (Stanford Research Systems, Inc.). The developed experimental set-up can be used over a wide frequency range (from DC to several kHz). The maximum driving voltage this setup can handle is 300 Volt RMS.

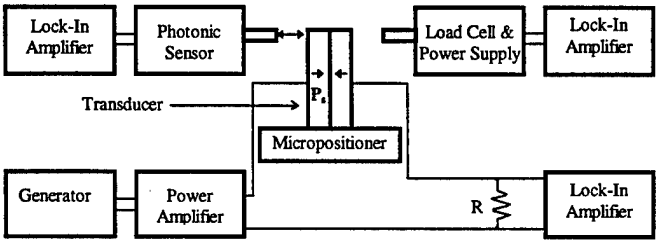

Fig. 3. Block diagram of the experimental set-up adopted to measure electromechanical properties of piezoelectric actuators.[4] $\mathbf{P}_s$ denotes the vector of spontaneous polarization.

Electromechanical characteristics were measured in the quasistatic regime at room temperature. The measurement frequency 100 Hz was at least ten times smaller than the fundamental resonant frequency.

4. EXPERIMENTAL RESULTS

The values of the piezoelectric d_{33} coefficient of the CRESCENT and unimorph actuators are given in Table 1. It is evident that the d_{33} coefficient decreases with increasing device fabrication temperature. Thus the CRESCENT actuator fabricated at 350°C has the lowest value whereas the unimorph actuator has the highest value.

Table 1. Values of the piezoelectric d_{33} coefficient of the CRESCENT and unimorph actuators

TYPE OF PIEZOELECTRIC ACTUATOR	piezoelectric d_{33} coefficient
CRESCENT (fabricated at 250°C)	518
CRESCENT (fabricated at 350°C)	512
Unimorph	570

Fig. 4 and Fig. 5 show the variation of quasistatic tip displacement, blocking force and admittance of the CRESCENT actuator fabricated at 250°C with increasing electric field upto about 2 kV/cm. Fig. 6 and Fig. 7 show the variation of these parameters with electric field for the CRESCENT actuator fabricated at 350°C. The variation of these parameters with electric field for the unimorph actuator is depicted in Fig. 8 and Fig. 9. As seen from the figures, for all the three actuators under consideration, the quasistatic tip displacement and blocking force vary linearly with electric field for low fields but the variation becomes increasingly non-linear at higher electric fields. The slope of tip displacement and blocking force vs. electric field monotonically increases with electric field at higher levels of field.

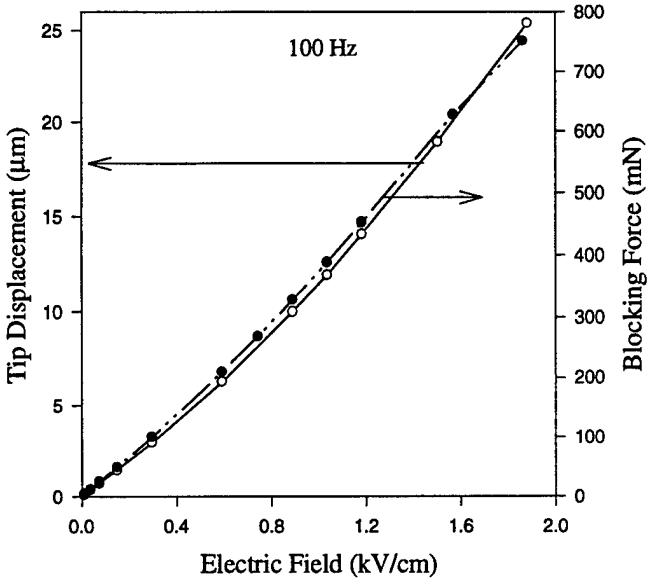

Fig. 4. Variation of tip displacement and blocking force of CRESCENT fabricated at 250°C with electric field.

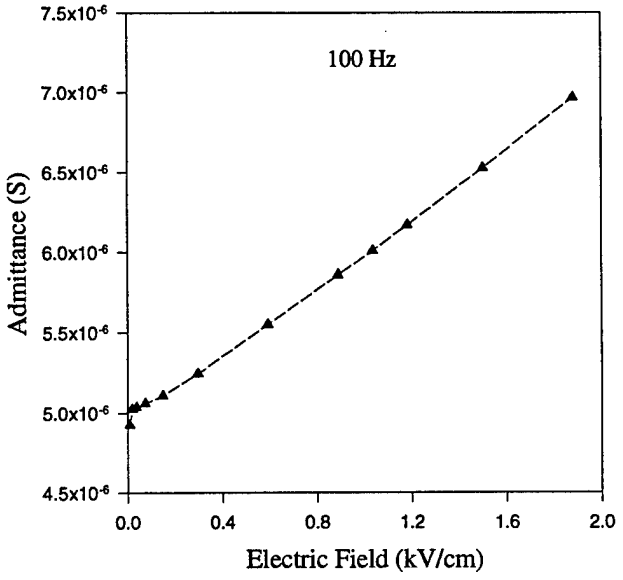

Fig. 5. Variation of relative admittance of CRESCENT fabricated at 250°C with electric field.

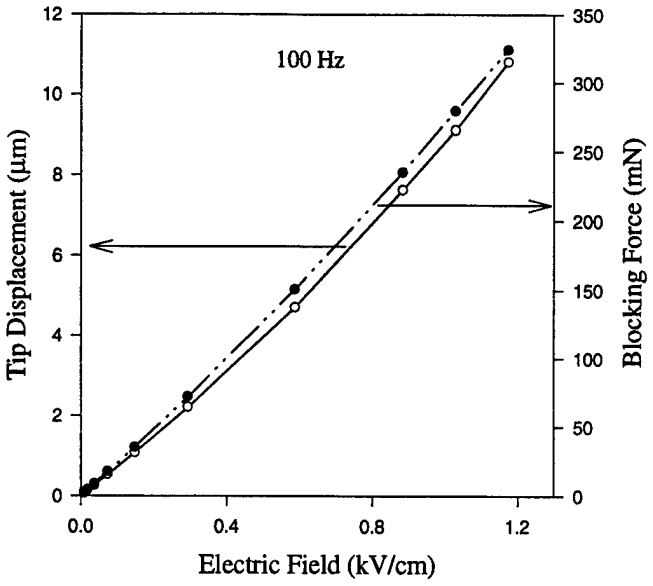

Fig. 6. Variation of tip displacement and blocking force of CRESCENT fabricated at 350°C with electric field.

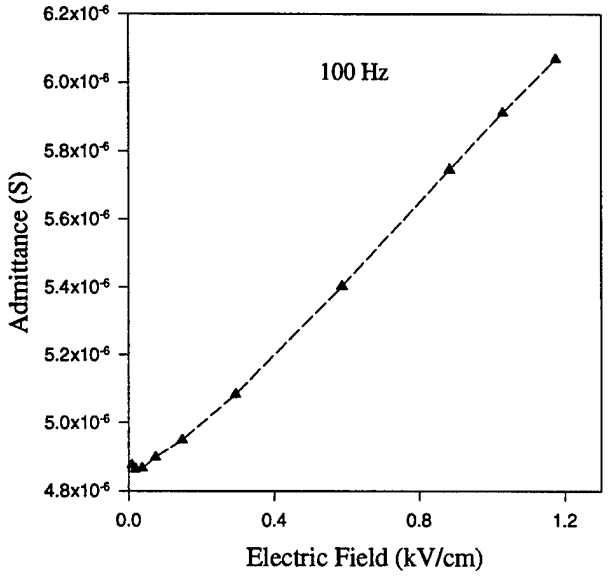

Fig. 7. Variation of relative admittance of CRESCENT fabricated at 350°C with electric field.

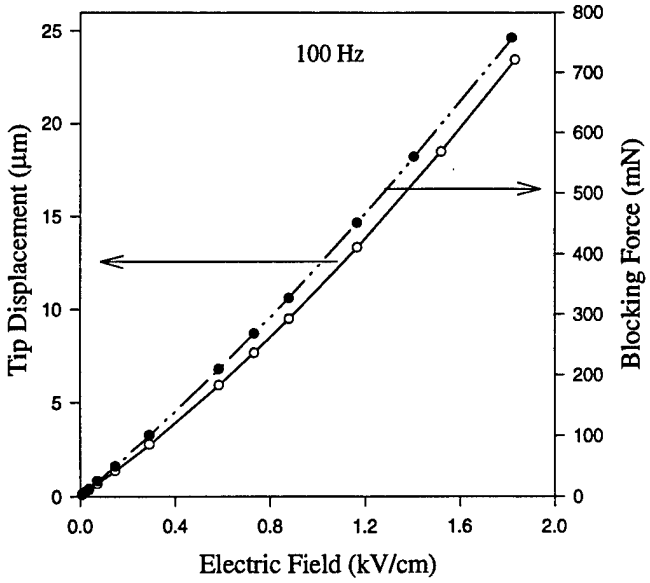

Fig. 8. Variation of tip displacement and blocking force of unimorph with electric field.

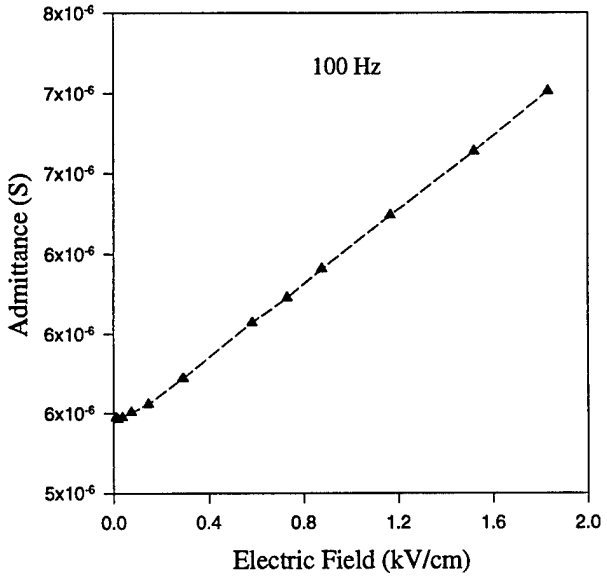

Fig. 9. Variation of relative admittance of unimorph with electric field.

5. DISCUSSION AND SUMMARY

The experimental results show that the CRESCENT actuator fabricated at 250°C exhibits a larger tip displacement but a smaller blocking force and electrical admittance than the unimorph actuator. However, the CRESCENT actuator fabricated at 350°C shows a smaller tip displacement, blocking force and electrical admittance than the unimorph. It is indeed useful to compare the various electromechanical parameters of the three actuators and arrive at an overall figure of

merit which can be used to evaluate their electromechanical performance relative to one another. This comparison can be done using the analysis given below.[5] This analysis can be applied only to actuators consisting of plates with rectangular cross-section.

The actuators were studied in the cantilever configuration in which the mechanical load is usually applied to the vibrating end of the cantilever. Therefore the most important characteristics under quasistatic conditions are the free displacement η (Fig. 1) of the vibrating end and the blocking force F_{bl} when η=0. For piezoelectric unimorph actuators[6]

$$\begin{aligned} \eta &= \frac{3}{2} d_{31} \frac{l^2}{t} k_d E, \\ F_{bl} &= \frac{3}{8} \frac{d_{31}}{s_{11}^E} \frac{w t_c^2}{l} k_{df} E, \end{aligned} \tag{1}$$

where d_{31} and s_{11}^E are the piezoelectric coefficient of ceramics, and the mechanical compliance of ceramics in the direction X under the constant electric field E (Fig. 1) respectively, k_d and k_{df} are displacement and blocking force coefficients respectively, and $E = U/t_c$.

For unimorph cantilevers (i.e. without internal mechanical stress) k_d and k_{df} can be expressed as[6]

$$\begin{aligned} k_d &= \frac{2xy(1+x)}{1+4xy+6x^2y+4x^3y+x^4y^2}, \quad x = \frac{t_m}{t_c}, \quad y = Y_m s_{11}^E, \\ k_{df} &= 2xy \frac{1+x}{1+xy}, \end{aligned} \tag{2}$$

where Y_m is the Young's modulus of the metal. As given in equation (2) factors k_d and k_{df} depend on the ratio of thicknesses x and ratio of Young's moduli y of metal and piezoelectric plates.

For CRESCENT actuators, internal mechanical stress produced during device fabrication and poling, changes the electromechanical properties of ceramics. Therefore equation (1) for these actuators can be written as[5]

$$\begin{aligned} \eta &= \frac{3}{2} d_{31} \frac{l^2}{t} k_d k_p E, \\ F_{bl} &= \frac{3}{8} \frac{d_{31}}{s_{11}^E} \frac{w t_c^2}{l} k_{df} k_{pm} E, \end{aligned} \tag{3}$$

where k_p is equal to relative change in d_{31} and k_{pm} is equal to the change in d_{31}/s_{11}^E as a result of the internal stress bias. k_d is not very sensitive to change in s_{11}^E. Hence k_p can be calculated from the ratio of the tip displacements of the CRESCENT and unimorph actuators using equation (1) and equation (3). However, k_{df} being a strong function of s_{11}^E, the value of k_{df} in equation (3) should be first calculated using the value of s_{11}^E under mechanical stress in equation (2). Then k_{pm} can be determined from the ratio of blocking forces and ratio of k_{df} for unimorph and CRESCENT actuators using equation (1) and equation (3).

Another important quasistatic electromechanical characteristic of the actuators is their electrical admittance Y :

$$Y = j\omega \frac{lw}{t_c} \varepsilon_{33}^T k_Y , \tag{4}$$

where ω is the angular frequency = $2\pi\nu$, ε_{33}^T is the component of the tensor of the dielectric permittivity of ceramics and coefficient k_Y depends on the electromechanical coupling coefficient and a change in the dielectric permittivity due to device fabrication.

An overall figure of merit representing the ratio of the mechanical work to the input electrical energy can be expressed as[6]

$$\text{overall figure of merit} \propto \frac{\eta F_{bl}}{Y} . \tag{5}$$

Equation (5) can be used to compare different actuators (in our case, CRESCENT and unimorph actuators) only if they are fabricated using the same piezoelectric ceramics and have the same dimensions of the active piezoelectric plate. All

quasistatic characteristics should be measured for the same amplitude and frequency of the applied electric field since electromechanical properties of piezoelectric ceramics depend on the amplitude and frequency of the electric field.[7]

Calculated relative values with respect to the unimorph actuator representing electromechanical characteristics of the actuators studied are given in Table 2. These values were obtained at low applied electric field (less than 20 V/cm). As seen from Table 2, the CRESCENT actuator fabricated at 250°C has the highest figure of merit.

Table 2. Figures of merit of bending-mode piezoelectric actuators in the cantilever configuration.

Type of Piezoelectric actuator	Tip displacement (relative)	Blocking force (relative)	Admittance (relative)	Overall figure of merit
Unimorph	1	1	1	1
CRESCENT (fabricated at 250°C)	1.09	0.97	0.91	1.16
CRESCENT (fabricated at 350°C)	0.88	0.85	0.90	0.83

Based on the relative values of tip displacement and blocking force and equations (1) and (3) the values of k_p and k_{pm} under quasistatic conditions and low applied electric field can be calculated. The calculated values of these coefficients are given in Table 3.

Table 3. k_p and k_{pm} values for CRESCENT actuators

Type of Piezoelectric actuator	k_p	k_{pm}
CRESCENT (fabricated at 250°C)	1.09	0.88
CRESCENT (fabricated at 350°C)	0.88	0.82

From Table 2, it is clear that the CRESCENT actuator fabricated at 250°C has a higher tip displacement and lower admittance than d_{31} unimorph fabricated from the same materials. This implies that the average piezoelectric d_{31} coefficient of the piezoelectric ceramic plate poled under a certain level of mechanical bending stress is higher and the corresponding dielectric permittivity ε_{33}^{T} lower than that of the starting material. This is very surprising because experimental results[8] show that longitudinal stress decreases piezoelectric d_{31} coefficient. Also, it is interesting to note that for a piezoceramic plate poled under a certain level of mechanical stress, the piezoelectric d_{33} coefficient is lower but the piezoelectric d_{31} coefficient is higher than the starting material. This enhanced electromechanical response can be attributed to specific domain structures which are formed during poling. A very important fact supporting this hypothesis is that there was a significant increase in the radius of curvature of the device after poling. For the CRESCENT actuator fabricated at 350°C (above the optimum temperature), excessive residual mechanical stress may decrease the piezoelectric d_{31} coefficient. This explains the inferior electromechanical characteristics exhibited by the actuator. The blocking force of both CRESCENT actuators is less than that of unimorph. This can be due to the increase in s_{11}^{E} due to mechanical stress during poling of the device.

It is evident from the results that the electromechanical and dielectric properties of the CRESCENT actuators are dependent on the level of the applied electric field. At high electric fields, they exhibit a non-linear variation. This can be attributed to the non-linear behavior of the soft PZT ceramics.[7] This non-linear behavior of ceramics has an extrinsic nature i.e. it is caused by domain wall and phase boundary motion.

Another important yardstick to evaluate the reliability of an actuator is the electric field at which mechanical failure occurs at resonance. Electromechanical resonance induces a very high level of mechanical vibrations which causes mechanical fracture. For unimorph and bimorph actuators, the fracture occurs at 30-50 MPa in the region where actuators were clamped since this region is subjected to the highest level of stress.[5] CRESCENT actuators have metal plates, and hence even if mechanical failure of ceramics occurs the actuators do not fracture since metals like stainless steel have much

higher fracture toughness than ceramics. Hence they can be expected to have a higher reliability than bimorphs. Work to study the reliability aspects of the CRESCENT actuators is currently in progress.

In summary, the electromechanical characteristics of CRESCENT and unimorph actuators in cantilever configuration have been investigated and compared. The tip displacement, blocking force, and electrical admittance under quasistatic conditions were chosen to evaluate electromechanical performance. The experimental results show that the CRESCENT actuator fabricated at close to optimum temperature exhibits superior characteristics as compared to conventional unimorph. This also shows that though in most cases stress has an adverse effect on the performance of piezoelectric devices, it can enhance performance if prudently designed and properly directed.

ACKNOWLEDGMENTS

This work was supported by the Office of Naval Research under the contract N00014-94-1-1140.

REFERENCES

1. M. R. Steel, F. Harrison, and P. G. Harper, "The piezoelectric bimorph: An experimental and theoretical study of its quasistatic response", *J. Phys. D: Appl. Phys.* **11**, pp. 979-989, 1978.
2. G. H. Haertling, "Rainbow ceramics - a new type of ultra-high-displacement actuator", *Amer. Cer. Soc. Bulletin* **73**, pp. 93-96, 1994.
3. G. H. Haertling, "Chemically reduced PLZT ceramics for ultra-high displacement actuators", *Ferroelectrics* **154**, pp. 101-106, 1994.
4. V. D. Kugel, Q. M. Zhang, Baomin Xu, Qing-ming Wang, Sanjay Chandran, and L. E. Cross, "Behavior of Piezoelectric Actuators under High Electric Field", Accepted in *IEEE Proceedings on Application of Ferroelectrics, ISAF'96* (1996).
5. V. D. Kugel, Sanjay Chandran, and L. E. Cross, "A comparative analysis of piezoelectric bending-mode actuators", submitted to *SPIE's 4th Annual Symposium on Smart Structures and Materials, Section : Smart Materials Technologies* (1997).
6. V. D. Kugel, Sanjay Chandran, and L. E. Cross, "Caterpillar-type piezoelectric d_{33} bimorph transducer", *Appl. Phys. Lett.* **69**, pp. 2021-2023, 1996.
7. S. Li, W. Cao and L. E. Cross, "The extrinsic nature of nonlinear behavior observed in lead zirconate titanate ferroelectric ceramic", *J. Appl. Phys.* **69**, pp. 7219-7224, 1991.
8. Q. M. Zhang, J. Zhao, K. Uchino, and J. Zheng, "Change in the weak field properties of $Pb(Zr,Ti)O_3$ piezoceramics with compressive uniaxial stresses and its links to the effect of dopants on the stability of the polarization in materials", to be published in *J. Mater. Research* **12**, 1997.

APPENDIX 64

Submitted to SPIE Proceedings "Smart Structures and Materials, Section: Smart Materials Technologies 1997" Paper No: 3040-09

A comparative analysis of piezoelectric bending-mode actuators

V. D. Kugel, Sanjay Chandran, and L. E. Cross
Intercollege Materials Research Laboratory, The Pennsylvania State University, University Park, PA 16802

ABSTRACT

During the last several years novel piezoelectric bending actuators have been developed: RAINBOW, CERAMBOW, CRESCENT, d_{33} bimorph and THUNDER. A comparative experimental investigation of electromechanical characteristics of these devices along with conventional d_{31} bimorph and unimorph actuators was conducted in this work. All transducers were fabricated from soft piezoelectric ceramics. The experimental results show that d_{33} bimorph and unimorph elements have superior quasistatic characteristics as compared to other type of bending-mode actuators. All these piezoelectric devices demonstrate a significant dependence of electromechanical performance on the magnitude of the driving electric field. It was found that the decrease in the mechanical quality factor and resonant frequency of bending vibrations in d_{31} unimorph. RAINBOW, CRESCENT (CERAMBOW) and THUNDER with increasing electric field is much smaller than that in bimorph and d_{33} unimorph actuators. The dependence of the behavior of these devices on the operating conditions governs the selection of a particular device for a specific application.

Keywords: piezoelectric actuators, bimorph, unimorph, RAINBOW, CRESCENT, CERAMBOW, THUNDER

1. INTRODUCTION

Piezoelectric ceramics have a relatively high electromechanical coupling coefficient which makes them very attractive for applications involving efficient transformation of electrical energy into mechanical energy and vice versa. Therefore piezoelectric actuators fabricated from these ceramics have significant potential for use as sensors and actuators in smart systems. Some of the most popular types of piezoelectric devices are bending actuators, in which applied electric field causes mechanical bending because of the piezoelectric effect. A classical example of such a device is piezoelectric bimorph actuator[1] consisting of two similar electroded piezoelectric plates poled along their thickness and adhesively bonded together. A schematic view of the piezoelectric bimorph cantilever with rectangular cross-section is shown in Fig. 1a. The flexural displacement η under applied voltage U (Fig. 1b) is caused by the piezoelectric effect in the direction perpendicular to the polar (Z) axis (piezoelectric d_{31} coefficient).

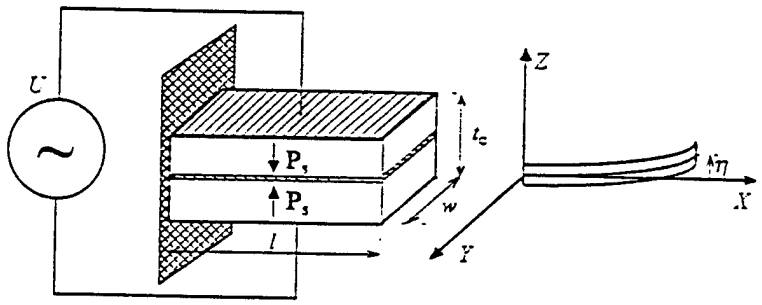

(a) (b)

Fig. 1. (a) A schematic view of the piezoelectric d_{31} bimorph cantilever with series connection. P_s denotes the vector of the spontaneous polarization. (b) Flexural displacement of the transducer in the ZY plane under the applied voltage.

Another widely used bending actuator is unimorph (Fig. 2).[2] The unimorph actuator consists of the non-piezoelectric and electroded piezoelectric plates bonded together. Here, like in the piezoelectric bimorph, the piezoelectric effect in the direction perpendicular to the polar axis (coefficient d_{31}) generates flexural displacement.

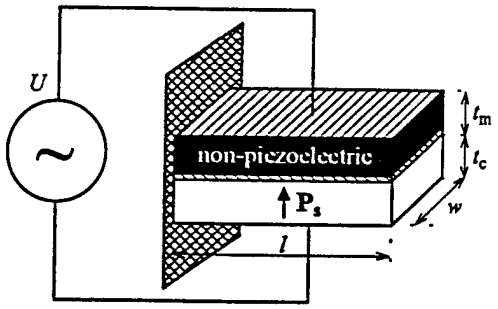

Fig. 2. A schematic view of the piezoelectric d_{31} unimorph cantilever with rectangular cross-section.

A new type of bending piezoelectric actuator named RAINBOW (standing for Reduced And Internally Biased Oxide Wafer) has recently been developed.[3] This is a monolithic bender in which the ceramic is subjected to a selective high temperature reduction with graphite in an oxidizing atmosphere resulting in a reduced non-piezoelectric layer with metallic electrical conductivity and an unreduced piezoelectric layer. The resulting stress-biased monolithic unimorph has domelike structure (Fig. 3) because of difference in the thermal contraction of reduced and non-reduced parts of the ceramic plate. It was stated that the actuator can generate significant axial displacement.[4]

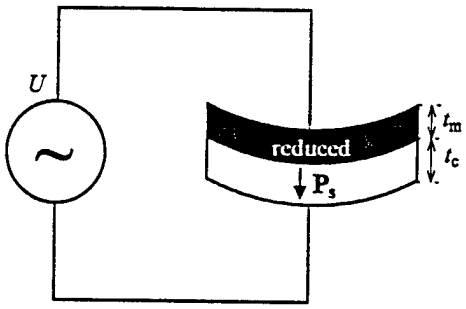

Fig. 3. A schematic view of RAINBOW actuator.

CERAMBOW (stands for CERAMic Biased Oxide Wafer) piezoelectric actuator is another stress-biased unimorph actuator in which metal and electroded ceramic plates are cemented together at an elevated temperature using appropriate solder.[5] Curvature develops as the CERAMBOW is cooled to room temperature since the metal and ceramics have different coefficients of the thermal expansion. CERAMBOW has the same shape as RAINBOW (Fig. 4). A much more reliable way for stress-biased actuators fabrication has been suggested by the authors. Dome shape of this stress-biased unimorph named CRESCENT (Fig. 4) is achieved by bonding metal and electroded piezoelectric plates at a high temperature using special epoxies (curing temperature is 200-400 °C). If fabricated at the same temperature, the CERAMBOW and CRESCENT have similar electromechanical properties.

Another new class of bimorph and unimorph actuators utilizing piezoelectric d_{33} coefficient has recently been developed.[6] This caterpillar-type piezoelectric d_{33} transducer consists of piezoelectric segments bonded by a polymeric agent by a dicing and layering technique (Fig. 5). It is the piezoelectric effect along polar axis $\mathbf{P}_s$ (coefficient d_{33}) that causes flexural displacement in these transducers. Since piezoelectric d_{33} coefficient in commercial piezoelectric ceramics is 2-2.2 time large than d_{31}, this transducer generates significantly higher displacement than conventional piezoelectric d_{31} bimorph and unimorph actuators.

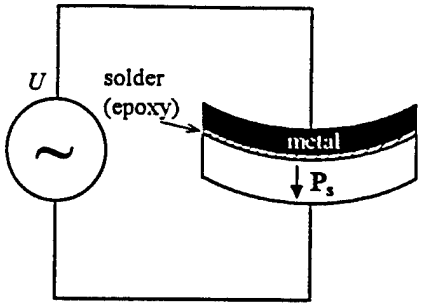

Fig. 4. Schematic view of CERAMBOW (CRESCENT).

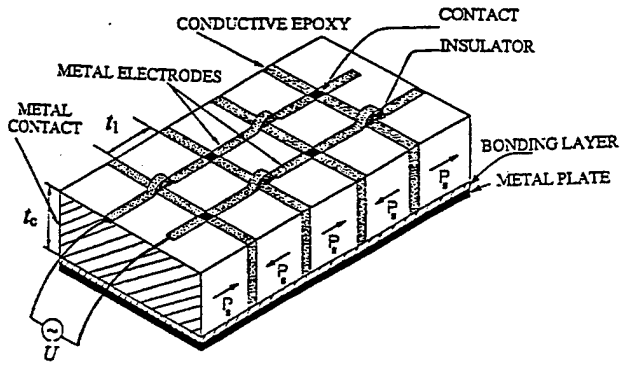

Fig. 5. A schematic view of the caterpillar-type d_{33} unimorph actuator. In the case of a bimorph consisting of two similar piezoelectric plates, the metal plate is replaced by the same piezoelectric plate.

Recently, another type of unimorph stress-biased piezoelectric actuator - THUNDER - (stands for THin layer Unimorph DrivER and sensor) has been reported.[7] The technique of THUNDER fabrication consists of high temperature bonding (300-350 °C) of an electroded ceramic plate with metal foils using LARC™-SI polyimide adhesive developed at NASA. The foils are cemented from both surfaces of the ceramic plate and the thickness of the metal foils on one surface of the ceramic plate is much thicker than on the other (Fig. 6). After the high temperature bonding the structure is given an additional bent by mechanical pressing to increase curvature. No published data are available to date for evaluating electromechanical properties of THUNDER.

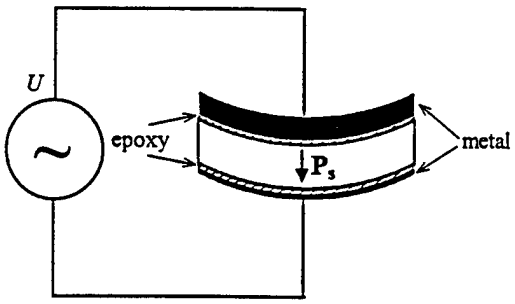

Fig. 6. Schematic view of THUNDER.

Thus, several new types of piezoelectric bending actuators have emerged during the last several years. A comparative analysis of their electromechanical properties is indeed the need of the hour. Therefore this work was undertaken in attempt to find and use unified criteria for the device characterization. The approach used is described in

section 2. Experimental procedure and results are presented in section 3. Finally, discussion and summary are given in section 4.

2. REPRESENTATION OF EXPERIMENTAL DATA

Actuators consisting of plates with rectangular cross-section have only been considered in this work. Since in many instances piezoelectric bending actuators are used in the cantilever configuration where one end of the actuator is clamped and the second one vibrates under or without an external load (Fig. 1), this configuration was used for the actuator characterization.

In the cantilever configuration mechanical load is usually applied to the vibrating end of the cantilever. Therefore the most important quasistatic characteristics are the free displacement η (Fig. 1) of the vibrating end and the blocking force F_{bl} when η=0. For piezoelectric bimorph and unimorph actuators[6]

$$\eta = \frac{3}{2} d \frac{l^2}{t} k_d E,$$
$$F_{bl} = \frac{3}{8} \frac{d}{s} \frac{w t_c^2}{l} k_{df} E, \tag{1}$$

where d is the piezoelectric coefficient of ceramics, s is the mechanical compliance of ceramics in the direction X under the constant electric field E (Fig. 1), $E = U/t_c$ for all actuators except for d_{33} bimorph and unimorph for which $E = U/t_1$ (Fig. 5), l, w, and t_c are the dimensions of the piezoelectric plate of the cantilevers (Figs. 1 and 2), and k_d and k_{df} are displacement and blocking force coefficients, respectively. For conventional piezoelectric d_{31} bimorph and unimorph actuators (Figs. 1 and 2) piezoelectric coefficient d_{31} and mechanical compliance s_{11}^E should be used in equation (1); for d_{33} transducers d_{33} and s_{33}^E should be used.

For bimorph cantilevers displacement and blocking force coefficients in equation (1) are equal to 1, for unimorph cantilevers without internal stress bias (Figs. 2 and 5) they can be expressed as[6]

$$k_d = \frac{2xy(1+x)}{1+4xy+6x^2y+4x^3y+x^4y^2}, \quad x = \frac{t_m}{t_c}, \quad y = Y_m s,$$
$$k_{df} = 2xy \frac{1+x}{1+xy}, \tag{2}$$

where t_m is the thickness of the non-piezoelectric plate (Fig. 2) and Y_m is the Young's modulus of the non-piezoelectric plate. As follows from the analysis of equation (2) factors k_d and k_{df} depend on the ratio of thicknesses x and Young's moduli y of non-piezoelectric and piezoelectric plates. The larger y is, the higher the value of k_d and k_{df} for optimum x. Analysis shows that maximum value of k_d is 0.5 and corresponding k_{df} is 2.

For stress-biased unimorph actuators like RAINBOW, CERAMBOW, and CRESCENT, mechanical stress arising in these structures during device fabrication and poling, changes electromechanical properties of ceramics. Therefore equation (1) for these actuators can be written as

$$\eta = \frac{3}{2} d_{31} \frac{l^2}{t} k_d k_p E,$$
$$F_{bl} = \frac{3}{8} \frac{d_{31}}{s_{11}^E} \frac{w t_c^2}{l} k_{df} k_{pm} E, \tag{3}$$

where d_{31} and s_{11}^E are the piezoelectric and mechanical compliance coefficients of the piezoelectric ceramics before the device fabricating, k_p and k_{pm} are coefficients equal to relative change in d_{31} and d_{31}/s_{11}^E respectively as a result of the acting mechanical stress. Coefficients k_d and k_{df} in equation (3) should be calculated using equation (2) for values of piezoelectric and electromechanical coefficients of the piezoelectric plate poled under mechanical stress. Equation (3) is also valid for THUNDER but in this case k_d and k_{df} are not described by equation (2).

One more important quasistatic electromechanical characteristic of the actuators is their electrical admittance Y:

$$Y = j\omega \frac{lw}{t_c} \varepsilon_{33}^T k_Y, \tag{4}$$

where ω is the angular frequency, ε_{33}^{T} is the component of the tensor of the dielectric permittivity of ceramics and k_Y is the factor depending on the corresponding mechanical coupling coefficient and a change in the dielectric permittivity as a result of the devices fabricating.

Thus as is seen from equations (1-4) quasistatic electromechanical characteristics of actuators with **the same dimensions** of piezoelectric part of the devices, **the same electric field**, and **the same frequency** can be normalized with respect to actuator chosen as a standard. It is convenient choose d_{31} **bimorph actuator** (Fig. 1) as this standard. Therefore the tip displacement η, blocking force F_{bl} and electrical admittance Y of all above described transducers fabricated using **the same piezoelectric ceramics** can be expressed as

$$\begin{aligned} \eta &= \eta^{\text{bimorph}} f_m^{\eta}, \\ F_{bl} &= F_{bl}^{\text{bimorph}} f_m^{F}, \\ Y &= Y^{\text{bimorph}} f_m^{Y}, \end{aligned} \tag{5}$$

where f_m^{η}, f_m^{F}, f_m^{Y} are individual figures of merit characterizing the tip displacement, blocking force and electrical admittance of a specific bending actuator, respectively.

The mechanical work W_{mc} that can be produced by the bending-mode actuators is proportional to the product of the multiplication of the tip displacement η and the blocking force :

$$W_{mc} \propto \eta F_{bl}. \tag{6}$$

Quasistatic electrical energy W_{el} accumulated in the transducer is proportional to its dielectric permittivity ε, the volume of the piezoelectric plate and the square of electric field E. Using equation (4), the following relation is obtained:

$$W_{el} \propto \frac{Y}{\omega} t_c^2 E^2, \tag{7}$$

The ratio of the mechanical work to the input electrical energy can serve as an overall figure of merit for the electromechanical efficiency of the piezoelectric actuator,

$$\text{integral figure of merit} = \frac{W_{mc}}{W_{el}} \propto \frac{\eta F_{bl}}{Y} \frac{\omega}{t_c^2 E^2}. \tag{8}$$

Using equation (5) the overall figure of merit relative to that of piezoelectric d_{31} bimorph, f_m, can be written as

$$f_m = \frac{f_m^{\eta} f_m^{F}}{f_m^{Y}}. \tag{9}$$

Thus, the relative factors f_m^{η}, f_m^{F}, f_m^{Y}, and f_m make it possible to describe quasistatic electromechanical characteristics of bending-mode piezoelectric actuators in the cantilever configuration. It is important to note that the actuators under consideration should be fabricated using the same piezoelectric ceramics and should have the same dimensions of the active piezoelectric part. All quasistatic characteristics should be measured for the same amplitude and frequency of the applied electric field since electromechanical properties of piezoelectric ceramics depend on the amplitude and frequency of the electric field.[8] Experimental results[6,8] show that despite a significant dependence of quasistatic electromechanical characteristics of piezoelectric actuators fabricated from soft piezoelectric ceramics on the applied electric field, the changes of these characteristics for different actuators show almost the same variation. Therefore it is enough to find f_m^{η}, f_m^{F}, f_m^{Y}, and f_m for one value of the applied electric field.

Since in many cases bending-mode actuators are operated near the fundamental frequency of bending vibrations, resonant characteristics of the actuators are also important. The values of the fundamental resonant frequency ν_r and the mechanical quality factor Q_m can be chosen to characterize resonant properties. The fundamental resonant frequency of the piezoelectric d_{31} bimorph cantilever with rectangular cross-section is[9]

$$\nu_r = \frac{1.875^2}{4\pi} \frac{t_c}{l^2} \frac{1}{\sqrt{3 s_{11}^{E} \rho_c}}, \tag{10}$$

where ρ_c is the density of the ceramics. The resonant frequency of the piezoelectric d_{31} unimorph with rectangular cross-section is expressed as[10]

$$\nu_r = \frac{1.875^2}{4\pi} \frac{t_c}{l^2} \frac{1}{\sqrt{3 s_{11}^{E} \rho_c}} \sqrt{\frac{k_{df}}{k_d (1 + xz)}}, \qquad z = \frac{\rho_m}{\rho_c}, \tag{11}$$

where ρ_m is the density of the non-piezoelectric plate. Thus, it is evident that the resonant frequency of the unimorph cantilever is a function of the resonant frequency of the piezoelectric plate (bimorph). For calculating the fundamental

resonant frequency of piezoelectric d_{33} bimorph and unimorph, s_{33}^E should be used in equations (10) and (11) instead of s_{11}^E. Equation (11) is also valid for RAINBOW, CERAMBOW, and CRESCENT cantilevers but in this case, the mechanical compliance of the stress-biased piezoelectric plate should be used in the calculations. For THUNDER too, the resonant frequency is a function of the resonant frequency of piezoelectric plate which is described by equation (10) but the actual dependence is a more complicated function of x, y and z. Based on the analysis described above, the resonant frequency of the bending mode actuators can be related to the resonant frequency of the piezoelectric d_{31} bimorph which has the same dimensions of the active piezoelectric plate, using the equation

$$\nu_r = \nu_r^{\text{bimorph}} f_m^{\nu}, \tag{12}$$

where f_m^{ν} is the figure of merit characterizing the fundamental resonant frequency of the bending-mode transducer. It is known[8] that the fundamental resonant frequency depends on the magnitude of the applied electric field. Therefore another important parameter to be considered is the relative change in the resonant frequency $\Delta\nu_r/\nu_r$ as a function of the electric field.

The mechanical quality factor Q_m is another important resonant characteristic. Since mechanical vibrations of the piezoelectric bending-mode actuators are described by fourth-order differential equation[9] and not by a second order one, Q_m should be defined appropriately. By analogy with the definition of Q_m for damped harmonic vibrator without frequency dispersion of the relevant electromechanical parameters of the system, Q_m can be expressed as[11]

$$Q_m = \frac{\eta_r}{\eta}, \tag{13}$$

where η_r is the amplitude of resonant vibrations. The amplitude of resonant vibrations depends on mechanical losses in the actuator[9] and is also very sensitive to the way the cantilever is clamped. Therefore it is preferable to compare the relative change $\Delta Q_m/Q_m$ as a function of the electric field instead of Q_m.

Thus, relative factors f_m^{η}, f_m^{F}, f_m^{Y}, and f_m are used to characterize quasistatic electromechanical characteristics and f_m^{ν}, $\Delta\nu_r/\nu_r$, and $\Delta Q_m/Q_m$ are used to characterize resonant properties of bending-mode piezoelectric actuators in the cantilever configuration.

3. EXPERIMENTAL PROCEDURE AND EXPERIMENTAL RESULTS

All transducers investigated were fabricated from soft piezoelectric ceramics and had a rectangular cross-section and the following dimensions: 0.4-2.5 mm in thickness, 5-15 mm in width, and 15-35 mm in length. Piezoelectric bimorph and metal/piezoelectric unimorph actuators were fabricated from PKI550 (Piezo Kinetic, Inc.) ceramic plates poled along their thickness. This category of piezoelectric ceramics is analogous to soft piezoelectric ceramics PZT5H. Stainless steel SS302 was used to make the unimorphs because of its very high Young's modulus and, consequently, high theoretical ratio of Young's moduli y=3.05 (equation (2)). The plates were bonded using commercial J-B Weld epoxy (J-B Weld Company). Piezoelectric d_{33} bimorphs were fabricated by a dicing and layering technique.[6] Theoretical ratio of Young's moduli for the d_{33} unimorph is y=3.90. The ceramic plates in the stack were bonded using commercial conductive adhesives EP21TDCS (Master Bond, Inc.) and E-Solder 3025 (Insulating Materials, Inc.). J-B Weld epoxy was used for bonding metal and sliced ceramic plates. Each piezoelectric segment in the piezoelectric plates (Fig. 5) had the following dimensions: $t_c = t_1 = 1.09$ mm, $w = 11$ mm. As follows from equation (2), electromechanical characteristics of d_{31} and d_{33} unimorph actuators depend on the ratio of thicknesses x and Young's moduli y of non-piezoelectric and piezoelectric plates. Theoretical analysis shows[10] that maximum value of the displacement factor f_m^{η} and overall figure of merit f_m correspond to different values of x. Therefore, only devices exhibiting maximum quasistatic tip displacement were chosen. Experimental study showed[6,10] that for SS302/PKI550 unimorphs optimum x lies between 0.2 and 0.35.

CRESCENTs were fabricated from PKI550 and SS302 using several types of high temperature epoxies. Since the Curie temperature ~200 °C was lower than the device fabrication temperature, the actuators were poled after their fabrication. It was found that tip displacement factor f_m^{η} for CRESCENT depends not only on the x and y factors but also on the curing temperature T_{cr}; therefore only CRESCENTs possessing maximum f_m^{η} were used for a comparative study. For actuators with t_c=1 mm and t_m=0.37 mm the optimal curing temperature was around 250-260 °C. The radius of the curvature of the transducer before poling was 0.4 m and after poling it increased to 0.8-0.9 m.

Since figures of merit are defined for elements with the same dimension of the piezoelectric part, the experimental data obtained for actuators fabricated from PKI550 with different dimensions were recalculated for a device with standard dimensions of piezoelectric plate.

RAINBOW actuators were cut from piezoelectric RAINBOW disks which were purchased from Aura Ceramics, Inc. RAINBOW disks are fabricated from C3900 ceramics which is analogous to PZT5H. The thickness of the devices was 0.46-0.48 mm, the thickness of the piezoelectric (unreduced) part t_c was approximately 0.27-0.29 mm. The thickness of the reduced layer was 0.12 mm and the thickness of conductive epoxy layer which served as electrode was 0.07 mm.

THUNDER actuators were fabricated from soft piezoelectric ceramics PZT5A and Al foil. Three layers of the foil were cemented on one side of the ceramic plate and one layer on the other side. Curing temperature was 300-320 °C. The thickness of the THUNDERs was 0.41 mm, the thickness of piezoelectric plates was 0.2 mm. The radius of the actuator curvatures after poling was approximately 0.33 m. After the high temperatures bonding followed by poling (first stage) the devices were additionally bent by mechanical pressing (second stage) and the radius of the curvature decreased to 0.14 m. Measurements of piezoelectric characteristics were conducted after the first and second stages.

Individual figures of merit of RAINBOW and THUNDER actuators were calculated using their experimental data and theoretical calculations for bimorph actuators from the same piezoelectric ceramics having the same dimensions.

The tip displacement of actuators was measured by a photonic sensor MTI 2000 (MTI Instruments Division). The blocking force was measured by means of a load cell ELF-TC500 (Entran Devices, Inc) and the electrical admittance was measured my means of a lock-in amplifier SR830 DSP (Stanford Research Systems, Inc). A complete description of the experimental set-up is given elsewhere.[8] Electromechanical characteristics were measured in quasistatic regime and at the fundamental frequency of bending vibrations. In the quasistatic regime the measurement frequency was at least ten times smaller than the fundamental resonant frequency.

Experimental figures of merit f_m^{η}, f_m^{F}, f_m^{Y}, f_m, and f_m^{v} representing electromechanical characteristics of the actuators studied are given in the Table. These values were obtained for low applied electric field (less than 20 V/cm). Dependencies of the resonant frequency and mechanical quality factors on the electric field are shown in Figs. 7 and 8, respectively. Resonant characteristics of CRESCENT actuators were similar to that of d_{31} unimorphs. No significant difference in almost all measured electromechanical properties of THUNDER actuators after the first and second stages of their fabrication was observed. Only mechanical quality factor decreased by 23% after the second stage.

Table. Figures of merit of bending-mode piezoelectric actuators in the cantilever configuration.

TYPE OF PIEZOELEMENT	Tip displacement factor f_m^{η}	Blocking force factor f_m^{F}	Admittance factor f_m^{Y}	Overall figure of merit f_m	Resonant frequency factor f_m^{v}
d_{31} Bimorph	1	1	1	1	1
d_{31} Unimorph x=0.34, y=3.05	0.41	1.8	1.0	0.74	1.7
RAINBOW	0.19-0.22	0.1-1.2	0.66	0.03-0.40	1.2-1.4
CRESCENT 250 °C (CERAMBOW) x=0.34, y≅3.05	0.44	1.75	0.91	0.85	1.7
THUNDER (3Al/PZT5A/Al)	0.12	0.36-1.0	0.90	0.05-0.13	2.1
d_{33} Bimorph	2.5	1.52	~1	3.80	0.84
d_{33} Unimorph x=0.34, y=3.90	0.72	3.5	~1	2.52	1.7

Analysis of d_{31} bimorphs experimental data showed that the experimental tip displacement and its theoretical value calculated according to equation (1) are in good agreement. Averaged experimental value of the blocking force was 33% less than theoretical one given by equation (1) and the averaged experimental value of the resonant frequency of cantilevers was 13% smaller that theoretical one (equation (10)). Nevertheless, the resonant frequency of these bimorph actuators with free-free boundary conditions (non of the ends is clamped) coincided with the theoretical one. For d_{31} unimorph actuators

the same tendency was observed: the blocking force was smaller by 13% and the resonant frequency was smaller by 12% than corresponding theoretical values. In d_{33} bimorphs the blocking force was smaller by 42% and the resonant frequency was smaller by 17% than corresponding theoretical values. The discrepancy was smaller for d_{33} unimorphs: the blocking force was smaller by 7% and the resonant frequency was smaller than the corresponding theoretical values by 3%. There may be several reasons for these discrepancies. Firstly, under the applied electric field, piezoelectric cantilever bends not only along the X axis but also along the Y axis (Fig. 1). In theoretical calculations bending along the Y axis was neglected. Bending along the Y axis may affect the blocking force and resonant frequency of actuators. The second reason is that the cementing epoxy whose thickness was neglected in the calculations, may also change electromechanical properties of the actuators. We were unable to conduct the same analysis for RAINBOW, CRESCENT and THUNDER actuators since exact electromechanical properties of these devices are unknown.

As seen from the Table, the blocking force factor for RAINBOW does not have an exact value. This is because the blocking force showed significant dependence on the external load. The force increased markedly with increasing mechanical pre-stress which can be generated externally by the horizontal displacement of the load cell stuck to the vibrating end of the actuator. It was also found that if the load cell was pressed against the vibrating end the measured blocking force was an order of magnitude large than that for the case when the load cell was glued to the vibrating end of RAINBOW cantilevers. A significant scattering in the measured blocking force factor f_m^r of THUNDERs (see Table) is probably caused by experimental limitations since it is very difficult to attach the vibrating end of THUNDER having a curved shape and the load cell head having a flat surface.

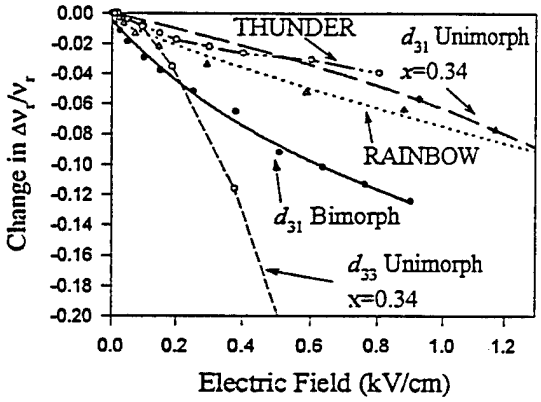

Fig. 7. Dependence of the resonant frequency ν_r of bending vibrations on the electric field (rms). Low-field resonant frequency is: 1394 Hz (d_{31} bimorph), 1015 Hz (d_{31} unimorph), 1029 Hz (d_{33} unimorph), 595 (RAINBOW), and 227 Hz (THUNDER).

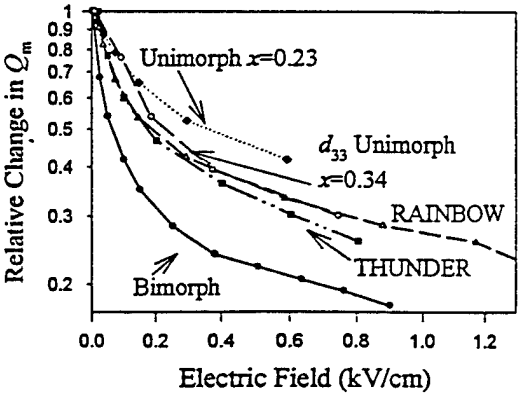

Fig. 8. Dependence of the relative mechanical quality factor on the electric field (rms). Low-field quality factor Q_m is: 55 (d_{31} bimorph), 48 (d_{31} unimorph), 25 (d_{33} unimorph), 62 (RAINBOW), and 137 (THUNDER, after first stage).

4. DISCUSSION AND SUMMARY

As follows from the Table, d_{33} bimorph and unimorph actuators have the best quasistatic electromechanical characteristics with respect to the blocking force and overall figure of merit. The reason for this is that piezoelectric d_{33} coefficient and corresponding coupling factor k_{33} are 2-2.2 times large than d_{31} and k_{31}. d_{31} bimorph generates higher tip displacement than d_{33} unimorph but its blocking force is significantly lower. d_{31} bimorph is followed by CRESCENT (CERAMBOW) and d_{31} unimorph actuators. It is interesting that the CRESCENT fabricated at the optimal temperature has a higher tip displacement, and overall figure of merit than d_{31} unimorph fabricated from the same materials. It means that the average piezoelectric d_{31} coefficient of the piezoelectric plate poled under certain mechanical bending stress is higher and corresponding dielectric permittivity ε_{33}^{T} lower than that of the starting material. A probable reason is that there are specific domain structures that are formed during poling. Two experimental facts support this hypothesis: the first one is a significant increase in the radius of the transducer curvature after poling. The second fact is that after separation of the metal and ceramic plates in the poled CRESCENT, the ceramic plate retained its curved shape which implies that there is practically no mechanical stress in the transducer. Moreover, effect of the longitudinal stress cannot explain the increase in the tip displacement since experimental results[12] show that longitudinal stress decreases piezoelectric d_{31} coefficient. If the CRESCENT is prepared above the optimal temperature residual mechanical stress may decrease piezoelectric d_{31} coefficient.

As is seen from the Table, RAINBOW and THUNDER actuators have lowest quasistatic figures of merit. Since reduced layer in RAINBOW actuator has a Young's modulus[13] much lower than stainless steel used for d_{31} unimorph fabrication, displacement factor k_d for this actuator is less than that for unimorphs. In addition as follows from the analysis of equation (2), the ratio of thickness of the reduced and active piezoelectric layers is less than the optimal one. The same reason can explain inferior quasistatic behavior of THUNDERs. Also, these devices have metal foils from both sides that decrease tip displacement. Since the thickness of the piezoelectric plates in the device was relatively small, the adhesive layers can also decrease f_m^n.

As seen from Fig. 7, the fundamental resonant frequency of bending-mode actuators depends on the applied electric field. Large sensitivity of the resonant frequency of d_{33} unimorph to electric field can be due to the fact that at a high level of mechanical stress which exists at a high level of resonant vibrations the epoxy bonding the piezoelectric segments becomes soft due to non-linear strain-stress relationship in the polymer materials. Resonant properties of d_{33} bimorph were not measured but based on the above discussion, this device should be even more sensitive to high electric field because it does not have the stabilizing metal plate. Relatively high dependence of v_r of d_{31} bimorph can be caused by an increase of the mechanical compliance of the piezoelectric ceramics with increasing electric field.[8] The effect of mechanical "softening" of the piezoelectric ceramics in all d_{31}-type unimorph devices is less significant since they have non-piezoelectric part whose properties do not depend on the electric field.

All actuators demonstrate a significant decrease of the mechanical quality factor with increasing electric field (Fig. 8). The most sensitive device studied was the d_{31} bimorph. Since the amplitude of resonant vibrations is inversely proportional to the mechanical losses at the resonance[9], the mechanical losses increase significantly under high electric field. At the electric field 1 kV/cm the mechanical quality factor decreases by an order of magnitude as compared to its low-field value. Since in unimorph-type structures there is non-piezoelectric part in which the mechanical losses do not depend on the applied electric field, the decrease of Q_m in these actuators is more gradual.

It should be noted that there is one more important figure of merit that has not been considered in this work. It is mechanical failure at resonance. Our results showed that at a high level of mechanical vibrations at resonance the actuators fracture. The fracture occurred at the surface of ceramic plates in the region where actuators were clamped since this area is subjected to the highest level of stress. Analysis of experimental data showed that fracture of d_{31} bimorph and unimorph transducers at resonance occurs if the maximum stress at the clamped surface reaches 30-50 MPa. In this case mechanical failure occurs in several seconds. Clearly, unimorph actuators having metal plates, such as d_{31} and d_{33} unimorph, CRESCENT, CERAMBOW, and especially THUNDER, are more reliable in a sense that even if mechanical failure of ceramics occurs the actuators do not fracture since metals like steel or Al have much higher fracture toughness than ceramics.

It is worthwhile to note that the straight or slightly curved shape of bending-mode actuators is not optimal in terms of overall figure of merit f_m. For instance, theoretical calculations show that L-shaped d_{31} bimorph cantilever (Fig. 9) has higher blocking force factor f_m^F and overall figure of merit f_m than straight d_{31} bimorph with the same dimensions. This is because in a conventional straight structure, bending moment generated in the actuator works against the blocking force

applied to the vibrating end. Therefore this force blocks the movement of the actuator's tip only. In the L-shaped structure, application of the horizontal force produces a mechanical moment on the horizontal part of the actuator. Thus, the blocking force should almost prevent displacement in the whole bottom part of the transducer consequently the magnitude of the corresponding blocking force should be higher in this case.

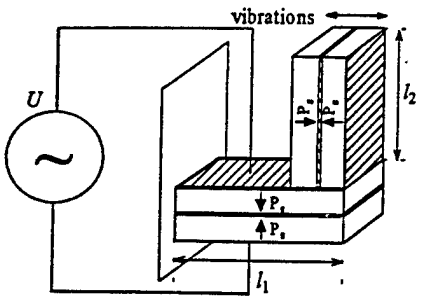

ELEMENT	Tip displacement factor f_d^n	Blocking force factor f_d^F	Admittance factor f_d^Y	Overall figure of merit f_m	Resonant frequency factor f_d^v
d_{31} Bimorph	1	1	1	1	1
L-shaped d_{31} Bimorph (l_1=l_2=0.5l)	0.75	1.5	1.0	1.125	1.32

Fig. 9. Schematic view of L-shaped d_{31} bimorph and theoretical figures of merit of this device with l_1=l_2=0.5l.

In summary, a comparative experimental investigation of electromechanical characteristics of piezoelectric d_{31} and d_{33} bimorph and unimorph actuators, RAINBOW, CRESCENT (CERAMBOW), and THUNDER actuators in cantilever configuration has been conducted. The tip displacement, blocking force, and electrical admittance were chosen to characterize quasistatic properties and the resonant frequency and mechanical quality factor were chosen to characterize the behavior at the fundamental frequency of bending vibrations. The experimental results show that d_{33} bimorph and unimorph actuators have superior quasistatic characteristics as compared to other types of bending-mode actuators. It was found that resonant frequency and especially mechanical quality factor of all actuators depend on the applied electric field. d_{31} unimorph, RAINBOW, CRESCENT (CERAMBOW), and THUNDER were found to be less dependent on the applied electric field than d_{31} bimorph and d_{33} bimorph and unimorph actuators. These results indicate that the choice of devices for a particular application depends on conditions under which the device will operate.

ACKNOWLEDGMENTS

The authors would like to thank R. L. Fox, R. G. Bryant, and J. M. Bacon for supplying THUNDER samples. This work was supported by the Office of Naval Research under the contract N00014-94-1-1140.

REFERENCES

1. W. P. Mason, *Electromechanical Transducers and Wave Filters* (D. Van Nostard Company, New York, 1942). pp. 199-200, 209-215.

2. M. R. Steel, F. Harrison, and P. G. Harper, "The piezoelectric bimorph: An experimental and theoretical study of its quasistatic response", *J. Phys. D: Appl. Phys.* **11**, pp. 979-989, 1978.

3. G. H. Haertling, "Rainbow ceramics - a new type of ultra-high-displacement actuator", *Amer. Cer. Soc. Bulletin* **73**, pp. 93-96, 1994.

4. G. H. Haertling, "Chemically reduced PLZT ceramics for ultra-high displacement actuators", *Ferroelectrics* **154**, pp. 101-106, 1994.

5. E. Furman, "Stress-enhanced ferroelectric materials and structures", *Annual report Part III "Studies of RAINBOW and CERAMBOW electromechanical properties"*, The Gilbert C. Robinson Department of Ceramic Engineering, Clemson University, 1995.

6. V. D. Kugel, Sanjay Chandran, and L. E. Cross, "Caterpillar-type piezoelectric d_{33} bimorph transducer", *Appl. Phys. Lett.* **69**, pp. 2021-2023, 1996.

7. R. L. Fox, R. G. Bryant, and J. M. Bacon "THUNDER ACTUATOR" (NASA Langley Research Center), private communication, 1996.

8. V. D. Kugel, Q. M. Zhang, Baomin Xu, Qing-ming Wang, Sanjay Chandran, and L. E. Cross, "Behavior of Piezoelectric Actuators under High Electric Field", Accepted to *IEEE Proceedings on Application of Ferroelectrics, ISAF'96* (1996).

9. V. D. Kugel, Baomin Xu, Q. M. Zhang, and L. E. Cross, "Bimorph-Based Piezoelectric Air Acoustic Transducer: Model", Submitted to *Sensors and Actuators A* (1996).
10. V. D. Kugel and L. E. Cross, unpublished.
11. R. F. Steidel, Jr., *An Introduction to Mechanical Vibrations* (John Willey & Sons: New York, 1979). pp. 212-216.
12. Q. M. Zhang, J. Zhao, K. Uchino, and J. Zheng, "Change in the weak field properties of $Pb(ZrTi)O_3$ piezoceramics with compressive uniaxial stresses and its links to the effect of dopants on the stability of the polarization in materials", To be published in *J. Mater. Research* **12**, 1997.
13. E. Furman, G. Li, and G. H. Haertling, An investigation of the resonance properties of RAINBOW devices", *Ferroelectrics* **160**, pp. 357-369, 1994.

APPENDIX 65

Submitted to the Proceedings of the 10th Annual International Symposium on Applications of Ferroelectrics (ISAF), 1996.

CHARACTERISTICS OF SHEAR MODE PIEZOELECTRIC ACTUATORS

Qing-ming Wang, Baomin Xu. V. D. Kugel and L. E. Cross

187 Intercollege Materials Research Laboratory
The Pennsylvania State University
University Park. PA 16802

Abstract: **Characteristics of cantilever shear mode piezoelectric actuator have been investigated. In this actuator configuration, soft PZT ceramic plate was poled along length and driven across its thickness, with one end mechanically clamped and the other free. Experimental results indicated that relative large tip displacement can be obtained through nonlinear piezoelectric response at high driving field. Due to lateral shear force, mechanical bending also contributes to the tip displacement of shear mode actuator. The fundamental bending resonant frequency was observed in the frequency range from 150 Hz to 600 Hz, depending on thickness and length of actuator. We also found that the resonant frequency of bending vibration is dependent on the driving field because of elastic nonlinearities. Two layer and multilayer shear mode actuators were also developed to reduce the driving voltage, while shifting the bending resonance to higher frequency range by increasing the total thickness of actuator.**

Key words: PZT, Ceramic actuator, Shear mode

I. Introduction

Piezoelectric ceramic materials such as lead zirconate titanate (PZT) have been designed as solid-state actuators and sensors for many applications such as precision positioning , noise and vibration sensing and cancellation, louder speaker, linear motor, and many others [1]. The three most common types of piezoelectric actuators are multilayer ceramic actuators, bimorph or unimorph actuators and flextensional composite actuators. Multilayer actuators, in which about 100 thin ceramic sheets are stacked together with internal electrodes utilizing the direct extentional mode (d_{33} mode), are characterized by large generated force, high electromechanical coupling, high resonant frequency, low driving voltage and quick response but small displacement level. On the other hand, bimorph or unimorph actuators consist of two thin ceramic sheets or one ceramic and one metal sheet bounded together with the poling and driving directions normal to the interface. When driving, the alternative extension and shrinkage of ceramic sheets due to transverse mode (d_{31}) result in a pure bending vibration. Bimorph and unimorph actuators can generate large displacement level but low electro-mechanical coupling, low resonant frequency and low driving force. For flextensional composite actuator, two typical examples are so-called "moonie" and "cymbal" actuators [2], [3] which consist of a piezoelectric or electrostrictive ceramic disk and metal end-caps. The ceramic is excited in an extensional mode and the metal caps in a flexure mode. The metal end-caps act as a mechanical transformer converting and amplifying the radial displacement ceramic disk into linear axial motion. Very large effective d_{33} coefficient can be obtained in "moonie" and "cymbal" actuators which results in quite large displacement levels.

Monomorph actuator [4], basically a modified unimorph actuator, made from a semiconductive piezoelectric ceramic thin sheet coated with certain electrodes. Quite a large tip displacement (100μm) arises from the non-uniform distribution of the electric field which occurs at semiconductor-metal electrode interface. The monomorph actuator has a simple structure in which bonding problems usually found in unimorph or bimorph structure can be avoided. A more recent device, Rainbow actuator, developed by Haertling[5], is also a monolithic unimorph-type ceramic actuator which is produced by selectively reducing one surface of a PLZT ceramic wafer on carbon black at high temperature. The reduced layer is a good electrical conductor and it acts as both the electrodes and inert part of the actuator. There is a very large internal pre-stress developed in the Rainbow actuator during reducing processing. It was reported [6] that Rainbow actuator is capable of achieving very high axial displacement (>1000 μm) and sustaining moderate pressures.

Obviously, mechanical motion generated by all the above ceramic actuators utilizes or is related to either d_{33} longitudinal mode or d_{31} transverse mode. It is interesting to note that although the d_{15} which couples to the shear mode is the highest coefficient in soft PZT ceramic materials, piezoelectric shear vibration mode is seldom used in actuator and transducer applications. In this paper, cantilever shear mode actuator and its characteristics will be presented. In this actuator, ceramic plate is poled along length and driven across its thickness with one end clamped and the other end free. The advantage of cantilever shear mode actuator is its simple, monolithic structure which allows for easy fabrication. However, its displacement level is relatively low comparing with bimorph or unimorph actuators.

II. Experimental Procedures

(1) Sample preparation:

In this study, Soft PZT 3203HD (Motorola Ceramic Product, Albuquerque, New Mexico) ceramic material was used to prepare shear mode actuator. Rectangular ceramic block with dimensions of 38.1 mm x 38.1 mm x 25.4 mm was electroded with air-dry silver paste and poled at a temperature of 90°C in oil bath for 45 minute under dc electric field of 1.8 kV/mm along its length. After poling, the ceramic block was aged for more than one week at room temperature. Then d_{33} coefficient was measured by using Berlincourt d_{33} meter. The measured value, 684 x 10^{-12} m/V, comparing with 650 x 10^{-12} m/V provided by manufacturer data sheet, indicates the ceramic block was well poled. Then the silver electrodes were removed and the poled ceramic block was cut into thin plates with 38.1 mm length, 12.3 mm width and thickness from 0.3 mm to 1.6 mm. Gold electrodes were sputtered on the major surfaces for applying electric field across thickness. One end of ceramic plate was clamped with rigid plastic support which is mounted on an optic plate with micropositioner (Ealing Electro-Optics, Inc.) while the other end free.

(2) Measurement

To characterize the shear mode actuators, the tip displacement was measured as function of both frequency and driving field. The measurement system was schematically shown in Fig. 1. MTI 2000 Fotonic Sensor (MTI Instrument) was used for displacement measurement. A small mirror was attached on the actuator tip for reflecting the incident light from optic fiber. When actuator vibrates under ac field driving, the reflected light is detected and transferred to voltage signal or displacement signal by the sensor. The optic fiber head was mounted on an XYZ micropositioner which provides distance adjustment against the measured actuator. Manual calibration was performed to determine the correspondence of displacement and output signal of the sensor. The AC signal generated by DS345 function generator (Stanford Research System, Inc.) was amplified through a powder amplifier (790 series, PCB Piezotronics, Inc.). The output of the power amplifier was then applied on the ceramic actuator. A lock-in amplifier (SR830 DSP, Stanford Research System, Inc.) which synchronized with the output voltage of the power amplifier was used to measure the output signal from MTI sensor. An Oscilloscope was also used to monitor the applied voltage and output signal from MTI sensor. The maximum output voltage of the power amplier is 300 volts RMS. When even higher driving field is needed, a power source with maximum output voltage of 500 Volts is used.

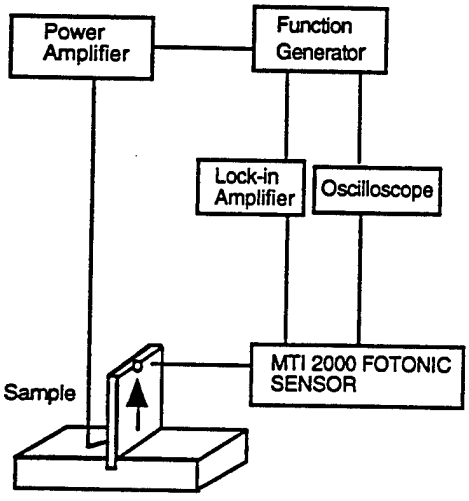

Fig.1. Experimental Set-up for displacement measurement

III. Results and Discussions

Linear piezoelectric shear strain, tip displacement and blocking for pure shear mode actuator can be written as:

$$x_5 = d_{15} E_1, \qquad (1)$$

$$\delta = d_{15} E_1 L, \qquad (2)$$

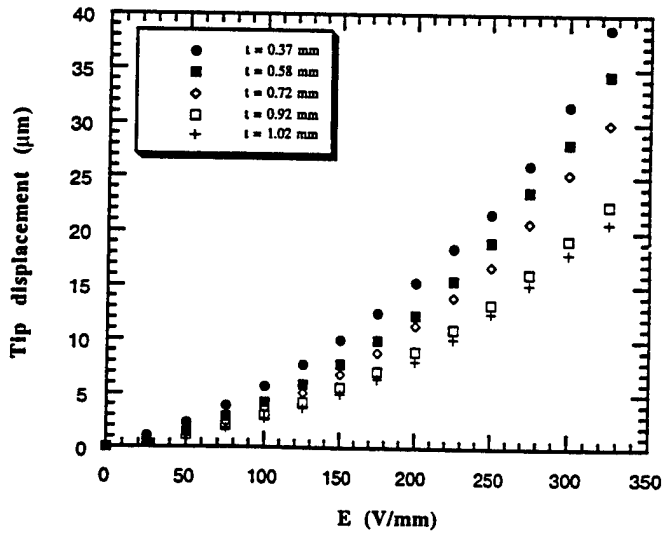

Figure 2. Driving field dependence of tip displacement of shear actuators with different thichness (L = 32.2mm, w = 12.3 mm)

$$F_b = \frac{d_{15}\, E_1\, w\, t}{s_{44}^E}. \qquad (3)$$

Where L, w, and t are actuator length, width and thickness, s_{44}^E is the shear component of the elastic compliance of PZT ceramics. Clearly, according to equations (2) and (3), both tip displacement and blocking force are proportional to driving field. Moreover, tip displacement is independent of actuator thickness at a given field. Shown in Fig. 2 is the electric field dependence of tip displacement for shear mode actuator with different thickness. We can see that rather than predicted by eq. (2), tip displacement is dependent on actuator thickness . Quite a large tip displacement level (40μm) was obtained by shear mode actuator with thickness of 0.37 mm under electric field of about 325 V/mm. For a given field, as the actuator thickness decreases, the tip displacement increases. And also, tip displacement is not linearly proportional to electrical field in this wide driving field range. Two reasons may account for these results: nonlinear piezo-electric response under high driving field level for soft PZT ceramics; and induced mechanical bending due to lateral shear force.

For ferroelectric ceramics such as PZTs, linear piezoelectric response is observed only under very small signal level. The materials properties provided by manufacturers are all measured under small signal level. However, as driven field amplitude increases, the charge output or strain response due to electric field will increase nonlinearly. Consequently, the effective dielectric constant and piezoelectric coefficients will increase[7]. Our experimental results[8] on various PZT ceramic materials indicate that piezoelectric d_{15} coefficient increases as driving field amplitude. Especially for soft PZT, nonlinearity occurs even at relatively low electric field level which consequently contributes to the nonlinear electric field response of tip displacement of the cantilever shear mode actuators. On the other hand, for cantilever shear mode actuator, one end is mechanically clamped thus can not generate pure shear motion under high driving field. Due to this boundary condition, a lateral force which perpendicular to the actuator surface will be produced when driving under electric field. In the case of thin ceramic plate, mechanical bending will then be easily resulted which enhances the tip displacement of ceramic actuator. The thinner the ceramic plate, which is easier to be bent thus the larger the tip displacement. The induced mechanical bending mode can be further clarified by Fig. 3 which shows frequency response of tip displacement for shear actuator with 0.9 mm thickness under driving field of 100 V/mm. The observed fundamental bending resonant frequency is 278 Hz. Experimental results also shows that at a given driving field level, as actuator thickness increases, resonant frequency linearly increases, as shown in Fig. 4. Using the assumption of a homogeneous ceramic plate, the fundamental bending resonant frequency of a cantilever actuator can be expressed as:

$$f_r = 0.161\,(t/L^2)\frac{1}{\sqrt{\rho\, s_{11}^E}} \qquad (4)$$

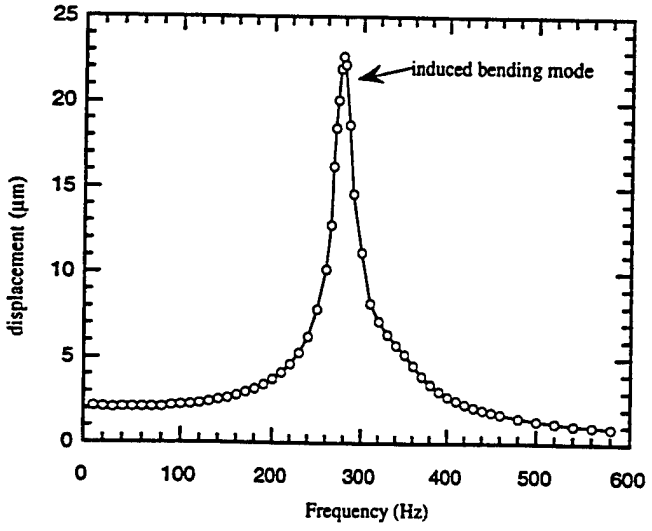

Figure 3. Tip displacement as function of frequency for shear actuator with t = 0.9 mm (L = 32.2 mm, w = 12.3 mm, driving field E = 100 V/mm)

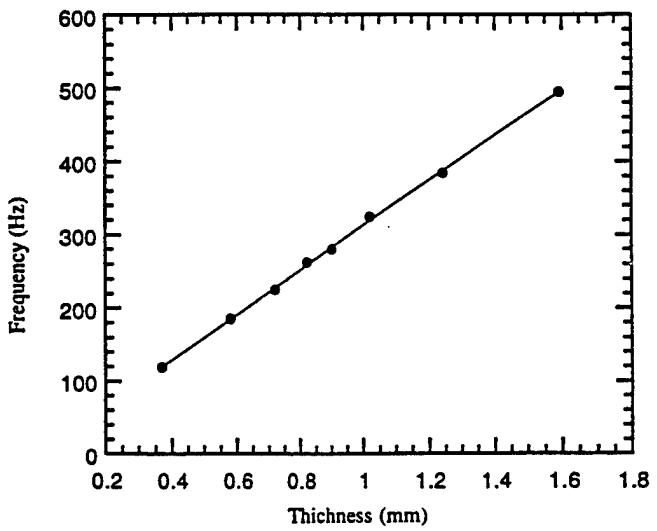

Figure 4. Bending resonant frequency as function of actuator thickness (L = 32.2 mm, w = 12.3 mm)

indicating f_r is proportional to actuator thickness, which is in good agreement with experimental data. By Eq. (4), using the measured resonant frequency, mechanical compliance s_{11}^E could be calculated. However, further experimental results (Fig. 5) show that the bending resonant frequency is strongly dependent on driving electric field: as the amplitude of driving field increases, resonant frequency decreases. Therefore mechanical compliance s_{11}^E in Eq. (4) is dependent on driving field amplitude. This is due to elastic nonlinearities of piezoelectric ceramics. In Eq. (4) s_{11}^E is the linear elastic compliance. When piezoelectric ceramic is driven under high electric field, nonlinear elastic coefficients have to be taken into account.

$$x_i = s_{ij}^E T_j + s_{ijk}^E T_j T_k + s_{ijkl}^E T_j T_k T_l \qquad (5)$$

The nonlinear elastic coefficients are directly related to and account for the shift of resonant frequency [9].

Quite a large blocking force can be generated in pure shear mode vibration and this shear force is independent of actuator length (Eq. (3)). However, when induced bending vibration occurs under high driving field level, blocking force will be greatly reduced and can be written as:

$$F_b = \frac{Y t^3 w \delta}{4L^3} \qquad (6)$$

Where Y is Young's modulus of ceramic actuator, δ is tip displacement. The blocking force is now dependent on electric field in a quite complex way since tip displacement is not a linear function of driving field for cantilever shear mode actuator.

It should be noted that in piezoelectric shear mode actuator, large tip displacement can only be achieved when using thin ceramic plate. under high driving field. In some applications which require low displacement level but large force, two-layer or multilayer shear mode actuator could be used. In these actuators, thin ceramic plates with anti-parallel poling direction are bonded together mechanically in series and electrically in parallel. Low driving voltage could be used due to reduced individual layer thickness. Experimental results on two-layer actuators indicate that bending resonant frequency is proportional to the total actuator thickness thus can be shift to higher frequency range by using more layers.

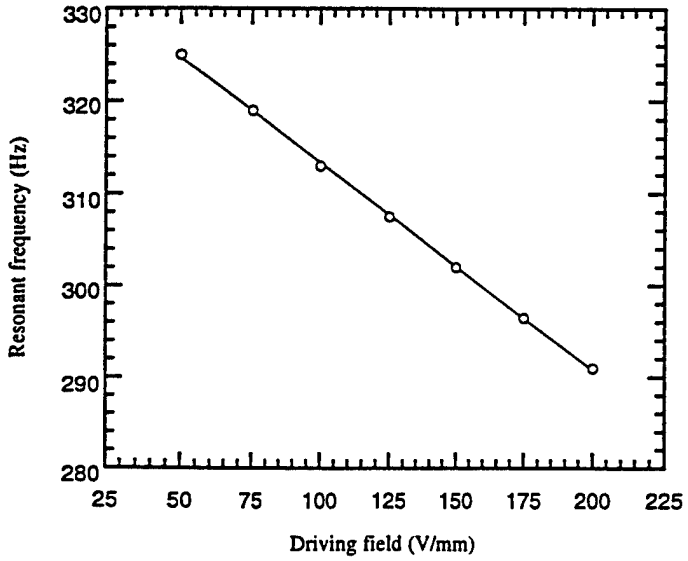

Figure 5. Bending resonant frequency as a function of driving field for shear actuator with t = 1.02 mm

IV. Summary

Characteristics of piezoelectric shear mode actuator have been investigated. Due to both nonlinear piezoelectric response and electric field induced mechanical bending, quite a large tip displacement can be obtained. The resonant frequency of bending vibration is dependent on the driving field because of elastic nonlinearities.

ACKNOWLEDGMENT

This work was supported by the Office of Naval research under the contract N00014-94-1140

Reference

(1) Uchino, *Bull. Am. Ceram. Soc.*, 65(4), 647 (1986)
(2) Y. Sugawara, K. Onitsuka, S. Yoshikawa, Q. C. Xu, R. E. Newhnam, and K. Uchino, "Metal-Ceramic Composite actuators," *J. Am. Ceram. Soc.*, 75[4] 996-98 (1992)
(3) Q. C. Xu, A. Dogan, J. Tressler, S. Yoshikawa and R. E. Newhnam, "Ceramic-Metal Composite Actuator", *Ferroelectrics*, Vol. 160, pp. 337 -346 (1994)
(4) K. Uchino, M. Yoshizaki and A. Nagao, "Monomorph Characteristic in $Pb(Zr,Ti)O_3$ Based Ceramics", *Ferroelectrics*, Vol. 95, pp. 161-164 (1994)
(5) Gene H. Haertling, "Rainbow Ceramics - A New Type of Ultra-High-Displacement Actuator", *Am. Ceram. Bull.* Vol. 73, No. 1, 93 - 96 (1994)
(6) Gene H. Haertling, " Chemically Reduced PLZT Ceramics for Ultra-High Displacement Actuators", *Ferroelectrics*, Vol. 154, pp. 101-106 (1994)
(7) Q. M. Zhang, H. Wang and J. Zhao, " Effect of Driving Field and Temperature on the Response Behavior of Ferroelectric Actuator and Sensor Materials", *Journal of Intelligent Material Systems and Structures*, Vol. 6, 84 - 94 (1996)
(8) Qing-Ming Wang, L. E. Cross, "Electric Field and Temperature Dependence of Piezoelectric d_{15} coefficient of PZT Ceramics", to be published.
(9) Horst Beige, "Elastic and Dielectric Nonlinearities of Piezoelectric ceramics", *Ferroelectrics*, Vol. 51, pp. 113 - 119 (1983)

INTEGRATION STUDIES

APPENDIX 66

journal

J. Am. Ceram. Soc., 79 [8] 2041–48 (1996)

Structural–Property Relations in a Reduced and Internally Biased Oxide Wafer (RAINBOW) Actuator Material

Catherine Elissalde,* L. Eric Cross,† and Clive A. Randall†

Materials Research Laboratory, The Pennsylvania State University, University Park, Pennsylvania 16802

Reduced and internally biased oxide wafer (RAINBOW) actuators are fabricated by a controlled reduction of $Pb(Zr,Ti)O_3$-based piezoelectric material. The reduction process results in a conductive layer composed of an interconnected metallic lead phase and refractory oxides ($ZrTiO_4$, ZrO_2, La_2O_3, etc.). The nature of the reduction is discovered to be the result of a complex volume change leading to a nanoscale interconnected metallic structure. The distribution of phases within the cermet vary within the thickness of the wafer. Within the piezoelectric ceramic phase, the reduction process modifies the grain-boundary structure to give two distinct types of fracture: transgranular and intergranular. The complexed microstructures of the RAINBOW actuator materials are discussed in relation to their dielectric and piezoelectric properties.

I. Introduction

RECENTLY, there has been a continuous effort to improve the performance of piezoelectric materials for electromechanical actuator applications. Novel piezoelectric structures, such as unimorph or bimorph cantilevers and flextensional composite structures all have been developed to produce higher strains than the basic monolithic materials.[1–4] As an example, the ceramic–metal composite actuator, the so-called "Moonie," is able to provide large displacements and generative forces.[5,6] A new type of monolithic ceramic, known as the reduced and internally biased oxide wafer (RAINBOW), is of extreme interest, because it presents the advantage of a wide range of stress/strain characteristics.[7] The RAINBOW device can be described as a monolithic structure with a piezoelectric layer (nonreduced) and a reduced cermet layer (electrically conductive); a cermet is a ceramic–metal composite material often used for mechanical applications. The controlled reduction of a stoichiometric $Pb(Zr,Ti)O_3$ (PZT) is achieved by placing the bottom surface of the ceramic on a carbon substrate and protecting the top surface with a ZrO_2 plate. The RAINBOW actuator is heated at high temperatures and cooled to room temperature. An internal radial stress develops during the reduction process and distorts the wafer to the domelike structure of the actuator.[7] This transformation process gives the RAINBOW actuator unique elastodielectric properties. Our objective is to understand the microstructure of the RAINBOW material, with relation to the electrical and mechanical properties of the two phases (reduced and nonreduced).

II. Experimental Techniques

Lead lanthanum zirconate titanate- (PLZT-) based RAINBOW ceramics were used (Aura Ceramics, Inc., Minneapolis, MN). The composition was given as 5.5/56/44, in terms of the respective constituent lanthanum/zirconium/titanium ions.

The electromechanical resonant behavior of the RAINBOW material was measured using an impedance/gain phase analyzer (Model HP4194A, Hewlett-Packard Co., Palo Alto, CA) in the frequency range 100 Hz–1 MHz. Dielectric measurements were conducted from room temperature up to 250°C at various frequencies using a multifrequency inductance–capacitance–resistance (LCR) meter (Model HP4274A, Hewlett-Packard). An acoustic microscope (Sontex) was used to determine longitudinal and transverse sound velocities of the samples.

Thermal expansion measurements were performed from room temperature up to 650°C to measure the thermal strains. A vertical push-rod dilatometer equipped with a high-sensitivity linear variable-differential transformer (LVDT) was used.[8] X-ray diffractometry (XRD) analysis was conducted for phase identification using a diffractometer (Model PAD V, Scintag, Inc., Sunnyvale, CA). Scanning and transmission electron microscopy studies, SEM and TEM, respectively, were conducted to evaluate the microstructural details of the RAINBOW structures. The SEM microscope was a field-emission model (Model 6300f, JEOL, Tokyo, Japan), and a scanning tunneling electron microscope (STEM) (Model 420, Philips Electronic Instruments, Mahwah, NJ) operated at 120 kV was used for TEM. The TEM samples were prepared in planar and cross-sectional views. The samples were polished to a thickness of 40 μm and then mounted on 3 mm copper grids with epoxy. Ion-beam thinning was performed on a dual mill (Gatan, Pleasanton, CA) at 4 kV at 12°.

III. Results and Discussion

(1) *Microstructural Characterization*

Figure 1(a) shows a typical XRD analysis for the reduced layer on the cermet phase. The dominant phase was identified as metallic lead; the presence of the additional oxide materials, identified as La_2O_5–4PbO and $ZrTiO_4$, varies throughout the thickness of the cermet layer. The surface in contact with the unreduced PLZT still contained metallic lead, but the presence of La_2O_3, PbO, and $ZrTiO_4$ are more prevalent, as shown in Fig. 1(b). The metallic phase is continuous throughout the cermet and serves as one of the electrode contacts to pole and drive the piezoelectric phase. The gradient of phases throughout the thickness of the cermet also is reflected in the spatial variation of the resistance, as previously reported by Haertling.[9]

Thermal expansion measurements of the unreduced layer and of the cermet show large differences, which readily could be the origin of radial stress on cooling to form the dome structure. The thermal expansion coefficient (α) of the cermet is dominated by the metallic lead to give $\alpha_{cermet} = 8.4 \times 10^{-6}$ °C^{-1}, whereas the corresponding unreduced PLZT layer is only 44×10^{-6} °C^{-1}. The thermal expansion coefficient of the cermet is lower than that expected for pure lead metal (29×10^{-6} °C^{-1}),

W. Huebner—contributing editor

Manuscript No. 192497. Received June 30, 1995; approved February 21, 1996.
Supported in part by the Office of Naval Research, NASA, and the Jet Propulsion Laboratory.
†Member, American Ceramic Society.
*Laboratoire de Chemie du Solide du CNRS, Université Bordeaux, 33405 Talence Cedex, France.

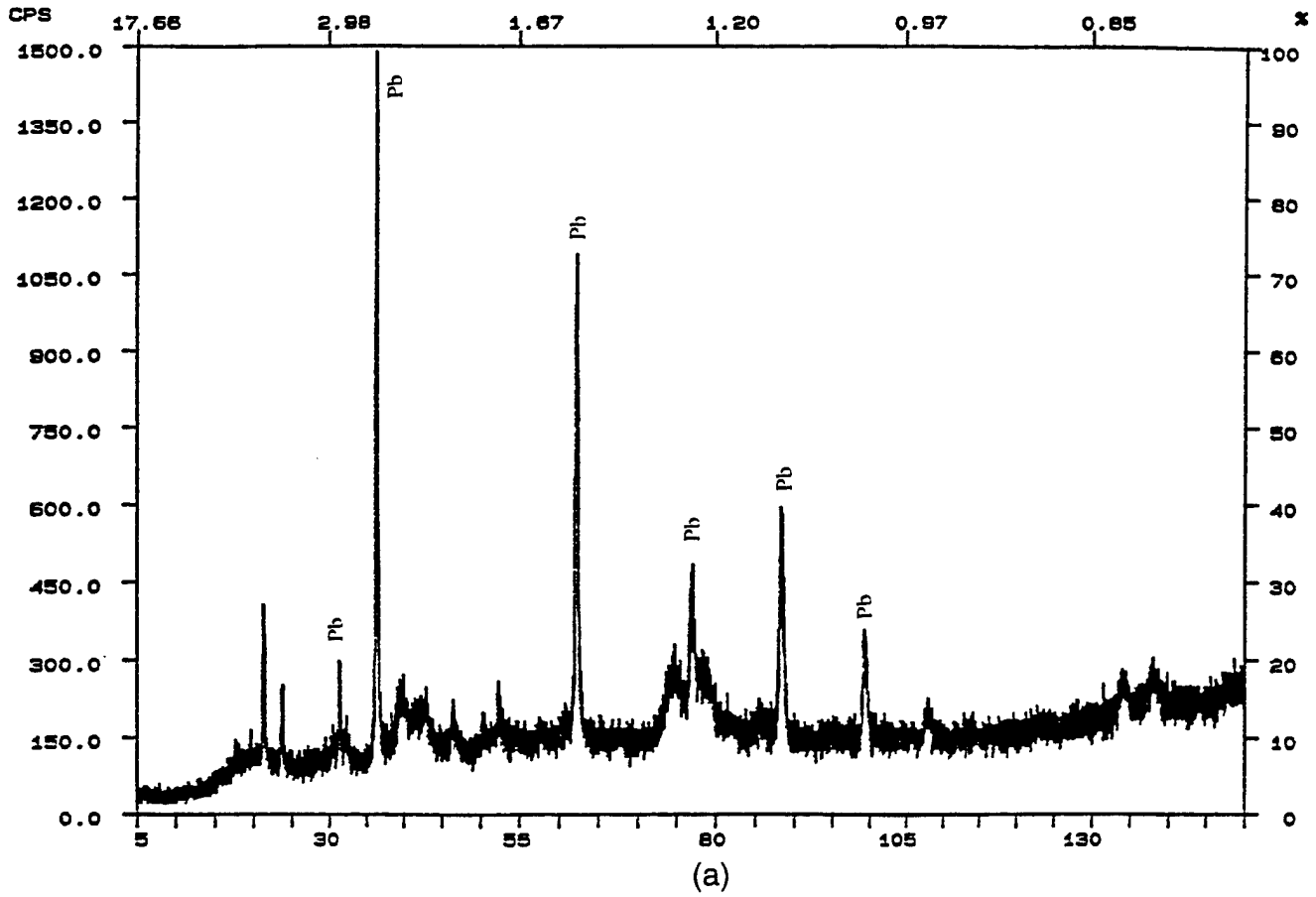

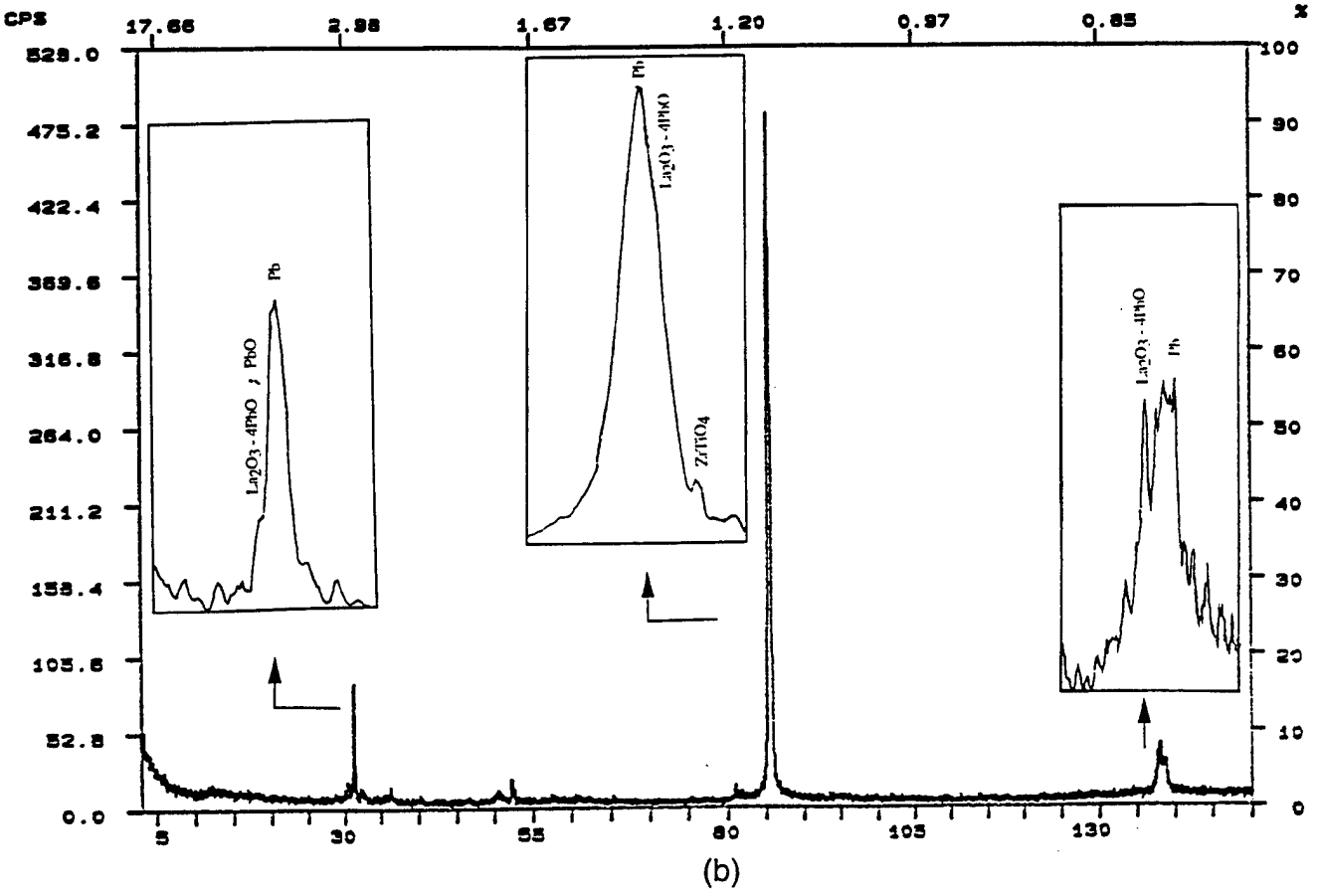

Fig. 1. XRD patterns for (a) the reduced layer and (b) a different thickness region of the cermet.

which is caused somewhat by the unreduced oxide inclusions but predominantly is associated with the interconnected porosity, which is discussed below.

Figures 2(a)–(e) show the general microstructural characteristics of the cermet phase. Figure 2(a) is an SEM micrograph that shows the pore and channel structures contained within the cermet; these pores and channels have cross-sectional diameters of ~100 nm. Figure 2(b) shows the equivalent TEM micrograph of these structures; the TEM study revealed that these channels and pores are real features distributed homogeneously throughout the cermet up to the piezoelectric interface. Additionally, the channels are percolating throughout the cermet with a 3–3 connectivity.[10] The size of the oxide phase inclusions is ~100 nm (Fig. 2(c)). Figure 2(d) shows a Moire fringe

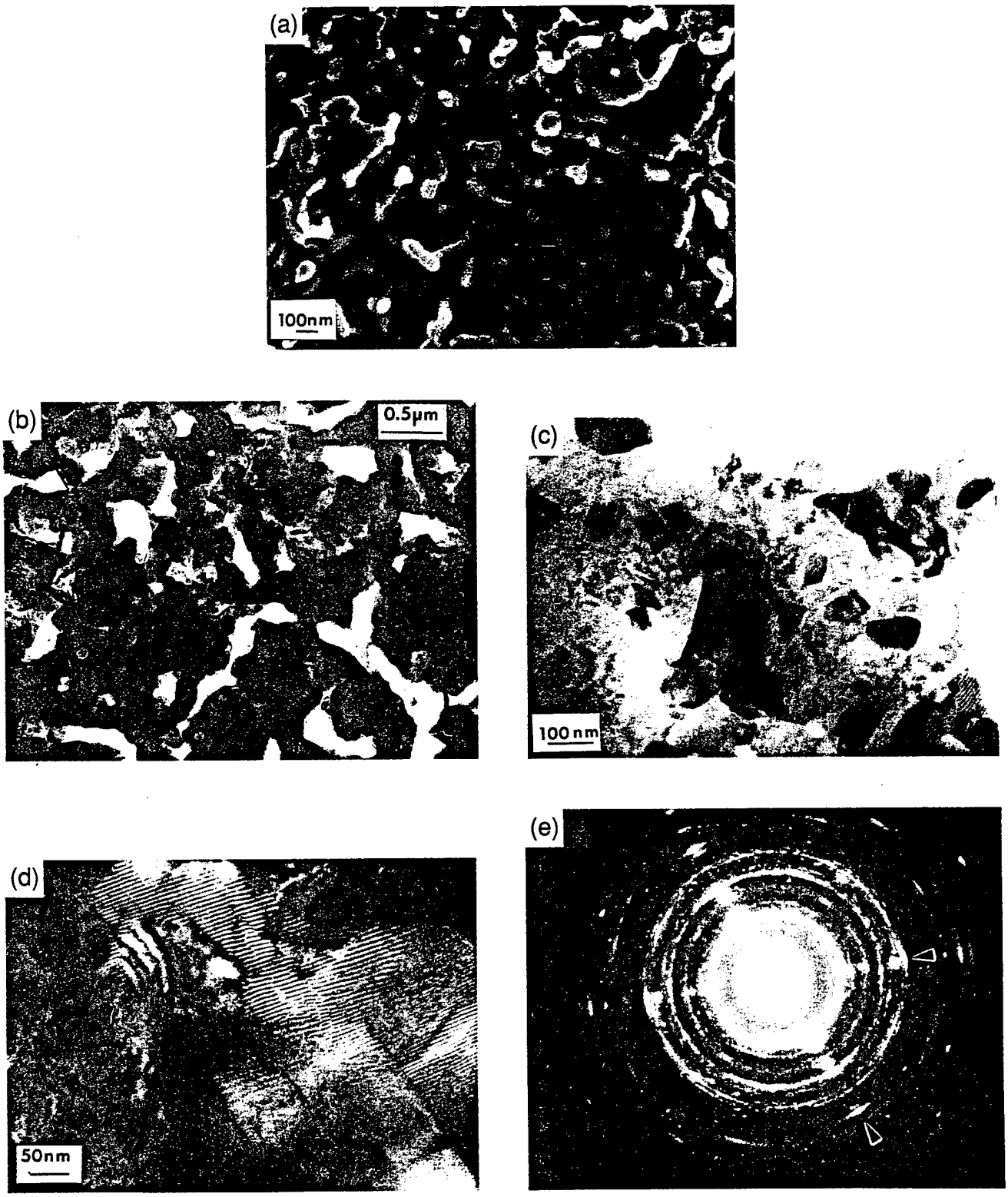

Fig. 2. (a) SEM image of the cermet; (b) TEM planar view image of the cermet; (c) TEM bright-field image of the multiple oxide inclusions within the metallic lead phase; (d) Moiré patterns within the cermet lead crystallites; and (e) selected-area diffraction photograph of the cermet, showing ring patterns of the phases.

Table I. Comparison between Lattice Spacings Obtained from TEM and International Centre for Powder Diffraction Data Files

Material	*d*-spacing (Å) TEM	XRD	ICPDD* Card No.
$ZrTiO_4$	3.59	3.61	34-415
	2.93	2.93	
	2.53	2.516	
	2.11	2.15	
	1.81	1.806	
$PbO_{1.57}$	3.87	3.856	26-577
	2.879	2.872	
	2.23	2.235	
	1.59	1.584	
	2.879	2.872	
Lead	2.879	2.855	4-086
	2.49	2.475	

*International Centre for Powder Diffraction Data, Newtowne Square, PA.

pattern contained within the metallic lead crystallites. Closer inspection of the Moire fringe contrast reveals a dislocation structure associated with lattice parameter changes and very little suggestion of lattice rotation as the source of the internal stresses.[11] Figure 2(e) is a selected-area diffraction pattern revealing ring patterns of the oxide phase $ZrTiO_4$. The systematic diffraction rows noted in Fig. 2(d) are associated with the larger metallic lead crystallites. The obtained lattice spacings are compared to the International Centre for Diffraction Data (Newtowne Square, PA) files for these different phases and listed in Table I.

Electron micrographs of the cross-sectional region between the cermet and the ceramic are shown in Figs. 3(a)–(d). Figure 3(a) is an SEM micrograph of the cermet/ceramic interface. A typical bright-field micrograph of the interface is illustrated in Fig. 3(b); the volume reduction of the cermet phases, along with the pores and channel formation, is shown. No special crystallographic orientation relationships have been found in this study; we believe this is the result of the textured lead-metal crystallites being first nucleated and grown from the random orientation of the piezoelectric ceramic grains. Figure 3(c) shows a diffraction pattern from the piezoelectric grain; the elongated spots in the ⟨110⟩ direction are typical of the ferroelectric twin structures found in PZT grains.[12] From the microscopy, it is clear that the interface between the cermet and ceramic is relatively uniform. The roughness of the interface, being only over a few grains along the length of the cermet–ceramic, is represented schematically in Fig. 3(d). Figure 4(a) shows that there are two regimes within the perovskite oxide resulting from the reduction process; these regions are labeled I and II in the SEM micrograph of a fractured

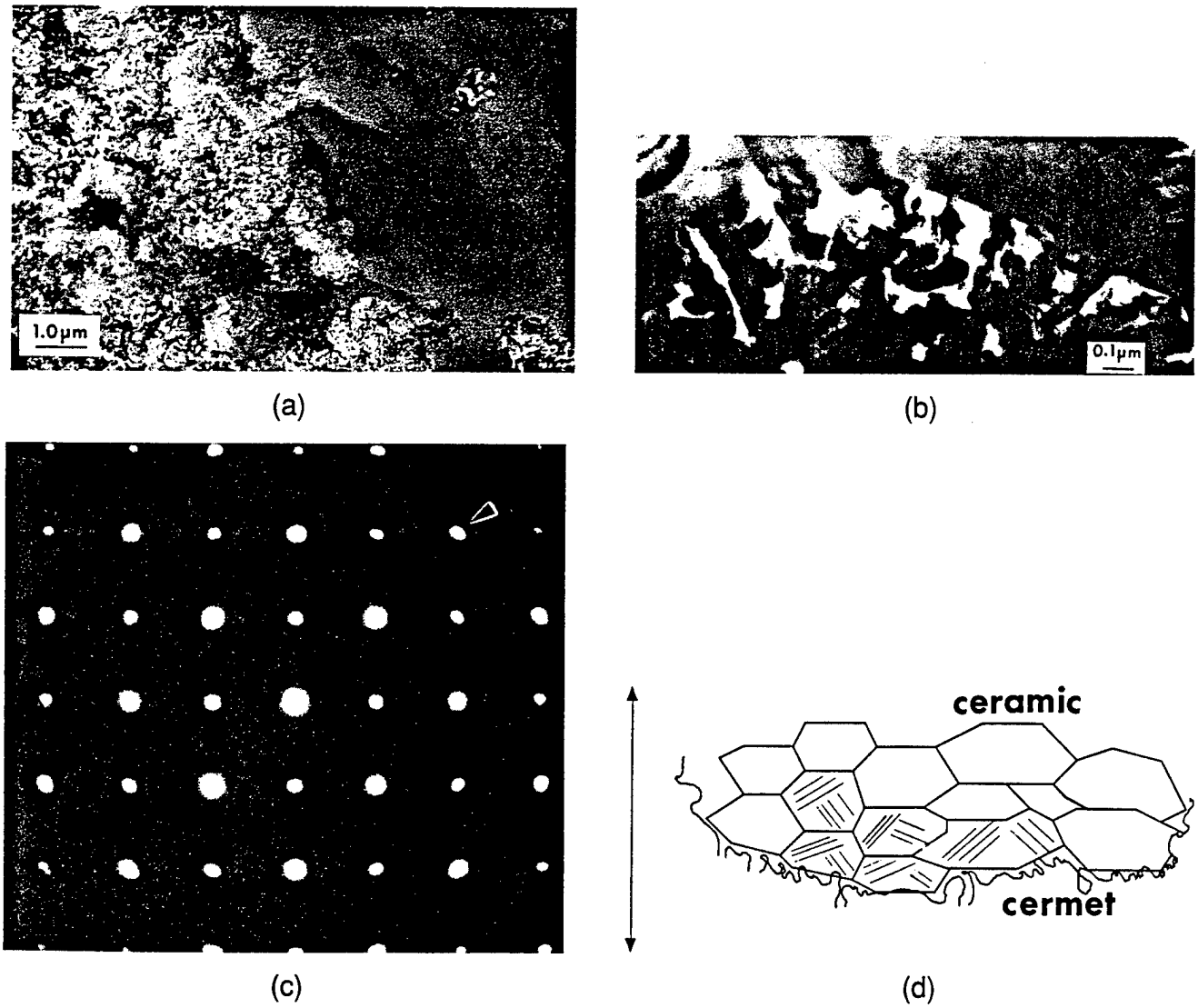

Fig. 3. (a) SEM image of the cermet/ceramic interface; (b) TEM bright-field image of the interface; (c) diffraction pattern of the PLZT ceramic, showing split reflections [001] zone (spot splitting consistent with {110} twins domains); and (d) schematic representation of the cermet/ceramic interface.

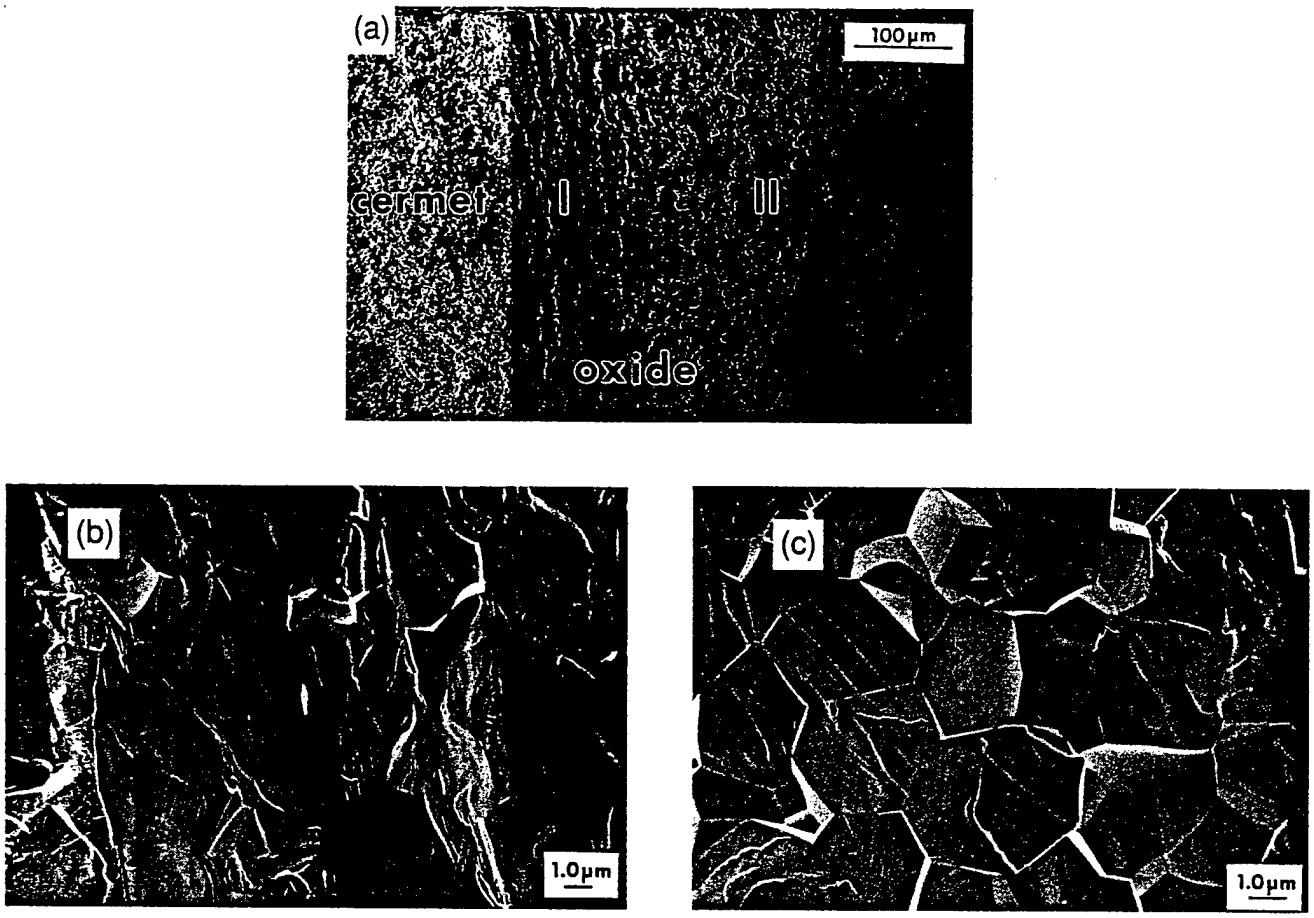

Fig. 4. SEM micrographs of (a) the interface, showing the two regions existing within the perovskite oxide; (b) fracture of region I; and (c) fracture of region II.

cermet/ceramic interface. Region I reveals transgranular fracture, whereas region II reveals intergranular and transgranular fracture but is predominantly intergranular. Also observed within the grains is the complex ferroelastic domain structure typical of a PZT ferroelectric.[12]

The difference in the fracture behavior is believed to be the result of an initial modification of the grain boundaries in the form of lead oxide loss and reduction from the grain boundaries. The process is the first stage of the reduction process, with the second stage being the full reduction of the PZT grains into the cermet.

The microstructure features observed above account for the evolution of the cermet phase in the reduction process, as noted by Haertling.[13] Figure 5 summarizes the general features of the reduction process; the evolution of the thickness (x) versus reduction time (t) does not follow the ideal parabolic relation ($x = (Dt)^{1/2}$, where D is the diffusion coefficient). The micrographs above, with the volume reduction and the channel formation, could account for this departure. The chemical reduction processes also are listed.[9]

(2) Physical Properties

In our previous study of the resonance behavior of RAINBOW materials, we modeled the impedance data assuming similar elastic behavior between the ceramic and cermet phases. Considering the new microstructural evidence, we reconsidered this basic assumption.

The determination of the fundamental thickness mode allows precise measurement of the elastic stiffness coefficient, C_{33}^D, using the following relationship:

$$2f_p t = \left(\frac{C_{33}^D}{\rho}\right)^{1/2} \tag{1}$$

where t is the thickness of the sample, f_p the parallel resonance frequency, and ρ the density. Geometrically determined densities reveal similar values for sections of the cermet phase and ceramic phase; $\rho = 7.5 \times 10^3\ \text{kg}\cdot\text{m}^{-3}$. This similarity is a direct consequence of the porosity contained within the cermet phase. The obtained C_{33}^D value for the nonreduced material is $15.5 \times 10^{10}\ \text{N}\cdot\text{m}^{-2}$, within the typical range expected for soft PZT.[14] For the RAINBOW material, this value is only $C_{33}^D = 14.4 \times 10^{10}\ \text{N}\cdot\text{m}^{-2}$. By varying the relative thickness of the piezoelectric and modeling the composite elastic stiffness with the series mixing:

$$\frac{1}{C_{33\text{tot}}^D} = \frac{t_{nr}}{t_{tot}}\left(\frac{1}{C_{33nr}^D}\right) + \frac{t_{cer}}{t_{tot}}\left(\frac{1}{C_{33cer}^D}\right) \tag{2}$$

where t_{nr} is the piezoelectric thickness, t_{cer} the cermet thickness (the total thickness is simply the sum of the components; i.e., $t_{tot} = t_{nr} + t_{cer}$), C_{33nr}^D the piezoelectric elastic stiffness, and C_{33cer}^D the cermet elastic stiffness. Then, knowing C_{33nr}^D and varying t_{nr}, deduction of C_{33nr}^D is possible. An average value of $10.04 \times 10^{10}\ \text{N}\cdot\text{m}^{-2}$ was obtained. Further verification of the elastic coefficients was obtained from acoustic microscopy. Acoustic microscopy allows direct determination of the elastic coefficients via the velocity of the acoustic wave transmitted through the material. A comparison of the two techniques is presented in Table II, where good agreement is shown between these measurements. A reduction in stiffness within the cermet structure is noted; the metallic lead and interconnected porous structure account for this result.

Additionally, the lateral extensional mode of the RAINBOW cantilever can be determined. Figure 6 shows the resonant frequency versus inverse width ($1/w$) of the nonreduced piezoelectric cantilever with both ends free. Under these boundary conditions, the resonant frequency can be expressed as

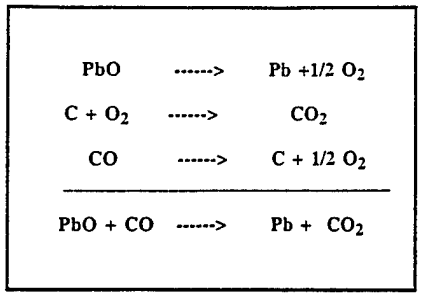

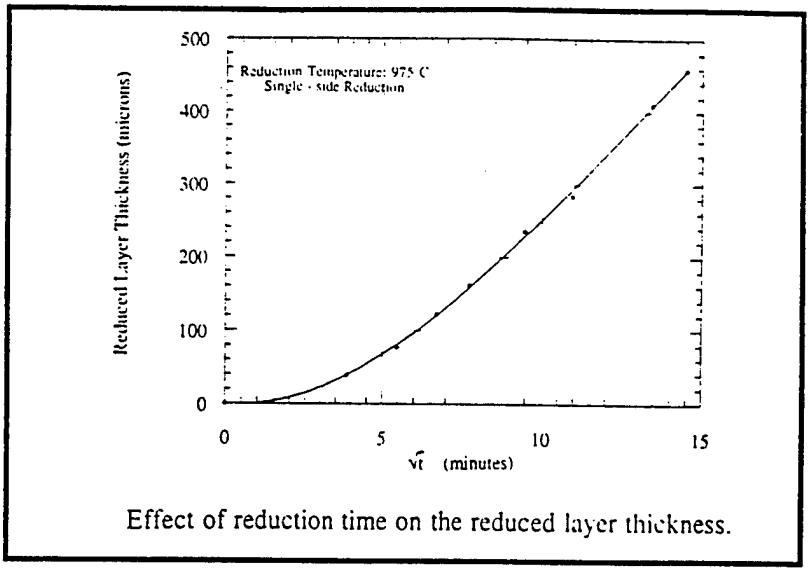

Effect of reduction time on the reduced layer thickness.

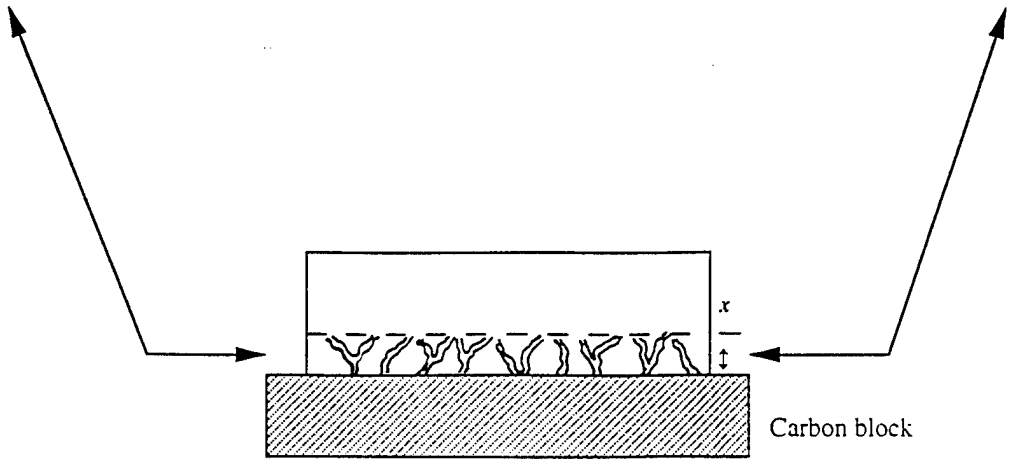

Fig. 5. Schematic representations of the general features involved in the reduction process of the ceramic to the RAINBOW material.

Table II. Elastic Stiffness Constant (C_{33}^D) Values Obtained from Resonance Method and Acoustic Microscopy

Technique	C_{33}^D ($\times 10^{-10}$ N·m^{-2})	
	Cermet	Piezoelectric
Resonance	10.04	15.49
Acoustic microscopy	9.93	15.52

$$f_r = 0.5\left(\frac{1}{w}\right)\left(\frac{C_{\text{eff}}^E}{\rho}\right)^{1/2} \tag{3}$$

where w is the width of the piezoelectric sample, ρ the density, and C_{eff}^E is the effective elastic constant where

$$C_{\text{eff}}^E = \frac{1}{S_{11}^E(1-\sigma^2)} \tag{4}$$

S_{11}^E is the elastic compliance, and σ is the Poisson ratio. From Fig. 6, we can obtain $C_{\text{eff}}^E = 8.63 \times 10^{10}$ N·m^{-2}. Also, via the bending mode, the scan is obtained directly:[15]

$$f_r = 1.0279\frac{t}{L^2}\left(\frac{1}{S_{11}^E\rho}\right)^{1/2} \tag{5}$$

where L is the length of the cantilever. S_{11}^E was determined to be 13.36×10^{-12} N·m^{-2}. From Eq. (4), σ for the nonreduced phase was determined to be 0.366. Such a value is in good agreement with a previous reference[16] and confirms the validity of the technique. In the lateral direction, the resonant frequency was independent of the reduced and nonreduced phase thicknesses (Fig. 7).

To complete this characterization, the coefficient d_{31} of the piezoelectric element was determined. From the resonance method, the d_{31} value obtained was -150×10^{-12} C/N. A direct technique, the double-beam laser interferometer, was used to verify the d_{31} value.[17] Under an alternating-current- (ac-) driven electric field along the polarization direction (E_3), the sample deformation ($\Delta L_1/L_1$) and the strain (S_1) are measured. Through the converse piezoelectric effect:

$$d_{31} = \frac{S_1}{E_3} = \frac{(\Delta L_1/L_1)}{E_3} \tag{6}$$

The obtained d_{31} value of -141×10^{-12} C/N is in good agreement with the previous value deduced from the resonance method. Such a value is more characteristic of a hard PZT than that expected for the soft PZT studied.[14] This lower d_{31} value can be explained by a reduction in the extrinsic domain wall contribution to d_{31} in the soft PLZT due to the high transverse constraining stress.[18] From these piezoelectric resonance measurements, the cermet microstructure clearly influences the density and elastic stiffness of the RAINBOW structures, which, in turn, controls the resonant modes.

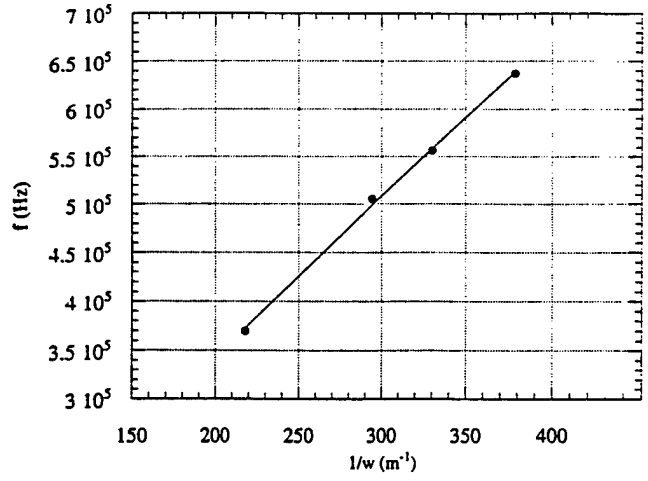

Fig. 6. Resonant frequency of the lateral extensional mode versus inverse width (nonreduced phase).

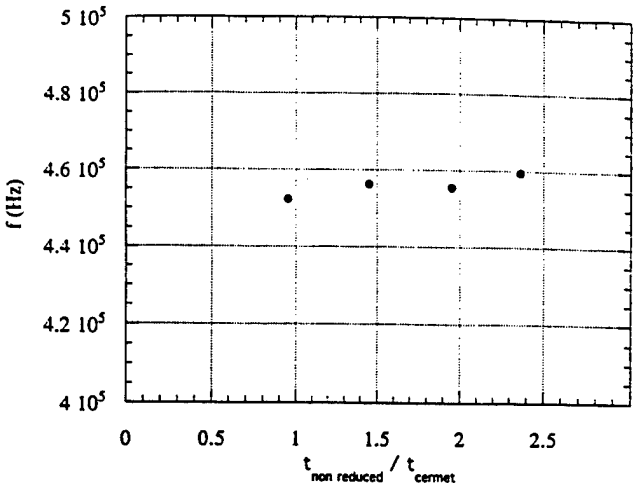

Fig. 7. Resonant frequency of the lateral extensional mode versus the nonreduced-layer-thickness:cermet-thickness ratio.

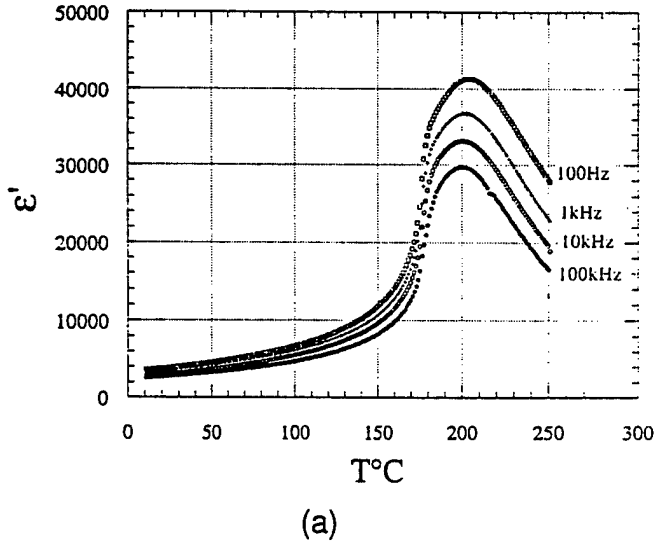

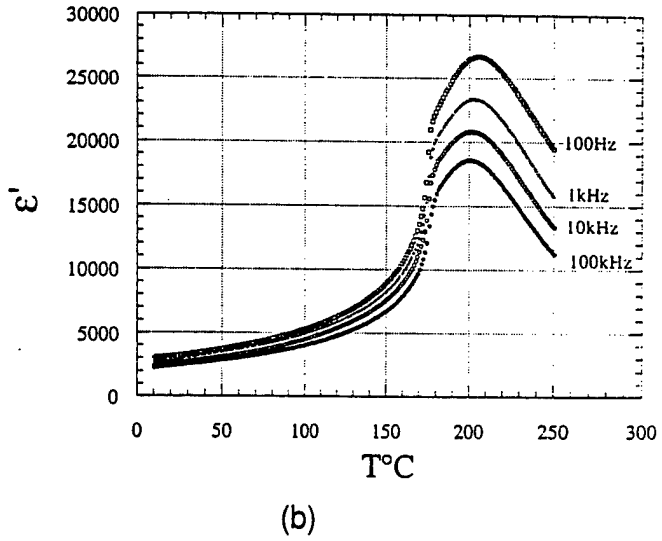

Fig. 8. Dielectric constant as a function of temperature for (a) RAINBOW material and (b) the nonreduced phase.

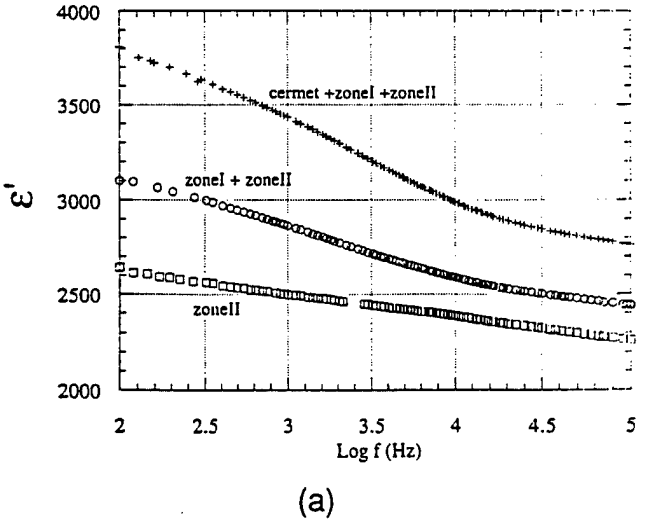

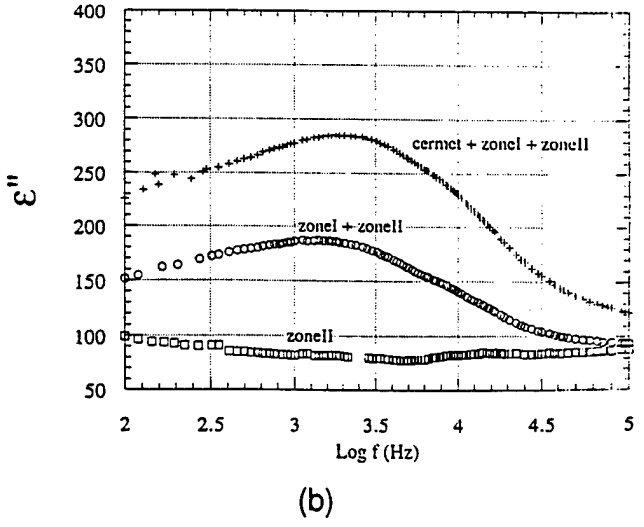

Fig. 9. Frequency dependence of (a) the real part of the permittivity, ε', and (b) the imaginary part of the permittivity, ε'', at room temperature.

Dielectric measurements have been performed from room temperature up to 250°C for nonreduced PLZT and RAINBOW samples. Figures 8(a) and (b) show the corresponding temperature dependence of the dielectric constant, ε', at different frequencies. It is interesting to note that removing the electrode on the reduced face of the RAINBOW material does not change the obtained results, verifying the conductive cermet phase to be suitable as an electrode material. The Curie temperature is ~200°C and remains the same when the frequency increases. Such a result is in agreement with a nonrelaxor such as PLZT and corresponds to a composition similar to 6/65/35, which is that of a typical soft PZT. The dielectric permittivity of the RAINBOW material shows a dispersion typical of a space relaxation over the measured temperature range. The room-temperature dielectric behavior shows a relaxation, characterized by a simultaneous maximum of the imaginary part of the permittivity, ε'', and decrease of the real part of the permittivity, ε'. (Figs. 9(a) and (b)). The microstructure observed in Fig. 4(a) is believed to be the origin of this space-charge relaxation. By systematically polishing away the cermet layer and region I and making impedance measurements, the dielectric response confirms this hypothesis on each combination of layers (Fig. 9). The physical removal of region I, the prereduced grain-boundary piezoelectric region, leaves no space-charge polarization effects at room temperature in region II. Therefore, the differences in capacitance and resistance from these mixed regions give the space-charge contribution. The relaxation observed at ~1 kHz depends only on the electrical boundary conditions, and this is not believed to be the result of the stress inherent in the RAINBOW material. This last effect is considered only on the elastic properties.

IV. Summary and Conclusions

A structure–property relationship study of the RAINBOW cermet–ceramic has revealed new insights into the formation process, the microstructure, and electromechanical properties. The cermet microstructure consists of an interconnected metallic lead phase and an interconnected porous structure, with unreduced oxides $ZrTiO_4$ and La_2O_3 embedded in the lead metal matrix as inclusions. The cermet/ceramic interface is relatively sharp, but there is a prereduction of the grain-boundary phase in the ceramic. The prereduction modifies the grain boundary, as observed in the fracture properties of the ceramic. The prereduction and nonreduced regimes (regions I and II) in the ceramic create a space-charge polarization.

Physical properties that determine the resonance behavior, such as density and elastic stiffness, are given consideration with the observed microstructure. Measurements of the elastic stiffness of the cermet were obtained via a thickness resonance mode and acoustic microscopy and showed excellent agreement.

Acknowledgments: The authors wish to thank Michael Hill of NIST (Maryland) for the acoustic microscopy measurements. Many thanks also go to Mark S. Angelone for his technical input on the SEM microscope.

References

[1]K. Uchino, *Piezoelectric and Electrostrictive Actuators*. Morikita Publications, Tokyo, Japan, 1986.
[2]J. K. Lee and M. M. Marcus, "The Deflection–Bandwidth Product of Poly Benders and Related Structures," *Ferroelectrics*, **32**, 93–101 (1981).
[3]M. R. Steel, F. Harrison, and P. G. Harper, "The Piezoelectric Bimorph: An Experimental and Theoretical Study of its Quasistatic Response," *J. Phys. D: Appl. Phys.*, **11**, 979–89 (1978).
[4]J. Van Randeraat and R. E. Setterington, *Piezoelectric Ceramics*. N. V. Philips' Gloeilampenfabricken, Eindhoven, The Netherlands, 1974.
[5]Y. Sugawara, K. Onitsuka, S. Yoshikawa, Q. Xu, R. E. Newnham, and K. Uchino, "Metal–Ceramic Composite Actuators," *J. Am. Ceram. Soc.*, **75** [4] 996–98 (1992).
[6]K. Onitsuka, "Effects of Bonding and Geometry on the Flextensional Transducer 'Moonie' "; Ph.D. Thesis. The Pennsylvania State University, University Park, PA, 1993.
[7]G. Haertling, "Rainbow Ceramics—A New Type of Ultra-High Displacement Actuator," *Am. Ceram. Soc. Bull.*, **73** [1] 93–96 (1994).
[8]R. Guo, "Ferroelectric Properties of Lead Barium Niobate Near the Morphotropic Phase Boundary"; Ph.D. Thesis. The Pennsylvania State University, University Park, PA, 1990.
[9]G. Haertling, "Reduction/Oxidation Effects in PLZT Ceramics"; pp. 699–711 in *4th International SAMPE Electronics Conference* (Albuquerque, NM, 1990). Edited by R. E. Allred, R. J. Martinez, and K. B. Wischmann. Society for the Advancement of Materials and Process Engineering, Covina, CA, 1990.
[10]R. E. Newnham, "Composite Electroceramics," *Annu. Rev. Mater. Sci.*, **16**, 47–68 (1986).
[11]J. W. Edington, *Practical Electron Microscopy in Materials Science*. N. V. Philips' Gloeilampenfabricken, Eindhoven, The Netherlands, 1976.
[12]C. A. Randall, R. W. Whatmore, and D. J. Barber, "Ferroelectric Domain Configurations in a Modified PZT," *J. Mater. Sci.*, **22**, 925–31 (1987).
[13]G. Haertling, "Chemically Reduced PLZT Ceramics for Ultra-High Displacement Actuator," *Ferroelectrics*, **154**, 101–106 (1994).
[14]B. Jaffe, W. R. Cook, and H. Jaffe, *Piezoelectric Ceramics*. Academic Press, New York, 1971.
[15]W. G. Cady, *Piezoelectricity*, Vol. I. Dover Press, New York, 1964.
[16]W. P. Mason, *Physical Acoustics*, Vol. I, Part A. Academic Press, New York, 1964.
[17]W. Y. Pan and L. E. Cross, "A Sensitive Double Beam Laser Interferometer for Studying High-Frequency Piezoelectric and Electrosensitive Strains," *Rev. Sci. Instrum.*, **60** [8] 2701–703 (1989).
[18]Q. M. Zhang, H. Wang, N. Kim, and L. E. Cross, "Direct Evaluation of Domain Wall and Intrinsic Contributions to the Dielectric and Piezoelectric Response and Their Temperature Dependence on Lead Zirconate-Titanate Ceramics," *J. Appl. Phys.*, **75** [1] 454–59 (1994).

APPENDIX 67

To be published in the proceedings on the 10th Annual International Symposium on Applications of Ferroelectrics (ISAF), 1996.

Optimization of Bimorph Based Double Amplifier Actuator under Quasistatic Situation

Baomin Xu, Q. M. Zhang, V. D. Kugel, Qingming Wang, L. E. Cross

Materials Research Laboratory, Pennsylvania State University, University Park, PA 16802

Abstract -- Bimorph based double amplifier actuator is a new type of piezoelectric actuation structure which combines both bending and flextensional amplification concepts. As a result the displacement of the actuator can be more than ten times larger than the tip displacement of bimorphs and can be used in air acoustic transducers as an actuation element. This paper studied the dependence of displacement on actuator parameters and optimum design issues for the cover plate (the flextensional part of the actuator) theoretically and experimentally.

I. INTRODUCTION

How to get larger displacements is always a main objective in the development of piezoelectric transducer and actuator devices. Since the direct extensional strain in most piezoelectric ceramic materials is at best a few tenths of one percent, the means of enhancing or amplifying the displacement is essential in many device designs[1].

Except for multilayer type actuators, which enhance the displacement by a direct dimension effect, presently there are two ways to amplify the extensional strain of piezoelectric materials[2]. One is to make use of bending amplification mechanism, which leads to the development of bimorph type actuators. Another way is the utilization of flextentional amplification scheme, which leads to the development of flextensional transducers widely used in underwater acoustics, moonie and cymbal actuators[3].

Recently, we presented a new kind of piezoelectric actuation structure named bimorph based double amplifier[4], because it can be considered as the combination of bending-type actuators and flextensional elements, as shown in Fig. 1. As a result the displacement of the new actuator can be more than ten times larger than the tip displacement of bimorphs, and can be used in air acoustic transducers as an actuation element. Some theoretical analyses have been given earlier[5]. In this work, the displacement of the actuator is studied in detail, with emphasis on the optimum dimension design of the cover plate of the actuator.

II. PRINCIPLE AND THEORETICAL ANALYSIS

This work was supported by the Office of Naval Research under the contract No. N00014-94-1-1140.

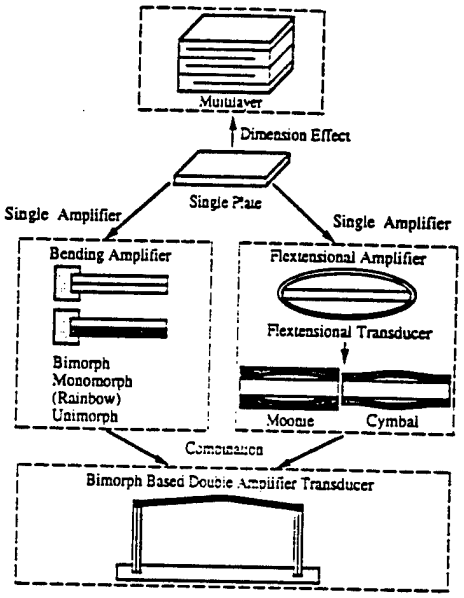

Fig. 1. Evolution of piezoelectric actuators with larger displacement

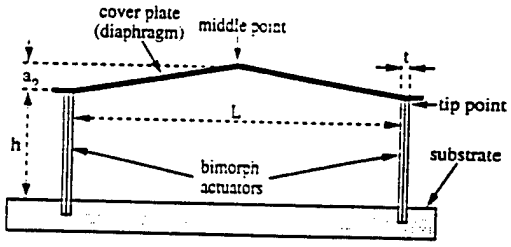

L: length of the cover plate h: height of bimorphs
t: thickness of bimorphs a_0: initial height of the cover plate

Fig. 2. Basic configuration of bimorph based double amplifier

The basic configuration of bimorph based double amplifier is shown in Fig. 2. The structure mainly consists of two parallel-mounted bimorphs with a triangle shaped cover plate as an active diaphragm fixed on the top of the bimorphs. Higher displacement is achieved by converting the tip displacement of bimorphs to the motion of the cover plate. Since one of the objective of the actuator is to work in air acoustic transducers as an actuation element, loudspeaker

paper is chosen as cover plate material in this work because of its excellent mechanical-acoustic property and light weight.

The relationship between displacement of the cover plate (middle point) and actuator parameters is explained below: as shown in Fig. 3, letters A, B, and C represent the joint parts of the cover plate, which are called as hinge regions. Generally, the deformation of the cover plate can be considered to concentrate in these hinge regions. When a displacement of the cover plate is generated, moments will be induced in these hinge regions due to the deformation, which will balance the moments produced by the bimorphs. Therefore, the motion of the cover plate is rotation-dominated and can be treated as two rigid beams connected by a torsional spring at the middle point. When a voltage V is applied to the bimorphs, a tip displacement Δ and force F are generated, which in turn produces a displacement ξ at the middle point of the cover plate and induces a moment M in the torsional spring due to the displacement. From the geometric consideration, it can be found that:

$$\xi = a_1 - a_0 = \sqrt{a_0^2 + L\cdot\Delta} - a_0 \qquad (1)$$

The moment balance equation is:

$$2F\cdot(a_0+\xi) = M = k\cdot 2\cdot(\theta_1 - \theta_0)$$

or
$$F(a_0+\xi) = k(\theta_1-\theta_0) \approx k\cdot 2\xi/L \qquad (2)$$

Since ξ is much smaller than L. k in equation (2) is the spring constant. It has been known that[6]:

$$F = \frac{t^3 w}{4h^3 s_{11}^E}(\Delta_0 - \Delta) = c_0(\Delta_0 - \Delta) \qquad (3)$$

where w is the width and s_{11}^E is the elastic compliance of the piezoelectric material, Δ_0 is the tip displacement under free condition, and

$$\Delta_0 = 3d_{31}V(h/t)^2 \qquad (4)$$

if parallel type bimorph is used.

The equivalent torsional spring constant k can be determined in this way: Suppose the original length of the hinge region is b, and it is also the neutral line length of the deformation area. R_A, R_B and R_C are the elastic curvature radii at hinge regions A, B, and C respectively. From Fig. 3 we can get:

$$R_{B,i} = R_{C,i} \approx b/\tan\theta_i \text{ , and } R_{A,i} \approx b/(2\tan\theta_i),\ i = 0,\ 1$$

Let M_A, M_B and M_C represent the induced moments at areas A, B and C due to the displacement, then the total induced moment is[7]:

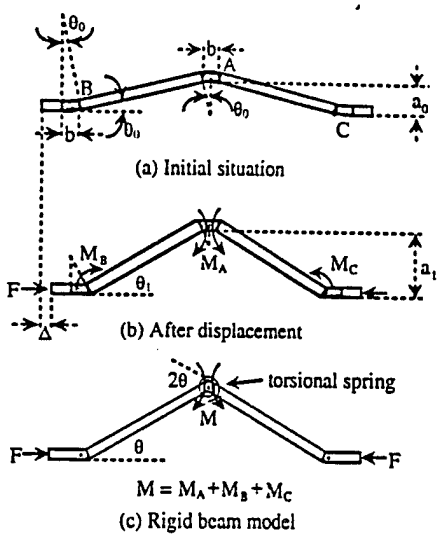

Fig. 3. Rigid-beam model for rotation-dominated cover plate motion

$$\begin{aligned} M &= M_A + M_B + M_C \\ &= EI(1/R_{A,1} - 1/R_{A,0}) + 2\cdot EI(1/R_{B,1} - 1/R_{B,0}) \\ &= 4EI(\tan\theta_1 - \tan\theta_0)/b \\ &\approx 4EI(\theta_1 - \theta_0)/b \end{aligned}$$

where E is the Young's modulus of the cover plate material and I is area moment of inertia of cross section of the hinge region. Compare to equation (2) we get the spring constant:

$$k = 2EI/b \qquad (5)$$

This means that k just depends on the properties of the cover plate material. Substituting equations (3) and (5) in equation (2) yields:

$$c_0(\Delta_0 - \Delta)(a_0 + \xi) = (2EI/b)\cdot(2\xi/L) \qquad (6)$$

From equations (1), (6) and (4), the dependence of Δ and ξ on the actuator parameters and driving voltage can be obtained, so that optimization on actuator design can be conducted. However, the analysis is rather complicated because the relationship between Δ and ξ is nonlinear according to equation (1).

Considering a simple situation, that is, if $L\cdot\Delta << a_0^2$, we get the linear approximations for equations (1) and (6):

$$\xi = L\cdot\Delta/(2a_0) \qquad (7)$$

$$c_0(\Delta_0 - \Delta)\cdot a_0 = (2EI/b)\cdot(2\xi/L) \qquad (8)$$

Hence Δ and ξ can be obtained as:

$$\Delta = \frac{\Delta_0}{1 + 2EI/(a_0^2 c_0 b)} \tag{9}$$

$$\xi = \frac{L \cdot \Delta_0}{2a_0 + 4EI/(a_0 c_0 b)} \tag{10}$$

Equation (10) indicates that ξ will increase linearly with L, but there is an optimum value for a_0 where ξ is maximum. This optimum value is:

$$2a_0 = 4EI/(a_0 c_0 b), \text{ or } a_0 = \sqrt{2EI/(c_0 b)} \tag{11}$$

However, as the initial height a_0 is very small, another possibility is that the deformation of the cover plate becomes larger and can not be neglected, that is, flextensional motion of the cover plate will occur. Hence the rigid-beam model shown in Fig. 3 is not valid. From elastic theory[8,9], when a triangle shaped continuous beam is under the action of compressed axial force P, the displacement of middle point is:

$$\xi = a_0 \left(\frac{\tan(\pi/2)\sqrt{P/P_{cr}}}{(\pi/2)\sqrt{P/P_{cr}}} - 1 \right) \tag{12}$$

where $P_{cr} = \pi^2 EI/L^2$ is Euler load.

Equation (12) shows that ξ will increase linearly with a_0. Actually, this is the situation similar for cymbal actuators where the displacement is linearly related to the cavity depth of endcaps and exponentially related to the cavity diameter because of the flextensional motion of endcaps[10].

Therefore, if flextensional motion of the cover plate occurs above the optimum a_0 value determined from the rotation-dominated situation, the real optimum cover plate height will be in the vicinity from rotation-dominated situation to the flextension-dominated situation.

III. EXPERIMENTS

The bimorphs used in this work are operated in parallel configuration and made from Motorala 3203HD (PZT type 5H) material. Their dimensions are 20.0 × 7.7 × 1.5mm. The loudspeaker paper with the same width and 0.56mm thickness is fixed on the top of bimorphs by super glue. The displacement of middle point and tip point are measured by using MTI 2000 Fotonic Sensor under different dimensions of cover plate. The applied voltage on bimorphs is fixed at 150V (p-p value) and frequency is 1Hz.

IV. RESULTS AND DISCUSSIONS

Fig. 4 is the dependence of middle point displacement and tip point displacement on the height of cover plate. The

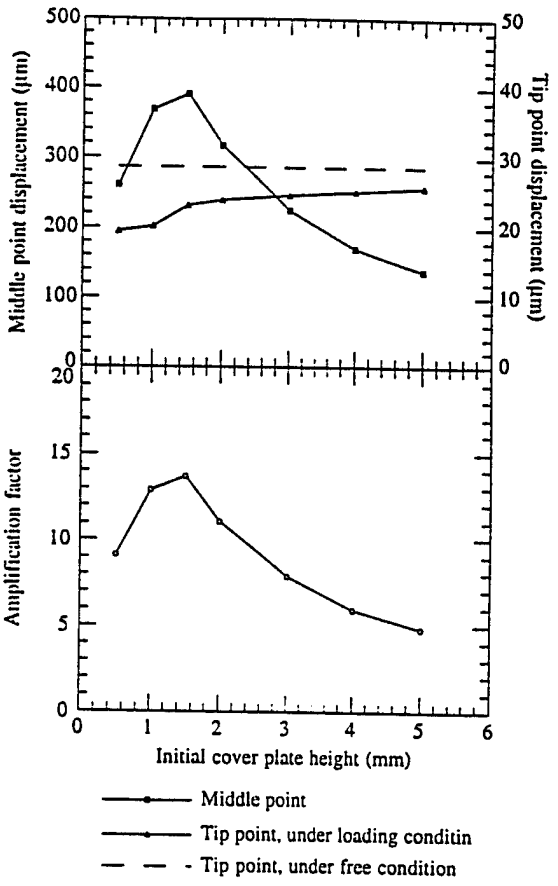

Fig. 4. Dependence of displacement and amplification factor on the initial cover plate height

length of cover plate is fixed at 56.0mm in this experiment. It really shows that there is an optimum value for initial cover plate height (about 1.5mm) at which middle point displacement reaches the maximum. Defining the amplification factor as the ratio of middle point displacement to the free tip displacement of bimorphs, Fig. 4 shows that the amplification factor is more than 10 in the vicinity of optimum initial cover plate height.

In order to determine the motion situation of the cover plate, the middle point displacement is also calculated by using equations (1) and (7) with measured tip point displacement and compared to experimental values in Fig. 5. It can be seen that when the cover plate height is larger than 3.0mm, the linear approximation can be used. When the cover plate height is between 1.5mm and 3.0mm, the calculated value using equation (1) is consistent with experimental results. This means it is still rotation-dominated situation but nonlinear effect must be considered. When the cover plate height is smaller than 1.5mm, the calculated value still increases but the measured value decreases, which means

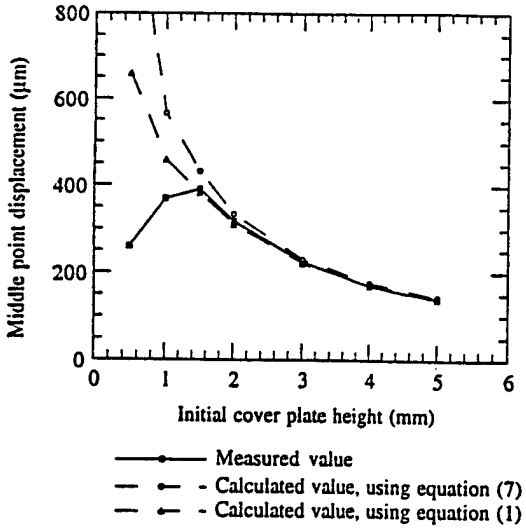

Fig. 5. Measured and calculated middle point displacement

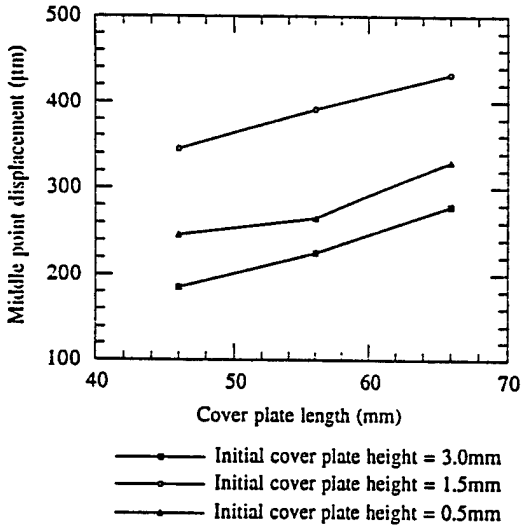

Fig. 6. Dependence of middle point displacement on cover plate length

flextensional motion of cover plate becomes obvious. Therefore, the optimum initial cover plate height for the present design is in the vicinity from rotation-dominated to flextention-dominated situation.

Fig. 6 shows the dependence of middle point displacement on the length of cover plate. When the cover plate height is 3.0mm, the linear approximation can be used so that the middle point displacement will linearly increase with the length of cover plate. When the cover plate height is 0.5mm, flextensional motion becomes dominated, and the middle point displacement increased with cover plate length more rapidly than linearly. This is consistent with our theoretical analysis.

V. CONCLUSIONS

The displacement of bimorph based double amplifier actuators can be more than ten times larger than the tip displacement of bimorphs. The displacement strongly depends on the initial height of cover plate. When the cover plate height decreases, the motion of cover plate is from rotation-dominated to flextension-dominated. And the optimum cover plate height is in the transfer region of these two kinds of situations. The displacement increases with cover plate length, but the relationship in detail is quite different according to rotation-dominated or flextension-dominated situation.

REFERENCES

[1] G. H. Haertling, "Rainbow ceramics – a new type of ultra-high-displacement actuator", *Amer. Ceram. Soc. Bull.*, Vol. 73, pp. 93 - 96, Jan. 1994.

[2] K. Uchino, "Ceramic Actuators: Principles and Applications", *MRS Bulletin*, Vol. 18, pp. 42 - 47, April 1993.

[3] A. Dogan, "Flextensional 'moonie' and 'cymbal' actuators", Ph.D. thesis, Pennsylvania State University, 1994.

[4] Baomin Xu, Q. M. Zhang, V. D. Kugel, L. E. Cross, "Piezoelectric air transducer for active noise control", *SPIE Proc.*, Vol. 2717, pp. 388 - 398, Feb. 1996.

[5] V. D. Kugel, Q. M. Zhang, Baomin Xu, Qingming Wang, L. E. Cross, "Bimorph-based air transducer: a model", presented at 1996 ONR Transducer Materials and Transducer Workshop, State College, Pennsylvania, March 25 - 27, 1996.

[6] J. G. Smits, S. I. Dalke, T. K. Cooney, "The constituent equations of piezoelectric bimorphs", *Sensors and Actuators A*, Vol. 28, pp. 41 -61, Jan. 1991.

[7] L. D. Landau and E. M. Lifshitz, *Theory of Elasticity*, 3rd. ed., Oxford: Pergamon Press, 1986, Chapter 2.

[8] S. P. Timoshenko, J. P. Gene, *Theory of Elastic Stability*, 2nd. ed., New York: McGraw-Hill, 1961, Chapter 1.

[9] H. G. Allen, P. S. Bulson, *Background to Buckling*, London: McGraw-Hill, 1980, Chapter 1.

[10] A. Dogan, J. F. Fernandez, K. Uchino, R. E. Newnham, "New piezoelectric composite actuator designs for displacement applications," in press *Proc. Euroceram 95* (1995).

APPENDIX 68

Piezoelectric air transducer for active noise control

Baomin Xu, Qiming Zhang, V. D. Kugel and L. E. Cross

Intercollege Materials Research Laboratory, Pennsylvania
State University, University Park, PA 16802

ABSTRACT

A new type of piezoelectric air transducer has been developed for active noise control and other air acoustics applications. The transducer is based on the composite panel structure of a bimorph-based double amplifier, that is, two parallel bimorphs or bimorph arrays with a curved cover plate as an active face attached to the top of the bimorphs. The electro-mechanical and electro-acoustic properties of the double amplifier structure and the transducer are investigated in this paper. The displacement of the cover plate of the double amplifier structure can reach millimeter scale with a relatively low driving voltage, which is more than ten times larger than the tip displacement of bimorphs. The sound pressure level (SPL) of the transducer can be larger than 90dB (near field) in the frequency range from 50 to 1000Hz and be larger than 80dB (far field) from 200Hz to 1000Hz, with the largest value more than 130dB (near field). Because of its light weight and panel structure, it has the potential to be used in active noise control.

Keywords: piezoelectric transducers, bimorphs, double amplifier structure, air acoustics, active noise control

1. INTRODUCTION

The electromechanical transducers based on piezoelectric materials have been widely used for many decades. However, most of these transducers are used in the areas of ultrasonics and underwater acoustics.[1] It is still difficult to apply piezoelectric materials or devices in air acoustics, especially at low frequency range. On the other hand, because of their unique properties, such as high electromechanical coupling efficiency, the ability of both sensing and transmitting, low loss, light weight and panel structure, it is highly desirable to use piezoelectric transducers at low frequency range and active noise control.[2]

There are two main problems to be solved to apply piezoelectric transducers in air acoustics and active noise control. One is that the displacement must be much larger than that of the common ceramic actuators because the radiated acoustic energy is proportional to the square of the displacement amplitude.[3] Another one is that the acoustic impedance should be matching to air to ensure an effective acoustic flow from the transducer to the medium.

Among all the piezoelectric actuators, bimorph type actuators generate the largest displacement (tip displacement).[4] However, the displacement is still not large enough to be used in air acoustics at low frequency range. In this paper, a new type of piezoelectric transducer based on the idea of bimorph-based double amplifier structure is presented. The displacement generated by the double amplifier structure can be more than ten times larger than the tip displacement of bimorphs. The acoustic impedance matching between the transducer and air can be obtained by carefully choosing the cover plate (active face) materials and its geometric configurations. As a result of these new designs, the transducer is promising to be used in active noise control as a sound transmitter.

2.DESIGN PRINCIPLES

The basic configuration of the bimorph-based double amplifier structure is shown in Fig. 1. The structure mainly consists of two parallel bimorphs with a curved (triangle shape) cover plate as an active face attached to the top of the bimorphs. Higher displacement is achieved by changing the tip displacement of bimorphs to a flexural motion of the cover plate. That is, when the bimorphs vibrate horizontally, the cover plate vibrates vertically with larger amplitude. Fig. 1(b) is the schematic of the displacement of the cover plate and bimorph actuators. From the geometric consideration, the vertical displacement of the middle point on the cover plate can be described as:

0-8194-2092-1/96/$6.00

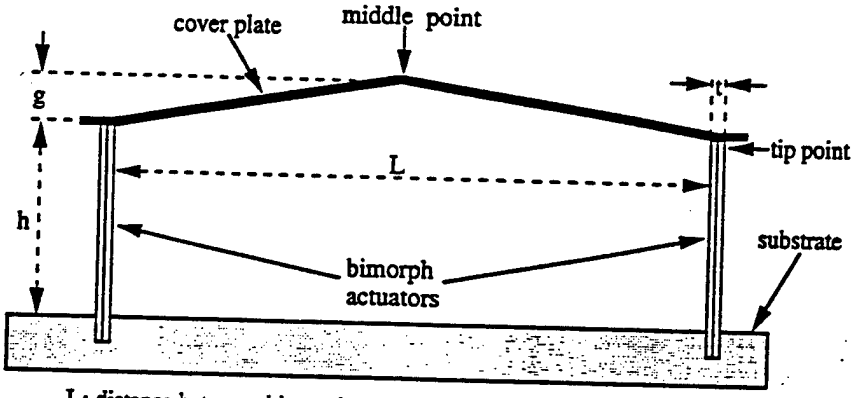

L: distance between bimorphs h: height of bimorphs
t: thickness of bimorphs g: height of the cover plate

(a) Cross section of the double amplifier structure

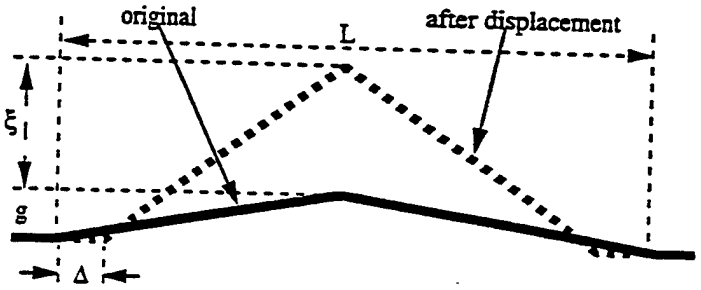

Δ: tip displacement of bimorphs ξ: displacement of the middle point of the cover plate

(b) Displacement of the double amplifier structure

Fig. 1. Configuration of the Bimorph Based Double Amplifier Structure

$$\xi = \sqrt{g^2 + L \cdot \Delta} - g \tag{1}$$

where ξ is the displacement of the middle point;
g is the height of the cover plate;
L is the distance between bimorph actuators;
Δ is the tip displacement of bimorphs.

We define the amplification factor of the displacement as:

$$\alpha = \frac{\text{middle point displacement of cover plate}}{\text{tip displacement of bimorph}} = \frac{\xi}{\Delta}$$

so,

$$\alpha = \frac{\sqrt{g^2 + L \cdot \Delta} - g}{\Delta} \tag{2}$$

If $L \cdot \Delta << g^2$, then

$$\sqrt{g^2 + L \cdot \Delta} \approx g\left(1 + \frac{L \cdot \Delta}{2g^2}\right) = g + \frac{L \cdot \Delta}{2g}$$

Therefore,

$$\xi = \frac{L \cdot \Delta}{2g} \tag{3}$$

and,

$$\alpha = \frac{\xi}{\Delta} = \frac{L}{2g} \tag{4}$$

This is why the displacement of the cover plate is much larger than the tip displacement of bimorphs.

Shown in Fig. 2 is the transducer constructed from the bimorph-based double amplifier structure. Instead of two parallel bimorphs, two parallel bimorph arrays are used here and the cover plate is fixed on the top of the bimorph arrays so that larger radiation area is obtained. Loudspeaker paper is chosen as the cover plate because of its excellent mechanical and acoustic properties and light weight. The other two lateral faces were also sealed by loudspeaker papers so that the transducer can work effectively as a monopole source.[5]

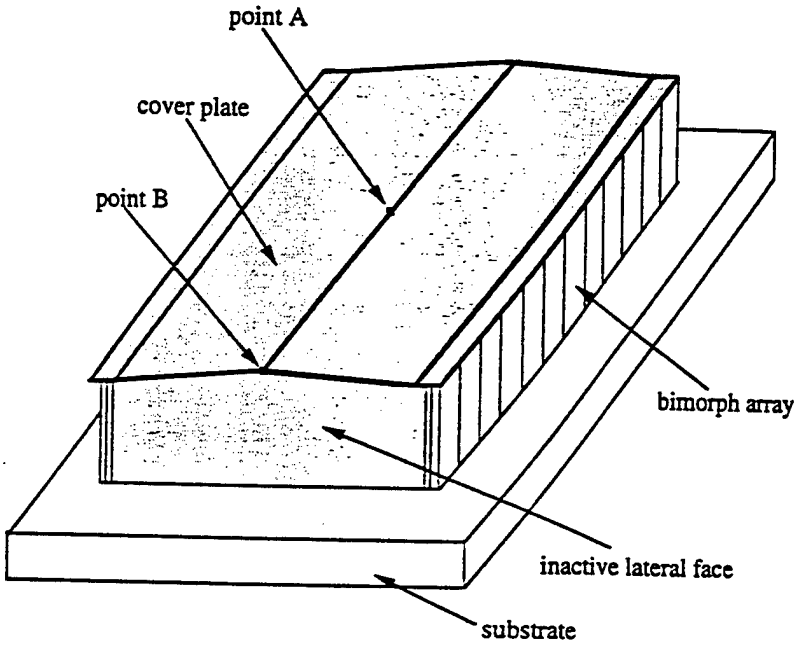

Fig. 2. Configuration of the Double Amplifier Transducer

3. SAMPLE PREPARATION AND MEASUREMENT TECHNIQUE

Bimorph actuators can be operated in series (the poling directions of the two piezoelectric plates are opposite) or in parallel (the poling directions of the two piezoelectric plates are consistent) configurations. All the bimorphs used in this paper are in parallel structure. They are made from a kind of PZT 5H type piezoelectric material[6] and the dimensions are 20.0mm X 7.0 X 1.0mm. The loudspeaker paper is from Nu-Way Company with the thickness of 0.56mm.[7] The experiments were conducted both on the double amplifier structures and the transducer. For the double amplifier structure experiment, the bimorphs are mechanically clamped at one end, and the cover plate is fixed on the top of bimorphs by super glue. The displacement of middle point and tip point are measured by using MTI 2000 Fotonic Sensor[8] under quisistatic and dynamic conditions. Fig. 3 is the schematic drawing of the measurement setup. The resonant frequency of the structure was determined by an HP-4194 Impedance Analyzer. For the transducer study, the bimorph arrays were fixed in the slots on the plastic substrate by super glue. The displacement at the central point (point A in Fig. 2) of the cover plate and at the intersection point of the central line and edge of the cover plate (point B in Fig. 2) was measured. The sound pressure level of the transducer was also studied in an anechoic chamber by using B & K 4135 type condenser microphone.[9] In measurement, the

transducer is baffled in a large rigid plane and the measurement points are on the axis which goes through the central point and perpendicular to the substrate as shown in Fig. 4. The distances between the measurement points and the central point are 5.0mm and 1.0m respectively. The former situation is called near field and the latter is far field.[10]

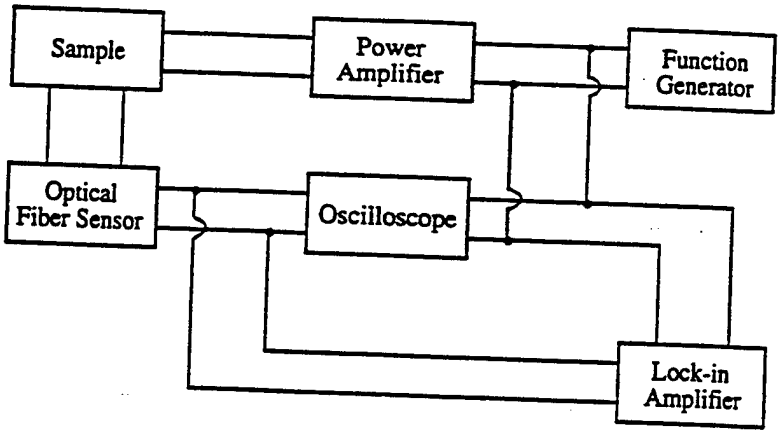

Fig. 3. Schematic Drawing of the Displacement Measurement Setup

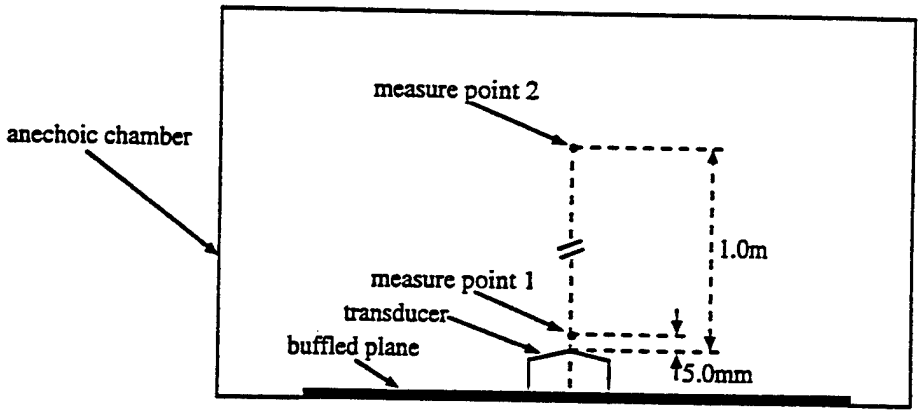

Fig. 4. Schematic Drawing of Sound Pressure Level Measurement Setup

4.RESULTS AND DISCUSSOINS

4.1. Displacement and resonant frequency of the double amplifier structures

The dependence of the middle point displacement and amplification factor on the height of the cover plate was evaluated under quisistatic condition (driving frequency = 1Hz) for the double amplifier structures with L = 50.0mm and 60.0mm (see Fig. 1) respectively, and the results were presented in Fig. 5. As the height of cover plate g decreases, the middle point displacement increases first, and then decreases. The largest displacement was obtained when the distance between bimorphs was 50mm and the height of cover plate was 1.0mm. The largest displacement can reach 450μm (0.450mm) with a driving voltage of 100V (peak-peak value). Fig. 5 also reveals that the amplification factor always increases as the height of the cover plate is reduced. The amplification factor can reach more than ten easily. When the driving voltage is 100V (peak-peak value), the tip displacement of the bimorphs without loading is 37.63μm, which is called free tip displacement.[11] Hence the middle point displacement can be more than ten times larger than the free tip displacement of the bimorphs. Fig. 6 shows the

displacement of the middle point as a function of the driving voltage. The displacement of the middle point increases almost linearly with the driving voltage. It is expected that the displacement of the middle point can reach about 1.5mm when the driving voltage is raised to 300V (peak-peak value) or 110V (rms value).

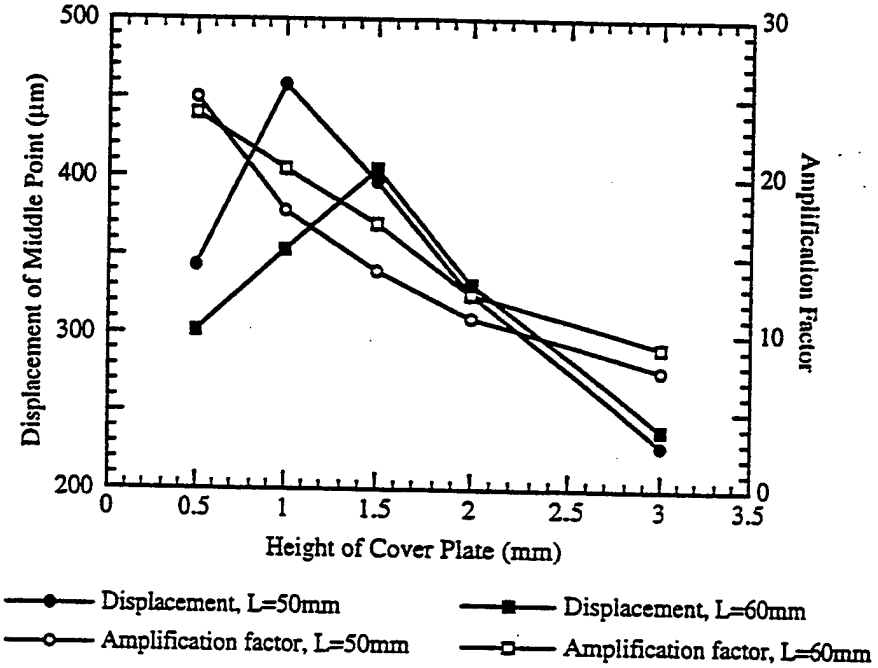

Fig. 5. Displacement and Amplification Factor of the Double Amplifier Structure (f=1Hz, Vp-p=100V)

Equations (1) to (4) show that the middle point displacement should always increase as the cover plate height is reduced, so does the amplification factor. However, when the height of the cover plate decreases, the effective loading of the cover plate will increase, and a larger force is needed to push the cover plate. The relationship between the generated force and tip displacement of bimorph can be described as:[12]

$$F = \frac{Y_c t^3 w}{4h^3}\left(\frac{3d_{31}h^2E}{2t} - \Delta\right) \tag{5}$$

where Yc is Young's modules of ceramic material;
d_{31} is piezoelectric constant of ceramic material;
w is width of bimorph;
E is applied electric field.

When a larger force is needed, the tip displacement of bimorph will reduce. Therefore, when the height of cover plate decreases, there are two competing factors which influence the middle point displacement of the cover plate. One is that the middle point displacement will increase according to the geometric relationship, so does the amplification factor. Another one is that the tip displacement of bimorph will decrease, which will reduce the middle point displacement. Therefore, there is an optimum point where the maximum value of the middle point displacement is obtained. However, the amplification factor will always increase when the cover plate height decreases as long as the geometric relationship is valid. The similar situation will happen when the distance between the bimorphs is changed.

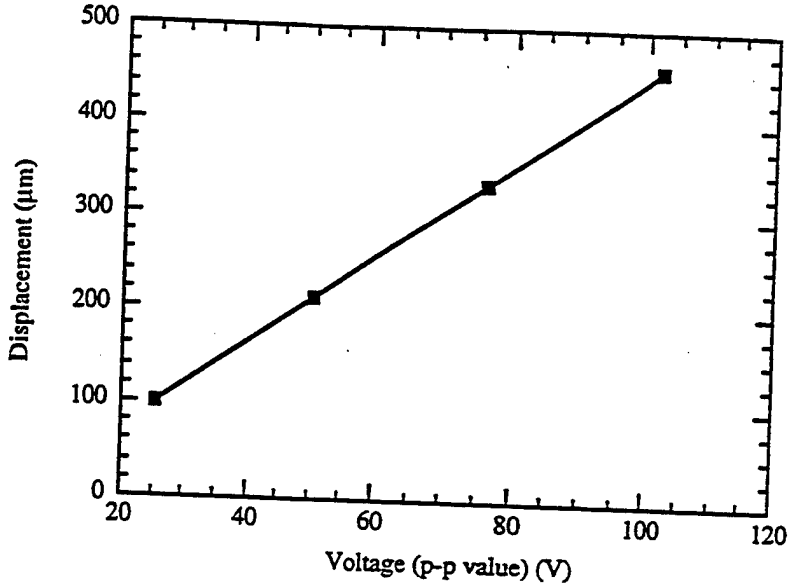

Fig. 6. Displacement of the Middle Point as a Function of Driving Voltage (f=1Hz, L=50mm, g=1.0mm)

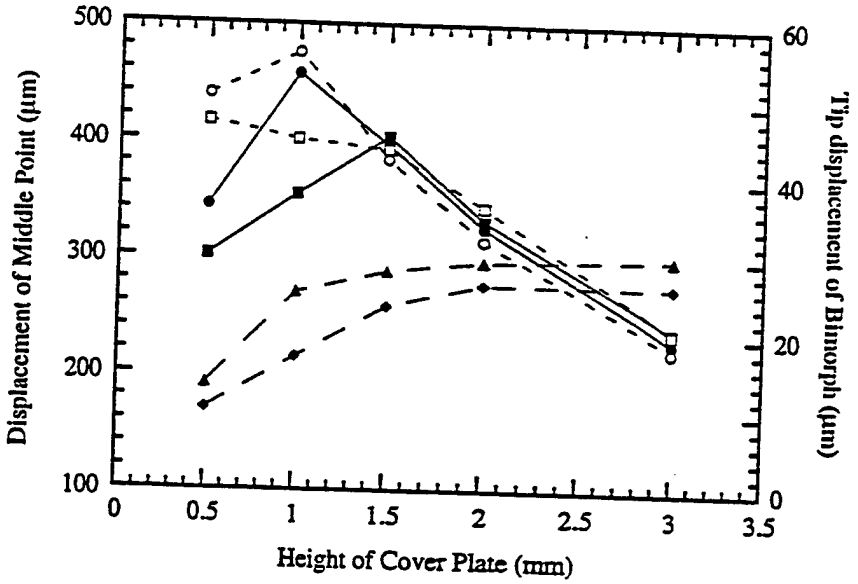

Middle point, measured value, L=50mm
Middle point, measured value, L=60mm
Tip point, measured value, L=50mm
Middle point, calculated value, L=50mm
Middle point, calculated value, L=60mm
Tip point, measured value, L=60mm

Fig. 7. Displacement of the Double Amplifier Structure (f=1 Hz, Vp-p=100V)

Besides these two factors, there is an additional factor should be considered is the buckling of the cover plate. If the buckling of the cover plate happens, the geometric relationship (equation (1)) will not be hold, and the middle point displacement of cover plate will become smaller.

The tip displacement of bimorphs, the measured displacement of the middle point, and the calculated displacement of the middle point according to equation (1) are presented in Fig. 7. The tip displacement decreases rapidly when g is below 1.0mm for L = 50.0mm and 1.5mm for L = 60.0mm, which results in a decrease in the middle point displacement. When g is larger than 1.0mm for L = 50mm and 1.5mm for L = 60mm, there is no buckling of the cover plate since the calculated middle point displacement is nearly the same as the measured value. Below these values buckling of the cover plate occurs.

The dependence of the resonant frequency on the height of the cover plate is shown in Fig. 8 for L = 50.0mm and 60.0mm. For this amplifier structure, the cover plate can be considered as an effective mass loading attached on the top of the bimorph beams, which reduces the resonant frequency of the bimorph beams.[13] As the height of the cover plate decreases and the distance between bimorphs increases, the effective loading of the cover plate increases, resulting in a decrease of the resonant frequency. This is consistent with the experimental results.

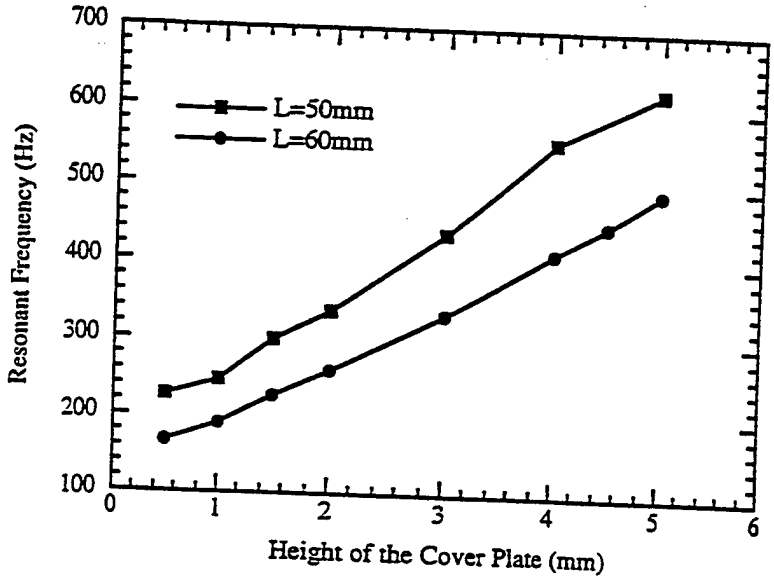

Fig. 8. Resonant Frequency of the Double Amplifier Structure

The relationship between the displacement and frequency is shown in Fig. 9 for L = 50.0mm, g = 1.0mm. From the comparison of the tip displacement of bimorphs, the calculated displacement of middle point, and the measured displacement of middle point, it can be concluded that the cover plate can keep its shape from buckling during vibration in the frequency range up to about two times of the resonant frequency, that is, the transducer can work effectively in the frequency range up to the two times of the resonant frequency.

4.2. Displacement and sound pressure level of the double amplifier transducer

Based on the experimental results and analyses of the double amplifier structures, the bimorph-based double amplifier transducer was constructed. The dimensions of the transducer are:

the distance between the bimorphs L = 50.0mm;
the height of the cover plate g = 3.5mm;
the width of the bimorph arrays W = 60.0mm;
the height of bimorphs h = 18.0mm.

Therefore, this transducer can be expected to work effectively up to 1000 Hz, which is the frequency range desirable for the active noise control.

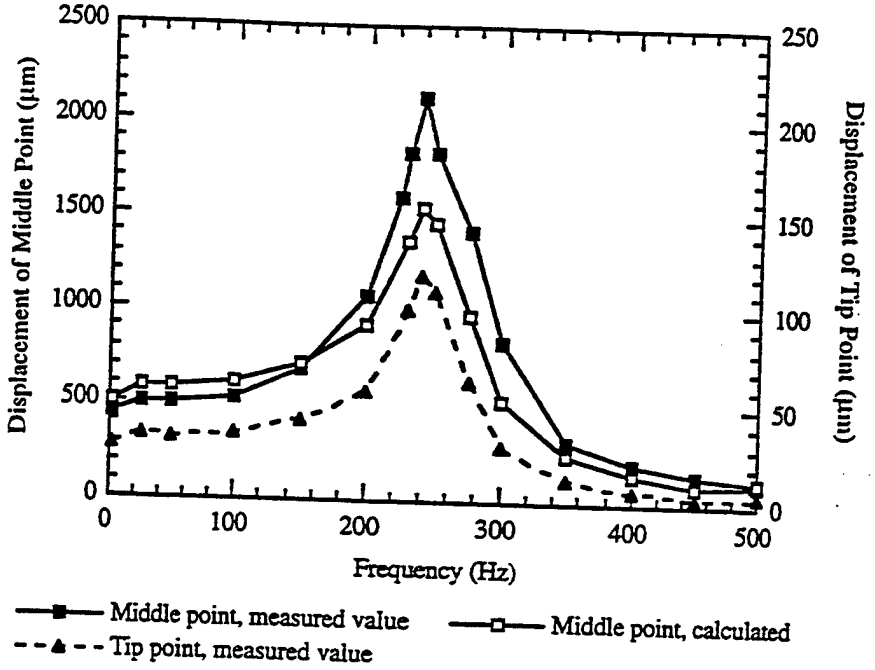

Fig. 9. Dependence of the Displacement on Frequency (L=50mm, g = 1.0mm, Vp-p = 100V)

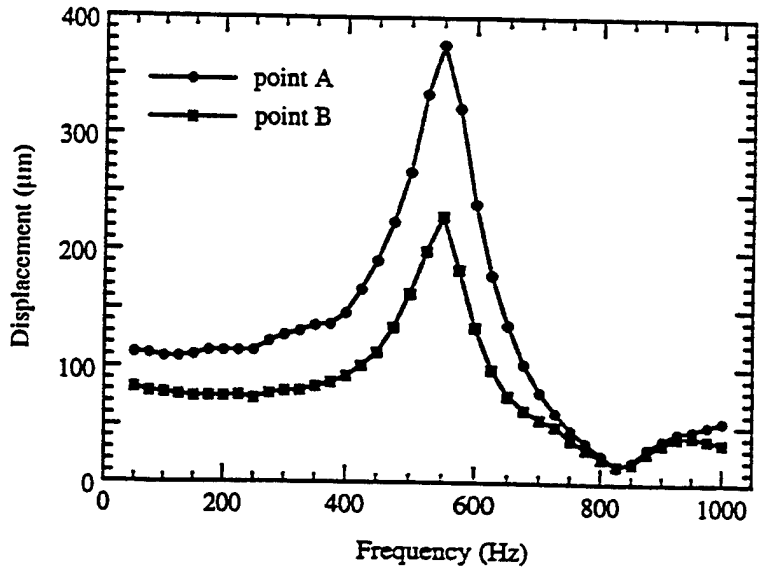

Fig. 10. Frequency Dependence of the Displacement of the Transducer (Vp-p = 100V)

The dependence of the displacement of the point A and point B of the cover plate (see Fig. 2) on frequency is shown in Fig. 10. Due to clamping effect of the two lateral faces which are made of loudspeaker paper and are inactive, and due to the loading effect of the air in the closed chamber of the transducer, the displacement of point A is some smaller than that of the middle point displacement of the double amplifier structure with the same L and g values, and the displacement of point B is smaller than that of point A, but the displacement of the cover plate is still much larger than the tip displacement of bimorphs. The height of the peak in the resonant frequency also becomes weaker and smooth due to these clamping and loading effects.

The frequency dependence of the sound pressure level (SPL) was presented in Fig. 11. The SPL of the near field can be larger than 90dB in the frequency range from 50 to 1000Hz, and the largest value can reach more than 130dB. For the far field, the SPL can reach more than 80dB when the frequency is higher than 200Hz, which is suitable for active noise control. Larger SPL value can be easily obtained by increasing the width of the bimorph arrays. Another approach to get larger SPL value is to construct the transducer with multi-double amplifier structure, as shown in Fig. 12.

5. CONCLUSIONS

Bimorph-based double amplifier structure and the transducer based on this structure have been constructed and studied in this paper. It was demonstrated that with relatively low voltage, the displacement of the active face can reach millimeter scale, which is more than ten times larger than the tip displacement of bimorphs. The sound pressure level of the piezoelectric transducer can be larger than 90dB (near field) between 50 to 1000Hz and 80dB (far field) between 200 to 1000Hz. And the largest value can reach 130dB (near field). Because of its light weight and panel structure, it is potential to use this new piezoelectric air transducer in active noise control.

As the first result of the bimorph-based double amplifier transducer, further improvements in transducer performance are expected using improved materials and design. Instead of bimorph, some other ceramic actuators such as unimorph or monomorph can also be used in the double amplifier structure and transducer design.

6. ACKNOWLEDGMENT

This work was supported by the Office of Naval Research under the contract No. N00014-94-1-1140.

7. REFERENCES

1. L. E. Cross and K. H. Hardtl, "Ferroelectrics," in *Piezoelectricity*, Ed. by C. Z. Rosen, B. V. Hiremath and R. E. Newnham, pp.1-31, American Institute of Physics, New York, 1992.
2. E. K. Dimitriadis and C. R. Fuller, "Active control of sound transmission through elastic plates using piezoelectric actuators," AIAA Journal, Vol. 29, pp. 1771-1777, 1991.
3. L. L. Beranek, *Acoustics*, Chapter 4, the Acoustical Society of America, New York, 1993.
4. K. Uchino, *Piezoelectric/Electrostrictive Actuator*, Chapter 4, Morikita Publishers, Tokyo, Japan, 1986.
5. D. E. Hall, *Basic Acoustics*, Chapter 11, Harper & Row Publishers, New York, 1987.
6. PZT 3203HD Piezoelectric Materials, Motoralo Company, Albuquerque, New Mexico.
7. NW 2200A Loudspeaker Paper, Nu-Way Speaker Products, Antioch, Illinois.
8. MTI-2200 Fotonic Sensor, MTI Instruments, Latham, New York.
9. Cartage Type 4135 1/4" Condenser Microphone, Bruel & Kjael Instruments, Marlborough, Massachusetts.
10. L. E. Kinsler, A. R. Frey, A. B. Coppens and J. V. Sanders, *Fundamentals of Acoustics*, 3rd Edition, Chapter 8, John Wiley & Sons, New York, 1982.
11. J. K. Lee and M. A. Marcus, "The deflection-bandwith product of poly(vinylidene fluoride) benders and related structures," Ferroelectrics, Vol. 32, pp. 93-101, 1981.
12. J. G. Smits, S. I. Dalke and T. K. Cooney, "The Constituent equations of piezoelectric bimorphs," Sensors and Actuators A, Vol. 28, pp. 41-61, 1991.
13. D. J. Gorman, *Free Vibration Analysis of Beams and Shafts*, Chapters 1 and 2, John Wiley & Sons, New York, 1975.

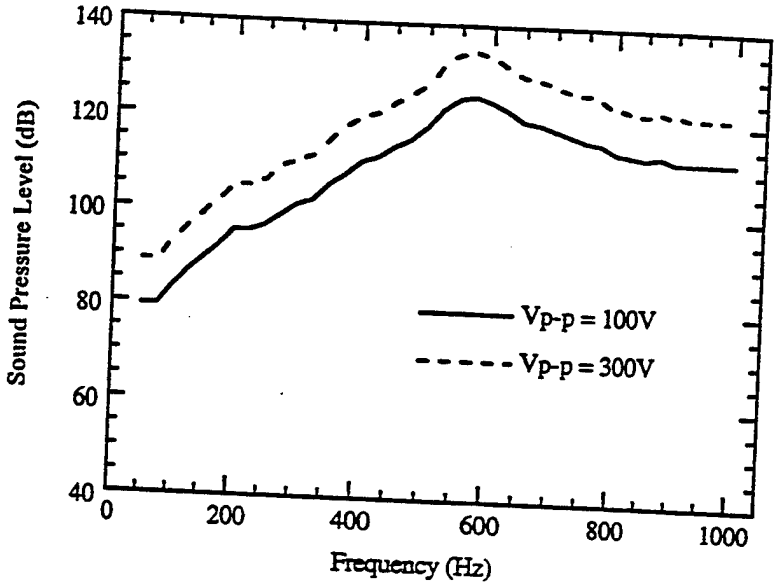

(a) Near field

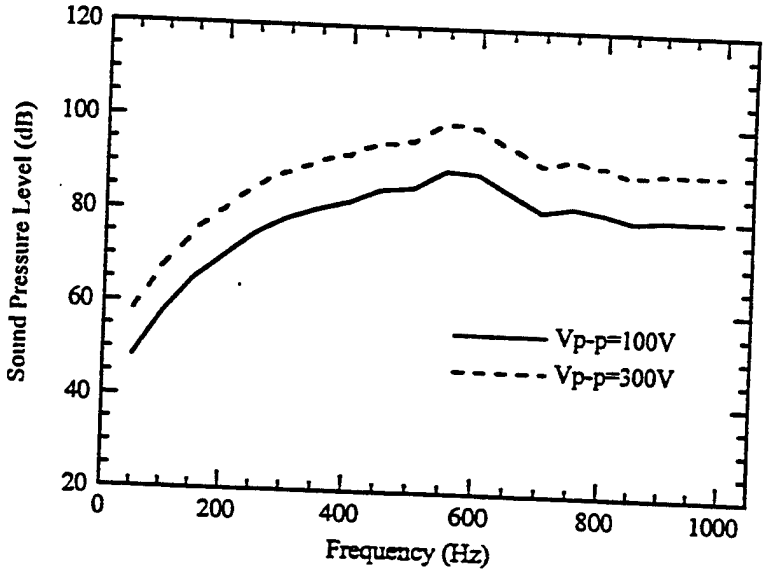

(b) Far field

Fig. 11. Sound Pressure Level of the Transducer

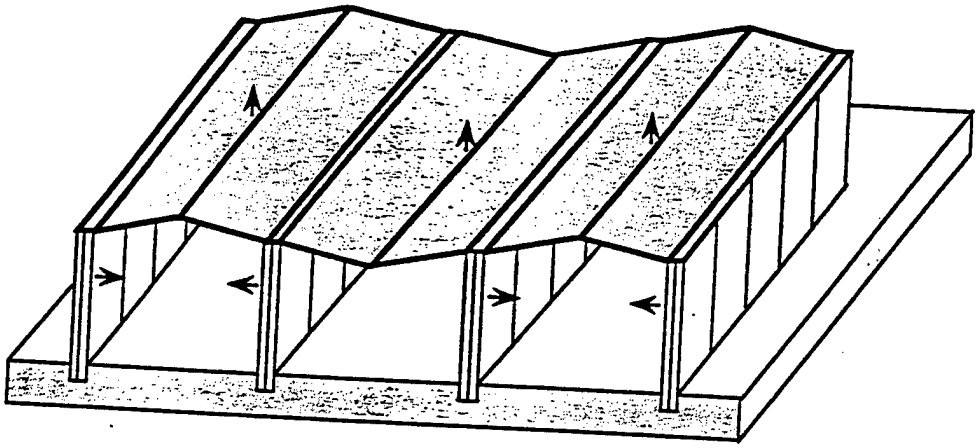

Fig. 12. Configuration of the Transducer Constructed from Multi-Double Amplifier Structure (the arrows represent the moving direction)